Design and development of a torsional guided-waves inspection system for the detection and sizing of defects in pipes

Mohamed Kharrat

Numéro d'ordre : 2012-16 Année 2012

UNIVERSITÉ DE LYON

THÈSE

présentée pour obtenir le titre de

DOCTEUR

de l'**ÉCOLE CENTRALE DE LYON**

Spécialité : MÉCANIQUE

préparée au

LABORATOIRE DE TRIBOLOGIE ET DYNAMIQUE DES SYSTÈMES

dans le cadre de l'École Doctorale

MÉCANIQUE, ENERGÉTIQUE, GÉNIE CIVIL, ACOUSTIQUE

par

Mohamed KHARRAT

DESIGN AND DEVELOPMENT OF A TORSIONAL GUIDED-WAVES INSPECTION SYSTEM FOR THE DETECTION AND SIZING OF DEFECTS IN PIPES

Soutenue publiquement le 6 Juillet 2012, devant le jury d'examen

Jan Holnicki-Szulc, Professeur, IPPT, Pologne	Rapporteur
Mohamed Haddar, Professeur, ENIS, Tunisie	Rapporteur
Lin Li, Professeur, BUAA, Chine	Examinateur
Michel Massenzio, Professeur, UCBL1, France	Examinateur
Manuel Collet, Chargé de recherche HDR, FEMTO-ST, France	Examinateur
Mohammed Ichchou, Professeur, ECL, France	Directeur de thèse
Olivier Bareille, Maître de conférences, ECL, France	Co-encadrant

ÉCOLE CENTRALE LYON **Direction de la recherche**

Liste des personnes Habilitées à Diriger des Recherches en poste à l'Ecole Centrale de Lyon

Nom-Prénom	*Corps grade*	Laboratoire ou à défaut département ECL	Etablissement
BEROUAL Abderrahmane	*professeur*	AMPERE	ECL
BURET François	*professeur*	AMPERE	ECL
JAFFREZIC-RENAULT Nicole	*directeur de recherche*	AMPERE	CNRS/ECL
KRÄHENBÜHL Laurent	*directeur de recherche*	AMPERE	CNRS/ECL
NICOLAS Alain	*professeur*	AMPERE	ECL
NICOLAS Laurent	*directeur de recherche*	AMPERE	CNRS/ECL
SCORLETTI Gérard	*professeur*	AMPERE	ECL
SIMONET Pascal	*directeur de recherche*	AMPERE	CNRS/ECL
VOLLAIRE Christian	*professeur*	AMPERE	ECL
		Nbre Ampère 9	
HELLOUIN Yves	*maître de conférences*	DER EEA	ECL
		Nbre DER EEA 1	
GUIRALDENQ Pierre	*professeur émérite*	DER STMS	ECL
VINCENT Léo	*professeur*	DER STMS	ECL
		Nbre DER STMS 2	
LOHEAC Jean-Pierre	*maître de conférences*	ICJ	ECL
MAITRE Jean-François	*professeur émérite*	ICJ	ECL
MARION Martine	*professeur*	ICJ	ECL
MIRONESCU Elisabeth	*professeur*	ICJ	ECL
MOUSSAOUI Mohand	*professeur*	ICJ	ECL
MUSY François	*maître de conférences*	ICJ	ECL
ZINE Abdel-Malek	*maître de conférences*	ICJ	ECL
		Nbre ICJ 7	
DAVID Bertrand	*professeur*	ICTT	ECL
		Nbre ICTT 1	
CALLARD Anne-Ségolène	*professeur*	INL	ECL
CLOAREC Jean-Pierre	*maître de conférences*	INL	ECL
GAFFIOT Frédéric	*professeur*	INL	ECL
GAGNAIRE Alain	*maître de conférences*	INL	ECL
GARRIGUES Michel	*directeur de recherche*	INL	CNRS/ECL
GENDRY Michel	*directeur de recherche*	INL	CNRS/ECL
GRENET Geneviève	*directeur de recherche*	INL	CNRS/ECL
HOLLINGER Guy	*directeur de recherche*	INL	CNRS/ECL
KRAWCZYK Stanislas	*directeur de recherche*	INL	CNRS/ECL
LETARTRE Xavier	*chargé de recherche*	INL	CNRS/ECL
O'CONNOR Ian	*professeur*	INL	ECL
PHANER-GOUTORBE Magali	*professeur*	INL	ECL

ROBACH Yves	*professeur*	INL	ECL
SAINT-GIRONS Guillaume	*chargé de recherche*	INL	CNRS/ECL
SEASSAL Christian	*directeur de recherche*	INL	CNRS/ECL
SOUTEYRAND Eliane	*directeur de recherche*	INL	CNRS/ECL
TARDY Jacques	*directeur de recherche*	INL	CNRS/ECL
VIKTOROVITCH Pierre	*directeur de recherche*	INL	CNRS/ECL

Nbre INL 18

CHEN Liming	*professeur*	LIRIS	ECL

Nbre LIRIS 1

BAILLY Christophe	*professeur*	LMFA	ECL
BERTOGLIO Jean-Pierre	*directeur de recherche*	LMFA	CNRS/ECL
BLANC-BENON Philippe	*directeur de recherche*	LMFA	CNRS/ECL
BOGEY Christophe	*chargé de recherche*	LMFA	CNRS/ECL
CAMBON Claude	*directeur de recherche*	LMFA	CNRS/ECL
CARRIERE Philippe	*directeur de recherche*	LMFA	CNRS/ECL
CHAMPOUSSIN J-Claude	*professeur émérite*	LMFA	ECL
COMTE-BELLOT geneviève	*professeur émérite*	LMFA	ECL
FERRAND Pascal	*directeur de recherche*	LMFA	CNRS/ECL
GALLAND Marie-Annick	*professeur*	LMFA	ECL
GODEFERD Fabien	*directeur de recherche*	LMFA	CNRS/ECL
GOROKHOVSKI Mikhail	*professeur*	LMFA	ECL
HENRY Daniel	*directeur de recherche*	LMFA	CNRS/ECL
JEANDEL Denis	*professeur*	LMFA	ECL
JUVE Daniel	*professeur*	LMFA	ECL
LE RIBAULT Catherine	*chargée de recherche*	LMFA	CNRS/ECL
LEBOEUF Francis	*professeur*	LMFA	ECL
PERKINS Richard	*professeur*	LMFA	ECL
ROGER Michel	*professeur*	LMFA	ECL
SCOTT Julian	*professeur*	LMFA	ECL
SHAO Liang	*directeur de recherche*	LMFA	CNRS/ECL
SIMOENS Serge	*chargé de recherche*	LMFA	CNRS/ECL
TREBINJAC Isabelle	*maître de conférences*	LMFA	ECL

Nbre LMFA 23

BENAYOUN Stéphane	*professeur*	LTDS	ECL
CAMBOU Bernard	*professeur*	LTDS	ECL
COQUILLET Bernard	*maître de conférences*	LTDS	ECL
DANESCU Alexandre	*maître de conférences*	LTDS	ECL
FOUVRY Siegfrid	*chargé de recherche*	LTDS	CNRS/ECL
GEORGES Jean-Marie	*professeur émérite*	LTDS	ECL
GUERRET Chrystelle	*chargé de recherche*	LTDS	CNRS/ECL
HERTZ Dominique	*past*	LTDS	ECL
ICHCHOU Mohamed	*professeur*	LTDS	ECL
JEZEQUEL Louis	*professeur*	LTDS	ECL
JUVE Denyse	*ingénieur de recherche*	LTDS	ECL
KAPSA Philippe	*directeur de recherche*	LTDS	CNRS/ECL
LE BOT Alain	*directeur de recherche*	LTDS	CNRS/ECL
LOUBET Jean-Luc	*directeur de recherche*	LTDS	CNRS/ECL
MARTIN Jean-Michel	*professeur*	LTDS	ECL
MATHIA Thomas	*directeur de recherche*	LTDS	CNRS/ECL
MAZUYER Denis	*professeur*	LTDS	ECL
PERRET-LIAUDET Joël	*maître de conférences*	LTDS	ECL
SALVIA Michelle	*maître de conférences*	LTDS	ECL

SIDOROFF François	*professeur*	LTDS	ECL
SINOU Jean-Jacques	*professeur*	LTDS	ECL
STREMSDOERFER Guy	*professeur*	LTDS	ECL
THOUVEREZ Fabrice	*professeur*	LTDS	ECL
TREHEUX Daniel	*professeur*	LTDS	ECL
VINCENS Eric	*maître de conférences*	LTDS	ECL

Nbre LTDS 25

Total HdR ECL	91

Acknowledgment

Few lines for those who deserve the gratitude.

First of all, I wish to express my thanks to my supervisors Prof. Mohammed Ichchou and Dr. Olivier Bareille, mostly for their confidence, for their rigorous and patient supervision, and for offering me the opportunity to learn a lot by their side. I thank also my colleague Wenjin Zhou for his practical help throughout my thesis.

I would like to thank the jury members for accepting to report my work and taking part in my PhD defense.

Huge thanks to my family for their encouragement during my thesis. A special thanks to Fatma for her patience, confidence and understanding throughout the time I spent far from her.

My sincere acknowledgments are also extended to all my friends for their continuing personal support.

Last but definitely not least, I must thank all my colleagues and members of the lab who have helped me during my research activities.

Résumé

Plusieurs industries manipulent des substances liquides et gazeuses qui circulent souvent dans de longues canalisations. La technique d'ondes guidées est couramment utilisée dans ce domaine. Cette technique est en progrès continu. Dans cette thèse, un système d'inspection a été conçu et développé. Il est basé sur des transducteurs piézoélectriques qui génèrent des ondes guidées de torsion pouvant se propager le long du tube testé. Les signaux réfléchis des défauts et singularités rencontrés sont détectés aussi par des capteurs piézoélectriques. Des simulations numériques utilisant par la méthode d'éléments finis standard et la méthode Wave Finite Element (WFEM) ont été effectuées afin de vérifier et de visualiser le phénomène de propagation des ondes dans des tubes intacts et endommagés. Un ensemble de tests a été mis en place sur des tubes droits et courbés avec deux matériaux différents: PVC et acier. L'interaction entre les ondes générées et les défauts usinés a été prouvée. Les résultats numériques et expérimentaux confirment certaines caractéristiques spécifiques concernant le coefficient de réflexion de l'onde. Par la suite, un pipeline industriel d'environ soixante mètres de long et contenant plusieurs défauts et singularités a été testé par le système d'inspection. Les signaux enregistrés ont soumis certains traitements numériques afin de les rendre exploitables. Les signaux traités sont analysés afin d'identifier et de distinguer les réflexions des défauts de celles des singularités structurés. La méthode WFEM a été employée pour construire une base de données numérique des coefficients de réflexion en variant la profondeur et les extensions axiale et circonférentielle du défaut modélisé. Le calcul a été établi en fonction de la fréquence. La corrélation des tailles des défauts est effectuée en balayant la base de données numérique pour trouver la combinaison appropriée de dimensions pour un défaut donné. Les réflexions à partir des singularités structurées (coudes, blocs de béton, colliers, et les soudures) sont traitées ainsi en comparant des coefficients de réflexion obtenus par WFEM à ceux évalués expérimentalement. Enfin, on a étudié numériquement l'effet de la position angulaire d'un défaut sur les coefficients de réflexion et de transmission tout en excitant à différents types d'ondes. La méthode WFE est aussi utilisée pour effectuer le calcul. Cette étude donne un guide à la localisation circonférentielle des défauts dans les tubes.

Mots clés : Contrôle Non Destructif, détection des défauts, ondes de torsion; transducteurs piezoélectriques; méthode éléments finis d'ondes; coefficient de réflexion; dimensionnement des défauts; position angulaire du défaut.

Abstract

Long pipelines are widely used in several industries transporting liquid or gas. The guided wave technique is commonly used in this field and it is under continuing progress. In this thesis, an inspection system has been designed and developed. Piezoelectric transducers are employed to generate torsional guided waves that could propagate along the tested pipe; and receive reflected signals from encountered features and damages. Numerical simulations using standard FE and Wave Finite Element methods have been carried out in order to verify and visualize the wave propagation phenomenon in both intact and damaged pipes. A set of tests has been performed on straight and curved pipes with two different materials: PVC and steel. The interaction between generated waves and machined defects has been proven. Numerical and experimental results confirm some specific features in the wave reflection coefficient. Thereafter, an industrial pipeline of about sixty meters long and containing several features has been tested by the inspection system. Recorded signals had submitted some numerical treatments in order to make them interpretable. Processed signals are analyzed to identify defects reflections from structured singularities echoes. The Wave Finite Element Method (WFEM) has been used to construct a numerical database of reflection coefficients from modeled defects by varying thickness, axial and circumferential extents. Calculation was made depending on frequency. The approximation of defect sizes is carried out by sweeping the numerical database to find the suitable combination of dimensions for a given defect. Reflections from structural singularities (elbows, concrete blocks, clamps, and welds) are treated as well by comparing reflection coefficients obtained by WFEM to those evaluated experimentally. Finally, a numerical investigation deals with the effect of defect angular-position on reflection and transmission coefficients while exciting by different types of waves. The spectral method Wave Finite Element has been used to carry out calculation. This study gives guidance to circumferential localization of defects in pipes.

Keywords: NonDestructive Testing; damage detection; torsional waves; piezoelectric transducers; Wave Finite Element Method; reflection coefficient; defect sizing; defect angular position.

Contents

Introduction

Background

Long pipelines are often used in petro-chemical industry for transporting liquid and gaseous substances. These pipes need to be regularly monitored and inspected for both safety reasons and environmental impact control. Non-Destructive Tests (NDT) techniques are required to assess the integrity of pipes in service. A lot of NDT methods exist with several industrial applications [1]. Conventional point-by-point methods such as ultrasonic thickness gauging imply a slow inspection process and consequently very expensive. Many other NDT techniques are also employed in pipe testing such as magnetic flux [2, 3], eddy current [4, 5] and radiography [6].

A quick and reliable method for the detection of corrosion and defects under insulation which does not involve removal of all the insulation is therefore required. The problem is even more severe in cases such as road crossings where the pipe is underground (often in a sleeve) for a limited distance; excavation of the pipe for visual or conventional ultrasonic inspection is extremely expensive so a technique to address this problem is particularly beneficial. Therefore, it is useful to find an effective method capable of screening long distances of pipes from one access position and to be fast and sufficiently accurate to identify defects in the inspected areas. Guided waves have been increasingly used in nondestructive evaluations. Many researchers have been interested in the application of ultrasonic guided waves for the nondestructive inspection of pipes [7–10]. They have recognized the possibility for rapid, accurate, and inexpensive nondestructive assessment of these structures that exist in the infrastructure of many industries. Guided wave inspection method is a fast screening technique for pipe testing. It ensures the inspection over larger distances from limited and distant points of observation. The use of low frequency ultrasonic guided waves propagating along the pipe wall is potentially a very attractive solution to this problem since they can propagate a long distance under insulation and may be excited and received using transducers positioned at a location where a small section of insulation has been removed.

One of the first works on guided wave inspection of pipes has been done by Mohr and Höller [11] for small diameter heat exchanger tubes. They used axially symmetric (axisymmetric) longitudinal guided waves to detect transverse failures in ferritic tubes and torsional guided waves to inspect for longitudinal defects. Thompson et al. [7, 12] developed an EMAT device to inspect from the inside of pipes. The generation of ultrasonic wave modes in thin-walled metal tubing has been investigated experimentally using piezoelectric ultrasonic probes by Silk and Bainton [8]. A prototype system with full computer support for ultrasonic inspection of ferritic

tubes using guided waves has been described by Böttger et al. [13]. The ultrasonic waves are launched and received with the aid of electromagnetic acoustic transducers which are laid out as linear phased arrays.

Cylindrically guided waves could be excited using an array of piezoelectric transducers distributed around the circumference of the pipe. These waves stress the whole pipe wall and propagate over long distance. When they encounter features, such as flanges, elbows, welds, branches or corrosion that change geometry of the pipe and thereafter its acoustic impedance, these guided waves are partially reflected. These echoes can be received by the same transducers used for excitation of the guided waves or other sensors, and then analyzed in order to provide information about the location, size and nature of discontinuities that caused the reflections. Practically, the reflection arrival-time gives an indication of the axial location of the reflecting feature and the amplitude of the reflection gives an indication of the severity of the cross sectional area change. However, guided wave propagation in pipes and their interaction with defects is complex, making accurate information about defects difficult to extract from the reflected signals.

In principle, both axisymmetric and non-axisymmetric modes can be used for long-range inspection. Axisymmetric modes are in general preferable because they are easier to excite and have relatively simple acoustic fields. Initial practical testing was done by many researchers using the longitudinal L(0,2) mode. This latter has the advantage to achieve the entire pipe wall coverage since it is axisymmetric and has a near constant mode shape through the wall thickness. Defects located at any circumferential position and anywhere the pipe wall thickness can be detected. The L(0,2) mode is dispersive but has been employed in relatively non-dispersive frequency regimes around 50-100 kHz. Alleyne and Cawley [9] have reported on the development of dry-coupled piezoelectric transducers for the excitation and detection of the guided waves. Alleyne et al. [14, 15] and Lowe et al. [16] have studied the reflection of the L(0,2) axially symmetric mode from notches in pipes, and examined the reflection of mode-converted guided waves with L(0,2) as incident mode [17]. Alleyne and Cawley [18] measured reflections of the same mode from welds, flanges and pipe supports, and demonstrated that the mode can be propagated under wet or dry insulation.

However, more recent testings gave a considerable research interest to the fundamental torsional mode T(0,1). Many researchers have employed it at lower frequencies (10-50 kHz) [19–21]. This mode has similar advantages to the longitudinal L(0,2) mode in terms of ease of excitation and full pipe-wall coverage due to axisymmetry. But in contrast to the L(0,2) mode, T(0,1) is entirely non-dispersive making post-processing of signals less complex, and its propagation characteristics are not affected by the presence of liquid in the pipe. Since shear waves cannot propagate in liquids, so there is no energy leakage for the T(0,1) mode, which consists of shear displacement only, whereas the L(0,2) mode can excite waves in the liquid. Moreover, there is no other axially symmetric torsional mode in the frequency range used, so axially symmetric torsional excitation will only excite the T(0,1) mode, whereas when the L(0,2) mode is used, the transducer system must be carefully designed to suppress the L(0,1) mode.

A detailed explanation by Rose et al. [22] has been presented along with the

various design aspects of a comb transducer. This latter is a finger-like device that is placed on the structure, whereby pumping ultrasonic energy into the comb with the appropriate spacing can produce guided waves of choice inside the piping material. The comb structure can go entirely around the pipe producing longitudinal axisymmetric waves or be placed partially around the circumference of the pipe, say from twenty to ninety degrees around the circumference, and in this case produce longitudinal non-axisymmetric or flexural modes in the pipe.

The subject of guided wave tuning principles and focusing for defect detection is introduced in many works [23–28]. This hypothesis is being explored in detail today, that of establishing wave resonances from a defect inside a structure by controlling phase velocity and frequency. It becomes possible to focus the ultrasonic energy onto the defect of interest that gives us the best dynamic response and hence the best potential for detection classification and sizing of the particular defect. Guided waves via a four dimensional tuning process of adjusting circumferential loading length, circumferential position, phase and frequency, can create a natural focusing effect almost anywhere inside the pipe. Shin and Rose [29] discussed the use of both axisymmetric and non-axisymmetric surface loading in hollow cylinders and illustrates the basic principles behind non-axisymmetric wave propagation. Use of these flexural mode waves are being tried in order to assist in the flaw detection classification and sizing process. Further work on the excitation of non-axisymmetric guided waves is reported by Li and Rose [30]. It is shown in this paper how it becomes possible to load the upper surface of a pipe and to inspect, for example, the bottom side of a pipe, at a certain distance away.

One of the potential difficulties in pipe inspection is the presence of viscoelastic coatings that are commonly used for corrosion protection. These coatings tend to attenuate the propagating energy and can severely degrade the performance of a guided wave test with regard to test sensitivity and the distance of propagation. A lot of work has been established on this issue [21, 31–33] to describe the effect of such coatings on the wave propagation in pipes.

Another issue that has been treated is the presence of features in pipeline like elbows. Rose and Zhao [34] carry further the flexural mode tuning concept for pipe elbow inspection. It is shown that it becomes possible to send ultrasonic energy into an elbow region and even beyond the elbow region in carrying out a reliable and efficient inspection. Also a semi-analytical finite element method has been used by Hayashi and Rose [35, 36] in order to show how an axisymmetric wave in a straight pipe is modified as it passes through an elbow. A. Demma et al. [37] has studied the propagation of guided waves in curved pipes. The modes propagating in toroidal structures have been found using an FE procedure.

Furthermore, guided waves can be also employed for the sizing of defects, which is much more difficult and requires detailed knowledge about the interaction of the incident wave with different possible defect types. Indeed, the reflection or transmission signal depends not only the defect size or shape, but also the mode type and frequency, potential mode conversion, and the attenuation due to dissipation, leakage or geometry. However, the wave-defect interaction analysis will help to find out which types of modes are sensitive to a given type of defects. The character of scattering should be quite different if the defect is transverse such as crack or notch,

axially distributed such as delamination in layered structures, or due to the loss of mass, presence of inclusions, etc., which probably causes the failure of the inspection if the mode is not properly chosen. In the other hand, the numerical wave-defect interaction analysis will provide a reference of the sizing in the practical test, at least to some extent. The effect of defect size on the reflection and transmission characteristics in pipes has been investigated by many researchers [15,17,19,38–44]. These studies deal with many types of defects like cracks [19,41], notches [15,17,38, 42], and circular holes [43,44]. J.L. Rose et al. [45] have used the boundary element analysis in seeking out some techniques that might be used for flaw sizing potential with guided waves. It is shown that a very simple algorithm of examining amplitude of the reflection or transmission from a defect as being proportional to depth of the defect is indeed sometimes true. A long range ultrasonic guided wave test system was used by Jing Mu et al. [46] to measure the circumferential size of volumetric corrosion defects and a transverse saw cuts by sweeping the focal position around the pipe. A quantitative study of the reflection of the T(0,1) mode from defects in pipes was carried out by A. Demma et al. [19], finite element predictions being validated by experiments on selected cases. Another work by A. Demma et al. [39] presents a systematic analysis of the effect of pipe size, defect size, guided wave mode and frequency on the reflection from notches. J. Davies and P. Cawley [47] quantify the performance of a synthetically focused guided-waves technique for detection, location, and sizing of circumferential crack-like defects in pipelines.

Many useful frequency-domain informations, such as wave dispersibility, reflection from damage, interface or boundary, sensitivity of specific mode to various types of damages, mode conversions, etc [48], can be obtained directly from the eigensolutions in spectral methods, or by the global-local techniques such as hybrid methods [49–54]. The Wave Finite Element Method (WFEM), which is a simple spectral method based on the standard finite element (FE) formulation, can be applied to examine the wave interaction with the local defects and the structural features [51–54]. The hybrid WFE/FE method is one of the hybrid methods for global-local analysis , which is very suitable to the case that wavelength is larger than the axial extension of FE model for complex local defect.

Contribution of the thesis

In this work, an inspection system has been designed and developed to excite the pipe under test with well-defined waves that propagate along the structure; and receive reflected signals from encountered features and damages. The torsional mode was chosen to be generated by the system. This choice is based on the intrinsic properties of this mode. The generation of torsional waves is operated by using a number of piezoelectric transducers clamped around the circumference of the pipe. After positioning the transducer ring around the pipe, the operator starts a rapid test, which automatically sweeps several frequencies collecting data from either side of the ring at once. The propagation of the ultrasonic signal depends on the conditions of the pipe under test. A wide range of about one hundred meters in either direction from the transducer ring position can be obtained when the pipe is in generally good condition and there is a low density of features encountered. The range can

be reduced, in one hand, if the pipe is heavily corroded over its length, and in other hand if pipes are buried or coated by viscoelastic materials, which increase wave attenuation. Dispersion curves for PVC and steel pipes are computed using the Wave Finite Element Method in order to obtain the wave velocity in the tested structures. The same method is employed also to determine numerically time signals from damaged pipe.

An important information retrieved from recorded signals is the reflection coefficient of each defect. This information can be very useful for defect sizing. For this purpose, a hybrid WFE/FE method has been used to construct a numerical database of reflection coefficients from rectangular defects by varying thickness, axial and circumferential extents. Calculation is made depending on frequency. The approximation of defect sizes is carried out by sweeping the numerical database to find the suitable combination of dimensions for a given defect. Axial and circumferential extents are evaluated by limited intervals for each possible thickness. Reflections from structural singularities (elbows, concrete blocks, clamps, and welds) are also treated by comparing reflection coefficients obtained by WFEM to those evaluated experimentally.

The hybrid WFE/FE has been used also to investigate numerically reflection and transmission coefficients from a defined defect in a pipe while varying its angular position at a fixed axial location. Three different waves are tested: the torsional mode T(0,1), the longitudinal L(0,2) mode, and the flexural F(1,2) mode are incident separately. In each case reflections and transmissions of all possible wave modes are checked in order to find guidance for the angular localization of the defect.

Outline of the thesis

This thesis consists of six chapters. The first one is an overview of the state of the art in fields of interest. Nondestructive testing methods are introduced in the first section. The more common techniques are described: Radiography Testing, Ultrasonic Testing, Magnetic Particle Inspection, Eddy Current Testing and, Guided Wave Testing. The principle, applicability as well as their advantages and drawbacks are clearly presented. The second section focuses deeply on Guided Wave Testing. The mathematical foundation of wave propagation in an isotropic unbounded media is described. Lamb wave dispersion equations are derived starting from the wave equations, which must be satisfied by all waves in elastic isotropic media. Guided wave propagation in pipes is then presented with the main characteristics and different modes description. Thereafter, major advantages and some limitations of Guided Wave Testing are considered. Finally, three most used technologies for generating guided waves are introduced. These technologies are: Piezoelectric transducers, ElectroMagnetic Acoustic Transducer and, Magnetostrictive Sensors.

Next five chapters include papers accepted and ready for submitting to international peer reviewed journals. The first paper (chapter 2) is entitled "Distributed piezoelectric guided-T-wave generator, design and analysis" and has been published in *Mechatronics* journal. This paper presents the definition and design of a specific torsional wave generator concept. Numerical simulations confirm the design. An experimental test bench is also provided in order to validate the concept. The ability

of the distributed system in generating pure T waves is discussed. Numerical and experimental results confirm some specific features in the wave reflection coefficient based on the interaction between the damaged waveguide dynamics and torsional waves propagation.

The second paper (chapter 3) is entitled "Defect detection in pipes by a torsional guided-wave inspection system: design and experiments" and is intended to be submitted to *Ultrasonics* journal. In this work, numerical simulations using standard FE and Wave Finite Element methods have been carried out in order to verify and visualize the wave propagation phenomenon in both intact and damaged pipes. An experimental test bench is provided in order to perform a set of tests on straight and curved pipes with two different materials: PVC and steel. In each case, time signals from intact and damaged structures were analyzed. The interaction between the generated waves and machined defects has been proven, as well as the ability of damage detection within the curved structure. Numerical and experimental comparison, in terms of reflection coefficients, has shown a good agreement.

The third paper (chapter 4) is entitled "Pipeline inspection using a torsional guided-waves inspection system. Part 1: Defect identification". A steel pipeline of about sixty meters long has been tested in this work using a guided-waves technique. The inspection system is a pair of transducer rings operating with the torsional mode T(0,1) and allows the long-range fast screening of the structure from defined measurement points. Recorded signals had submitted some numerical treatments in order to make them interpretable. Wavelet package analysis was one of them and has allowed the denoising of raw signals. Besides, the Hilbert transform was applied in order to obtain the wave envelope which is easier to interpret. Processed signals were analyzed to identify defects reflections from structured singularities echoes.

The fourth paper (chapter 5) is the second part of the previous paper and is entitled "Pipeline inspection using a torsional guided-waves inspection system. Part 2: Defect sizing by the Wave Finite Element Method". This paper deals with the torsional-mode reflection from defects and structural singularities in an industrial pipeline in order to perform the defect sizing. The Wave Finite Element Method (WFEM) has been used to construct a numerical database of reflection coefficients from rectangular defects by varying thickness, axial and circumferential extents. Calculation was made depending on frequency. The approximation of defect sizes is carried out by sweeping the numerical database to find the suitable combination of dimensions for a given defect. Axial and circumferential extents are evaluated by limited intervals for each possible thickness. Reflections from structural singularities (elbows, concrete blocks, clamps, and welds) were also treated by comparing reflection coefficients obtained by WFEM to those evaluated experimentally. Results show a good agreement for most of the structured singularities but not for the others. Results may be improved by including damages in the structural singularities.

The last paper (chapter 6) is entitled "Effect of defect angular-position on the wave reflection and transmission coefficients: numerical investigation by the Wave Finite Element Method". This paper provides a numerical investigation concerning the effect of defect angular-position on reflection and transmission coefficients while exciting by different types of waves. The spectral method Wave Finite Element has been used to carry out calculation. Twelve angular positions were studied while

impinging the modeled defect by torsional mode T(0,1), longitudinal mode L(0,2) and flexural mode F(1,2). Results show that the type of incident wave as well as the examined reflected and transmitted waves play an important role in circumferential localization of the defect.

Chapter 1

State of the art

1.1 Nondestructive Testing methods

Nondestructive testing (NDT), nondestructive evaluation (NDE) or nondestructive inspection (NDI) are commonly used to describe the technology of defect detection in solids. This technology covers a group of analysis techniques used in science and industry to evaluate the properties of a material, component or system without causing damage. It is an essential part of quality control of engineering systems for their safe and successful use in practical situations. However, applications of NDT go much deeper and are much broader in scope than the detection of gross defects. They concern all aspects of the characterization of solids as well as their method of preparation.

Whilst being a high technology concept, evolution of the equipment has made it robust enough for application in any industrial environment at any stage of manufacture, from steel making to site inspection of components already in service. A certain degree of skill is required to apply the techniques properly in order to obtain the maximum amount of information concerning the product, with consequent feedback to the production facility. Modern nondestructive tests are used by manufacturers to ensure product integrity, and in turn, reliability; to avoid failures, prevent accidents and save human life; to make a profit for the user; to ensure customer satisfaction and maintain the manufacturer's reputation; to aid in better product design; to control manufacturing processes; to lower manufacturing costs; to maintain uniform quality level; and to ensure operational readiness.

NDT can be applied on metals or nonmetals, small to large structures, and stationary as well as moving components. It is used in a variety of settings that covers a wide range of industrial activity like medical imaging, automotive, aviation, aerospace, construction, maintenance, manufacturing, industrial plants (pressure vessels, storage tanks, boilers, heat exchangers...), as well as pipelines, railways and others.

NDT includes various methods, each based on a particular scientific principle. These methods may be further subdivided into various techniques. The choice of the specific method depends on many factors including availability, accessibility, and suitability based on analysis and past experience. It may sometimes be necessary to use one method of NDT to confirm the findings of another. Thereafter, some

common methods are introduced.

1.1.1 Radiography Testing (RT)

The purpose of radiography is to show the presence and nature of defects or other structural discontinuities in the interior of the materials under examination. This technique makes use of the ability of short wavelength electromagnetic radiations, such as X-rays or gamma rays, to penetrate objects. In general, the shorter the wavelength, the greater is the penetrating power. The image obtained is an X-ray shadow projection of the interior of the material (see figure 1.1). Such a shadow picture is called a radiograph. The contrast in a radiograh is due to different degrees of absorption of x-rays in the specimen and depends on variations in specimen thickness, different chemical constituents, nonuniform densities, flaws, discontinuities, or to scattering processes within the specimen [55,56]. With conventional radiographic methods, the difference in attenuation produced by a change of the order of 1-2% in object thickness can be visualized. Thickness or density changes of as little as 0.5% and high-contrast features as small as several micrometers in size can be detected under optimum circumstances (good geometry, thin object, low x-ray energy, fine-grain photographic film, etc...). As the contrast decreases to a few percent, the resolution capability is degraded.

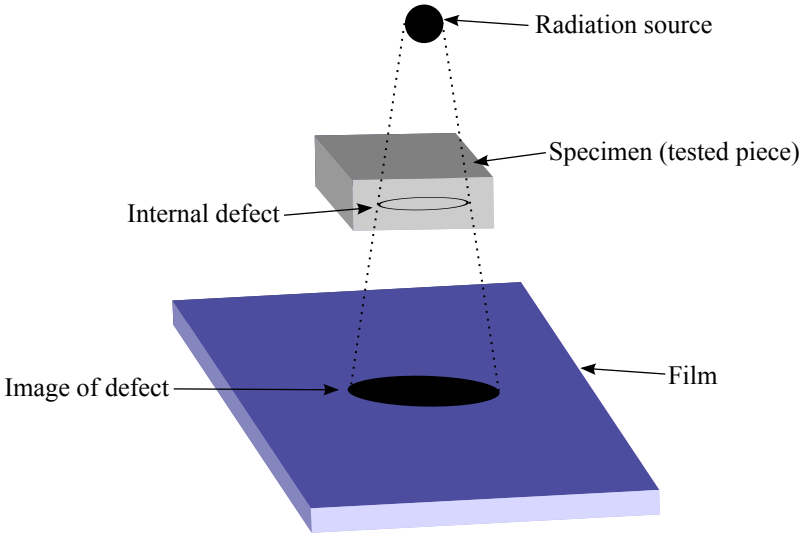

Figure 1.1: Principle of radiography testing.

Radiographic applications fall into two distinct categories: evaluation of material properties and evaluation of manufacturing and assembly properties. Material property evaluation includes the determination of composition, density, uniformity, and cell or particle size. Manufacturing and assembly property evaluation is normally concerned with dimensions, flaws (voids, inclusions, and cracks), bond integrity (welds, brazes, etc.), and verification of proper assembly of component pieces. Radiography is quite useful for detecting wall thickness variations, water ingress, scale build-up and some voids and areas lacking adhesive, as well as the presence of damages caused by impact, porosity or inclusion, and other volumetric defects. Besides,

cracks can also be also detected, as well as incorrect insertion of pipes in adhesive sockets and internal excess of adhesive. It is important to mention that radiographic technique is not sensitive to surface roughness, but it is sensitive to the orientation of the defect.

1.1.2 Ultrasonic Testing (UT)

Sound waves of frequency above 20 kHz are known as ultrasound or ultrasonics. Ultrasonic testing includes different types of methods: Acoustic Resonance Technology (ART), Electro Magnetic Acoustic Transducer (EMAT), Laser Ultrasonics, Internal Rotary Inspection System (IRIS), Phased Array, Time Of Flight Diffraction (TOFD), and Time Of Flight Ultrasonic Determination of 3D Elastic Constants. The range of frequencies used in ultrasonic testing is from less than 0.1 MHz to greater than 15 MHz, and typical values of wavelengths are from 1 to 10 mm. Ultrasonic wavelengths are on the same order of magnitude as visible light, giving them many of the same properties of light. For example, ultrasonic wavelengths can be focused, reflected, and refracted. Ultrasonic waves are transmitted through air, water, and solids such as steel by high-frequency particle vibrations. These waves are transmitted in homogeneous solid objects much like pointing a flashlight around a room with various objects that reflect light. The directed energy in an ultrasonic wave is reflected by boundaries between materials regardless of whether the material is gas, liquid, or solid. Ultrasonic waves are also reflected by any cracks or voids in solid materials. These reflected waves, which are caused by internal defects, can be compared to the reflected waves from the external surfaces, enabling the size and severity of internal defects to be identified. Ultrasonic inspection can be used for flaw detection/evaluation, dimensional measurements, material characterization, and more [55].

A typical UT inspection system consists of several functional units, such as the pulser/receiver, transducer, and display devices. A pulser/receiver is an electronic device that can produce high voltage electrical pulses. Driven by the pulser, the transducer generates high frequency ultrasonic energy. The sound energy is introduced and propagates through the materials in the form of waves. The ultrasonic wave is carried from the transducer to the unit under test (UUT) by a couplant – typically water, oil, or gel – and is reflected back to the transducer by both external surfaces and internal defects. An example of an ultrasonic testing is shown in figure 1.2. When there is a discontinuity (such as a crack) in the wave path, part of the energy will be reflected back from the flaw surface. Imperfections or other conditions in the space between the transmitter and receiver reduce the amount of transmitted sound, thus revealing their presence. The reflected wave signal is transformed into an electrical signal by the transducer and is displayed on a screen.

When operating in pulse-echo mode, ultrasonic transducers act as both emitters and receivers. The reflected ultrasonic waves vibrate the piezoelectric crystal within the ultrasonic transducer and generate voltages that are measurable by data acquisition hardware. When operating in through-transmission mode, two ultrasonic transducers are used; one transducer generates the wave and the other receives the wave.

The most primitive method to analyze the reflected ultrasonic signals is time-of-flight (TOF) display, or A-scan. Discontinuities that are closer to the ultrasonic transducer are received sooner than those further away from the transducer. Figure 1.3 shows the TOF display of the previous example.

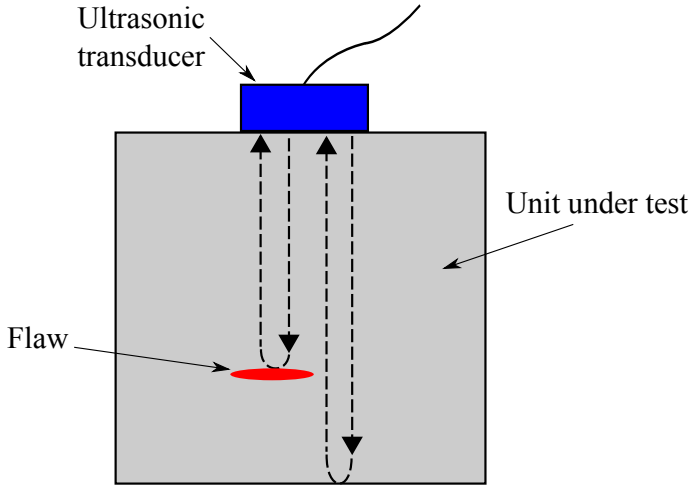

Figure 1.2: Principle of ultrasonic testing.

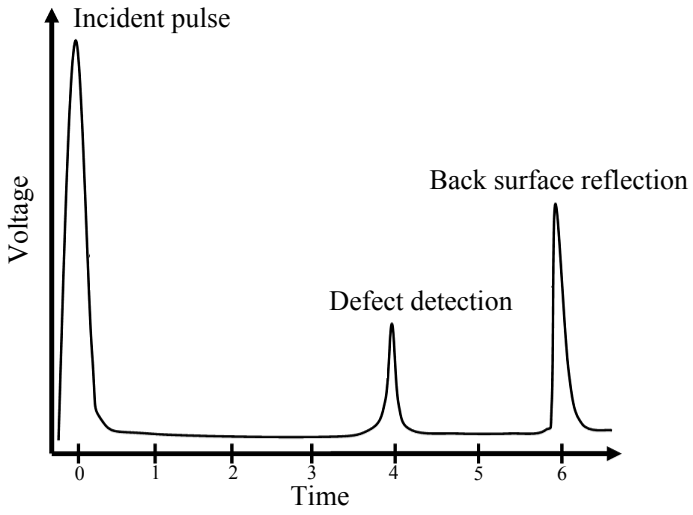

Figure 1.3: TOF display of an ultrasonic test.

1.1.3 Magnetic Particle Inspection (MPI)

MPI uses magnetic fields and small magnetic particles (i.e. iron filings) to detect flaws in components. The object being inspected must be made of a ferromagnetic material. The process applies a magnetic field into the tested piece. This latter can be magnetized by direct or indirect magnetization. Direct magnetization occurs when the electric current is passed through the test object and a magnetic field is formed in the material (Figure 1.4). Indirect magnetization occurs when no electric

current is passed through the test object, but a magnetic field is applied from an outside source. If any defects on or near the surface are present, the defects will create a leakage field. After the component has been magnetized, iron particles are applied to the surface of the magnetized part. The particles will be attracted and cluster at the flux leakage fields, thus forming a visible indication that the inspector can detect [57].

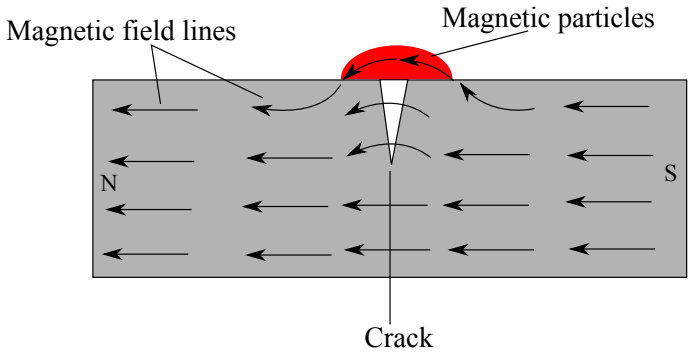

Figure 1.4: Principle of a magnetic particle inspection.

There are many methods of generating magnetic flux in the test piece, the most simple one being the application of a permanent magnet to the surface, but this method cannot be controlled accurately because of indifferent surface contact and deterioration in magnetic strength. Modern equipments generate the magnetic field electrically either directly or indirectly. In the direct method a high amperage current is passed through the subject and magnetic flux is generated at right angles to the current flow. Therefore the current flow should be in the same line as the suspected defect. If it is not possible to carry out this method because of the orientation of the defect, then the indirect method must be used. This can be one of two forms: passing a high current through a coil which encircles the subject, or making the test piece form part of a yoke which is wound with a current carrying coil. The effect is to pass magnetic flux along the part to reveal transverse and circumferential defects.

MPI have many advantages. It can detect both surface and near sub-surface defects and inspect parts with irregular shapes easily. Besides, precleaning of components is not as critical as it is for some other inspection methods. Fast method of inspection and indications are visible directly on the specimen surface. This method is characterized by a considered low cost compared to many other NDT methods. It is also a very portable inspection method especially when used with battery powered equipment. However, some limitations of this technique exit. In fact, it cannot inspect non-ferrous materials such as aluminum, magnesium or most stainless steels. Inspection of large parts may require use of equipment with special power requirements. Moreover, some parts may require removal of coating or plating to achieve desired inspection sensitivity. It has also a limited subsurface discontinuity detection capabilities. Post cleaning and post demagnetization is often necessary.

1.1.4 Eddy Current Testing (ECT)

The Eddy Current method is employed in two aspects of Non-Destructive Testing. Firstly, as a means of finding surface and subsurface flaws, and secondly as a means of determining different metallurgical characteristics in place of destructive methods.

Eddy currents are created through a process called electromagnetic induction. When alternating current is applied to the conductor, such as copper wire, a magnetic field develops in and around the conductor. This magnetic field expands as the alternating current rises to maximum and collapses as the current is reduced to zero. If another electrical conductor is brought into the close proximity to this changing magnetic field, current will be induced in this second conductor. Eddy currents are induced electrical currents that flow in a circular path. Variations in the electrical conductivity or magnetic permeability of the test object, or the presence of any flaws, will cause a change in eddy current and a corresponding change in the phase and amplitude of the measured current (see figure 1.5. However, ECT can detect very small cracks in or near the surface of the material, the surfaces need minimal preparation, and physically complex geometries can be investigated. It is also useful for making electrical conductivity and coating thickness measurements [58].

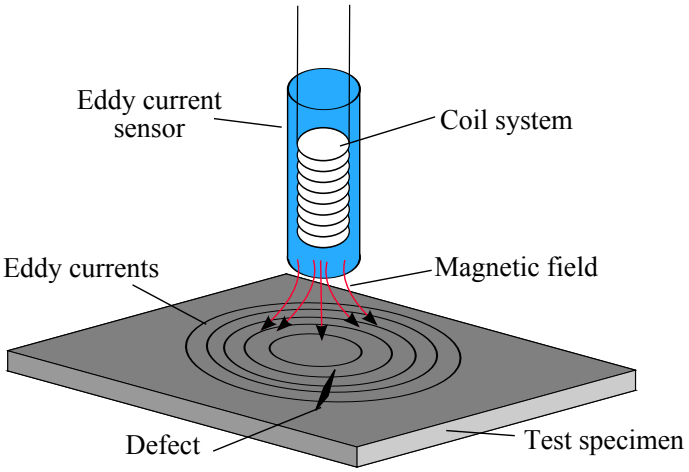

Figure 1.5: Principle of eddy current testing.

Normally equipments have two separate test coils, each of which houses a primary and a secondary winding. In one coil the known standard is placed, the unknown subject being placed in the second coil. The differences are displayed on the instrumentation. It is not strictly necessary that the coils encircle the subject. Recent developments use a single coil which uses impedance generated by the eddy currents. This means that probe systems have evolved which can be scanned over the surface of the part to be tested.

The depth of penetration of eddy currents depends on the material. At a given composition the lower the frequency of the A.C. current fed to the primary the deeper the penetration. However, the lower the frequency the less sensitive the method is to small changes.

Being a purely electrical method eddy current testing is easily automated, since the encircling coil or probe need not come into contact with the test piece. The

mechanical handling makes it a requirement that the pieces are of a simple geometric shape.

By summarizing the benefits of ECT, we can say that it is suitable for the determination of a wide range of conditions of conducting material, such as defect detection, composition, hardness, conductivity, etc... in a wide variety of engineering metals. Moreover, information can be provided in simple terms: often go/no go. Phase display electronic units can be used to obtain much greater product information. The equipment is extremely compact and portable units are available. Furthermore, this technique offers a flexibility in selection of probes and test frequencies to suit different applications, and it is also suitable for total automation. However, the technique presents some disadvantages. The wide range of parameters which affect the eddy current responses means that the signal from a desired material characteristic, e.g. a crack, can be masked by an unwanted parameter, e.g. hardness change. Careful selection of probe and electronics will be needed in some applications. Also, tests are generally restricted to surface breaking conditions and slightly subsurface flaws.

1.1.5 Guided Wave Testing (GWT)

Guide wave testing is one of latest techniques in the NDT field, which is under continuous development. The method uses mechanical stress waves that propagate along an elongated structure while guided by its boundaries. The propagating waves can travel a long distance and reflect from defects and features encountered in the structure. Nowadays, GWT is widely used to inspect and screen many engineering structures, particularly for the inspection of metallic pipelines around the world. In some cases, hundreds of meters can be inspected from a single location. There are also some applications for inspecting rail tracks, rods and metal plate structures. GWT is different to conventional ultrasonic testing. Unlike conventional testing, GWT can inspect a large area of the tested component since waves are guided by the structure as seen in figure 1.6. It uses very low ultrasonic frequencies compared to those used in conventional UT, typically between 10 to 100 kHz. Higher frequencies can be used in some cases, but detection range is significantly reduced. The next section will give more details about guided waves and focuses on their principles and mode propagation.

1.2 Guided waves

Ultrasonic guided waves technique have been developed for the rapid survey of structures for the detection of damages. The primary advantage is that long lengths may be examined from a single test point. The second one is that it reduces the costs of gaining access to the pipes for testing as well as avoidance of removal and reinstallation of insulation (where present), except for the area on which the transducers are mounted. Another advantage is the ability to test inaccessible areas, such as sleeved or buried pipes and areas under clamps. Finally, it allows the test of the entirely of the pipe wall.

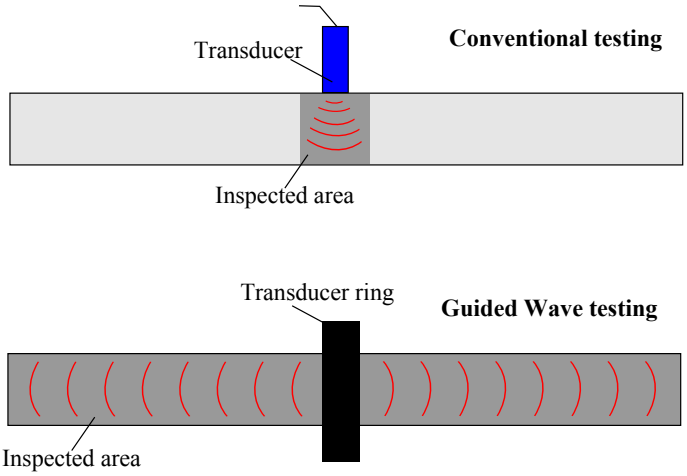

Figure 1.6: Principle of GWT vs. conventional testing.

Guided waves can travel either at the boundaries (surface waves) or between boundaries (Lamb waves), and they are the result of the interaction occurring at the interface between two different materials. This interaction produces reflection, refraction and mode conversion between longitudinal and shear waves which can be predicted using appropriate boundary conditions. The guided-waves propagation is dependent on the material properties and the material boundaries. The solution of guided waves is in general complex because they are characterized by an infinite number of modes associated with a given partial differential equation solution. Thus, guided waves are highly dependent on wavelength and frequency, and propagating guided waves can only exist at specific combinations of frequency, wavenumber and attenuation.

Before going to inspect a structure, it is with great interest that we understand thoroughly how guided waves operate and by which rules they are dominated. This section introduces the mathematical foundation of guided waves and focuses on the main concepts of the technique.

1.2.1 Wave propagation in an isotropic unbounded media

This subsection summaries the derivation of the Lamb wave dispersion equations, starting from the wave equations, which must be satisfied by all waves in elastic isotropic media.

Wave propagation in elastic infinite media was reported by many authors and can be found in a lot of textbooks [59–62]. For a linearly elastic solid with neglected body forces and constant density ρ, the Euler's equation of motion can be derived from the Newton's second law and may be written as follows:

$$\rho \cdot \left(\frac{\partial^2 \mathbf{u}}{\partial t^2} \right) = \nabla \cdot \overrightarrow{\overrightarrow{\sigma}} \tag{1.1}$$

where $\mathbf{u}$ is the displacement vector, ∇ is the three dimensional Laplace operator and $\overrightarrow{\overrightarrow{\sigma}}$ is the stress tensor. Using Hooke's law, the stress tensor can be expressed in

terms of the strain tensor $\overrightarrow{\overrightarrow{\epsilon}}$ and the stiffness tensor C:

$$\overrightarrow{\overrightarrow{\sigma}} = C \cdot \overrightarrow{\overrightarrow{\epsilon}} \tag{1.2}$$

Equation 1.2 can be written differently as follows:

$$\overrightarrow{\overrightarrow{\sigma}} = \lambda \mathbf{I} \nabla \cdot \mathbf{u} + \mu(\nabla \mathbf{u} + \mathbf{u}\nabla^T) \tag{1.3}$$

where λ and μ are the *Lamé* constants of the material. Combining equations 1.1 and 1.3 yields Navier's differential equation for isotropic elastic medium:

$$\rho \left(\frac{\partial^2 \mathbf{u}}{\partial t^2} \right) = \mu \nabla^2 \mathbf{u} + (\lambda + \mu) \nabla \nabla \cdot \mathbf{u} \tag{1.4}$$

Equation 1.4 can be expanded in the three spatial components x, y, z:

$$\begin{aligned}
\rho(\frac{\partial^2 u_x}{\partial t^2}) &= \mu(\frac{\partial^2}{\partial x^2} + \frac{\partial^2}{\partial y^2} + \frac{\partial^2}{\partial z^2})u_x + (\lambda + \mu)\frac{\partial}{\partial x}(\frac{\partial u_x}{\partial x} + \frac{\partial u_y}{\partial y} + \frac{\partial u_z}{\partial z}) \\
\rho(\frac{\partial^2 u_y}{\partial t^2}) &= \mu(\frac{\partial^2}{\partial x^2} + \frac{\partial^2}{\partial y^2} + \frac{\partial^2}{\partial z^2})u_y + (\lambda + \mu)\frac{\partial}{\partial y}(\frac{\partial u_x}{\partial x} + \frac{\partial u_y}{\partial y} + \frac{\partial u_z}{\partial z}) \\
\rho(\frac{\partial^2 u_z}{\partial t^2}) &= \mu(\frac{\partial^2}{\partial x^2} + \frac{\partial^2}{\partial y^2} + \frac{\partial^2}{\partial z^2})u_z + (\lambda + \mu)\frac{\partial}{\partial z}(\frac{\partial u_x}{\partial x} + \frac{\partial u_y}{\partial y} + \frac{\partial u_z}{\partial z})
\end{aligned} \tag{1.5}$$

These equations represent the differential equations of motion. They are called *wave equations* and must be satisfied by all elastic waves propagating in the media. Any displacement field which satisfies the wave equations implicitly satisfies the equilibrium and compatibility conditions, so the only remaining constraints on the displacement field must come from external boundary conditions.

The equation of motion 1.4 can be also expressed in a more simplified form. By using a Helmholtz decomposition, the displacement field $\mathbf{u}$ can be divided into a rotational component $\nabla \times \mathbf{H}$ and an irrotational component $\nabla\phi$, where ϕ is a compressional scalar potential and $\mathbf{H}$ is an equivoluminal vector potential:

$$\mathbf{u} = \nabla\phi + \nabla \times \mathbf{H}, \tag{1.6}$$

with

$$\nabla \cdot \mathbf{H} = \mathbf{0}. \tag{1.7}$$

The expression 1.6 can be substituted into Navier's equation of motion. Thus, we obtain the following equation:

$$\nabla[(\lambda + 2\mu)\nabla^2\phi - \rho(\frac{\partial^2 \phi}{\partial t^2})] + \nabla \times [\mu\nabla^2\mathbf{H} - \rho(\frac{\partial^2 \mathbf{H}}{\partial t^2})] = 0. \tag{1.8}$$

Equation 1.8 leads to the following couple of equations for the two unknown potentials:

$$\frac{\partial^2 \phi}{\partial t^2} = c_l^2 \nabla^2 \phi, \quad \frac{\partial^2 \mathbf{H}}{\partial t^2} = c_s^2 \nabla^2 \mathbf{H} \tag{1.9}$$

where c_l and c_s represent the phase velocities of longitudinal and shear waves respectively,and have the following expressions:

$$c_l = \sqrt{\frac{\lambda + 2\mu}{\rho}}, \quad c_s = \sqrt{\frac{\mu}{\rho}}. \tag{1.10}$$

Equations 1.9 are called the Helmholtz differential equations. The first one governs longitudinal waves and the second one governs shear waves. So, there are only two types of waves which can propagate in an unbounded isotropic medium. Equations 1.9 are independent, so longitudinal and shear waves can propagate without interaction in an unbounded media. The general solution of the Helmholtz differential equations that fully describes the propagation of the two waves is

$$\begin{cases} \phi = \phi_0 e^{i(\mathbf{k_l} z - \omega t)} \\ \mathbf{H} = \mathbf{H}_0 e^{i(\mathbf{k_s} z - \omega t)} \end{cases} \tag{1.11}$$

where ϕ_0 and $\mathbf{H}_0$ are arbitrary initial constants, $\mathbf{k_l}$ and $\mathbf{k_s}$ are the longitudinal and shear wavevectors, and z is the propagation direction.

1.2.2 Guided waves in pipes

In guided wave testing of pipelines, an array of low frequency transducers is attached around the circumference of the pipe to generate an axially symmetric wave that propagate along the pipe in both the forward and backward directions of the transducer array. A one directional wave can be generated by adding additional transducer arrays. The equipment operates in a pulse-echo configuration where the array of transducers is used for both the excitation and detection of the signals. At location where there is a change of cross-section or a change in local stiffness of the pipe, an echo is generated. Based on the arrival time of the echoes, and the predicted speed of the wave mode at a particular frequency, the distance of a feature in relation to the position of the transducer array can be accurately calculated.

The propagation of guided waves in pipes, also called hollow cylinders, has been reported in several investigations [63–66] and the solution can be found in a variety of textbooks [61, 67]. The problem of harmonic waves in an infinite-long hollow cylinder was analytically founded in three-dimensional cylindrical coordinates by Gazis in 1959 [63,64]. Confirmation of the analytical predictions given by Gazis was presented by Fitch [68] who carried out experiments using both axially symmetric and non-symmetric modes in hollow cylinders.

Considering a guided wave propagation in an infinitely long hollow cylinder, as shown in figure 1.7. The boundary conditions for the pipe geometry, for free motion are

$$\sigma_{rr} = \sigma_{rz} = \sigma_{r\theta} = 0 \quad \text{at } r = a \text{ and } r = b. \tag{1.12}$$

The displacement components would therefore be

$$\begin{aligned} u_r &= U_r(r)\cos(n\theta)\cos(\omega t + kz), \\ u_\theta &= U_\theta(r)\sin(n\theta)\cos(\omega t + kz), \\ u_z &= U_z(r)\cos(n\theta)\sin(\omega t + kz), \end{aligned} \tag{1.13}$$

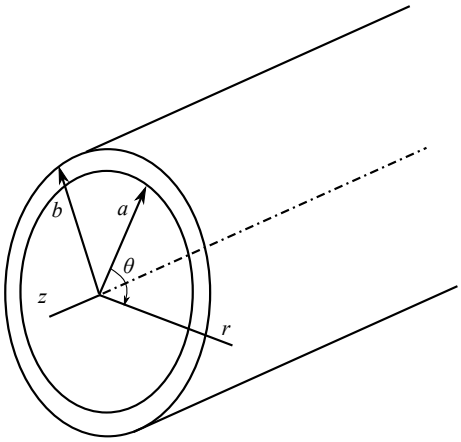

Figure 1.7: Hollow cylinder with cylindrical coordinates.

where n is the circumferential order; k is the wavenumber; the terms u_r, u_θ, u_z are the displacement components in the radial, circumferential, and axial directions respectively; U_r, U_θ, U_z are the corresponding displacement amplitudes composed of Bessel functions (or modified Bessel functions, depending on the arguments).

Guided waves can propagate in hollow cylinders according to three different mode types: longitudinal, torsional, and flexural modes. The first and second are axisymmetric modes, while the third mode is non-axisymmetric. In equations 1.13, the displacements for $n = 0$ correspond to the axisymmetric modes and the displacements for $n = 1, 2, 3 \ldots$ correspond to the flexural modes. Using the notation of Silk and Bainton [8], longitudinal modes are noted L(0,m), torsional modes are noted T(0,m), and flexural modes are noted F(n,m). The first index n is the harmonic order of circumferential variation. Thus, all modes whose first integer is zero are axially symmetric, all modes whose first integer is 1 have one cycle of variation of displacement and stresses around the circumference, and so on. The second index m is the mode number. The value 1 is associated with fundamental modes; the higher order modes are numbered consecutively.

1.2.3 Dispersion

Dispersion in guided waves is due to velocity variations with frequency. Rayleigh [69] had already noted that the velocity of a group of waves could be different from the velocity of the individual waves. He was describing the concept of phase and group velocity. The group velocity, V_{gr}, is the velocity at which a guided wave packet will travel at a given frequency while the phase velocity, V_{ph}, is the speed at which the individual peaks within that packet travel. The two velocities are defined by

$$V_{ph} = \frac{\omega}{k}, \quad V_{gr} = \frac{\partial \omega}{\partial k} \tag{1.14}$$

where ω is the circular frequency and k is the wavenumber.

Phase and group velocities are related to each other through the following equation [67]

$$V_{gr} = V_{ph} + k\frac{\partial V_{ph}}{\partial k}. \tag{1.15}$$

The physical manifestation of dispersion is that when a particular mode is excited by a signal of finite duration, the signal is distorted in time and space as it propagates away from the source. The dispersion curves for a system describe the solutions to the modal wave propagation equations and give the properties of guided waves (phase velocity, energy velocity, attenuation and mode shape). In general this information enables the prediction of the optimum test conditions and helps the understanding of the experimental results. Dispersion curves show all of the constructive interference zones that could occur as the waves reflect inside a structure, demonstrating the kinds of waves and modes that could actually propagate. A tremendous amount of information can be found on the dispersion curves that can be used to design and analyze a guided wave nondestructive testing experiment. Phase velocity spectrum leads to a zone of excitation as we try to excite a particular mode and frequency. The zone of excitation is such that we often produce several modes at once. The phase velocity and frequency spectrum principles must be considered when designing a guided wave experiment. Another tremendously important consideration in the selection of guided wave modes for a particular experiment is associated with wave structure. The in-plane displacement, out-of-plane displacement, or actual stress distribution itself varies across the thickness of the structure, often quite significantly [10, 67].

Dispersion curves can be plotted using a spectral method called Wave Finite Element (WFE). This method was previously implemented and used for the analysis of wave propagation in structures [51–54,70–72]. Figures 1.8 and 1.9 show the group and phase velocities for a 140 mm outer diameter steel pipe with a thickness of 4 mm. From these curves, several important observations can be made. First of all, it is obvious that, for a given frequency, lots of waves can propagate. Besides this, when the frequency varies not only the number but also the types of waves change (longitudinal, flexural, and torsional). In the next subsection, the main characteristics of these modes are described.

1.2.4 Mode types

Longitudinal mode

Longitudinal modes can have displacements u_r and u_z which are independent of θ. The particle motion being predominantly axial and the strain being roughly uniform through the pipe wall, which makes it equally sensitive to internal or external defects. It is therefore well suited to the detection of corrosion which may initiate at either surface of the pipe. The dispersion curves of figure 1.8 show that the L(0,2) mode in the frequency range 20-100 kHz is practically nondispersive – that is to say its group velocity is essentially constant with frequency so that there is minimal distortion of the wave packet over long propagation distances. L(0,2) is also the fastest mode, which means that it will be the first signal to arrive at the receiver and so can readily be separated by time-domain gating.

However, the L(0,1) mode will be generated and received along with L(0,2). It may be possible to remove the L(0,1) mode by adjusting the length of the transducer elements and/or by employing multiple rings of transducers. However, figure 1.8 shows that the velocity of the L(0,2) mode is approximately twice that of

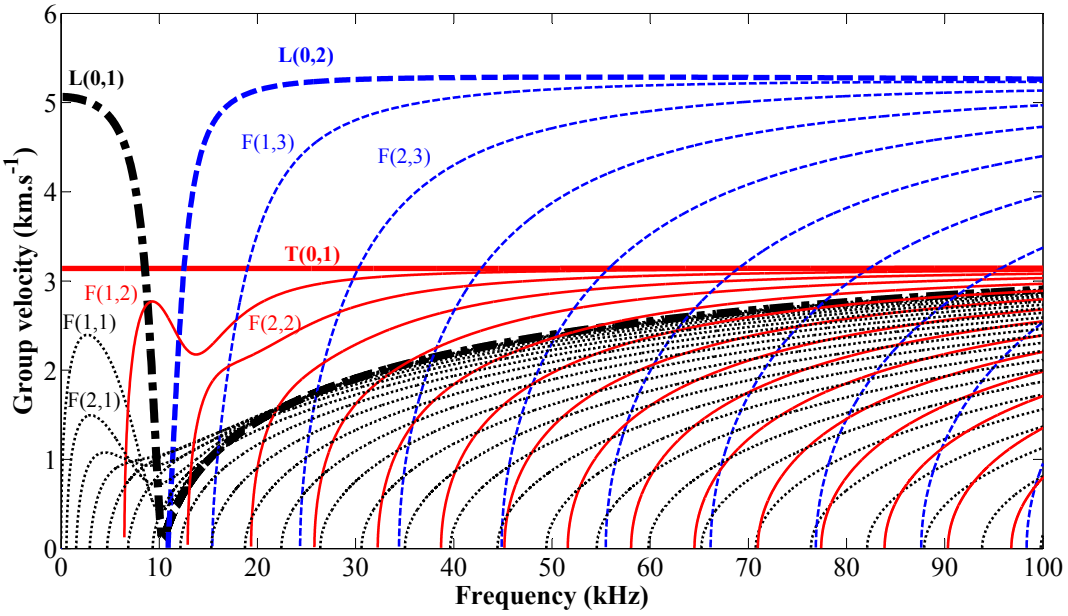

Figure 1.8: Group velocity dispersion curves for a 140 mm outer diameter steel pipe with 4 mm-thick.

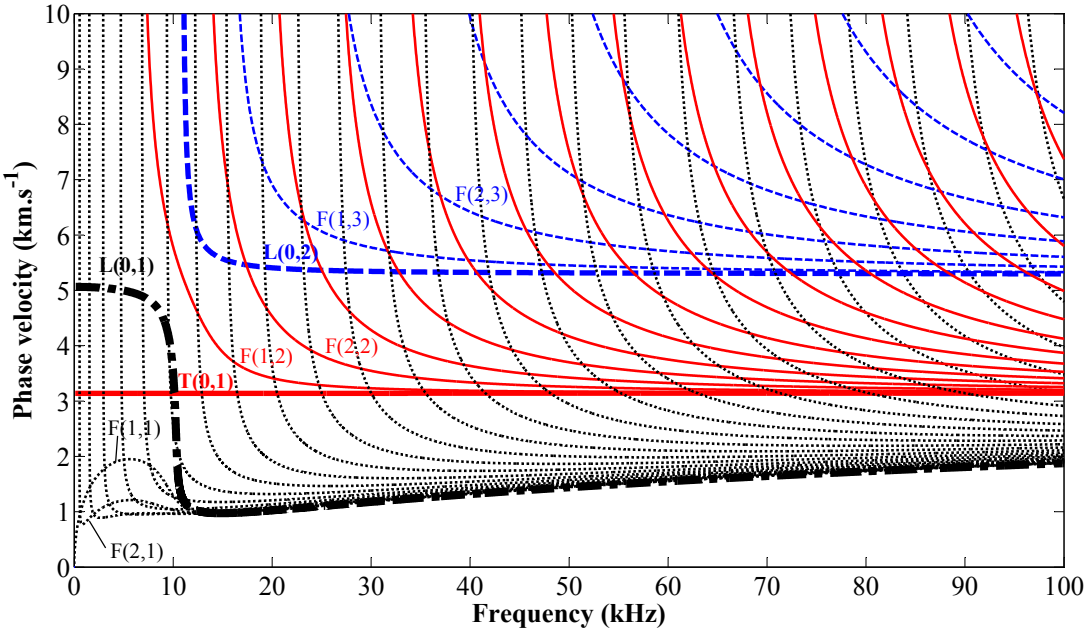

Figure 1.9: Phase velocity dispersion curves for a 140 mm outer diameter steel pipe with 4 mm-thick.

the L(0,1) mode, so in a simple pipe system with a limited number of reflectors, it is straightforward to separate the signals corresponding to the two modes in the time domain [39].

Torsional mode

Torsional pipe modes involve displacements u_θ. T(0,1) is the only true torsional mode, as it exists with purely torsional characteristics at any frequency. Higher order modes that show torsional characteristics are also flexural in nature. T(0,1) is a non-dispersive mode and the fastest among torsional waves. It has a high sensitivity to axial and circular defects, as well as to internal and external defects. By comparing L(0,2) to T(0,1) mode, the latter exists at all frequencies whereas the former is present only at frequencies above its cut-off as shown in figure 1.8. Also T(0,1) propagates in pipes filled with liquid without any interference problem whereas typically some additional reverberation is present when L(0,2) travels in a pipe fully filled with liquid. Furthermore, the transduction is much simpler when using the T(0,1) mode because there is no other axisymmetric torsional mode, whereas when the L(0,2) mode is used, the transducer system must be carefully designed to suppress unwanted excitation of the L(0,1) mode.

Flexural mode

In flexural mode propagation, all three displacement components u_r, u_θ and u_z can exist. Flexural modes are non-axisymmetric and dispersive waves as seen in figures 1.8 and 1.9. They converge to either a longitudinal or torsional mode at high frequencies where the wavelength to radius ratio is small. For example, F(n,1) modes converge to L(0,1), F(n,2) modes converge to T(0,1), F(n,3) converge to L(0,2) and so on. When non-axisymmetric guided waves are generated, the acoustic field is more complicated and the energy distribution of the wave propagation needs to be known in order to evaluate the guided wave inspection ability and to perform frequency and angle tuning.

Guided wave inspection in pipes operates typically at frequencies at which the wavelength is much larger than the pipe wall thickness. In this frequency regime, only the modes which converge to the fundamental torsional mode T(0,1), the fundamental symmetric mode L(0,2) and the fundamental antisymmetric mode L(0,1) can propagate in the pipe. Usually, only the lower circumferential order modes are used in most non-destructive testing situations, since practical measurement systems generally do not have enough resolution around the circumference to be able to clearly separate high circumferential orders.

1.2.5 Benefits and limitations of guided waves

Guided waves have a lot of advantages comparing to other techniques. Some of their major benefits are considered here. First of all, GWT allows inspection over long distances from a single probe position. This technique is also able to inspect structures under water, coatings, insulation, multi-layer structures or concrete with excellent sensitivity.

Moreover, inspection coverage is a very important parameter that affects the efficiency of an NDT method (including equipment and procedure) to identify a threat to the normal operation of a pipe. Typically UT, RT and other volumetric NDT methods have relatively high probability of detection (POD), however it is

difficult and expensive to achieve large coverage. GWT has relatively low POD (will not find small defects such as single pits) and high coverage (nearly 100%). As a result of the combined effect of POD and coverage, GWT is in several cases the most efficient method to identify a threat before failure (this will depend on the critical defect size and inspection interval). After a potential threat is identified using GWT, standard NDT methods must be used to size the defect and further evaluate the fitness for service of the pipe. The combination of NDT methods that complement each other for improved POD and ability to accurately size is therefore recommendable.

Furthermore, using multi-mode and frequency Lamb type, surface or horizontal shear waves, we have a potential to detect, locate, classify and size defects; and it is possible to establish wave resonances and excellent overall defect detection potential by mode and frequency tuning.

Therewith, the sensitivity achieved by GWT is often greater than obtained in standard normal beam ultrasonic inspection or other NDT techniques. Using Guided Waves it is possible to inspect pipes while they are in service. Liquid or gas phases may be free flowing and the measured pipe temperature must be between -40°C and 200°C [73].

Finally, the use of guided waves induces a cost effectiveness due to the inspection simplicity and speed. Generally, less than about 1/20 of the cost of standard normal beam ultrasonic and other inspection techniques. When planning an inspection, one of the items to consider is the access to the part to be inspected. In some cases several solutions may be available to carry out the inspection but due to limited access the choice is drastically reduced. Normally access can be achieved but the cost can be prohibitive and well above the cost of the inspection.

Nevertheless, although of these relevant benefits some drawbacks can exit. In fact, interpretation of recorded data is highly operator dependent and requires some experience in GWT due to the complexity of signals. Besides, it is difficult to find small pitting defects. Several parameters can affect the efficiency of GWT. One of these parameters is the pipe geometry. GWT is not very effective at inspecting areas close to accessories. The flange represents the end of test. Other features such as Ts, valves, changes in direction and welded supports strongly reduce the test range. It is more productive and effective the further the pipe features are apart from each other. Viscoelastic coatings (such as bitumen or polyethylene) can also reduce the test range. The effect is more severe when the coating is soft, thick and well adhered to the pipe wall. Wide frequency range must be used to optimize test range. Another parameter is the content of the tested structure. Gas and non-viscoelastic fluids do not affect the test range when using torsional waves, whereas viscoelastic fluids or heavy deposits reduce the test range. Ambient noise have also an influence on the efficiency of GWT. Noise may be caused by pumps or compressor at a location close to the inspection area, the fluid flow inside the pipe and repair or construction work on the pipe under inspection. In some isolated cases the GWT may not be carried out while the source of noise is active. Most commonly the noise is at a lower frequency than the range used for the pipe inspection and the GWT can be completed using standard procedures. The pipe condition is also an affecting parameter. Light general corrosion (e.g. 10-20% wall loss) may reduce the test

range. When the general corrosion on the pipe is extended over a long length and severe (e.g. 40% wall loss) GWT may not be suitable to carry out the inspection.

1.2.6 Generation of guided waves

Guided waves can be generated using piezoelectric transducers, electromagnetic acoustic transducers (EMAT) or magnetostrictive sensors (MsS). The technology used is quite different from a method to another but the result in term of generated and received guided waves is usually the same.

Piezoelectric transducers

Piezoelectric transducers are polarized ceramics and belong to the group of ferroelectric materials. Ferroelectric materials are crystals which are polar without an electric field being applied. When an electric field is applied across the material, the polarized molecules will align themselves with the electric field, resulting in induced dipoles within the molecular or crystal structure of the material. This alignment of molecules will cause the material to change dimensions. This phenomenon is known as electrostriction. In addition, a permanently-polarized material such as quartz (SiO2) or barium titanate (BaTiO3) will produce an electric field when the material changes dimensions as a result of an imposed mechanical force. This phenomenon is known as the piezoelectric effect.

The application of an electric voltage to an unrestrained piezoceramic body results in its deformation. The movement is a function of the polarity of the voltage applied and the direction of the polarization vector. Applying an AC voltage generates a cyclical change in the geometry (e.g. increase or reduction in the diameter of a disk). If the body is clamped, i.e. if free deformation is constrained, a mechanical stress or force is generated.

Piezoelectric ceramics can bend in different ways at different frequencies. This bending is called the vibration mode. The ceramic can be made into various shapes to achieve different vibration modes. For rectangular shapes, we can find either thickness and longitudinal oscillations or shear oscillation. Circular components can vibrate according to radial and thickness oscillations (disks case); or thickness, radial and longitudinal oscillations (hollow cylinders case).

The shear transducers could either be angled perpendicular to the pipe axis (i.e. in a circumferential direction) to excite a torsional mode, or parallel to the pipe axis to excite longitudinal modes. If the system is to excite a pure axisymmetric mode then the transducer spacing Δ around the pipe must satisfy the Nyquist-Shannon sampling criterion ($\Delta < \lambda/2$, where λ is the wavelength of the inspection mode) at the frequencies used for inspection [74]. The transducers are held in place and forced onto the pipe wall by either a fixed or flexible collar. The collar is designed to push each individual transducer onto the pipe with a comparable force thus allowing even coupling of the transducers' energy into the pipe wall. The transducers can be dry coupled to the pipe because of the low operating frequencies.

Alleyne et al. [9] suggested a transducer array of dry coupled piezoelectric shear transducers clamped around the outer pipe wall to excite the axisymmetric guided wave modes. Recently, permanently installed transducer rings have been developed

for long term integrity monitoring of pipelines by *Guided Ultrasonics Ltd.* [75]. Comb transducers and angle beam wedges have also been investigated for transduction of specific guided wave modes [22, 30, 76, 77]. A phased piezoelectric transducer array for the excitation of certain modes was implemented by Li et al. [78], and was used on a viscoelastic coated hollow cylinder [32, 33].

The torsional commercial system that employs piezoelectric transducer arrays as described above, includes two rings of transducers arranged around the pipe [20]. In order to achieve a directional control, the two rings are separated by a quarter of the wavelength and a phase shift of $\pi/2$ is applied to the excitation of the two rings, so that the energy is summed in one direction and cancels in the other [17, 79]. By this way, the guided wave mode can be excited in only one axial direction. The same principle may also be used in reception in order to detect waves traveling in one direction while suppressing the detection of waves traveling in the other direction.

ElectroMagnetic Acoustic Transducer (EMAT)

EMATs transmit and receive acoustic waves (including Lamb waves) in electrically conductive materials using the Lorentz principle. A magnetic field is produced in the material beneath the EMAT using either permanent magnets or DC electromagnets which are built into it. Also contained within the EMAT is a conducting wire, usually in the form of a meander or pancake coil. When the EMAT is transmitting, an alternating current is passed through the wire, eddy currents are induced in the material beneath the EMAT. These currents interact with the magnetic field to generate forces within the material which in turn generate acoustic waves. The orientation of the magnetic field and the position of the conducting wires can be configured in different ways in order to produce different types of acoustic waves.

EMATs have many advantages. In fact, they do not need to be in physical contact with the surface of the plate and do not need to be used with a coupling fluid, which makes them ideal for measurement of high temperature plate inspection. Moreover, this technique is less sensitive to surface condition and easier for sensor deployment. The major disadvantage of EMATs is their lower sensitivity than piezoelectric devices, which is mainly due to limitations on the strength of magnetic field which can be achieved in a practical device. The efficiency of EMATs is also affected by variations in the magnetic properties of materials on which they are used which can be significant.

EMATs have been used in a broad range of applications like thickness measurement, flaw detection in plates and pipes, weld and rail inspection, material characterization... Thompson et al. [7, 12] suggested an EMAT device to inspect from the inside of the tubes. Wilcox et al [80] have developed an EMAT array using the S0 mode at frequencies around 170 kHz for the inspection of plates between 5 and 25 mm thick.

Magnetostrictive Sensors (MsS)

The MsS generates and detects guided waves electromagnetically in the material under testing. For wave generation, it relies on the magnetostrictive (Joule) effect that refers to a small change in the physical dimensions of ferromagnetic materials

(on the order of several parts per million in carbon steel) caused by an externally applied magnetic field. For wave detection, it relies on the inverse-magnetostrictive (Villari) effect that refers to a change in the magnetic induction of ferromagnetic material caused by mechanical stress (or strain). Since the probe relies on the magnetostrictive effects, it is called a magnetostrictive sensor.

In the standard application, the sensor consists of a thin ferromagnetic material (such as nickel or an iron cobalt alloy) that is bonded to the pipe. A thin excitation coil is placed over the thin ferromagnetic material. The thin ferromagnetic material has a biasing magnetic field and the excitation coil is configured to apply a time-varying magnetic field to the ferromagnetic material. This generates a wave in the thin ferromagnetic material that is then coupled (usually by an epoxy bond) into the material being inspected. The same sensor is used to pick up magnetic induction changes in the material caused by the guided wave reflected by a discontinuity.

A single magnetostrictive sensor generates and detects the guided waves propagating in both directions. In practical inspection applications, the guided wave generation and detection are controlled to work primarily in one direction so that the areas of the structure on either side of the sensor can be inspected separately.

This technology can be used in plates, tubes and rods with slight differences in the probes. In the long-range guided wave inspection, a short pulse of guided waves in relatively low frequencies (up to a few hundred kHz) is launched along the structure under inspection. Signals reflected from geometric irregularities in the structure such as welds and discontinuities are detected in the pulse-echo mode. MsS have been suggested for excitation and reception of guided waves in pipes in several works [81, 82].

1.3 Conclusion

Nondestructive testing techniques have been introduced at first in this part. They are widely used in science and industry in several applications from evaluating the properties of a material, to detecting potential damages in components or systems without causing damage. NDT techniques cover a large variety of methods each based on a particular scientific principle. The choice of the specific method depends on many factors like availability, accessibility, and suitability. It may sometimes be necessary to use one method of NDT to confirm the findings of another. Radiography testing, ultrasonic testing, magnetic particle inspection and eddy current testing was described. All of them are conventional methods that inspect a limited zone of the tested structure.

Guided waves technique is one of nondestructive testing methods. Its specificity is that it can inspect long lengths of the structure from a single test position, as the waves are able to be guided by the structure. Guided waves are governed by the wave equations, which must be satisfied by all waves in elastic isotropic media. The displacement could therefore be computed depending on the geometry of the waveguide. Guided waves can propagate in pipes according to three different mode types: longitudinal, torsional, and flexural modes. The first and second are axisymmetric modes, while the third mode is non-axisymmetric. The dispersion curves for a system describe the solutions to the modal wave propagation equations and give

the properties of guided waves like phase velocity, energy velocity, attenuation and mode shape. Dispersion curves can be computed using the Wave Finite Element (WFE) method. This latter has been used in this work as numerical approach to validate some experimental results.

Guided waves can be generated using three different technologies: piezoelectric transducers, electromagnetic acoustic transducers (EMAT) or magnetostrictive sensors (MsS). In our investigation, piezoelectric transducers has been used in the designed inspection system to generate the desired waves.

Chapter 2

Distributed piezoelectric guided-T-wave generator, design and analysis

Mechatronics 22 (2012) 544–551

Contents lists available at SciVerse ScienceDirect

Mechatronics

journal homepage: www.elsevier.com/locate/mechatronics

Distributed piezoelectric guided-T-wave generator, design and analysis

O. Bareille *, M. Kharrat, W. Zhou, M.N. Ichchou

Laboratoire de Tribologie et Dynamique des Systèmes, École Centrale de Lyon, Université de Lyon, 36 Avenue Guy de Collongues, 69130 Ecully, France

ARTICLE INFO

Article history:
Available online 10 December 2011

Keywords:
Wave-guide
SHM – structural health monitoring
Pipe inspection
WFEM – wave finite element method

ABSTRACT

In this work, the definition and design of a specific wave generator concept is presented. The generator aims at providing well referenced *T* waves for structural health monitoring applications. A distributed network of piezoelectric patches network is considered. Shear effects is the most pertinent effect. An array of 16 piezoelectric stacks is found to be relevant. The numerical simulation confirms the finding. An experimental test bench is also provided in order to validate the concept. The ability of the distributed system in generating pure *T* waves is discussed. The concept is also employed in order to assess the distributed system overall performances. Numerical and experimental results confirm some specific features in the wave reflection coefficient based on the interaction between the damaged waveguide dynamics and torsional waves propagation.

1. Pipeline inspection using guided waves

The maintenance of pipeline networks represents an important technical and economical challenge. Oil or water transport and supply industries need to carry efficient and planned maintenance operations. Therefore they need to forecast any failure occurence by ensuring a reliable monitoring of the structure. The inspection process of such structures are the subject of current intensive researches. The classical Non-Destructive Technique (NDT) used so far could scan the state of the structure over a limited area. Recent advances in Structural Health Monitoring (SHM) make use of guided waves [1,2]. The inspection over larger distances from a limited and distant points of observation is now permitted. Yet, numerical based developments as well as experimental validations are still needed to analyse and to understand all the phenomena at stake [3].

Propagation of waves in waveguides has been studied for a long time as far as the question of propagation through periodic structures was addressed [4,5]. Experimental investigation have been intensively made on waveguide-like structures [1,6]. Such structures like pipeline were studied in order to design more efficient tools than conventional local Non-Destructive Testing (NDT) techniques to monitor large networks.

Some recent works use specific post-treatment like wavelet filtering in order to identify and to localize the defect's signature in time records [9]. However, some wave modes suffer a continuous wave distorsion. As a consequence, many of the available signal-processing tools, applied to these specific modes are rendered unaccurate. The choice of the generated wave is then the first important question to address.

Among the most recent results, the use of specific waves has emerged. For example, the well referenced torsional waves (*T*-waves) seem to be promising [7,8]. Once established, a specific wave generator has to be designed as well as the proper analysing process has to be defined. Based on these researches, the use of Wave Finite Element Methods (WFEM) are here first presented in order to justify the use and the design of a torsional-wave generator. Section 2 of this paper is devoted to the analysis of these guided waves' features.

The need for defining and designing a specific wave generator soon arises. Some mature systems, yet still a few, let us hope to, not only localize defects but also to identify their nature [2,3]. In Section 2, the design of a prototype actuator is presented. The ability, on an experimental mock-up, to detect a (small) alteration of a pipe with torsional wave is finally illustrated.

2. Wave-mode selection

Choosing the right wave to generate is crucial regarding the range of frequency that should be used. Regarding the traditional techniques in NDT, the idea was first to use high pitched signals in order to achieve precision in the location, the size and the shape of the defect. However, when the monitored facilities are large and the access points to the structure limited (buried structures, close inspection prohibited on operating facilities), the distance between sensors and areas to survey can limit or even prevent the efficient use of high frequency signals [10,11]. Yet, if lower frequency signals are used, the inspection distance is increased but the localiza-

* Corresponding author.
E-mail address: olivier.bareille@ec-lyon.fr (O. Bareille).

0957-4158/$ - see front matter © 2011 Elsevier Ltd. All rights reserved.
doi:10.1016/j.mechatronics.2011.11.005

tion precision is reduced along with the fact that the wave-mode initially chosen can present some distorsion.

An additional goal to the primary researches is now to identify the damage's level of severity. New advanced techniques try to improve the ability to characterize existing or developing defects during pipeline inspection. For example, Wang et al. [3] used longitudinal $L(0,2)$ waves, with frequency ranging from 100 to 240 kHz. Longitudinal modes are easy to excite and non-dispersive as long as the frequency is high enough. This point will be addressed in paragraph Section 2.2. In addition, the wave-amplitude damping along the pipe is inherent to the vibrations' propagation. This effect increases with the input signal's generating frequency at which the input signal is generated (see Section 4). The choice of torsional waves (T-waves) is motivated by their wide frequency range applicability [2]. Based on the analysis of calculated dispersion curves, this last property is detailed after the next section, where the method to obtain these dispersion curves is firstly described.

2.1. Dynamics of periodic waveguides

This study addresses the description of the dynamical behavior of a slender structure which is composed, along a specific direction (say x-axis), of N identical substructures. Note that this general description can be applied to homogeneous systems whose cross-sections are constant. The dynamic of the global system is formulated in terms of waves propagating along the x-axis.

Let us consider a finite element model of a given substructure r ($r \in \{1,\ldots,N\}$) belonging to the waveguide. The left and right boundaries of the discretized substructure are assumed to contain n degrees of freedom. Displacements $\mathbf{q}$ and forces $\mathbf{F}$ which are applied on these two boundaries are denoted by ($\mathbf{q}_{\mathrm{L}}$, $\mathbf{q}_{\mathrm{R}}$) and ($\mathbf{F}_{\mathrm{L}}$, $\mathbf{F}_{\mathrm{R}}$), respectively. It is assumed that the kinematic quantities are represented through state vectors $\mathbf{u}_{\mathrm{L}}^{(r)} = \left(\left(\mathbf{q}_{\mathrm{L}}^{(r)}\right)^{\mathrm{T}}\left(-\mathbf{F}_{\mathrm{L}}^{(r)}\right)^{\mathrm{T}}\right)^{\mathrm{T}}$ and $\mathbf{u}_{\mathrm{R}}^{(r)} = \left(\left(\mathbf{q}_{\mathrm{R}}^{(r)}\right)^{\mathrm{T}}\left(\mathbf{F}_{\mathrm{R}}^{(r)}\right)^{\mathrm{T}}\right)^{\mathrm{T}}$, and that the internal dof's of substructure r are not submitted to external forces. In this way, it can be shown that state vectors $\mathbf{u}_{\mathrm{L}}^{(r)}$ and $\mathbf{u}_{\mathrm{R}}^{(r)}$ are related in this way:

$$\mathbf{u}_{\mathrm{R}}^{(r)} = \mathbf{S}\mathbf{u}_{\mathrm{L}}^{(r)}. \tag{1}$$

$\mathbf{S}$ is a symplectic matrix [5]. The analysis of the dynamical behavior of the waveguide is based on Bloch's theorem [4], which states that solutions $\mathbf{u}_{\mathrm{L}}$ can be written in the following form (μ being the wave propagation constant).

$$\mathbf{u}_{\mathrm{L}}^{(r)} = \mu\mathbf{u}_{\mathrm{L}}^{(r-1)} \quad \forall r \in \{2,\ldots,N\}. \tag{2}$$

and that they derive from the following boundary value problem:

$$\mathbf{S}\Phi_i = \mu_i\Phi_i, \quad |\mathbf{S} - \mu_i\mathbf{I}_{2n}| = 0. \tag{3}$$

Solutions $\{(\mu_i, \Phi_i)\}_{i=1,\ldots,2n}$ of Eq. (3) refer to the wave modes of the heterogeneous waveguide. Matrix Φ of the eigenvectors can be described in this way:

$$\Phi = \begin{bmatrix} \Phi_{\mathbf{q}}^{\mathrm{inc}} & \Phi_{\mathbf{q}}^{\mathrm{ref}} \\ \Phi_{\mathbf{F}}^{\mathrm{inc}} & \Phi_{\mathbf{F}}^{\mathrm{ref}} \end{bmatrix}, \tag{4}$$

$\left(\left(\Phi_{\mathbf{q}}^{\mathrm{inc}}\right)^{\mathrm{T}}\left(\Phi_{\mathbf{F}}^{\mathrm{inc}}\right)^{\mathrm{T}}\right)^{\mathrm{T}}$ and $\left(\left(\Phi_{\mathbf{q}}^{\mathrm{ref}}\right)^{\mathrm{T}}\left(\Phi_{\mathbf{F}}^{\mathrm{ref}}\right)^{\mathrm{T}}\right)^{\mathrm{T}}$ stand for the modes which are incident to and reflected by a specific boundary (left or right) of the heterogeneous waveguide, respectively [5,12]. $\Phi_{\mathbf{q}}^{\mathrm{inc}}$, $\Phi_{\mathbf{F}}^{\mathrm{inc}}$, $\Phi_{\mathbf{q}}^{\mathrm{ref}}$ and $\Phi_{\mathbf{F}}^{\mathrm{ref}}$ are $n \times n$ matrices. The orthogonality properties of eigenvectors $\{\Phi_i\}_i$ [5] allow one to propose a simple criterion to classify the wave modes. Indeed, if $\Phi_i(\omega)$ stands for the ith mode at frequency ω, then the ith mode $\Phi_i(\omega + \Delta_\omega)$ at frequency $\omega + \Delta_\omega$ (Δ_ω represents the frequency step) must be chosen in order to achieve a maximum with the following quantity:

$$A_i(\omega) = (\Phi_l(\omega))^{\mathrm{T}}\mathbf{J}_n\Phi_i(\omega + \Delta_\omega), \quad \mu_l(\omega) = 1/\mu_i(\omega) \tag{5}$$

In fact, the validity of this criterion is based on the assumption that frequency step Δ_ω remains small enough such that eigenvector Φ_i variation is very little between ω and $\omega + \Delta_\omega$.

This technique is illustrated thereafter in Section 2.2 by results obtained for a pipe. Indeed, these eigenvectors and these eigenvalues let us obtain the propagative mode shapes and their corresponding wavenumbers. The method was previously implemented on similar structures and details about the methodology can be found in Refs. [13,14].

2.2. WFEM dispersion curves

The technique described in the previous part is here used in order to obtain the wave modes as well as the dispersion curves for a pipe. The structure is initially modeled using solid finite elements. The stiffness and mass matrices are then extracted from the finite element software (here Ansys). They are then used as basic materials for the wave mode identification process implemented in a classical C-based routine. The principle of this identification is shortly describe in Section 2.1 as details and some extended exemples about this wave-finite element method (WFEM) are available in [13,14].

Dispersion curves are numerically obtained for the steel pipe as seen in Figs. 1 and 2. The outer diameter is 140 mm and the thickness of the pipe's wall is 4 mm. From this curve, several important observations can be made. First of all, it is obvious that, for a given frequency, lots of waves can propagate. Besides this, when the frequency varies, not only the number but also the types of waves change (longitudinal, flexural, torsional). Among these waves, the torsional one $T(0,1)$ is the only one whose velocity remains constant with frequency. All the others suffer speed variations as the frequency changes. This is a major disadvantage for wave generators that could only generate longitudinal or flexural waves. Since the pulse's frequency adjustment is needed in order to ensure smaller singularities' detection. Reliability in all the other aspects of wave generation should be granted. This way, whatever type of wave or wave shape that could be detected would be due to the sole presence of singularities along the pipe. That is why, the

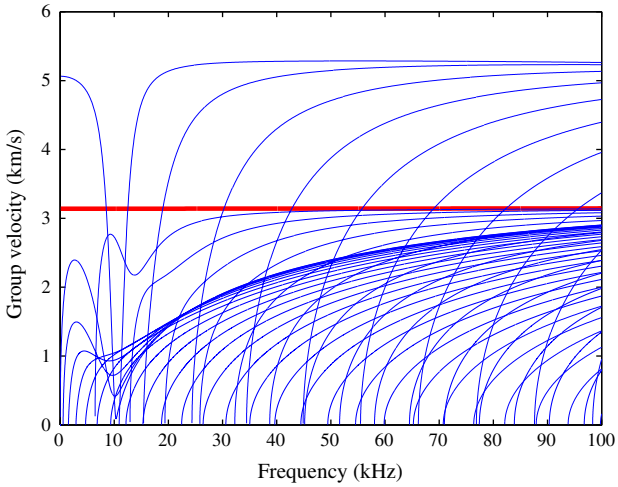

Fig. 1. Group velocities – dispersion curves for a steel pipe diameter 140 mm, thickness 4 mm – bold red line: torsional wave $T(0,1)$. (For interpretation of the references to colour in this figure legend, the reader is referred to the web version of this article.)

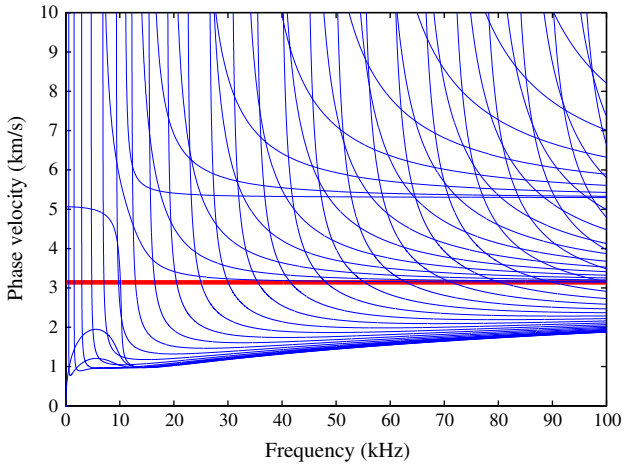

Fig. 2. Phase velocities – dispersion curves for a steel pipe diameter 140 mm, thickness 4 mm – bold red line: torsional wave $T(0,1)$. (For interpretation of the references to colour in this figure legend, the reader is referred to the web version of this article.)

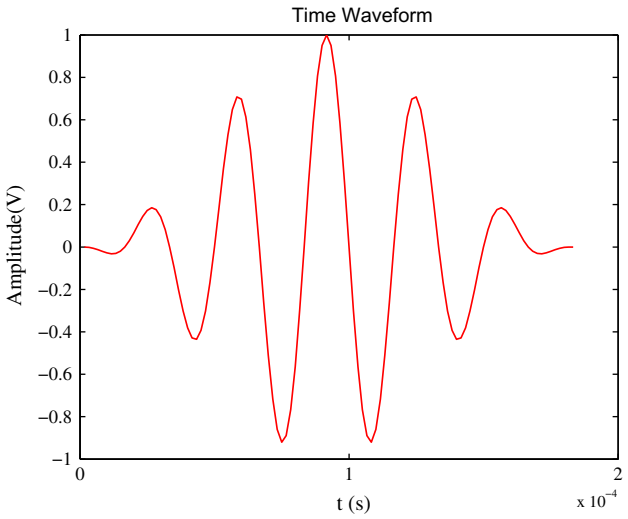

Fig. 3. Time impulse wave-form: 5.5 cycles at 30 kHz.

design of the actuator has to garantee that only torsional waves are generated. Then, the first experiments had to assess the generation of only torsional waves.

3. The actuator's design

The aim of the actuator is to generate torsional waves in a hollow cylinder. The idea is to apply a local torsional movement along the outerbound of the pipe's section. The time history of the displacement should be consistent with a pulse. The choice was made to use piezo patches that would convert the electric signal into shear strain (high d15 value). However, for a practical and economical concern, the continuity of the piezo round around the pipe could not be considered. Despite the fact that a piezo continuous ring could have been prefered, the idea was to generate a torsional torque via a ring of distributed rectangular piezo patches. Yet, the number of these piezo patches had to be estimated in order to ensure the generation of the desired waves.

Two ways of verifying that the pipe was submitted to the right wave impulse have been used: the analysis of the stress and strain patterns in sections along the pipe and the analysis of records for the time signal's shape at given points. Thanks to the first one, the homogeneity of the displacement in the pipe's section could be verified; whereas with the second way, the wave's running time to the measurement point was made consistent with the wave-speed of the torsional mode.

For that purpose, the finite element numerical model of a pipe was developed. The pipe's characteristics were the ones of the structure used in Section 2 for the WFEM wave speeds' calculation and in Section 4 for testings, namely a 3 m-long, 4 mm-thick steel pipe with a 140-mm outer diameter. The pipe's finite element model was exactly the same from which we previously obtained the mass and stiffness matrices to calculate the dispersion curves. A single layer of solid elements was used in the radial direction. The number of elements in the axial direction was choosen in order to have at least 6 elements per wavelength. In order to represent the piezo patches, solid-element rectangular shapes were attached at one end of the structure and evenly distributed around the exterior of the pipe. At the top of Fig. 5, three tested distributions are drawn. The actual dimensions of the piezo elements were used. Therefore there is a limit in the number of elements that can be attached around the pipe. Despite their overall rectangular shape, piezo elements were supposed to be fully in contact with the pipe on their bottom face.

The pulse time-signal input is shown in Fig. 3. This is a 5.5-cycle signal for frequencies ranging a few thousands Hz up to a few tenth of kHz. The magnitude and the number of cycles correspond to the total energy sent into the piezo array (and therefore used to shake the pipe). The magnitude, but also the frequency are the main characteristics of the wave input signal. Even if the torsional wave-speed is not frequency-dependent, the sensitivity of the propagative wave to the defects is closely correlated to its relative wavelength size vs. the defect's one. In addition, the magnitude and the frequency have both an influence on the ability of the waves to travel long distances before the structural damping makes them unperceivable. However these two parameters have practical limits due to the electronics of the voltage amplifier and of the measurement front-end.

3.1. Pipe's deformed shapes under distributed shear-stress input

Based on the finite element calculation for an electrical pulse time signal applied to the piezo patches, the stress and the strain patterns in sections spread along the pipe were used to re-construct the section displacement pattern (see Fig. 4). The same result was also used to calculate the section's generalized forces. Given that the simulated pipe had neither notches nor any other singularities but its ends, the waves' shapes could only be the result of the piezo patches' action.

Fig. 5 shows the results at 10, 15 and 30 kHz for three different configurations of piezo patches (sets of 4, 8 and 16 piezo patches around the pipe). The deformed shape of the pipe at a given time of the time simulation are compared. As one can expect the smaller and the more numerous the piezo patches were, the closer were the displacement and the force to the response of a pure torque excitation. In all other cases, some flexural waves were also excited. Regarding their dispersive properties with respect to frequency and the fact that they could interfer with the analysis of torsional wave reflexions and convertion on singularities, the number of piezo patches had to be as high as possible.

Yet, the piezo material's size and setting had to be taken into account. As a consequence, in order to ensure a good order of magnitude of shear stress, the thickness of the piezo patches should be large enough. However, as shown in Fig. 6, the shear strain in the piezo material can induce a local flexural motion on the pipe. The piezo mounting, connection and insulation emphasize this ef-

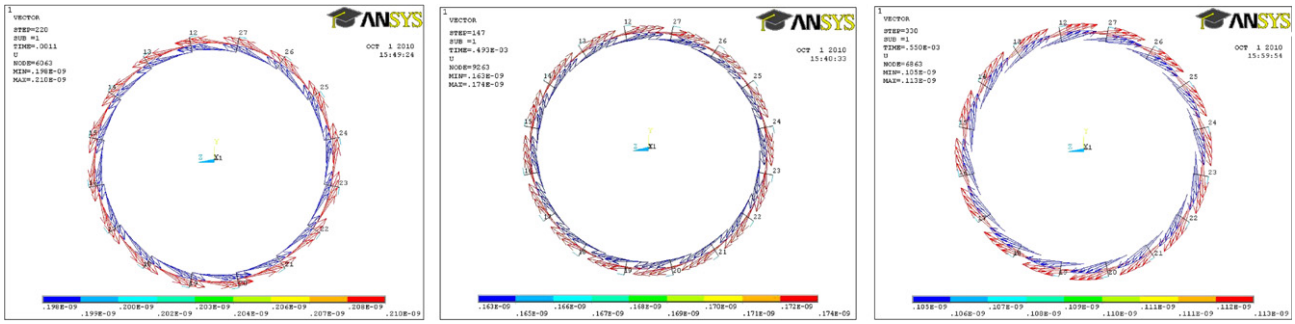

Fig. 4. Displacement vectors in the middle section of the pipe for 16 piezo patches at one end of the pipe: (a) 10 kHz, (b) 15 kHz and (c) 30 kHz.

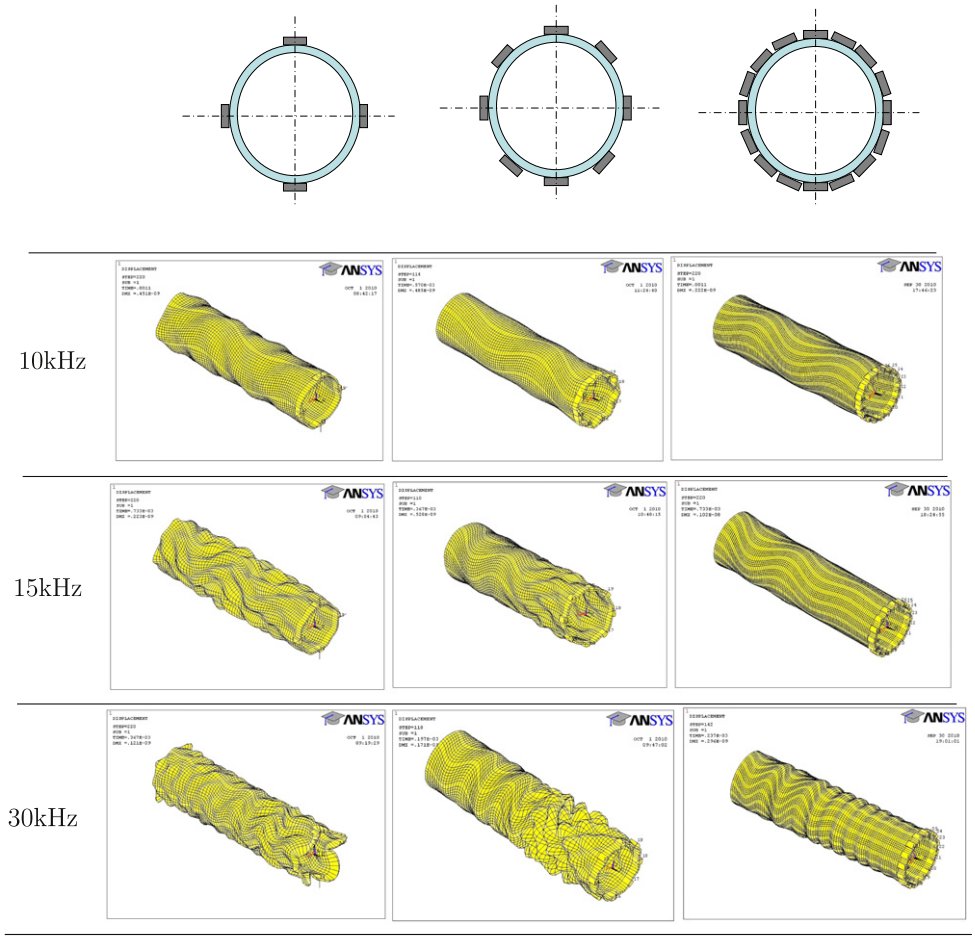

Fig. 5. Deformed shapes for different numbers of piezo patches, at different frequencies.

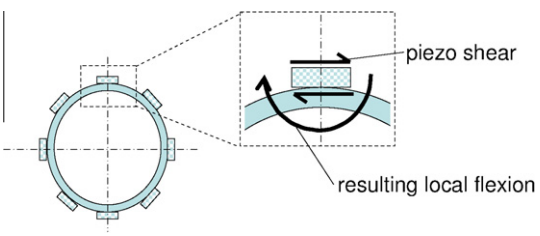

Fig. 6. Local flexural motion induced by piezo patches.

fect. The resulting practical solution will be a tradeoff between all these needs and drawbacks.

3.2. Simulation of measured time-signals along the pipe

For several points along the pipe, the time signal was observed and the time delay between the emission and the detection was divided by the wavespeed for the corresponding torsional wave in a steel pipe.

Results are shown in Fig. 7. Recorded time-signals are simulated for a 5.5-cycle 15 kHz impulse. They correspond to the orthoradial displacement in the middle of the pipe.

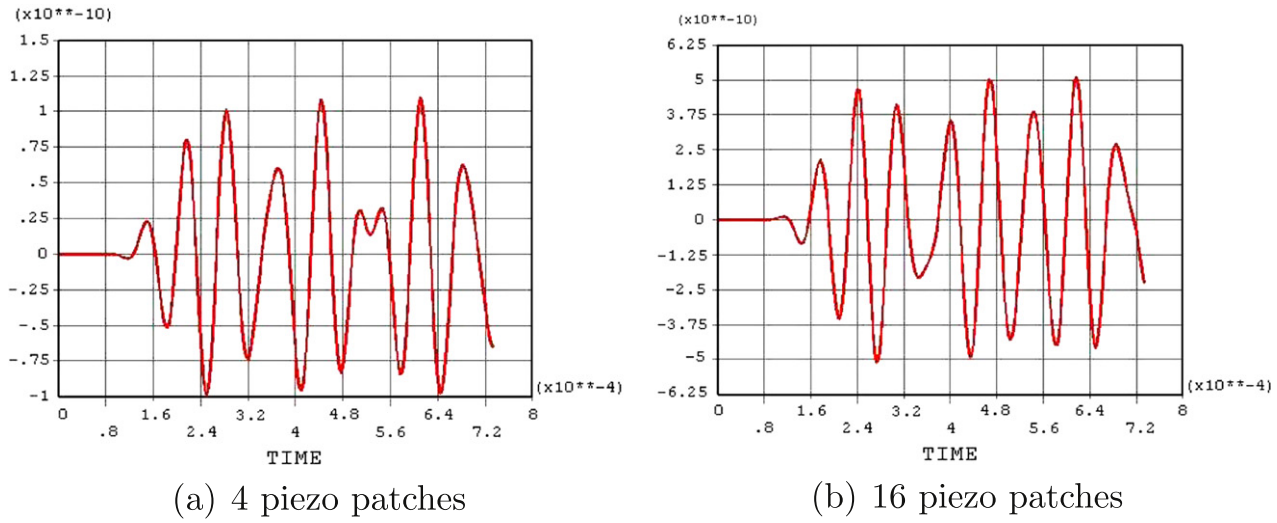

Fig. 7. Simulated record of the time signal in the middle of the pipe's length for different types of piezo arrays: (a) 4 patches and (b) 16 patches.

The distance hence obtained corresponded each time to the position of the measurement point along the pipe with no change in the pulse shape for the first impulse cycles. The duration of the pulse, $3.67e10^{-4}s$, corresponds to the 5.5 cycles at 15 kHz. Indeed, by the time the total torsional pulse had passed the measurement point, either the other (slower) flexural modes were arriving (see Fig. 7a) or the reflection of the wave on the end of the pipe was captured (see Fig. 7b). This result was kept as it is, since it corresponds to the length of the iron pipe that was used during the experiments. However, this assessment on the effect of the reflected wave was confirmed by measurements made closer to the excitation point and therefore farther form the reflecting pipe's end.

The conclusion was made that the size of the piezo parts was good enough to ensure the generation of the designated wave type, provided they were numerous enough. By means of time finite-element calculation, and according to the available piezo shear properties, the size and the number of piezo parts could be determined. Hence, a total number of 16 evenly distributed piezo was chosen, adapted to the 140 mm pipe. This rate of piezo patches to the pipe's size was also confirmed by the analysis from Lowe et al. [1].

3.3. Torsion mode – numerical results

Once the design of the actuator chosen, the next numerical simulations were performed in order calculate the dynamic response of the pipe with a notch. The torsional wave-mode proved to be very sensitive to the defect shape and size as it can be observed in Fig. 8. The numerical comparison, here presented, between a good pipe and a damaged one correspond to the actual pipes that were used for the experiments as reported in Section 5 (overall pipe's dimensions, size and shape of the defect).

The goal was to get an order of magnitude of the reflection coefficient that we could expect from a torsional wave. Theses values of the reflection coefficient with frequency are reported in Fig. 9 for different sizes of a through notch located at 2 m from the end of the pipe where the piezo-array actuator is placed. The notch is transverse to the pipe and its size is given in percentage of its circular length. The measurements are supposed recorded where the actuator is placed.

Generally speaking, the reflection coefficient increases with the frequency and (of course) the notch's size. However, above a given frequency, some peak values are observed on the numerical results. For a 12% notch, the refection coefficient between 10 and 30 kHz varies between 0.05 and 0.20 and does not evolves regularly. It reaches local peak values around 14 and 20 kHz and then drops sharply down to almost half of its values. The corresponding frequencies happen to be the eigen frequencies of pipe's section modes. These modes must be very sensitive to the occurence of such a singularity. Moreover, since the evolution of the reflection coefficient is not uniform across the frequency band, its value for a 12% notch can sometimes be lower than the one of a 8% notch. For instance, the value at 22.5 kHz is 0.08 for a 12% notch whereas, at 22 kHz, it is equal to 1.10 for a 8% one. Hence, depending on the frequency used to generate the traveling wave, this effect should seriously be taken into account in order to give the proper analysis on the pipe's health. The experimental results should confirm this evolution with frequencies.

4. Waves generation – time signal from the piezo actuator

The first measurements performed with the piezo-distributed actuator had to confirm the feasibility of a torsional wave generation on a pipe. Then, according to the quality of the measurements, the analysis of these latter should establish some observations in the way of processing the results. For instance, the impulse's duration must have an effect on the singularities visibility or the vibrations' attenuation has to be taken into account when considering the amplitude of the wave's reflexions. Then, the first measurements, comparing the time signal with and without a defect on a pipe, can be performed.

4.1. Wave propagation along the pipe

The actuator has here first to prove that it can generate pulsed propagative waves. Then, these waves have to be torsional waves only. The results of the following testing are presented in order to assess these features.

For that purpose, the actuator and the sensor are mounted on a straight 3 m-long PVC pipe without any defect. The actuator is attached at one end of the pipe; the sensor is placed at 1 m from the actuator. Fig. 10 shows the time record for the pipe without any defect, whereas Fig. 11 is the time record under the same experimental conditions but for a pipe with a defect. This defect is a single 6 cm radial cut. It is placed half way from both end of the pipe.

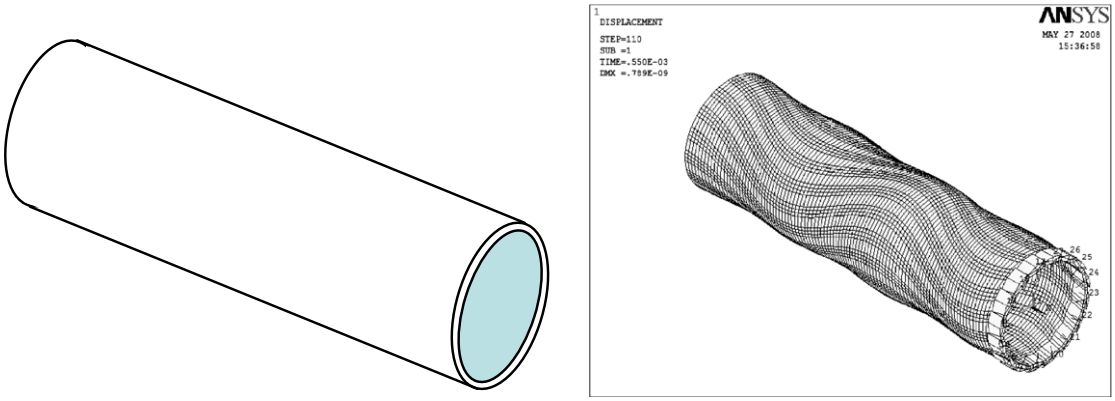

(a) pipe without notch

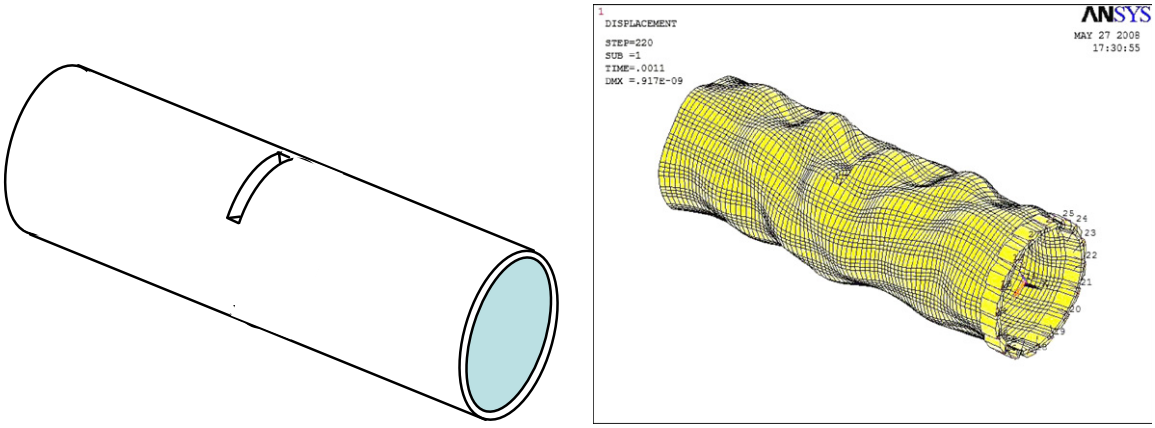

(b) pipe with a notch

Fig. 8. Finite element similuations with 16 piezo parts.

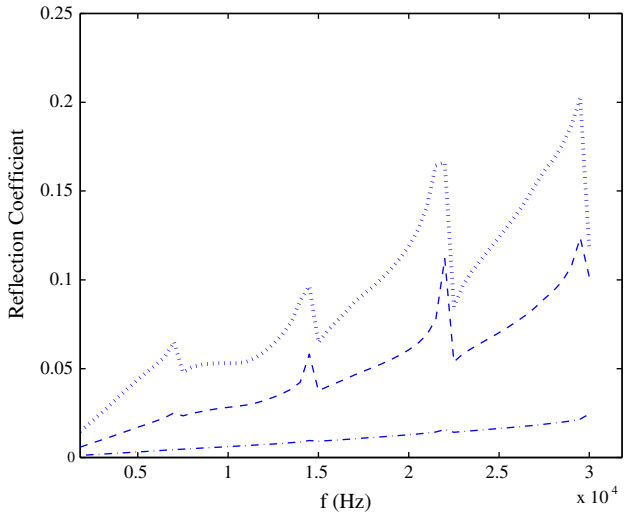

Fig. 9. Reflection coefficient for different notch's sizes (percentage of the pipe's circumference): 4% (dash-dotted line), 8% (dashed line), 12% (dotted line).

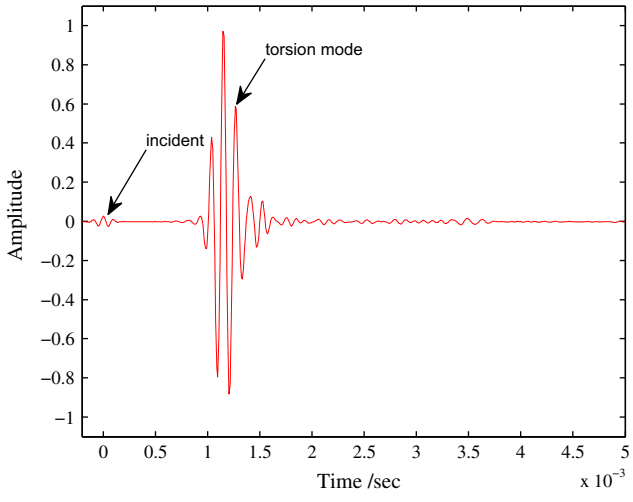

Fig. 10. Time signal recorded without defect: 3.5-cycle wave at 10 kHz.

The group speed of the torsional wave is here equal to 980 ms^{-1} in the PVC tube. Hence,the time delay between the emission of the pulse and its detection by the sensor corresponds to travel time of the torsional wave at this wavespeed. This signal corresponds to the large pulse recorded between $1.0e^{-3}$ s and $1.5e^{-3}$ s on both Figs. 10 and 11. The shape of the incident pulse is unchanged. This tends to confirm the ability of our actuator to generate only torsional waves.

After this large pulse, the two time results are different. A second pulse is visible in Fig. 11. The time delay ($1.0e^{-3}$ s) after the first pulse, at 980 ms^{-1}, is consistent with the time for the torsional wave to travel back to the sensor from the defect's location (1 m total length of path). Despite the important level of damping in such a PVC pipe, the movement can still be caught.

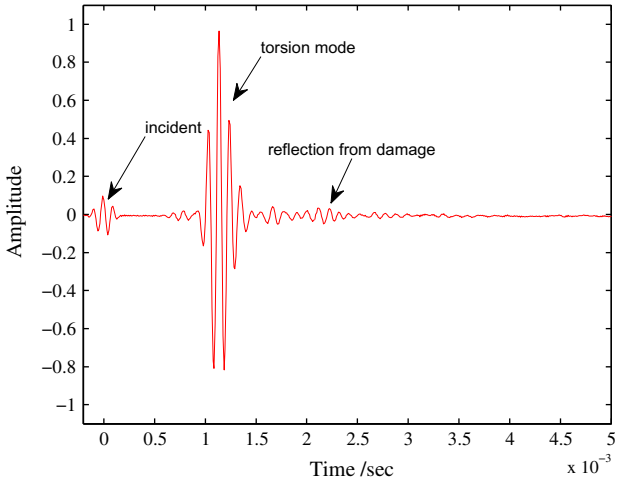

Fig. 11. Time signal recorded with defect: 3.5-cycle wave at 10 kHz.

The use of a PVC pipe was motivated not only by the easy way to process, to assemble and to cut it but also because of its important damping. Hence, no reflexion from the end could be detected as long as the sensor is not placed further than the middle of the pipe's length. We could then simulate the use of a semi-infinite pipe. With a steel pipe, the length needed would have been impossible to obtain reasonably.

4.2. Damping identification

Even if the torsional waves are not subjected to distorsion or any wave-type conversion, the attenuation of their amplitude is inherent to their propagation through a medium which is somehow dissipative. This effect even increases with the pulse signal frequency.

In order to properly appreciate the magnitude of the reflected signal as an effect of the severity of a singularity, the amplitude decrease with the distance of propagation has to be estimated. For that purpose, the following protocol was performed in order to measure this attenuation.

Taking a length of pipe with no singularity but the ends of it, a wave impulse is generated by the actuator placed at one of this ends. A single cell sensor is placed at a given distance from the actuator and the time signal is recorded. The time delay between the impulse emission and the sensor detection is measured for each position along the pipe. As seen in Fig. 12, the amplitude of the wave decays with the distance from the actuator. The interpolated curve corresponds to an exponential decrease with the distance. The calculated exponential decay is equal to 1.7 and in the range of the damping factor's values for this kind of material.

It must be mentioned that, for each measurement, the time delay was consistent with the wavespeed of the torsional wave. Moreover, when using a PVC pipe of such a length, the damping is so important that no reflexion from the pipe's end can reach the measurement point. Therefore, no doubt was possible about the origin of the measured pulse as the incident wave. Regarding the short distance over which the signal is damped, the PVC pipe can be used to simulate the equivalent long distance propagation in a more rigid material.

When a steel pipe is used instead of a PVC one, the wave can travel back and forth, reflecting itself several times at each end of the pipe. This effect is visible in Fig. 13, with the same kind of pulse as for the previous example. This figure presents the time signal on a straight 3 m-long steel pipe with no singularities but the ends of the pipe itself. The impulse wave is a 5.5-cycle wave at 15 kHz. The actuator is placed at one end of the pipe and the sensor is placed at 1.6 m from this point, on the outer surface of the pipe. The Hilbert transform is performed on the time signal in order to get the signal's amplitude only. When applied to such an input function, the Hilbert transform gives the envelop of the time varying signal [15,16].

Hence, even if the recorded pulses are not traveling the same way, their decrease in amplitude allows estimating the damping of the signal with the distance. Indeed, when performing the damping factor's measurement like in the PVC pipe case, the attenuation curves fits exactly to a line that would join all the recorded pulses' maxima (dashed line in Fig. 13).

When compared to the measured attenuation curve, the decrease of the time-signal amplitude's envelop is consistent with space attenuation of the wave traveling back and forth in the pipe. The wave's reflexions are due to the pipe's ends.

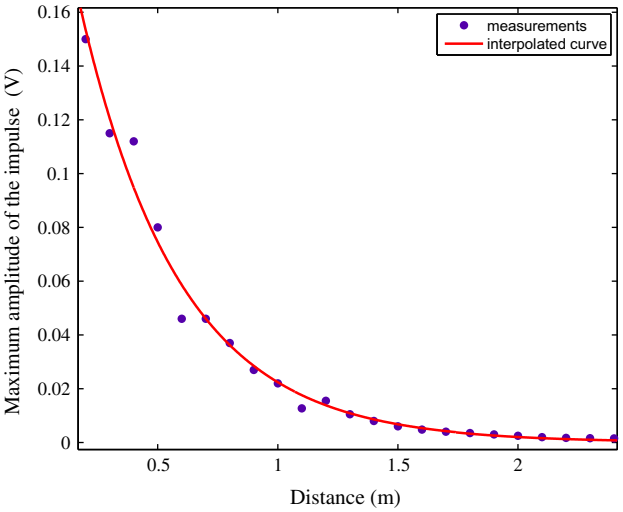

Fig. 12. Wave attenuation on PVC pipe: 5.5-cycle wave at 15 kHz. Dots: Measurements and continuous line: fitted exponential curve.

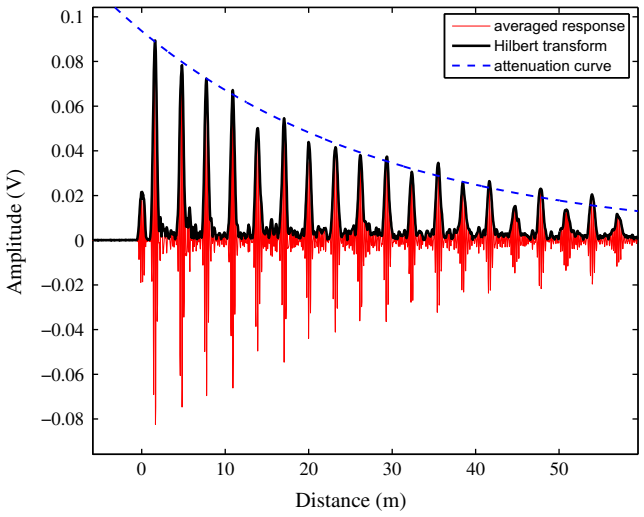

Fig. 13. Time signal attenuation with distance: 5.5-cycle wave at 15 kHz. Bold-line curve: Hilbert transform, dashed curve: attenuation curve, thin curve: time signal. (For interpretation of the references to colour in this figure legend, the reader is referred to the web version of this article.)

4.3. Results analysis

At this point, the experimental actuator–sensor device proved to actually generate and measure torsional waves traveling along a pipe waveguide. The feature of the wave's travel could be identified and evaluated like the spatial damping and the level of interaction with the defect. Long distance detection seems then to be reachable in the selected frequency range.

5. Measurements of the reflection coefficient

5.1. Reflection coefficients

A numerical vs. experimental comparison is made here, based on the reflexion coefficient. The experimental mockup uses a 4 m steel pipe. A notch is made at 2 m from the actuator location (this latter is mounted at one end of the pipe). The sensor is placed right after the actuator during these experiments. Future works will consider the fact of placing the sensor to some distance from the actuator in order to better estimate the defect location.

The reflection coefficient is calculated by establishing the ratio between the averaged reflected signal's amplitude and the amplitude of the generated wave on the pipe. This way, no matter how important is the energy input into the experimental setup, the comparison can still be drawn. The first wave's reflected signal is used to perform the comparison. Fig. 14 represents such a comparison. The reflection coefficient is calculated for a 5 mm-thick steel pipe with a 13.8% in circumference transverse notch. This settings for the numerical calculation correspond to the actual experimental ones. Experimental results seem to follow the numerical ones in the 10–20 kHz range. The interaction between the notch and the pipe's section mode is detected. However, in the upper end of the investigated frequency range, conclusions still difficult to draw. Yet, the measured reflection coefficient is always way above the numerical simulation. The technique used to get a "'reflection coefficient'" does not take into account the phase values of the time signal and hence this might be why there is a general overestimation.

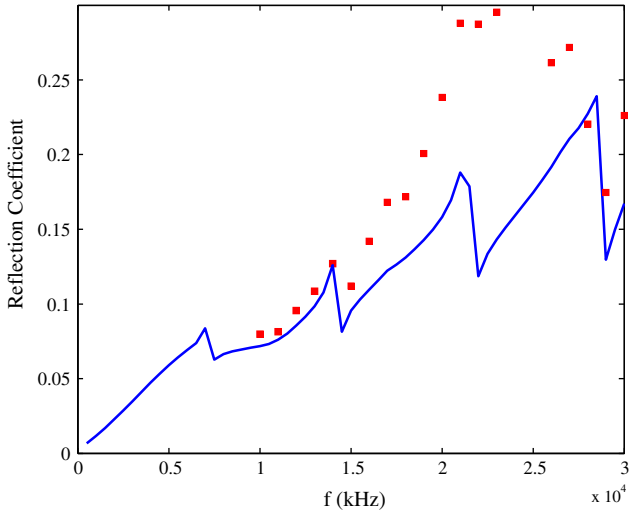

Fig. 14. Reflection coefficients for a steel pipe with a notch: numerical prediction (line curve), experimental results (square points).

5.2. Conclusion and comments for future works

This paper has presented the design and the validation process of a specific distributed piezoactuator. The use and the need of such a device for structural health monitoring was illustrated by preliminary numerical simulations. These simulations had shown the promising potential of torsional wave motion among all the propagative waves in pipe-like structure, namely waveguides.

The first experimental results validated the ability of our in-house manufactured actuator to generate the expected waves. Then, the first structure's properties could be identified and store as future parameters for monitoring the evolution the singularities and defects. Damping is one of them and it could be experimentally evaluated for two different homogeneous materials. These latter have shown the same pattern along with the distance of propagation.

The long distance application involving the treatment of reflected traveling waves is then the next step. Yet, regarding the complexity of the time signal for field applications, the current researches are led toward the post-treatment of such signals. The type and the extend of singularities are hence identified by mean of comparison to reference ones as well as knowing the sensitivity of mode conversion. Sensitivity analysis of the response quality needs also to be estimated regarding the relative inhomogeneity inherent to all real structures. For that purpose, not only specific numerical treatments but also newly designed sensor arrays are currently tested.

References

[1] Lowe MJS, Alleyne DN, Cawley P. Defect detection in pipes using guided waves. Ultrasonics 1998;36:147–54.
[2] Demma A, Cawley P, Lowe MJS. The reflection of guided waves from notches in pipes: a guide for interpreting corrosion measurements. NDT& E International 2004;37:167–80.
[3] Wang X, Tse PW, Mechefske CK, Hua M. Experimental investigation of reflection in guided wave-based inspection for the characterization of pipeline defects. NDT & E Int 2010. doi:10.1016/j.ndteint.2010.01.002.
[4] Brillouin L. Wave propagation in periodic structures. New-York: Mc Graw Hill,Publishing Compagny; 1946.
[5] Zhong WX, Williams FW. On the direct solution of wave propagation for repetitive structures. J Sound Vib 1995;181(3):485–501.
[6] Alleyne DN, Lowe MJS, Cawley P. The reflection of guided waves from circumferential notches in pipes. J Appl Mech 1998;65:635–41.
[7] Castaings Michel, Bacon Christophe. Finite element modeling of torsional wave modes along pipes with absorbing materials. J Acoust Soc Am 2006;119(2):3741–51.
[8] Demma A, Cawley P, Lowe MJS. The reflection of the fundamental torsional mode from cracks and notches in pipes. J Acoust Soc Am 2003;114:611–25.
[9] Ahadi Majid, Bakhtiar Mehrdad Sharif. Leak detection in water-filled plastic pipes through the application of tuned wavelet transforms to Acoustic Emission signals. Appl Acoust 2010;71:634639.
[10] Bartoli I, Lanza di Scalea F, Fateh M, Viola E. Modeling guided wave propagation with application to the long-range defect detection in railroad tracks. NDT& E Int 2005;38:325334.
[11] Siqueira MHS, Gatts CEN, da Silva RR, Rebello JMA. The use of ultrasonic guided waves and wavelets analysis in pipe inspection. Ultrasonics 2004;41:785797.
[12] Yong Y, Lin YK. Propagation of decaying waves in periodic and piecewise periodic structures of finite length. J Sound and Vib 1989;129(2):99–118.
[13] Mencik J-M, Ichchou MN. Multi-mode propagation and diffusion in structures through finite elements. European J Mech – A/Solids 2005;24(5):877–98.
[14] Mencik J-M, Ichchou MN. Wave finite elements in guided elastodynamics with internal fluid. Int J Solids Struct 2007;44(7-8):2148–67.
[15] Bracewell R. The Fourier transform and its applications. McGraw-Hill; 1965.
[16] Feldman M. Non-linear system vibration analysis using Hilbert transform – I. Free vibration analysis method 'FREEVIB'. Mech Syst Signal Process 1994;8(2):119–27.

Chapter 3

Defect detection in pipes by a torsional guided-wave inspection system: design and experiments

Abstract

Guided wave technique is becoming more and more usable in pipeline inspection due to its efficiency and its cost effectiveness. An inspection system has been designed and developed in this work. It is based on torsional wave generation and reception using piezoelectric transducers. Numerical simulations using standard FE and Wave Finite Element methods have been carried out in order to verify and visualize the wave propagation phenomenon in both intact and damaged pipes. An experimental test bench is provided in order to perform a set of tests on straight and curved pipes with two different materials: PVC and steel. In each case, time signals from intact and damaged structures were analyzed. Experimental results show that the torsional mode is well excited and could propagate along the pipe. The interaction between the generated waves and machined defects has been proven, as well as the ability of damage detection within the curved structure. Numerical and experimental comparison, in terms of reflection coefficients, has shown a good agreement.

Keywords: Structural health monitoring, defect detection, torsional guided-wave, piezoelectric transducers, reflection coefficient.

1. Introduction

Long pipelines are often used in petro-chemical industry for transporting liquid and gaseous substances. These pipes need to be regularly monitored and inspected for both safety reasons and environmental impact control. Non-Destructive Tests (NDT) techniques are required to assess the integrity of pipes in service. A quick and reliable method for the detection of corrosion and defects under insulation which does not involve removal of all the insulation is therefore required. The problem is even more severe in cases such as road crossings where the pipe is underground (often in a sleeve) for a limited distance; excavation of the pipe for visual or conventional ultrasonic inspection is extremely expensive so a technique to address this problem is particularly beneficial. Thus, it is useful to find an effective method capable of screening long distances of pipes from one access position and to be fast and sufficiently accurate to identify defects in the inspected areas.

Guided waves have been increasingly used in nondestructive evaluations. Many researchers have been interested in the application of ultrasonic guided waves for the nondestructive inspection of pipes [1–4]. They have recognized the possibility for rapid, accurate, and inexpensive nondestructive assessment of these structures that exist in the infrastructure of many industries. Guided wave inspection method is a fast screening technique for pipe testing [5–7]. It ensures the inspection over larger distances from limited and distant points of observation. The use of low frequency ultrasonic guided waves propagating along the pipe wall is potentially a very attractive solution since they can propagate a long distance under insulation and may be excited and received using transducers positioned at a location where a small section of insulation has been removed.

A detailed explanation by Rose, Pelts and Quarry on a comb transducer has been presented in reference [8], along with the various design aspects of a comb transducer. This latter is a finger-like device that is placed on the structure, whereby pumping ultrasonic energy into the comb with the appropriate spacing can produce guided waves of choice inside the piping material. The comb structure can go entirely around the pipe producing longitudinal axisymmetric waves or be placed partially around the circumference of the pipe, say from twenty to ninety degrees around the circumference, and in this case produce longitudinal non-axisymmetric or flexural modes in the pipe. Shin and Rose [9] have discussed the use of both axisymmetric and non-axisymmetric surface loading in hollow cylinders and illustrates the basic principles behind non-axisymmetric wave propagation. Use of these flexural mode waves are being tried in order to assist in the flaw detection classification and sizing process. Further work on the excitation of non-axisymmetric guided waves has been reported by Li and Rose [10]. It was shown in this paper how it becomes possible to load the upper surface of a pipe and to inspect, for example, the bottom side of a pipe, at a certain distance away.

In principle, both axisymmetric and non-axisymmetric modes can be used for long-range inspection. Axisymmetric modes are in general preferable because they are easier to excite and have relatively simple acoustic fields. Initial practical testing was done by many researchers using the longitudinal L(0,2) mode. Alleyne and Cawley [4] have reported on the development of dry-coupled piezoelectric transducers for the excitation and detection of the guided waves. Alleyne et al. [6, 11] and Lowe et al. [12] have studied the reflection of the L(0,2) axially symmetric mode from notches in pipes, and examined the reflection of mode-converted guided waves with L(0,2) as incident mode [13]. Alleyne and Cawley [14] have measured reflections of the same mode from welds, flanges and pipe supports, and demonstrated that the mode can be propagated under wet or dry insulation. However, more recent tests have employed the torsional mode [15–17]. This has the advantage that, in contrast to the L(0,2) longitudinal mode, the T(0,1) torsional mode propagation characteristics are not affected by the presence of liquid in the pipe and there is no other axially symmetric torsional mode in the frequency range, so axially symmetric torsional excitation will only excite the T(0,l) mode, whereas when the L(0,2) mode is used, the transducer system must be carefully designed to suppress the L(0,1) mode.

Another issue that has been treated is the presence of features in pipeline like elbows. Rose and Zhao, in [18], have carried further the flexural mode tuning concept for pipe elbow inspection. It was shown that it becomes possible to send ultrasonic energy into an elbow region and even beyond the elbow region in carrying out a reliable and efficient inspection. Also, a semi-analytical finite element method has been used by Hayashi and Rose [19, 20] in order to show how an axisymmetric wave in a straight pipe is modified as it passes through an elbow. A. Demma et al. [21] has studied the propagation of guided waves in curved pipes. The modes propagating in toroid structures have been found using an FE procedure.

Based on these previous researches, an inspection system has been designed and

developed to generate well-defined waves that propagate along the structure; and receive reflected signals from features and damages encountered. The torsional mode was chosen to be generated by the system. This choice is based on the intrinsic properties of this mode. The generation of torsional waves is operated by using a number of piezoelectric transducers clamped around the circumference of the pipe. The Wave Finite Element Method, which is a spectral approach, has been used to compute the response from damaged pipe in time domain. The same method has been employed to calculate reflection coefficients from the defect at different frequencies in order to be compared to experimental results.

In this paper, the design process of the torsional waves inspection system is presented at first, including finite element simulations on an intact and a damaged pipes. Time responses were examined in each case. Then, experimental tests have been performed on two pipes with different materials: PVC and steel. Some defects have been machined on these pipes. Their interaction with torsional waves has been proven by analyzing experimental time responses. Finally, the torsional wave propagation in a PVC straight-curved-straight structure was studied. The interaction with damage in a bend has been investigated.

2. Design of the guided-wave inspection system

In this section, the bases of the inspection-system design were introduced. Guided waves in pipes were described in order to achieve a suitable selection of the excitation mode. Once the choice made, the wave generation mechanism was detailed. Then, finite element simulations were performed on intact and damaged pipes in order to validate the concept.

2.1. Guided waves in pipes and mode selection

Guided-wave propagation in pipes is a complicated phenomenon due to the diversity of the generated waves. There is two different categories of wave modes: axisymmetric and non-axisymmetric. The first one includes longitudinal and torsional waves, and the second one includes flexural waves.

In order to achieve a good understanding of wave properties, dispersion curves were numerically obtained for a steel pipe using the Wave Finite Element Method. This method was previously implemented on similar structures and its methodology was detailed in references [22–24]. The outer diameter of the steel pipe is 140mm and the thickness of the pipe wall is 4mm. Figure 1 shows the group velocity dispersion curves of the modes that can propagate in the pipe.

The modes include a family of axially symmetric longitudinal, flexural and torsional motion of the pipe wall. However, in addition to the axially symmetric (zero-order) modes, there are modes which have harmonic variation of displacements and stresses around the circumference. The order 1 modes have one cycle of variation around the circumference, order 2 have two, and so on. For each of this infinite series of orders, there is a family of modes. The modes in the figure 1 are labeled after the convention of Silk and Bainton [3]: the first integer of the integer pair in each

mode label gives the harmonic order of circumferential variation; thus the axially symmetric modes have zero as their first integer. The letters L, F and T denote longitudinal, flexural and torsional modes, respectively.

The group velocity dispersion curves show the velocity at which finite-time wave packets travel; they are therefore useful for the calculation of the travel times of the wave signals which are used in the long-range testing. From this curves, several important observations can be made. First of all, it is obvious that, for a given frequency, lots of waves can propagate. Besides this, when the frequency varies not only the number but also the types of waves change (longitudinal, flexural, and torsional). Among these waves, the torsional mode T(0,1) is the only one whose velocity remains constant with frequency. All the others suffer speed variations as the frequency changes. Axisymmetric modes are preferred for the detection of defects in pipes. Previous studies have used the longitudinal mode L(0,2) due to its sensitivity to defects, its speed and non-dispersivity from cut-off frequency [6, 25]. These studies and others also have shown the benefit of using the torsional mode T(0,1). Indeed, its main advantages are:

- a non-dispersive mode, it keeps its speed constant.
- the fastest among torsional waves.
- it has a high sensitivity to axial and circular defects.
- it has a high sensitivity to internal and external defects.
- unique among the torsional modes in the frequency range used.
- it propagates through pipes filled with liquid without much leakage.

The design of the wave generator has to guarantee that only torsional mode is created which have to be verified by the first experiments.

2.2. Generation of torsional mode

The design of the inspection system has to take into account the selection and exploitation of a single mode. A lot of modes can be generated by an excitation source working in its frequency band. Obtained signals are much more complicated to interpret. Even, with a single mode, great care is necessary for the correct identification of reflections from defects and features that exist in the pipe (welds, supports, flanges...). Therefore, although it is not obvious to achieve, it is essential to design a wave generator able to excite only one mode.

The aim of the inspection system is, firstly, to generate torsional waves in a cylindrical pipe. Then, these waves must be guided by the pipe structure and have the necessary energy to travel along long distance. When they encounter features that change the geometry of the pipe such as structural singularities (flanges, elbows, welds, branches ...) or defects (corrosion, notches, metal loss ...), they have to be partially reflected. These echoes are then detected and analyzed in order to provide

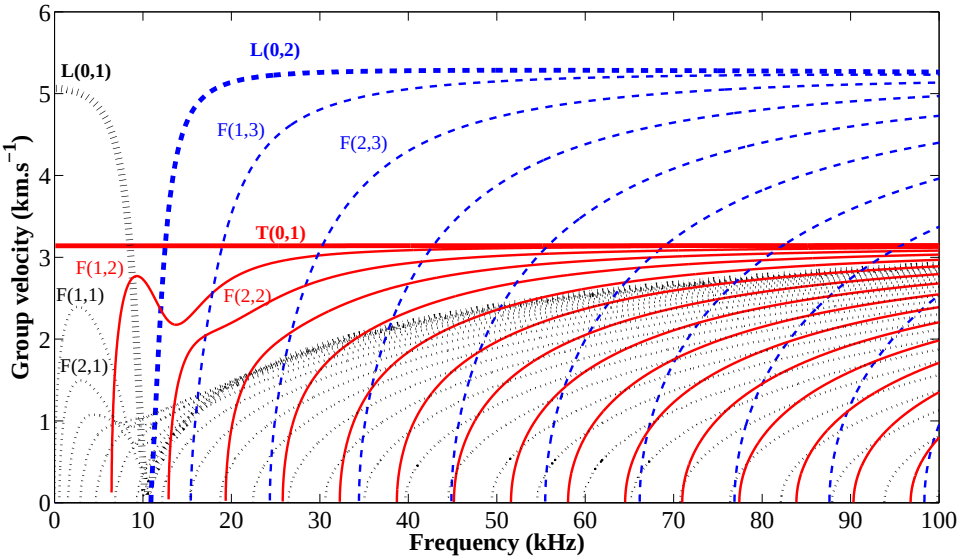

Figure 1: Group velocity dispersion curves computed by WFEM for a 140mm outer diameter steel pipe with a 4mm thickness.

information about the location and nature of every discontinuity in the pipe. So, our inspection system should have two parts: a wave-generator ring and, a wave-receiver ring. To design the generator ring, the idea is to apply a local shearing motion around the outer circumference of the pipe section. The time history of the displacement should be consistent with a pulse. The choice was made to use piezoelectric patches that would convert the electric signal into shear strain. However, for a practical and economical concern, the continuity of the piezoelectric round around the pipe could not be guaranteed. Therefore, instead of a piezoelectric ring, the idea was to generate a torsional torque via a ring of distributed rectangular piezo-transducers working with the inverse piezoelectric effect. Yet, the number of these piezoelectric parts has to be estimated in order to ensure the generation of the desired waves (Figure 2). Receiver side, the piezo-transducers should work with the direct piezoelectric effect. Received waves would be converted to electric signals and then would be sent to an acquisition instrumentation.

The first step in selective excitation is to use a narrow band signal. This also gives good signal strength and avoids dispersion over long propagation distances. A tone burst of 3 to 10 cycles in a Hanning window achieves this ideally. A typical time record for a 5.5 cycles signal and its frequency spectrum are shown in figure 3. The magnitude and the number of cycles correspond to the total energy sent into the piezoelectric array. The magnitude, but also the frequency are the main characteristics of the wave input signal. Even if the torsional wave-speed is not frequency dependent, the sensitivity of the propagative wave to the defects is closely correlated to its relative wavelength versus the defect size. In addition, the magnitude and the frequency have both an influence on the ability of waves to travel long

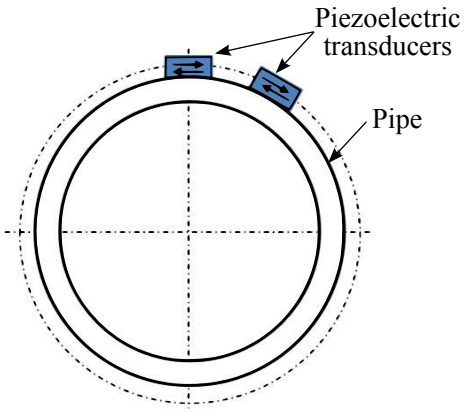

Figure 2: Mounting of the piezoelectric transducers on the pipe.

distances before the structural damping make them unperceivable. However these two parameters have practical limits due to the electronics of the voltage amplifier and of the measurement front-end.

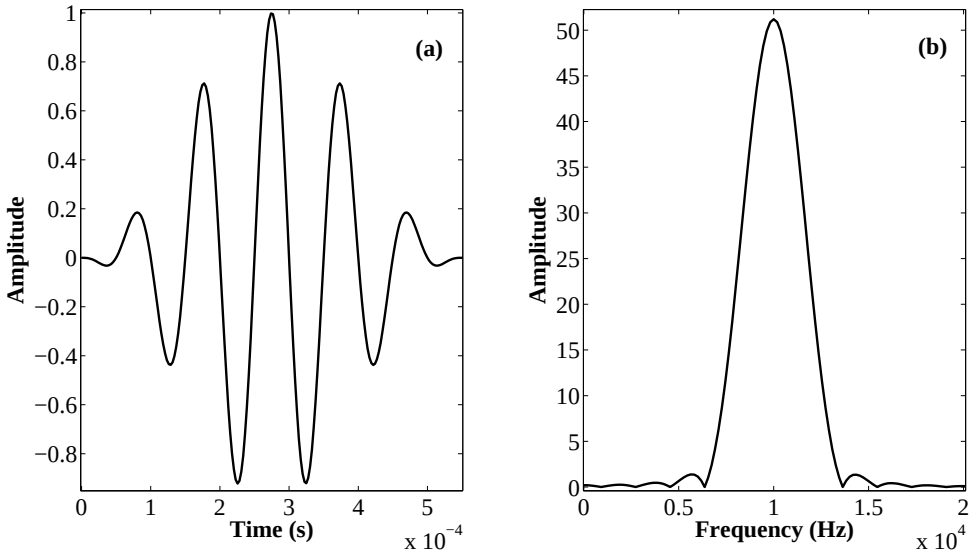

Figure 3: 5.5-cycles narrow-band signal at 10 kHz modulated by a Hanning window: (a) time record; (b) frequency spectrum.

2.3. Finite Element simulations on an intact pipe

2.3.1. Pipe deformed-shapes

In order to visualize the wave propagation phenomena and verify the homogeneity of the displacement in the pipe section, the finite element model of a pipe around which was clamped a number of piezoelectric transducers, was developed. The pipe is of steel with a 140mm outer diameter, a 4mm-thick and a 1m-long. If a sufficient number of equally spaced and equally driven transducers is excited around the

circumference, then only the axially symmetric (order 0) modes are excited. The number of transducers must be greater than the highest order of the modes which can be present in the frequency range of the signal [7]. For the 140mm pipe, it is suitable to use more than 15 transducers if we will reach the 40 kHz. Three configurations of piezoelectric-transducers numbers were studied here in order to find the optimal one and to be sure of to generate the desired waves. In the finite element model, we used 4, 8 and 16 piezo-elements equally spaced mounted around the circumference. We introduced the necessary piezoelectric-material properties for each of the elements and the electric signal was applied to the proper sides in order to have a shearing effect acting on the pipe circumference. The structure was excited at 10, 15 and 30 kHz. The resulting deformed shapes of the pipe at a given time of the time simulation are compared in figure 4.

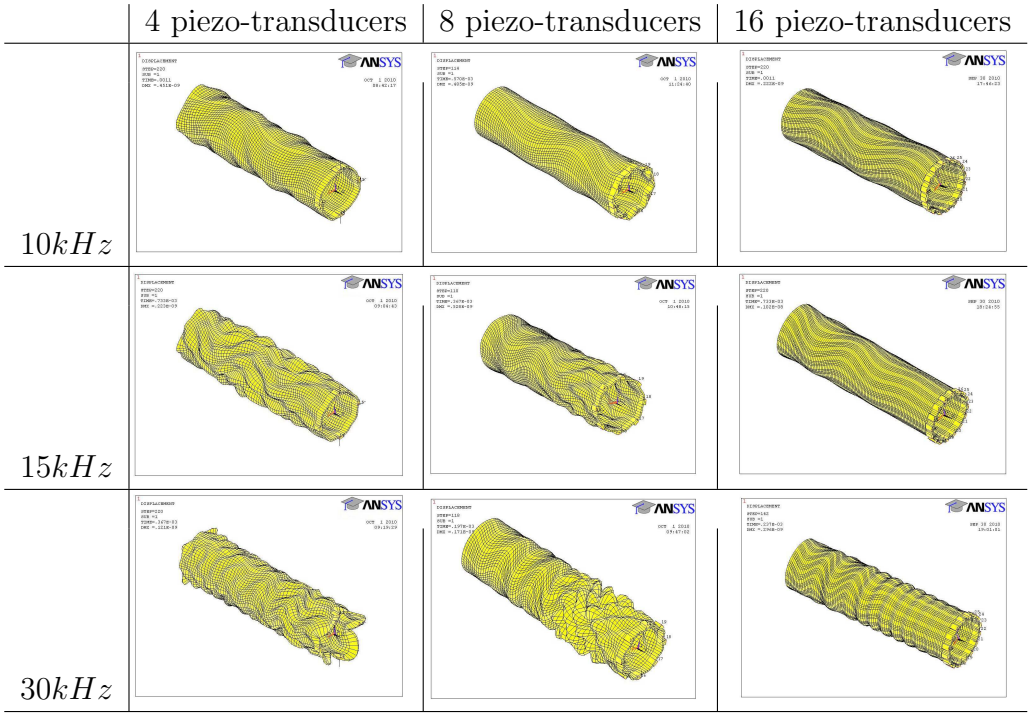

Figure 4: Deformed shapes of a steel pipe for different numbers of piezoelectric patches, at different frequencies.

We can notice that for the 4 piezo-transducers case, the torsional mode is not generated and there is flexural modes propagating in the pipe. In fact, the shearing effect is created locally but due to the limited number of transducers around the circumference the torsion effect was not generated. For the second case, 8 piezo-transducers induce torsional mode only at 10 kHz but if we go up the frequency flexural modes appear. Finally, the 16 piezo-transducers configuration seems to be convenient at the three frequencies and the torsional mode is well generated.

The number of piezo-patches to be used in the generator must take under account the necessity of creating a sufficient torsional motion on the one hand, and the surface

availability in the pipe on the other hand. Hence, a total number of 16 evenly distributed piezo-transducers was chosen, adapted to the 140mm pipe.

2.3.2. Simulated time-signals on the pipe

The wave speed of the presumed torsional mode created must be consistent with its real wave-speed which is $3140m.s^{-1}$ according to figure 1. The verification will be done using the numerical time-signals recorded in the FE simulation. For three points along the pipe in different axial locations (figure 5), the orthoradial displacement time-signals was observed and the time delay between the emission and the detection was divided by the wave speed for the corresponding torsional wave in a steel pipe. Recorded time-signals are simulated for an excitation impulse with 3.5 cycles at 10 kHz generated in x=0m (X being the axis of the pipe). The pipe is the same as in subsection 2.3.1. Results are shown on figure 6.

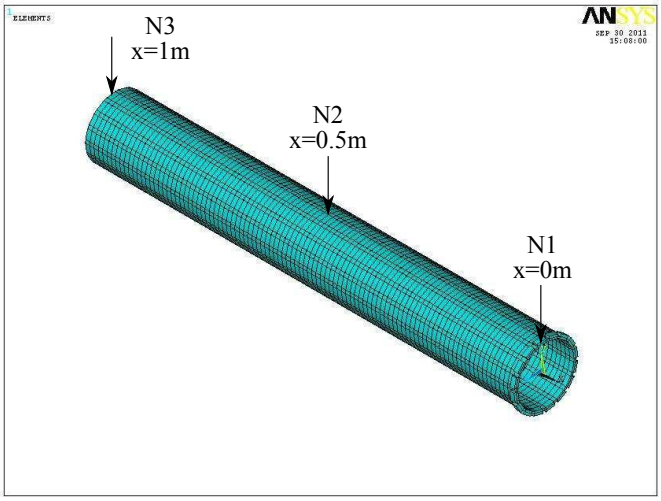

Figure 5: Observed-nodes locations in the pipe.

Figure 6(a) corresponds to the displacement recorded for the N1-node situated at $x = 0m$. If we examine this curve, we find two received impulses. The first one is due to the excitation since it begins at $t = 0s$. The second one corresponds to the end of the pipe echo received after the wave has traveled back and forth. The time duration between the first and the second impulses ($0.6 \times 10^{-3}s$) matches with the time needed by the wave to propagate 2m by the torsional wave-speed. Figure 6(b) shows the displacement recorded for the N2-node located at the middle of the pipe ($x = 0.5m$). This curve shows two whole impulses and a part of a third one. The first one is the passage of the incident wave arriving after a time-delay corresponding to the torsional wave traveling duration between the N1 and N2 nodes. The second impulse in the curve is the end of the pipe reflection received after the wave has traveled back and forth. The third impulse is not complete due to limited time simulation and comes from the other end of the pipe (at x=0m). Finally, figure 6(c) represents the displacement of the N3-node located in the end of the pipe.

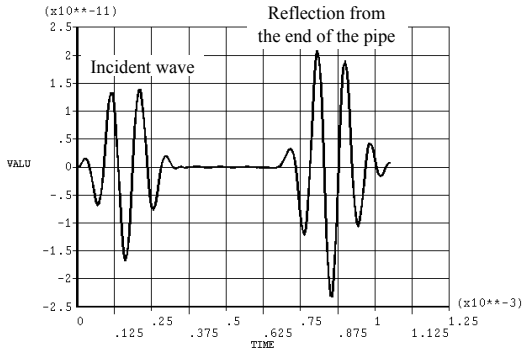

(a)

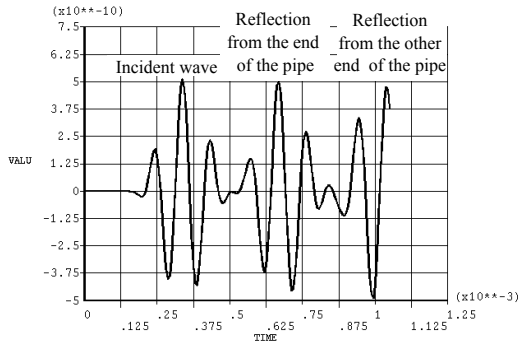

(b)

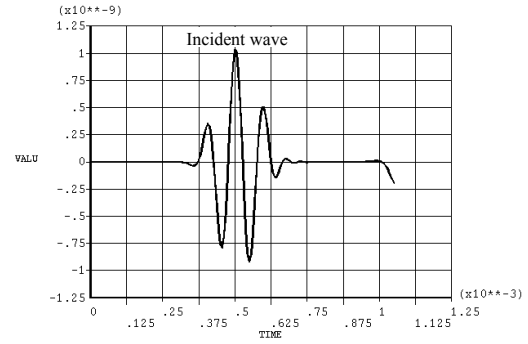

(c)

Figure 6: Displacement time-signals recorded at different locations in the pipe: (a) x=0m, (b) x=0.5m and (c) x=1m.

The received wave implies an impulse delayed by the time needed to travel from the excitation source until the measurement point. This duration matches with the torsional wave speed divided by the length of the pipe.

The FE simulations have shown the ability of the piezoelectric patches to generate torsional waves that can propagate along the pipe. The torsion wave-speed calculated by FEM was compared to the WFEM's one and verified. The next step is to validate, numerically, the sensibility of the torsional mode to the defect presence in the pipe.

2.4. Numerical simulations on a damaged pipe

2.4.1. Finite Element simulation

Once the design of the inspection system chosen, the next numerical simulations were performed in order to calculate the dynamic response of the pipe with a notch. The aim is to test the sensibility of the torsional waves generated by the inspection system to a defect. For this reason, a squared through-cut was modeled at the middle of a 1m-long pipe (Figure 7). Its circumferential extent is about 25% and its axial extent is 10mm. The diameter and the thickness of the pipe were the same as used previously. A piezoelectric array was positioned at one end of the pipe. The excitation signal has a 3.5 cycles and a frequency of 10 kHz.

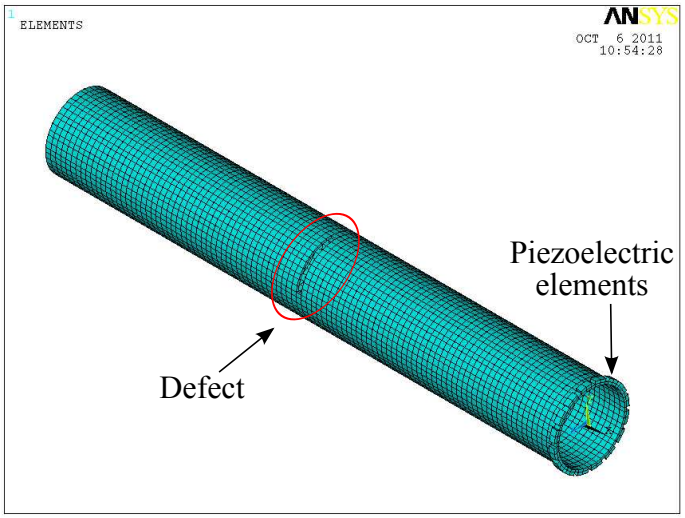

Figure 7: Finite Element model of the pipe with a defect.

Figure 8 shows the orthoradial-displacement time signals for two measurement points: at x=0m where the piezo-array is located, and at x=1m (the other end of the pipe). In figure 8(a), the time-signal is recorded for a node situated at the first end of the pipe, so we can see in the graph the incident wave impulse beginning at t=0s, then the defect echo is detected and its position can be verified knowing the torsional wave speed. Finally, the third impulse represents the reflection of the other end of the pipe. In figure 8(b), the time signal is recorded for a node situated at the other end of the pipe. The wave arrives with a delay corresponding to 1m propagation duration. The wave energy is affected by the structural attenuation and the presence of the defect in the pipe. The little impulse that appears later in the graph represents the echo of the defect from the returning wave.

Deformed shapes of the pipe can be extracted by this simulation in order to examine the wave propagation and its interaction with the defect (Figure 9). The wave created by the piezo-array begins to spread along the pipe as we can see in figure 9(a) where the torsion mode is observed here. After a while, the wave reaches the defect (fig. 9(b)). A part of the wave is reflected and turns back to the first end of the pipe where the piezo-array is located, whereas the other part of the wave

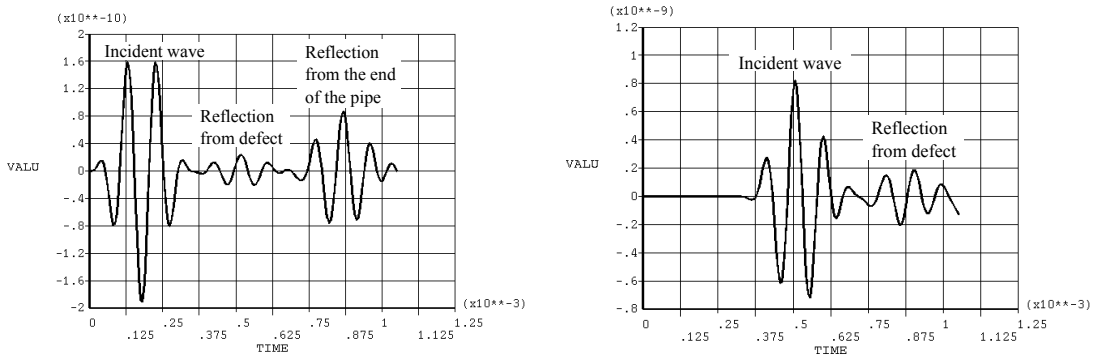

(a) (b)

Figure 8: Displacement time-signals recorded at different locations in the damaged pipe: (a) x=0m, (b) x=1m

continues traveling (fig. 9(c)). While the reflected wave attains the first end of the pipe, the transmitted wave catches the other extremity (fig. 9(d)) and then turns back completely. When it reaches the defect, a part of this wave is reflected and returns to the second end of the pipe at the same time that the transmitted one arrives at the first end (fig. 9(e)). The final deformed shape of the pipe in the simulation is presented in figure 9(f).

The presence of such non-axisymmetric defects creates mode conversion of the axisymmetric incident-wave to additional non-axisymmetric modes. In fact, an axially symmetric wave which is incident at an axially symmetric feature (eg a welded pipe joint) reflects energy only in axially symmetric modes. But, an axially symmetric wave which is incident at non-axially symmetric feature (eg a corrosion patch) mode-converts energy to non-axially symmetric modes. Thus, separate measurements of axially symmetric and non-axially symmetric reflections can discriminate between welds and defects [15, 17, 26]. The torsional mode T(0,1) tends to be converted mainly to the flexural modes F(1,2) and F(2,2). At 10 kHz, the frequency at which the simulation was performed, there is only the F(1,2) mode according to figure 1. Hence, the deformed shapes in figure 9 corresponds probably to the mode shapes of both T(0,1) and F(1,2). Since T(0,1) is faster than F(1,2), the first echo received at measurement point from the defect corresponds to a torsional one and the F(1,2) echo comes later.

2.4.2. WFE simulation

Brief introduction of WFE method.

Given a single or a set of incident modes, scattered modes (reflection and transmission) can be obtained via the governing equations for the scattering problem [27]:

$$\begin{bmatrix} \mathbf{S}^c_{ll}[\mathbf{q}^-] - [\mathbf{F}^-] & \mathbf{S}^c_{lr}[\mathbf{q}^+] \\ \mathbf{S}^c_{rl}[\mathbf{q}^-] & \mathbf{S}^c_{rr}[\mathbf{q}^+] + [\mathbf{F}^+] \end{bmatrix} \begin{Bmatrix} \mathbf{A}^{re} \\ \mathbf{A}^{tr} \end{Bmatrix} = \begin{bmatrix} [\mathbf{F}^+] - \mathbf{S}^c_{ll}[\mathbf{q}^+] \\ -\mathbf{S}^c_{rl}[\mathbf{q}^+] \end{bmatrix} \left\{ \mathbf{A}^{in} \right\}. \quad (1)$$

where $\mathbf{S}^c_{rl}$, $\mathbf{S}^c_{lr}$, $\mathbf{S}^c_{ll}$ and $\mathbf{S}^c_{rr}$ are block dynamic stiffness matrices of coupling structure, and subscripts l or r denote the left or right components respectively; $[\mathbf{q}^+]$ and

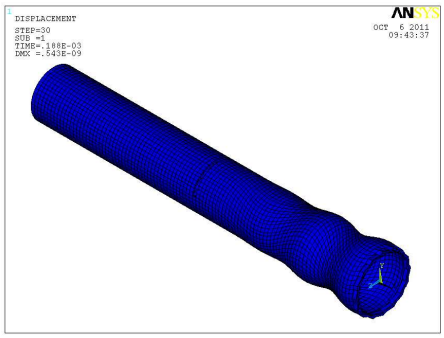

(a) At t=0.188ms

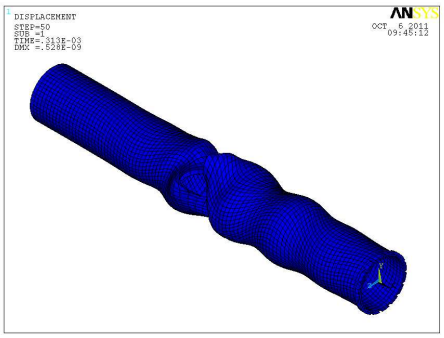

(b) At t=0.313ms

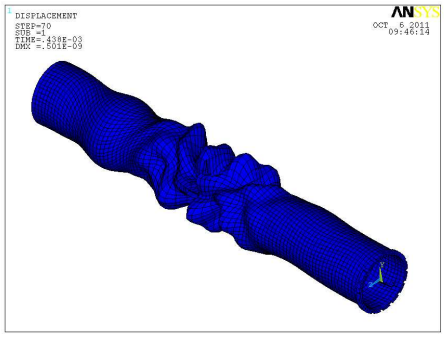

(c) At t=0.438ms

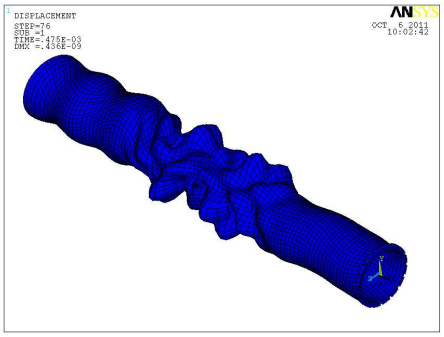

(d) At t=0.475ms

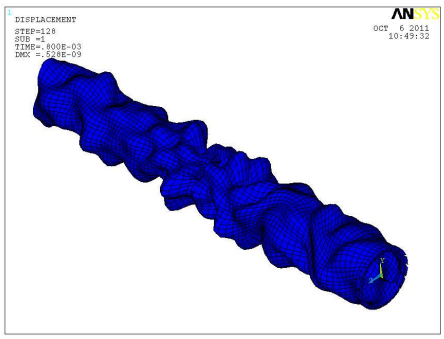

(e) At t=0.8ms

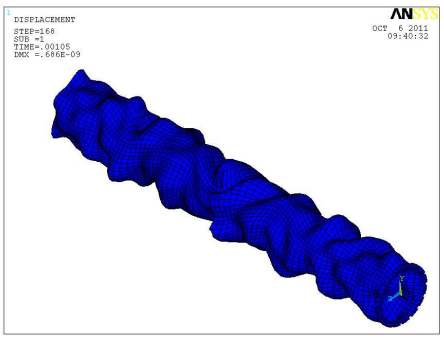

(f) At t=1.05ms

Figure 9: Results on a damaged pipe: FE deformed shapes variation over time.

$[\mathbf{q}^-]$ are displacement vectors relating respectively to the positive and negative going waves; $[\mathbf{F}^+]$ and $[\mathbf{F}^-]$ are force vectors; $\mathbf{A}^{in}$, $\mathbf{A}^{re}$, and $\mathbf{A}^{tr}$ denote respectively the amplitudes of the incident, reflected and transmitted waves.

In order to obtain the response of a damaged waveguide subjected to a given force input away from the location of defects, through Equation 1, the calculation needs to make use of the wave-modes solution under a given excitation from Equation 2.

$$\left\{\left(\hat{\mathbf{D}}_{we}\hat{\mathbf{D}}_{ee}^{-1}\hat{\mathbf{D}}_{ew}-\hat{\mathbf{D}}_{ww}\right)\left[\mathbf{q}^+\right]-\left[\mathbf{F}^+\right]\right\}\mathbf{A}^+=\hat{\mathbf{D}}_{we}\hat{\mathbf{D}}_{ee}^{-1}\mathbf{F}_e. \tag{2}$$

where $\mathbf{D}$ denotes the dynamic stiffness matrix of FE model of the damaged part; $\mathbf{F}_e$ is the external force applied on the end; the subscripts e and w denote the components associated with the excitation and wave mode interface.

If the waveguide is subjected to an force input, the short time response can be calculated from the frequency response function without taking into accounted the influence of the initial boundaries (if exist).

As to the wave response, a given mode at different frequency needs to be normalized for better recovering of the response of far field. The assumed incident wave form can be a wideband pulse or a well tuned sinusoid. As windowing functions can minimize the effect of spectral leakage to better represent the frequency spectrum of the signal, the functions with better frequency resolution and amplitude accuracy such as Hamming, Hanning or Gauss window functions are usually used for the active inspection of defects in NDT/E engineering. The sinusoidal pulse modulated by a window can be written as

$$\begin{cases} A^{in}(t)=A_0\sin(\omega_0 t)\,W(\omega_0 t,N_{cyc}) & 0\leqslant t\leqslant 2\pi N_{cyc}/\omega_0,\\ 0, & 2\pi N_{cyc}/\omega_0\leqslant t,\end{cases} \tag{3}$$

where $W(\omega_0 t, N_{cyc})$ is the window function; N_{cyc} is the cycle number and ω_0 is the signal frequency.

Let's consider a structural waveguide with a local defect as illustrated in Figure 10. l_1 is the location of the first interface between the reflection part and coupling part with defects and, l_2 is the location of the second interface between the transmission part and coupling part with defects.

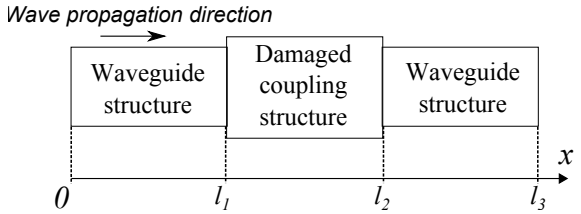

Figure 10: Wave propagation through a damaged coupling structure.

The Fourier transform of the wave mode response at $x = 0$

$$\int_{-\infty}^{+\infty}A_1(t)\,e^{j\omega t}dt=\left(1+R_i e^{-2jk_i l_1}\right)\int_{-\infty}^{+\infty}A^{in}(t)\,e^{j\omega t}dt \tag{4}$$

The mode response at $x = l_3,\ (l_3 > l_2)$

$$\int_{-\infty}^{+\infty} A_2(t)\, e^{j\omega t} dt = T_i e^{-jk_i(l_3-l_2)} \int_{-\infty}^{+\infty} A^{in}(t)\, e^{j\omega t} dt \tag{5}$$

where R_i and T_i are the reflection and transmission coefficients of the given incident i mode. The actual response in term of stress or strain needs to be scaled according to the eigensolution because the mode shape is frequency dependent in general. If the possible mode conversions due to the presence of coupling structure need to be considered, the reflection and transmission coefficient should also be scaled according to the mode structures. It is worth to note that the response due to specific mode does not need the tracing of all the eigenmodes except the incident mode itself.

Time responses.
The force response for unbounded waveguide has been used to compute time signals from the damaged pipe described in section 2.4.1. Responses were recorded from three different locations in the pipe. Sensor 1 is placed at 10 m from the defect to record the reflected signal. Whereas sensor 2 is located with the defect in the same position to record the incident wave. Finally, sensor 3 is placed at 10 m from the defect to detect the transmitted signal. Results are shown in figures 11–13. The excitation is a windowed sinusoidal signal with 5.5 cycles at 14 kHz. We can remark the detection of the defect echo by sensor 1 in figure 11. Travel duration confirms the wave velocity of T(0,1) wave. The attenuation in amplitude of the incident wave in figure 12 and the transmitted wave in figure 13 compared to the incident wave at $t = 0s$ can also be verified.

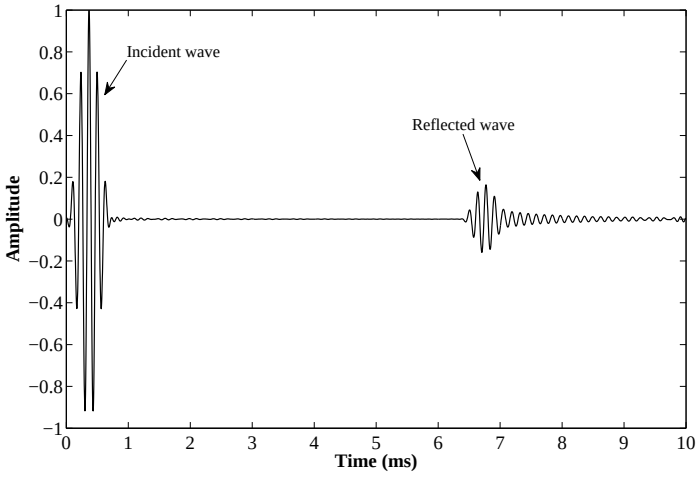

Figure 11: Time response of sensor 1 for reflected signal. Results obtained by WFEM for a damaged pipe with 140 mm outer diameter and 4 mm-thick with T(0,1) mode incident.

Once the inspection system concept verified numerically, the next work was to perform some experimental tests in order to assess its performances in wave generation and defect detection.

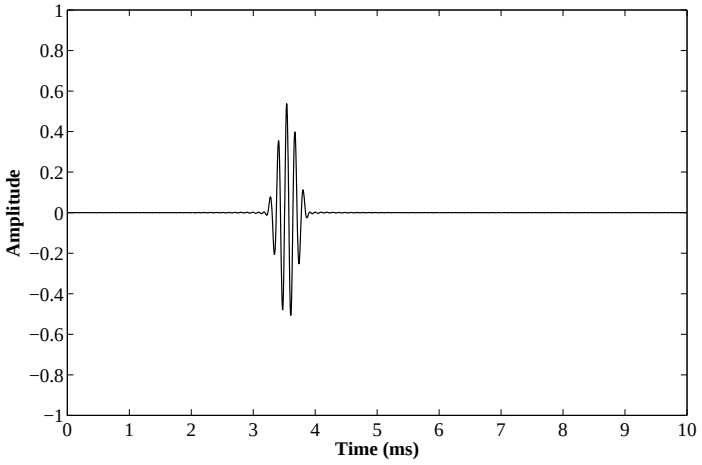

Figure 12: Time response of sensor 2 for incident signal. Results obtained by WFEM for a damaged pipe with 140 mm outer diameter and 4 mm-thick with T(0,1) mode incident.

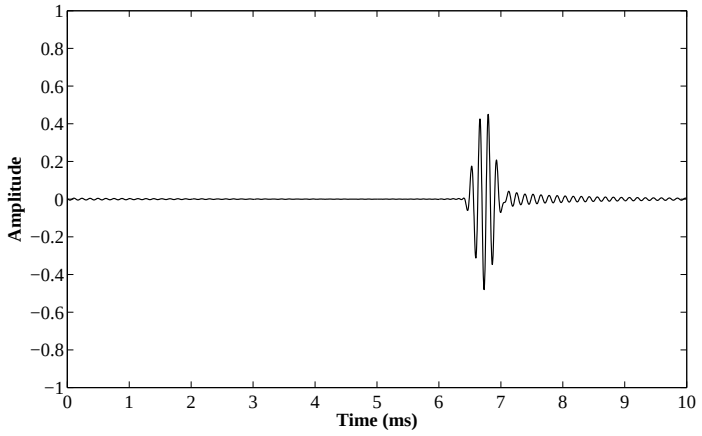

Figure 13: Time response of sensor 3 for transmitted signal. Results obtained by WFEM for a damaged pipe with 140 mm outer diameter and 4 mm-thick with T(0,1) mode incident.

3. Experimental tests and results

A set of experimental manipulations was implemented in order to evaluate the ability of the inspection system to generate torsional waves that can propagate long distances as well as the ability to detect defects in pipes. At first, some tests were performed in a PVC pipe with and without defect. Besides, the same tests were done on a steel pipe. In each case, the wave attenuation was observed and analyzed. Finally, torsional wave propagation in a PVC straight-curved-straight structure was studied and the interaction with damage in a bend has been investigated.

3.1. Test setup

The experimental setup is shown in figure 14. A computer controls the whole system through the LabView software. Digital excitation signal was created and subsequently was sent to the analog voltage output module (*National Instruments PXI-6120*). This latter converts the signal and delivers it to the power amplifier (*Trek Model PZD350A M/S*) whose output was sent to the generator transducers-ring; the individual transducers in the ring being connected in parallel. The voltage output by the power amplifier was from 0 to ±350 V peak AC. Signals captured by the receiver ring was transferred to a dynamic signal acquisition module (*National Instruments PXI-6120*) for digital conversion, and then to a PC for processing and display. In order to improve the signal quality and exclude unwanted modes, received signals from transducers were averaged. The inspection system has two separated rings: one for the excitation of incident waves and the other for the reception of reflected signals. Every ring contains 16 piezoelectric-transducers equally-distributed around the circumference.

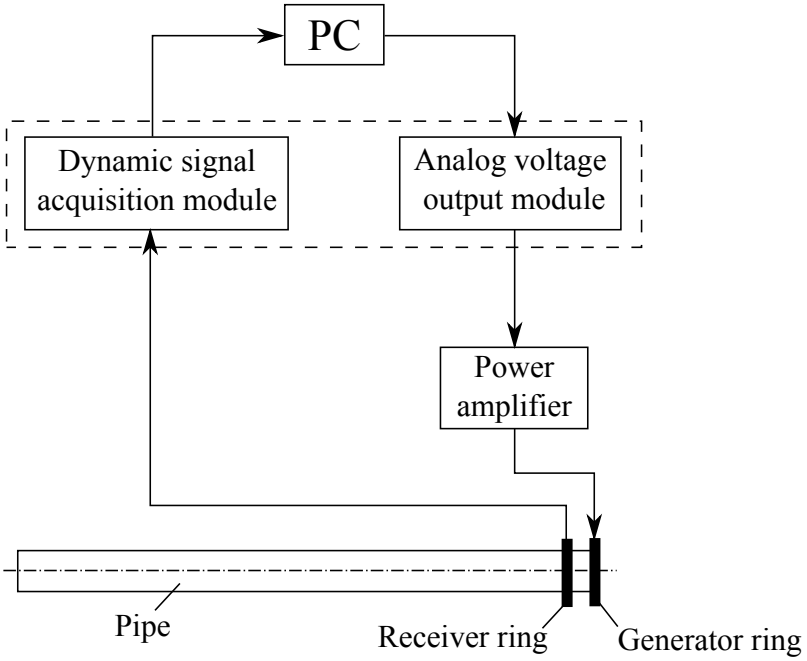

Figure 14: Schematic diagram of the experimental setup.

3.2. Wave propagation on a PVC pipe

Wave propagation depends on the waveguide material and structural damping which characterizes viscoelastic structures. Obviously, the propagation in a PVC material is different from that in steel. Hence, we should know the wave speed of torsional mode in such material to be able to analyze the received experimental signals. The dispersion curves of the group velocity for a PVC pipe with a 140mm outer diameter and a thickness of 3.2mm, that will be used in the next section, is

illustrated in figure 15. These curves were obtained by the Wave Finite Element Method [22–24].

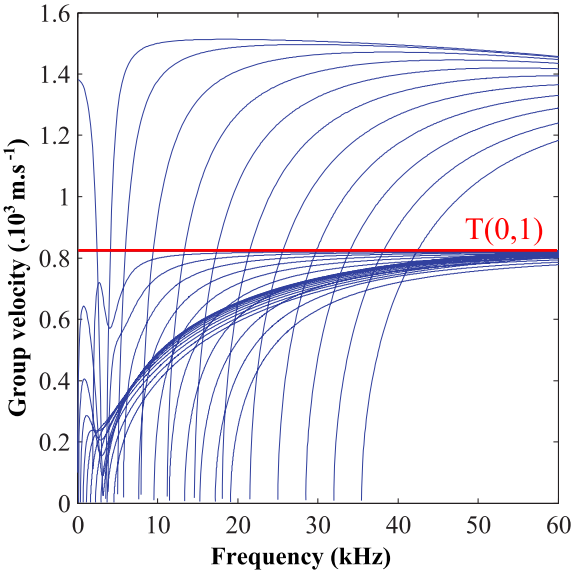

Figure 15: Group velocity dispersion curves for a 140mm outer diameter PVC pipe with a 3.2mm thickness.

The generator and the receiver were mounted on a straight 2.75m-long PVC pipe without any defect. The generator was attached at one end of the pipe; the receiver was placed at 1m from the actuator. Figure 16 shows the time record for the pipe without any defect, whereas figure 17 is the time record under the same experimental conditions but for a pipe with a defect. This latter was located at 1.6m from an end of the pipe where the wave generator was mounted. The defect was a squared through-thickness notch with a circumferential extent of 155mm (35%) and an axial extent of 20mm.

From these curves, we can note that the incident-wave speed corresponds to the torsional wave-speed in this PVC pipe ($\approx 850 m.s^{-1}$). Besides, the shape of the incident impulse is unchanged. This tends to confirm the ability of our generator to create only torsional waves. There is also a clear difference between the two time results. The occurrence of this difference is consistent with the time for a torsional wave to travel back to the receiver from the defect location. Despite the important level of damping in such PVC pipe, the movement can still be caught. The use of a PVC pipe was motivated not only by the easy way to process, to assemble and to cut it, but also because of its important damping. Hence, no reflection from the end could be detected as long as the receiver was not placed further than the middle of the pipe's length. We could then simulate the use of a semi-infinite pipe. With a steel pipe, the needed length would have been impossible to be reasonably obtained.

Even if the torsional waves are not subjected to distortion or any wave-type conversion, the attenuation of their amplitude is inherent to their propagation through a medium which is somehow dissipative. This effect is even increased with the fre-

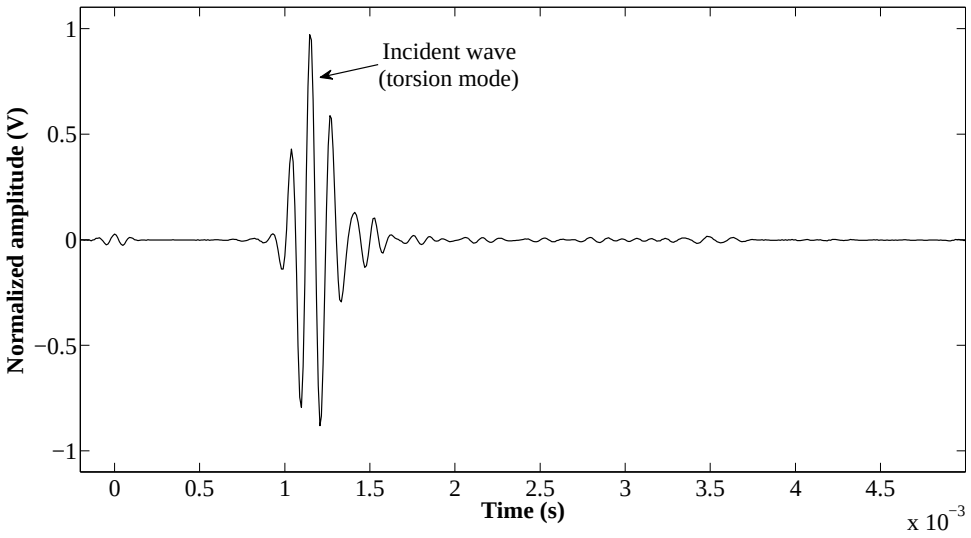

Figure 16: Receiver response from an intact PVC pipe, 3.5-cycle wave at 10 kHz.

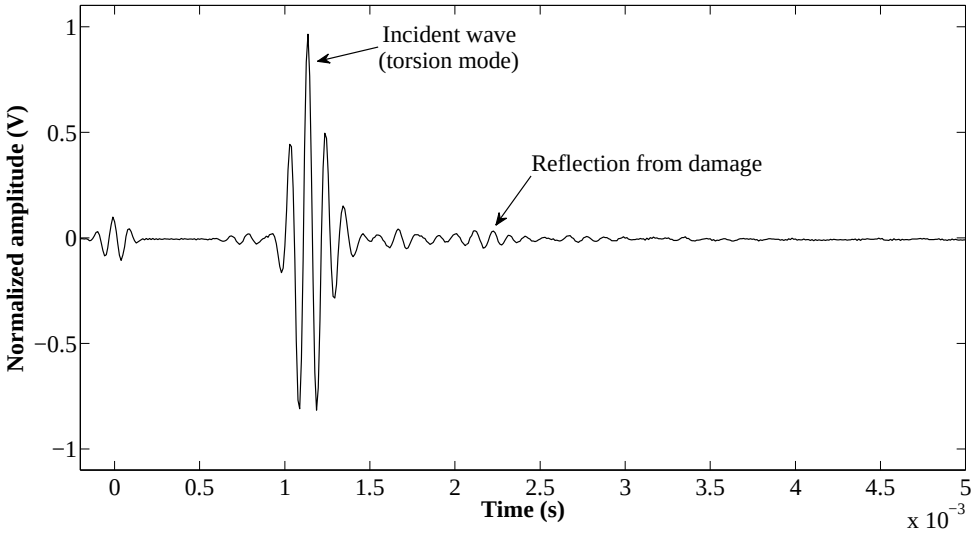

Figure 17: Receiver response from a damaged PVC pipe, 3.5-cycle wave at 10 kHz.

quency at which the input signal is generated. In order to properly appreciate the magnitude of the reflected signal as an effect of the severity of a singularity, the amplitude decrease has to be estimated. For that purpose, the following protocol was performed in order to measure this attenuation. Taking a length of pipe with no singularity but the ends of it, a wave impulse was created by the generator placed at one of this ends. A single cell sensor was placed at a given distance from the generator and the time signal was recorded. The time delay between the impulse emission and the sensor detection was measured for each position along the pipe. As seen on

figure 18, the amplitude of the wave decays with the distance from the generator. The interpolated curve corresponds to an exponential decrease with the distance. It must be mentioned that, for each measurement, the time delay was consistent with the wave-speed of the torsional mode. Moreover, when using a PVC pipe of such a length, the damping is so important that no reflection from the pipe end can reach the measurement point. Therefore, no doubt was possible about the origin of the measured impulse as the incident wave. Regarding the short distance over which the signal is damped, the PVC pipe can be used to simulate the equivalent long distance propagation in a more rigid material.

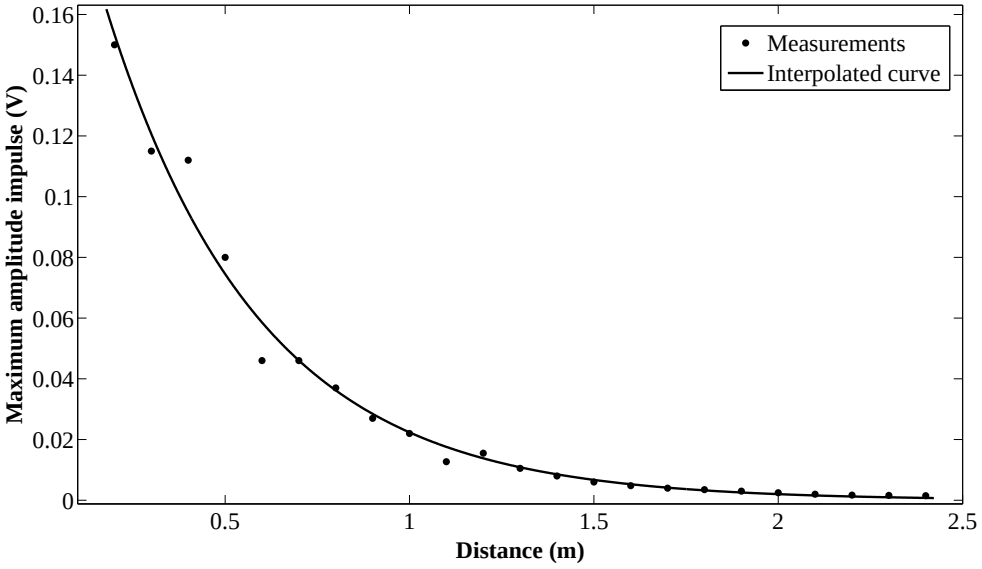

Figure 18: Wave attenuation on a PVC pipe, 5.5-cycles wave at 15 kHz.

3.3. Wave propagation on a steel pipe

3.3.1. Test on an intact pipe

The wave propagation in steel media is quite different from that in PVC one. Indeed, when a steel pipe is used, the wave can travel back and forth, reflecting itself several times at each end of the pipe. Figure 19 presents the time signal recorded on a straight 3m-long steel pipe, 140mm outer diameter, 4mm-thick, with no singularities but the ends of the pipe itself. The impulse wave is a 5.5-cycles signal at 15 kHz. The receiver ring is placed at 1.6m from one end of the pipe where the generator ring is mounted. The first big impulse shown in the figure represents the incident wave. The time delay was consistent with the torsional wave-speed. The second and the third received impulses were the reflections from the two ends of the pipe always traveling with the same speed. Hence, we can conclude that the torsional mode was well excited and was propagated with a sufficient energy to travel along the steel pipe and to reflect from its ends.

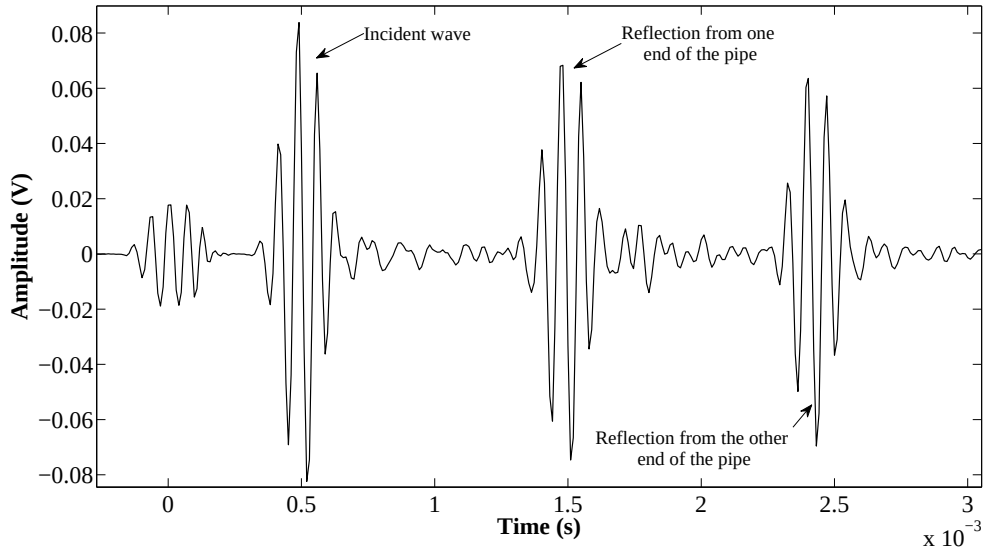

Figure 19: Time signal recorded on an intact steel pipe, 5.5-cycles wave at 15 kHz.

If we want to look more far away, the wave reflections were observed until its attenuation in order to view the damping effect on the wave propagation. The time axis was converted to distance axis basing on the torsional wave speed in steel pipe. Figure 20 shows the wave attenuation with distance. While the first big impulse recorded in the figure represents the incident wave, the other impulses are the successive torsional wave reflections from the ends of the pipe. Their discrepancies in amplitude let us estimate the damping of the signal with the distance. The Hilbert transformation is performed on the time signal in order to get the signal amplitude only. The attenuation in amplitude envelop is consistent with an exponential decrease with distance (e^{-ikx}) of the wave traveling back and forth in the pipe , k being the wavenumber and x being the wave propagation distance.

3.3.2. Test on a damaged pipe

In order to assess the performances of the inspection system for defect detection in steel pipes, a through thickness notch with about 60mm circumferential-extent and 5mm axial-extent was machined at 1.7m from one end of the pipe where the generator and the receiver were located one beside the other. The excitation signal was a 5.5-cycles impulse with a frequency of 10 kHz. Recorded time signal is shown in figure 21. In this curve, we can observe the defect echo located between the incident wave impulse at t=0s and the end of the pipe first-reflection. This confirmation is justified by the time delay of the defect reflection which is consistent with the wave speed of torsional mode.

The next tests performed on the pipe have to verify the sensitivity of the excited waves towards the frequency. Figure 22 shows the time signals responses recorded with a 5.5-cycles excitation impulse at frequencies from 11 kHz to 14 kHz. As we can see, the echo of the notch was detected in the time signals and its location was

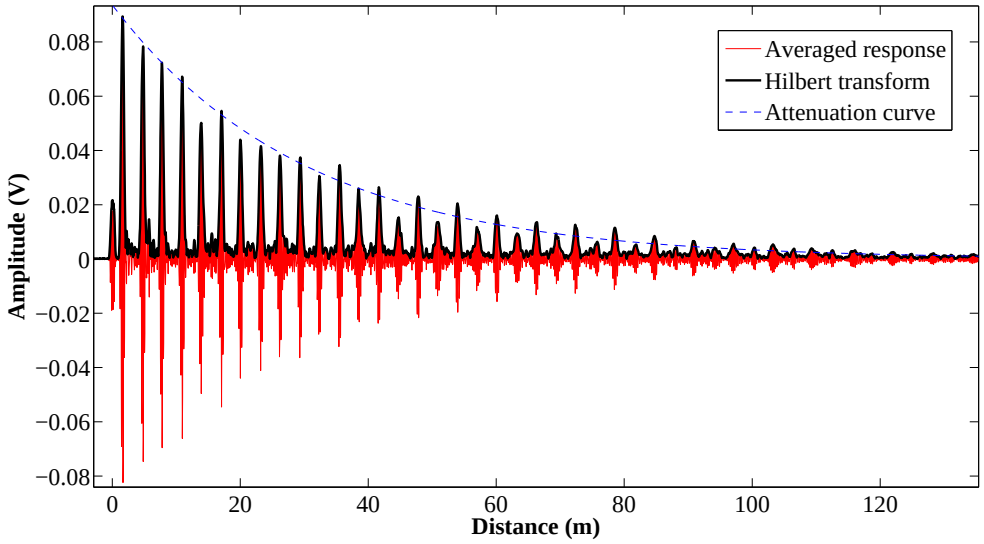

Figure 20: Time signal attenuation with distance on a steel pipe, 5.5-cycles wave at 15 kHz.

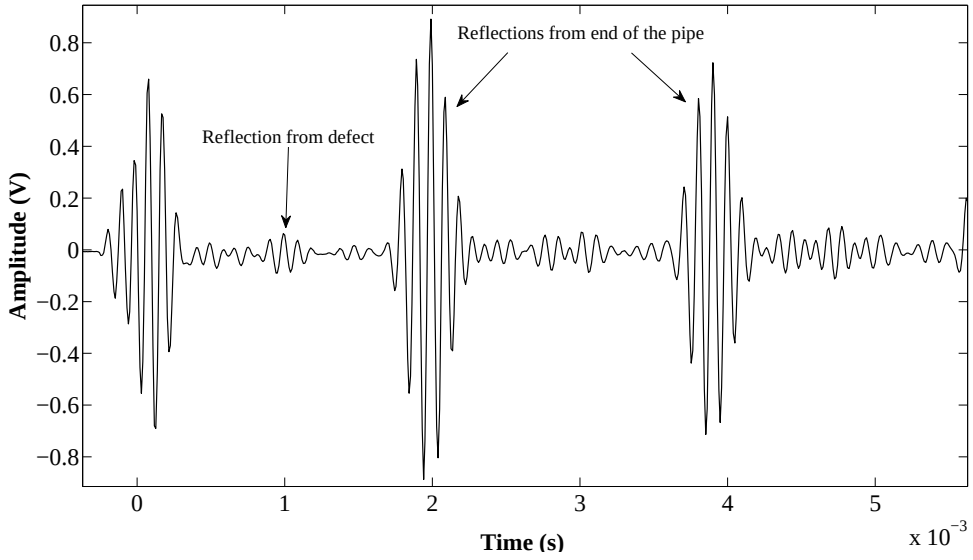

Figure 21: Time signal response from a 140mm outer diameter, 4mm-thick, steel pipe with a defect, 5.5-cycles wave at 10 kHz.

similar to that found by the test at 10 kHz. The generated waves were sensitive to the notch in the frequency range used.

3.3.3. Reflection coefficients calculation

The reflection coefficient is defined as the ratio between the averaged maximum-amplitude of reflected signal from the singularity and the maximum-amplitude of incident signal at the same moment of detection. The reflection coefficient is calcu-

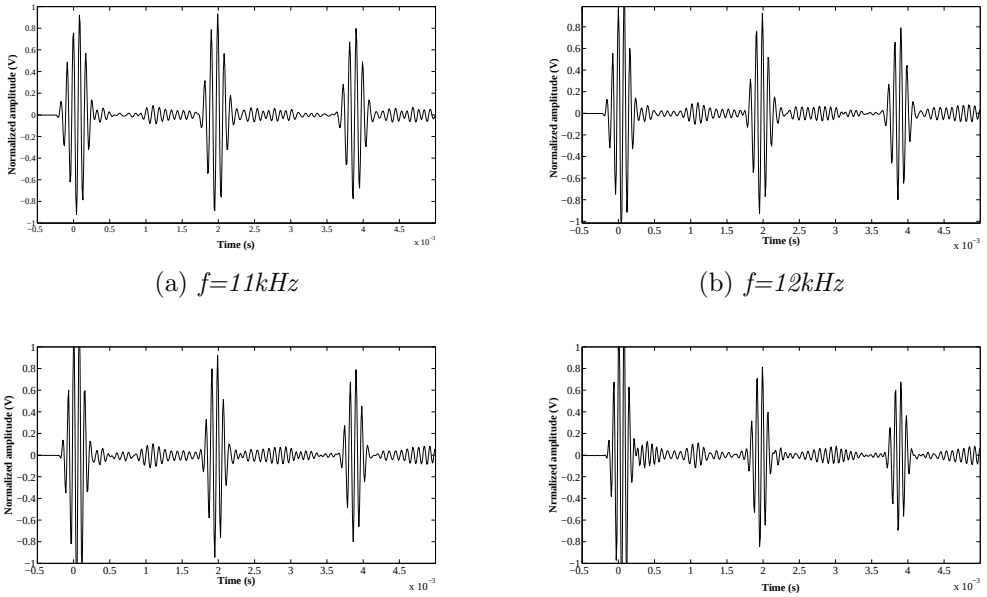

(a) *f=11kHz* (b) *f=12kHz*

(c) *f=13kHz* (d) *f=14kHz*

Figure 22: Time signals from a damaged pipe excited by a 5.5-cycles signal at different frequencies.

lated for the first reflected signal from the singularity, in other words we don't take into account multiple reflections.

Reflection coefficients can be obtained numerically by the Wave Finite Element Method (WFEM) for the steel pipe that was used in experiments with the same notch described in section 3.3.2. Experimentally, more tests were performed with an excitation frequency up to 30 kHz in order to calculate the defect reflection-coefficients associated to each frequency. Once done, the numerical vs. experimental comparison can be made. Figure 23 show the reflection coefficients curve calculated by WFEM, and the experimental points obtained from recorded time signals.

We can note that the experimental points are close to the numerical curve in the 10-15 kHz range. However, in the upper end of the investigated frequency range, the measured reflection coefficients are always way above the numerical ones. In fact, errors can occur in reflection coefficient measurement due to the wave attenuation when we go up in frequency. Signal perturbations such as the background noise may also be responsible for this overestimation. Another possible explanation for this gap, is the uncertainties in parameters that come into play in numerical simulations such as uncertainty in material properties (Young modulus, density ...) or in geometric parameters (pipe wall thickness, diameter, defect size ...).

3.4. Wave propagation through a PVC bend

The torsional wave propagation in PVC bend was studied here in order to investigate wave interaction with discontinuities in a curved pipe. The structure under test was composed of a bend connected to a 1m pipe in each end. The generator was maintained at one end of a pipe and the receiver was mounted in three different

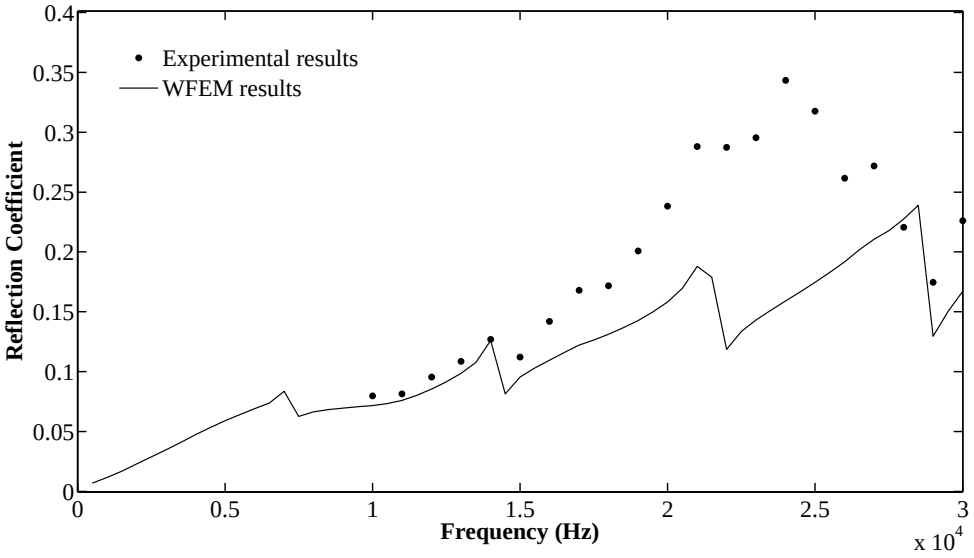

Figure 23: Reflection of the T(0,1) mode depending on frequency for a machined notch in a 140mm outer diameter steel pipe: WFEM and experimental comparison.

monitoring positions to inspect the structure and to control the wave propagation (see figure 24). The first experiments was established with an intact bend, whereas in the second a squared through-thickness notch was machined as described in figure 25. Its circumferential extent is 80mm and its axial extent is 10mm. Tests was made by a 5.5-cycles excitation signal at 15 kHz.

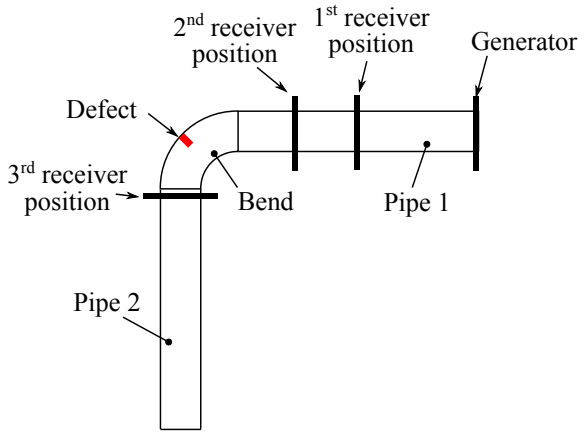

Figure 24: Schematic diagram of the setup used in experiments on straight pipes connected to a bend: different monitoring positions.

Time signals responses in the two cases, intact and damaged bend, was studied and compared. Figure 26 represents results obtained for 3 test configurations as already mentioned in figure 24. In the first configuration, the receiver ring was located at 0.5m from the free end of pipe 1 where the generator ring was mounted.

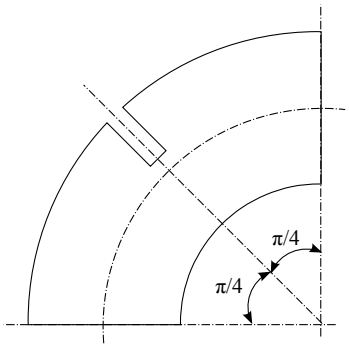

Figure 25: Description of the geometry and the position of the defect in the bend.

In the second configuration, the received ring was moved to a measurement position distant of 0.8m from the excitation point. Finally, the last configuration consists on the monitoring of the transmission wave through the bend; the receiver ring was placed at the end of the bend with which the pipe 2 was connected.

Figure 26(a) shows the time response for the first configuration, in which we can see the impulses corresponding to the incident wave detected by the receiver ring. Unfortunately, the echo of the defect in the bend, which must be detected at about $2.10^{-3}s$, was not observed. This could be justified by the strong structural damping in the PVC material as mentioned in subsection 3.2. Hence, it is necessary to bring even more the receiver ring from the bend, what was done in the second configuration. In figure 26(b), the incident wave was delayed by a 0.3m distance. The defect echo was clear by comparing the two curves of intact and damaged bend. The detection moment corresponds to its spatial location. At this stage, we could remark that no reflection from the free end of pipe 2 was received, always due to the strong damping in PVC media. The third configuration response in figure 26(c) shows the transmission of the incident T(0,1) wave through the bend for both curves. We might note here the appearance of other echoes in the time responses, that could be caused by the mode conversion of the torsional wave to non-axisymmetric mode. The reflection from the end of the pipe 2 was detected, because the transducer ring was more near from it. Comparing the two curves, the one corresponding to the intact bend shows maximum amplitude of the incident wave greater than the other corresponding to the damaged bend. This could be justified by the defect effect on the weakening of the wave transmitted through the bend. A part of the propagating energy was reflected by the defect, while the rest was transmitted and continued traveling.

4. Conclusion

An inspection system prototype for defect detection in pipes was designed in this work. It consists of two rings of 16 piezoelectric transducers for each one. The generator ring aims at creating torsional guided waves that can travel along the pipeline. When they encountered discontinuity in the structure, a part of these waves were

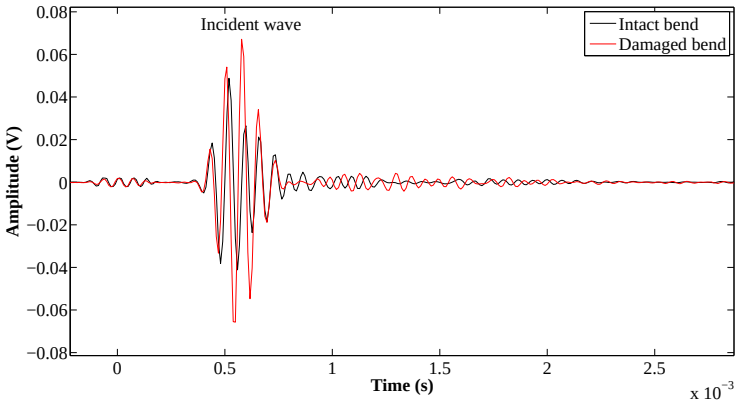

(a)

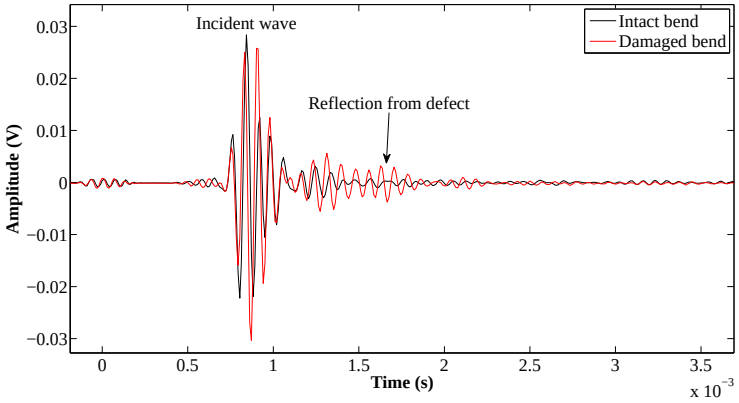

(b)

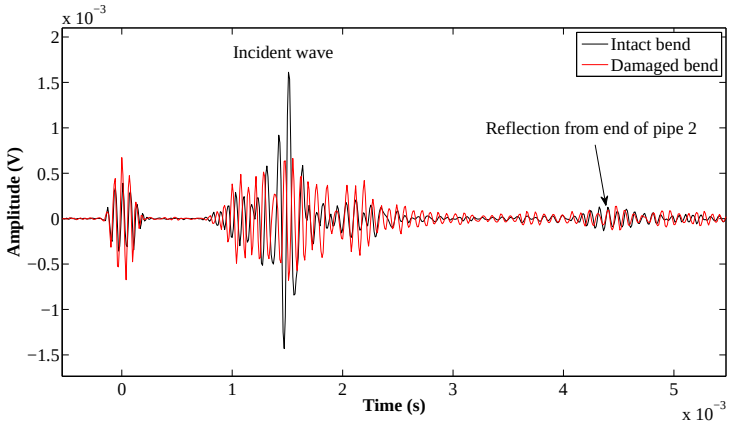

(c)

Figure 26: Time signals obtained for a PVC straight-curved-straight structure excited by a 5.5-cycles signal at 15 kHz. (a) First monitoring position, (b) second monitoring position and, (c) third monitoring position.

reflected back to the receiver ring. The received time signals were then analyzed in order to determine the position and the nature of defects. In the design process, many finite element simulations were carried out on intact and damaged pipes in order to visualize the torsional wave propagation and to verify the sensitivity to defects. Time responses obtained from standard FE and WFE methods have shown the generation of the torsional mode by clamping the piezoelectric transducers in the proper orientation. These simulated signals have proven also the defect detection. Many experimental tests have been performed by the prototype on intact and damaged pipes for two different materials: PVC and steel. Results validate the ability of the inspection system to generate the desired waves. Damping, as a property of structure, was identified and was evaluated experimentally for the two material types. The generated waves could propagate along the pipe and detect discontinuities like defects. The interaction between waves and a machined notch was determined by the estimation of reflection coefficients at different excitation frequencies. These values were compared with WFE results and have shown a good agreement. The wave interaction with curved structure was also evaluated by comparing intact and damaged bends. The obtained time signals have indicated a good detection potential.

This work, dealing with wave propagation and defect detection in simple structures with simple singularities, could be extended by testing more complex structures with more numerous defects. These latter need also to be sized in order to evaluate their severity. The defect-sizing issue should be addressed in future studies.

References

[1] J. Rose, A baseline and vision of ultrasonic guided wave inspection potential, Transactions-American society of mechanical engineers journal of pressure vessel technology 124 (3) (2002) 273–282.

[2] R. Thompson, G. Alers, M. Tennison, Application of direct electromagnetic lamb wave generation to gas pipeline inspection, in: 1972 Ultrasonics Symposium, IEEE, 1972, pp. 91–94.

[3] M. Silk, K. Bainton, The propagation in metal tubing of ultrasonic wave modes equivalent to lamb waves, Ultrasonics 17 (1) (1979) 11–19.

[4] D. Alleyne, P. Cawley, The excitation of lamb waves in pipes using dry-coupled piezoelectric transducers, Journal of nondestructive evaluation 15 (1) (1996) 11–20.

[5] Z. Sun, L. Zhang, J. L. Rose, Flexural torsional guided wave mechanics and focusing in pipe, Journal of Pressure Vessel Technology 127 (2005) 471–478.

[6] D. N. Alleyne, M. Lowe, P. Cawley, The reflection of guided waves from circumferential notches in pipes, Journal of Applied Mechanics 65 (3) (1998) 635–641.

[7] M. J. S. Lowe, D. N. Alleyne, P. Cawley, Defect detection in pipes using guided waves, Ultrasonics 36 (1-5) (1998) 147–154.

[8] J. Rose, S. Pelts, M. Quarry, A comb transducer model for guided wave nde, Ultrasonics 36 (1-5) (1998) 163–169.

[9] H. Shin, J. Rose, Guided waves by axisymmetric and non-axisymmetric surface loading on hollow cylinders, Ultrasonics 37 (5) (1999) 355–363.

[10] J. Li, J. Rose, Excitation and propagation of non-axisymmetric guided waves in a hollow cylinder, The Journal of the Acoustical Society of America 109 (2001) 457–464.

[11] D. N. Alleyne, P. Cawley, The long range detection of corrosion in pipes using lamb waves, Review of Progress in Quantitative NDE 14 (1995) 2073–2080.

[12] M. Lowe, Characteristics of the reflection of lamb waves from defects in plates and pipes, Plenum Publishing Corp., Review of Progress in Quantitative Nondestructive Evaluation.

[13] M. Lowe, D. Alleyne, P. Cawley, The mode conversion of a guided wave by a part-circumferential notch in a pipe, Journal of Applied mechanics 65 (1998) 649–656.

[14] D. Alleyne, P. Cawley, The effect of discontinuities on the long-range propagation of lamb waves in pipes, ARCHIVE: Proceedings of the Institution of Mechanical Engineers, Part E: Journal of Process Mechanical Engineering 1989-1996 (vols 203-210) 210 (35) (1996) 217–226.

[15] A. Demma, P. Cawley, M. Lowe, A. Roosenbrand, The reflection of the fundamental torsional mode from cracks and notches in pipes, The Journal of the Acoustical Society of America 114 (2003) 611–625.

[16] D. Alleyne, B. Pavlakovic, M. Lowe, P. Cawley, Rapid long range inspection of chemical plant pipework using guided waves, Key Engineering Materials 270 (2004) 434–441.

[17] J. Ma, F. Simonetti, M. J. S. Lowe, Scattering of the fundamental torsional mode by an axisymmetric layer inside a pipe, The Journal of the Acoustical Society of America 120 (4) (2006) 1871–1880.

[18] J. Rose, X. Zhao, Flexural mode tuning for pipe elbow inspection, Materials Evaluation 59 (5) (May 2001) 621–624.

[19] T. Hayashi, J. Rose, Guided wave simulation and visualization by a semianalytical finite element method, Materials evaluation 61 (1) (2003) 75–79.

[20] T. Hayashi, K. Kawashima, Z. Sun, J. Rose, Guided wave propagation mechanics across a pipe elbow, Journal of pressure vessel technology 127 (2005) 322–327.

[21] A. Demma, P. Cawley, M. Lowe, B. Pavlakovic, The effect of bends on the propagation of guided waves in pipes, Journal of pressure vessel technology 127 (2005) 328–335.

[22] W. Zhou, M. Ichchou, J.-M. Mencik, Analysis of wave propagation in cylindrical pipes with local inhomogeneities, Journal of Sound and Vibration 319 (1-2) (2009) 335–354.

[23] M. Ichchou, J. Mencik, W. Zhou, Wave finite elements for low and mid-frequency description of coupled structures with damage, Computer Methods in Applied Mechanics and Engineering 198 (15-16) (2009) 1311–1326.

[24] W. Zhou, M. Ichchou, Wave propagation in mechanical waveguide with curved members using wave finite element solution, Computer Methods in Applied Mechanics and Engineering 199 (33-36) (2010) 2099–2109.

[25] J. Barshinger, J. L. Rose, M. J. Avioli, Guided wave resonance tuning for pipe inspection, Journal of Pressure Vessel Technology 124 (3) (2002) 303.

[26] A. Demma, P. Cawley, M. Lowe, A. Roosenbrand, B. Pavlakovic, The reflection of guided waves from notches in pipes : a guide for interpreting corrosion measurements, NDT & E International 37 (3) (2004) 167–180.

[27] W. Zhou, M. Ichchou, Wave scattering by local defect in structural waveguide through wave finite element method, Structural Health Monitoring 10 (4) (2011) 335–349.

Chapter 4

Pipeline inspection using a torsional guided-waves inspection system. Part 1: Defect identification

Abstract

A steel pipeline of about sixty meters long has been tested in this work using a guided-waves technique. The inspection system is a pair of transducer-rings operating with the torsional mode T(0,1) and allows the long-range fast screening of the structure from defined measurement points. Recorded signals had submitted some numerical treatments in order to make them interpretable. Wavelet package analysis was one of them and has allowed the denoising of raw signals. Besides, the Hilbert transform was applied in order to obtain the wave envelope which is more easy to interpret. Processed signals was analyzed to identify defects reflections from structured singularities echoes. The inspection system seems to be efficient for defect detection and localization in long-range pipelines.

Keywords: Pipeline inspection, defect detection, guided-waves, piezoelectric transducers, wavelet denoise, Hilbert tansform.

1. Introduction

Pipelines are widely used in factories working with liquid or gaseous substances that need to be transported at different pressures and temperatures. They are composed of several pipes welded together and other features like bends, flanges, clamps, tees... Continuous monitoring of pipeline technical condition is important for ensuring their performance. However, doing this monitoring by regular non-destructive testing (NDT) methods is quite complicated, as pipelines were generally extended and can be bare, covered by some coatings as well as partially or totally buried underground.

Significant research has been conducted on topics related to pipeline inspection to meet the continuous requirements of civil and industrial users [1–8]. Characterizing existing or developing defects during pipeline inspection is important for the practical application of NDT techniques in order to carry out accurately and efficiently planned maintenance and replacement operations on pipelines. The long range, guided wave ultrasonic technique was developed for the rapid survey of pipelines [9–17]. The principal advantage is that long lengths of pipes in each direction can be examined from a single test point. So, this technique is able to inspect inaccessible areas, such as buried pipes, cased pipes and casings, wall penetrations and under clamps and supports. Consequently, we obtain reduction in the costs of gaining access to pipes for inspection, eliminating extensive removal and reinstallation of insulation, except in the area where the transducers are mounted. Otherwise, 100% of the pipe wall can be tested. Many studies have treated the guided wave technique. Rose et al. [18] have presented a comb transducer with its various design aspects. The comb structure can produce longitudinal axisymmetric waves or longitudinal non-axisymmetric or flexural modes in the pipe. Shin and Rose [19] have discussed the use of both axisymmetric and non-axisymmetric modes propagation

in hollow cylinders and showed the basic principles behind non-axisymmetric wave propagation. Flexural waves were used in defect detection classification and sizing process. Furthermore, other researchers were interested on the longitudinal L(0,2) mode. Alleyne and Cawley [16] have reported on the development of dry-coupled piezoelectric transducers for the excitation of the L(0,2) mode and the detection of reflected guided waves. Alleyne et al. [20, 21] and Lowe et al. [22] have studied the reflection of the L(0,2) axially symmetric mode from notches in pipes, and examined the reflection of mode-converted guided waves with L(0,2) as incident mode [23]. Alleyne and Cawley [24] have measured reflections of the same mode from welds, flanges and pipe supports, and demonstrated that the mode can be propagated under wet or dry insulation. Nevertheless, further tests have employed the torsional mode in the defect detection. A quantitative study of the T(0,1) mode reflection from defects in pipes has been carried out by A. Demma et al. [25] using finite element predictions validated by experiments. D. N. Alleyne et al. [26] have used the T(0,1) mode in the rapid inspection of chemical plant pipework, which includes uncoated or covered pipes. The scattering of the fundamental guided torsional wave by a local axisymmetrical layer coated inside a pipe has been studied by J. Ma et al. [27].

Based on all these previous works, an inspection system allowing generating and receiving guided waves has been designed by the authors. The generation of guided waves is obtained using piezoelectric-transducers array that creates torsional waves. Reflections are detected by other piezoelectric sensors and converted to electrical signals. The contact between the pipe and the transducers is dry and mechanical, so an applied force is used to ensure good coupling. After the transducer ring is positioned around the pipe, the operator starts a rapid test, which automatically sweeps several frequencies collecting data from either side of the ring at once. The propagation of the ultrasonic signal depends on the conditions of the pipe under test. A wide range of about a hundred meters in either direction from the transducer ring position can be obtained when the pipe is in generally good condition and there is a low density of features encountered. The range can be reduced, in one hand, if the pipe is heavily corroded over its length, and in other hand if pipes are buried or coated by viscoelastic materials, which increase wave attenuation. The Wave Finite Element Method, which is a spectral approach, has been employed to compute dispersion curves for the tested pipeline. These curves give relevant information about mechanism of wave propagation through the structure.

In this paper, the essential tools and means that were used to perform the series of experiments on the pipeline are firstly described, including the inspection system by which the tests was operated, the pipeline architecture with the different measurement points, and dispersion curves needed for the knowledge of wave velocities. In the second section, treatments that were applied to recorded signals are detailed as well as the resulting curves in which reflections identification was made.

2. Tools and means of experiments

2.1. The inspection system

The aim of the inspection system (figure 1) is, firstly, to generate torsional waves in a cylindrical pipe. Then, these waves must be guided by the pipe structure and have the necessary energy to travel along large distance. When they encounter features that change the geometry of the pipe such as structured singularities (flanges, elbows, welds, branches ...) or defects (corrosion, notches, metal loss ...) they have to be partially reflected. These echoes are then detected and analyzed in order to provide information about the location and nature of every discontinuity in the pipe.

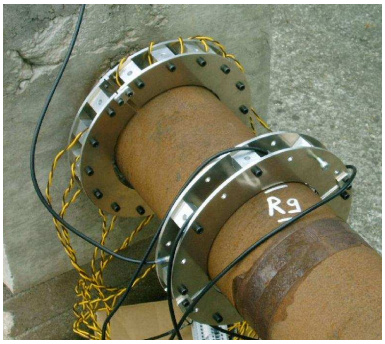

Figure 1: The inspection system: wave-generator and wave-receiver rings.

The choice of the torsional mode T(0,1) to be generated by the designed inspection-system was motivated by its properties. Indeed, it is a non-dispersive mode, i.e. it keeps its speed constant throughout the frequency range. Besides, it is the fastest among torsional waves. It has a high sensitivity to axial and circular defects as well as to internal and external defects. Moreover, T(0,1) is unique among torsional modes in the frequency range used. Finally, it propagates through pipes filled with liquid without much leakage.

The generation of torsional waves is operated by using a number of piezoelectric transducers clamped around the circumference of the pipe. Therefore, a ring of distributed rectangular piezo-transducers working with the inverse piezoelectric effect was provided to create a torsional torque. Receiver side, the piezo-transducers work with the direct piezoelectric effect. Received waves are converted to electric signals and then sent to an acquisition electronic instrumentation. The excitation signal is sinusoidal function modulated by a Hanning window. A typical time record for a 5.5 cycles signal at 10 kHz is shown in figure 2. The magnitude and the number of cycles correspond to the total energy sent into the piezoelectric array. The magnitude, but also the frequency are the main characteristics of the wave input signal. Even if the torsional wave velocity is not frequency dependent, the sensitivity of the propagative wave to the defects is closely correlated to its relative wavelength versus the defect size. In addition, the magnitude and the frequency have both an influence on the ability of waves to travel long distances before the structural damping make

them unperceivable. However, these two parameters have practical limits due to the electronics of the voltage amplifier and of the measurement front-end.

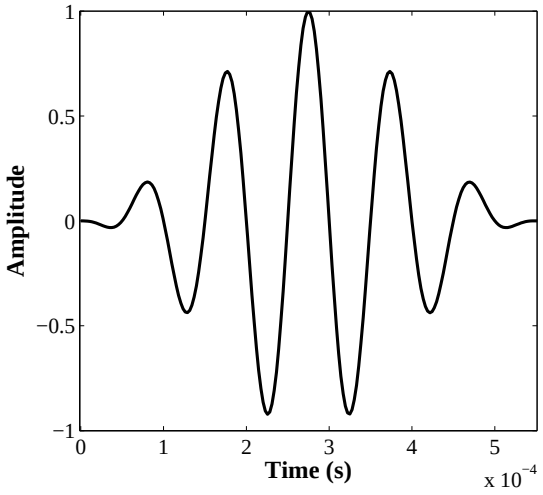

Figure 2: 5.5-cycles narrow-band signal at 10 kHz.

2.2. Pipeline under test

The pipeline under test shown on figure 3 is an industrial mock-up that brings together hollow pipes, structured singularities and machined defects. It was placed in conditions approximating the real industrial environment in order to simulate and involve almost all sources of influence on the measurements to perform. A detailed schema is presented on figure 4. It consists of thirteen pipes welded together coated differently. Pipes 3 and 7 were coated with polyethylene (PE), pipes 2 and 6 were covered with epoxy, and pipes 4 and 8 were wrapped with pitch. The remaining pipes were bare. All of them were in steel and have an outer diameter of 168 mm and a thickness of 11 mm. The material properties are: $E = 2.1 \times 10^{11}\ Pa$, $\rho = 7800\ Kg.m^{-3}$, $\nu = 0.3$. There were also some features in the pipeline: four bends, one tee, two clamps (C1 and C2) and eight concrete blocks (M1 - M8).

2.3. Measurement points

Measurements have been carried out according to nine different positions. For each measurement position, the two rings of the inspection system (generator and receiver) were positioned one far from the other by a known distance; the generator ring was kept in the same position while the receiver ring was mounted in two locations. The latter are required because our inspection system delivers waves in two directions, so two different receiver positions facilitate the analysis and identification of signals. This procedure allows us scanning the entire pipeline. Generator-ring positions are noted from E1 to E9, and receiver-ring positions are noted from R1 to R9 as we can see in figure 5.
Test positions can be classified under four categories:

Figure 3: Tested pipeline.

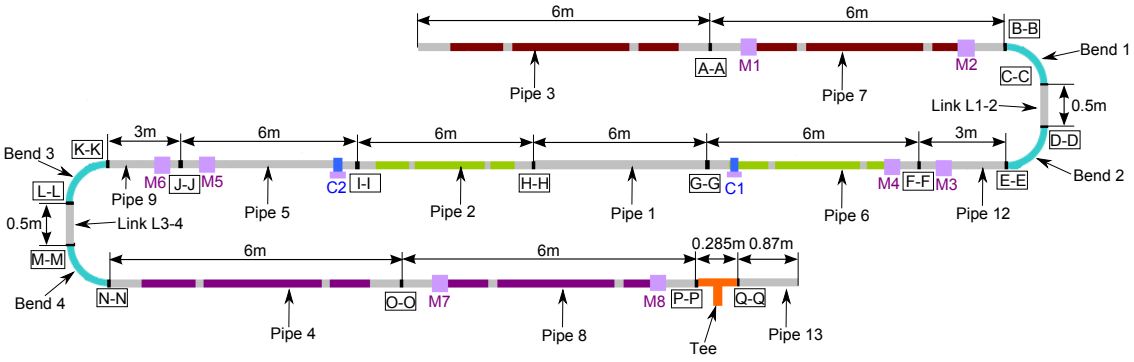

Figure 4: Schema of pipeline under test and geometric specificities.

- On straight pipes:
  - Points 5 and 6: the generator ring (E5/E6) was clamped at the free end of the pipe to ensure the wave propagation in one direction. The generator ring was kept at the same position while the receiver ring (R5) was moved to (R6).
  - Points 1 and 2: the inspection system was mounted in the middle of the pipeline, wave propagation in both directions was expected.
- Near curved pipes: points 3 and 4. The generator ring (E3/E4) was mounted near bend 2 while the receiver ring (R3) was clamped near bend 1 to study reflected and transmitted waves, then it was moved next to the generator ring (R4).
- Mixed zone: points 7 and 8. Here we have a combination of straight and curved pipes.

- Singular point in 9: this is a relatively narrow area and the presence of a tee was studied.

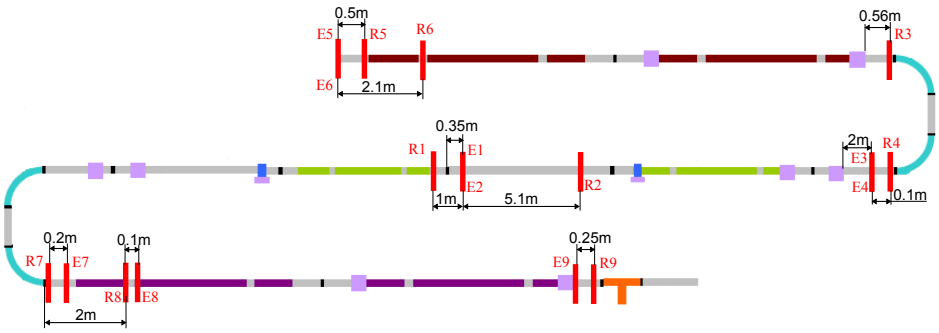

Figure 5: Schema of measurement points performed with the inspection system.

2.4. Dispersion curves

The knowledge of torsional-wave propagation-velocity is necessary for the experimental signals analysis and defects identification. Dispersion curves can be numerically determined using WFEM. Thereafter, the basis of this method is described.

2.4.1. Formulation of the WFE method

The structure can be discretized to identical cells as is shown in figure 6. The

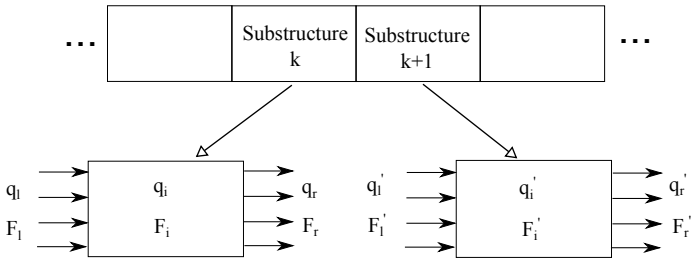

Figure 6: Structure discretized to identical cells (one-dimensional periodic system).

general FE formulation of a typical cell for the 1-D wave propagation in the pipe can be written as

$$\begin{bmatrix} \mathbf{D}_{ll} & \mathbf{D}_{li} & \mathbf{D}_{lr} \\ \mathbf{D}_{il} & \mathbf{D}_{ii} & \mathbf{D}_{ir} \\ \mathbf{D}_{rl} & \mathbf{D}_{ri} & \mathbf{D}_{rr} \end{bmatrix} \begin{Bmatrix} \mathbf{q}_l \\ \mathbf{q}_i \\ \mathbf{q}_r \end{Bmatrix} = \begin{Bmatrix} \mathbf{F}_l \\ \mathbf{F}_i \\ \mathbf{F}_r \end{Bmatrix}, \tag{1}$$

where [D] is the structure dynamic stiffness matrix, subscripts l, r and i denote the left, right and interior components, respectively. Assume that no external force be applied at interior dofs, Equation 1 is condensed as

$$\begin{bmatrix} \mathbf{S}_{ll} & \mathbf{S}_{lr} \\ \mathbf{S}_{rl} & \mathbf{S}_{rr} \end{bmatrix} \begin{Bmatrix} \mathbf{q}_l \\ \mathbf{q}_r \end{Bmatrix} = \begin{Bmatrix} \mathbf{F}_l \\ \mathbf{F}_r \end{Bmatrix}, \tag{2}$$

where

$$\mathbf{S}_{ll} = \mathbf{D}_{ll} - \mathbf{D}_{li}{\mathbf{D}_{ii}}^{-1}\mathbf{D}_{il} \ ; \quad \mathbf{S}_{lr} = \mathbf{D}_{lr} - \mathbf{D}_{li}{\mathbf{D}_{ii}}^{-1}\mathbf{D}_{ir} \ ;$$
$$\mathbf{S}_{rl} = \mathbf{D}_{rl} - \mathbf{D}_{ri}{\mathbf{D}_{ii}}^{-1}\mathbf{D}_{il} \ ; \quad \mathbf{S}_{rr} = \mathbf{D}_{ri} - \mathbf{D}_{ri}{\mathbf{D}_{ii}}^{-1}\mathbf{D}_{ir}.$$

Therefore, only the interface dofs are retained. Provided that there is no wave distortion induced by the material or geometric variation in the propagation direction, namely x axis, the wave motions can be theoretically treated using the exponential function e^{-ikx} ($i = \sqrt{-1}$). Hence, the displacement and force relationships between two adjacent cells are (see figure 6)

$$\mathbf{q}_l' = \mathbf{q}_l e^{-ikd}, \quad \mathbf{F}_l' = \mathbf{F}_l e^{-ikd}, \tag{3}$$

where d is the length of the cell in wave propagation direction. The time dependent term $e^{i\omega t}$ is omitted here, and elsewhere for other expressions.

Considering the displacement continuity $\mathbf{q}_l' = \mathbf{q}_r$ and force equilibrium condition $\mathbf{F}_l' = -\mathbf{F}_r$, Equation 2 can be written as

$$\begin{bmatrix} \mathbf{S}_{ll} & \mathbf{S}_{lr} \\ \mathbf{S}_{rl} & \mathbf{S}_{rr} \end{bmatrix} \begin{Bmatrix} \mathbf{q}_l \\ \lambda\mathbf{q}_l \end{Bmatrix} = \begin{Bmatrix} \mathbf{F}_l \\ -\lambda\mathbf{F}_l \end{Bmatrix}, \tag{4}$$

where $\lambda = e^{-ikd}$ denotes the propagation constant; $\mathbf{S}_{rl}$, $\mathbf{S}_{ll}$ and $\mathbf{S}_{rr} \in \mathbb{C}^{\mathbf{N}\times\mathbf{N}}$. Eliminating the force component of Equation 4 leads to a special case of quadratic eigenvalue problem for (λ, $\mathbf{q}_l$)

$$[\mathbf{S}_1/\lambda + \mathbf{S}_2 + \lambda\mathbf{S}_1^T]\boldsymbol{\varphi} = \mathbf{0}, \tag{5}$$

where $\boldsymbol{\varphi} = \mathbf{q}_l$, $\mathbf{S}_1 = \mathbf{S}_{rl}$, $\mathbf{S}_2 = \mathbf{S}_2^T = \mathbf{S}_{ll} + \mathbf{S}_{rr}$.

If the spectral problem for both propagating and evanescent modes is of interest, the propagation constant must be obtained for a given frequency in order to find the dispersion relationship. The eigenfunction may be solved using the classical linearization method to obtain the dispersion relationship and eigenmodes:

$$\begin{bmatrix} \mathbf{0} & \mathbf{S}_1 \\ -\mathbf{S}_1 & -\mathbf{S}_2 \end{bmatrix} \begin{Bmatrix} \boldsymbol{\varphi} \\ \lambda\boldsymbol{\varphi} \end{Bmatrix} = \lambda \begin{bmatrix} \mathbf{S}_1 & \mathbf{0} \\ \mathbf{0} & \mathbf{S}_1^T \end{bmatrix} \begin{Bmatrix} \boldsymbol{\varphi} \\ \lambda\boldsymbol{\varphi} \end{Bmatrix}. \tag{6}$$

The solution of such standard generalized eigenvalue problem yields the displacement vectors $\mathbf{q}_l^j$ ($j = 1, 2, \ldots, 2N$) for propagating and non-propagating waves. The corresponding force vectors can be written as

$$\mathbf{F}_l^j = \left(\mathbf{S}_{ll} + \lambda^j\mathbf{S}_{lr}\right)\mathbf{q}_l^j, \tag{7}$$

which can be obtained from Equation 4.

Another structured linearization method may be used to directly calculate both the displacement and the force vectors for propagating and non-propagating modes:

$$\begin{bmatrix} -\mathbf{S}_{ll} & \kappa\mathbf{I} \\ \mathbf{S}_{rl} & \mathbf{0} \end{bmatrix} \begin{Bmatrix} \boldsymbol{\varphi} \\ \boldsymbol{\psi} \end{Bmatrix} = \lambda \begin{bmatrix} \mathbf{S}_{rl}^T & \mathbf{0} \\ -\mathbf{S}_{rr} & -\kappa\mathbf{I} \end{bmatrix} \begin{Bmatrix} \boldsymbol{\varphi} \\ \boldsymbol{\psi} \end{Bmatrix} \tag{8}$$

where $\kappa = \|\mathbf{S}_{rl}\|$, $\boldsymbol{\psi} = \mathbf{F}_l/\kappa$.

The symmetry of the spectrum in Equation 6 might be lost due to roundoff errors, if no preservation routine is used in the eigenvalue computation. In the case of large matrices produced, it is better to employ the structured linearization method proposed by Zhong and Williams [28], which calculates the reciprocal pairs $(\lambda,\ 1/\lambda)$ by constructing Equation 9 to the eigenvalue problem about two skew symmetric matrices

$$\begin{bmatrix} \mathbf{S}_{rl} - \mathbf{S}_{rl}^T & -(\mathbf{S}_{rr} + \mathbf{S}_{ll}) \\ (\mathbf{S}_{rr} + \mathbf{S}_{ll}) & \mathbf{S}_{rl} - \mathbf{S}_{rl}^T \end{bmatrix} \begin{Bmatrix} \boldsymbol{\varphi} \\ \lambda\boldsymbol{\varphi} \end{Bmatrix} = \mu \begin{bmatrix} \mathbf{0} & \mathbf{S}_{rl} \\ -\mathbf{S}_{rl}^T & \mathbf{0} \end{bmatrix} \begin{Bmatrix} \boldsymbol{\varphi} \\ \lambda\boldsymbol{\varphi} \end{Bmatrix}, \tag{9}$$

where $\mu = (1/\lambda + \lambda)$. The pairing of eigenvalues is automatically guaranteed, as the linearization itself preserves the symmetry. However eigensolution of Equation 9 need specific iteration procedure to be developed [28], so does the linearization method proposed by Mackey et al. [29]. As the left system matrix is most likely well-conditioned, Equation 9 can be formulated as the standard eigenvalue problem:

$$[\mathbf{S}_{Std}] \begin{Bmatrix} \boldsymbol{\varphi} \\ \lambda\boldsymbol{\varphi} \end{Bmatrix} = \frac{1}{\mu} \begin{Bmatrix} \boldsymbol{\varphi} \\ \lambda\boldsymbol{\varphi} \end{Bmatrix}, \tag{10}$$

where $[\mathbf{S}_{Std}]$ equals to the left division of the right system matrix by the left one. This transformation may not be realized explicitly which usually leads to a dense matrix. The eigenvalues $1/\mu$ with the larger real parts correspond to the wavenumbers with the smaller amplitudes of imaginary parts, although not very strictly. This allows the ARPACK routine for nonsymmetric complex eigenvalue problems to be used [30], which is faster than the QZ algorithm if only a few eigenpairs are of interest.

It should be mentioned that if the dispersion relationships in undamped systems are of interest, Equation 5 can be re-formed to the generalized eigenvalue problem for ω^2, which provides a rapid dispersion calculation scheme

$$\tilde{\mathbf{K}}\boldsymbol{\varphi} = \omega^2\tilde{\mathbf{M}}\boldsymbol{\varphi} \tag{11}$$

where

$$\begin{cases} \tilde{\mathbf{K}} = \mathbf{K}_{rl}/\lambda + \mathbf{K}_{ll} + \mathbf{K}_{rr} + \lambda\mathbf{K}_{rl}^T \\ \tilde{\mathbf{M}} = \mathbf{M}_{rl}/\lambda + \mathbf{M}_{ll} + \mathbf{M}_{rr} + \lambda\mathbf{M}_{rl}^T \end{cases}$$

Both $\tilde{\mathbf{K}}$ and $\tilde{\mathbf{M}}$ are Hermitian matrices when $k \in \mathbb{R}$. The stable eigenfunction facilitates the mode tracing, since the property that eigenvectors of distinct eigenvalues

are mutually orthogonal can be used by introducing the criterion $\mid \boldsymbol{\varphi}_{i+1}^{T}\tilde{\mathbf{M}}\boldsymbol{\varphi}_{i} \mid$ to classify the waves with different normalized modal shape.

If the dispersion relation is available, the time-averaged axial energy flow in the pipe wall is

$$I = \frac{1}{T}\int_{0}^{T} \mathbf{F}^{H}\dot{\mathbf{q}}\, dt, \tag{12}$$

which is consist of the effective part and the standing part. Thus the power flow can be written in Poynting vector:

$$I_j = \langle P \rangle = \frac{1}{2} Re\left\{ i\omega \left(\mathbf{F}_l^j\right)^H \mathbf{q}_l^j \right\}, \tag{13}$$

where superscript H denotes Hermitian transpose.

The group velocity of a modulated wave is $V_g = \partial\omega/\partial k_R$, where k_R is the real part of the wavenumber. It equals to the energy velocity (or signal velocity) for the waves in undamped or slightly damped media. As to the waves in the highly absorptive media, it is well known that the group velocity cannot describe the manner that signal travels. The energy velocity is defined as the quotient of the time average energy flow and the energy density at the cross-section normal to the propagating axis

$$V_e = \frac{\langle P \rangle}{\langle E \rangle}, \tag{14}$$

where $E = T + U$, which stands for the sum of potential and kinetic energy density at the cross-section. Considering that the typical cell with length d, expression Equation 14 for energy velocity may be defined at the mid cross-section, where

$$\langle P_{mid} \rangle = \frac{1}{2} e^{k_I d} Re\left\{ i\omega \mathbf{F}_l^H \mathbf{q}_l \right\}, \tag{15}$$

where k_I is the imaginary part of the wavenumber. The average kinetic and potential energy density at the mid cross-section (at $d = 2$) is approximated as

$$\langle T \rangle = \frac{1}{4d}\omega^2 \mathbf{q}_{lr}^H \mathbf{M} \mathbf{q}_{lr},\ \langle U \rangle = \frac{1}{4d} \mathbf{q}_{lr}^H \mathbf{K} \mathbf{q}_{lr}, \tag{16}$$

where $\mathbf{q}_{lr} = (\mathbf{q}_l^T, \mathbf{q}_r^T)^T$, $\mathbf{M}$ and $\mathbf{K}$ are the mass and stiffness matrices condensed on the left and right boundaries. Thus, expression Equation 14 for energy velocity becomes

$$V_e = \frac{2de^{k_I d} Re\left\{ i\omega \mathbf{F}_l^H \mathbf{q}_l \right\}}{\mathbf{q}_{lr}^H (\mathbf{K} + \omega^2 \mathbf{M}) \mathbf{q}_{lr},} \tag{17}$$

which depend on the eigensolution of a given frequency.

The spectral eigensolutions sometimes need to be classified for the computational purpose. Equation 4 can be used to trace the kindred modes at different frequencies. However it concerns the operation of a large number of vectors. An alternative is to combine the curve tracing of the wave numbers with the mode assurance criterion (MAC). Polynomial fitting can be used to predict the eigenvalue of the subsequent

frequency step. In case of more than one solution being found within the prescribed tolerance δ, a criterion

$$\varepsilon = \left|\varphi_{f+\Delta f}^{H} \cdot \varphi_f\right|, \tag{18}$$

can be introduced to distinguish the kindred modes from the others when $\varepsilon\,(\varepsilon \leq 1)$ is maximum, where φ_f and $\varphi_{f+\Delta f}$ are the unitary displacement vectors at frequency step f and its subsequent frequency step $f + \Delta f$. Thus the eigenmodes can be traced by the consistency rather than the orthogonality. The unitary displacement vectors may not contain all the DOFs if only one or some of the low order modes need to be classified (partial modal assurance criterion, PMAC).

2.4.2. Numerical results

Dispersion curves of wave propagation in the pipe under test were obtained numerically by the WFEM. Figures 7 and 8 show, respectively, group velocity and phase velocity for the waves that can be present in the frequency range [0-100] kHz. From these figures, we can determine the wave velocity of T(0,1) mode: $V_T = 3230$ m/s. The knowledge of this velocity is very important because this parameter was used in signals analysis and interpretations. The T(0,1) mode keeps its velocity constant throughout the frequency range, so we can use its value at any excited frequency.

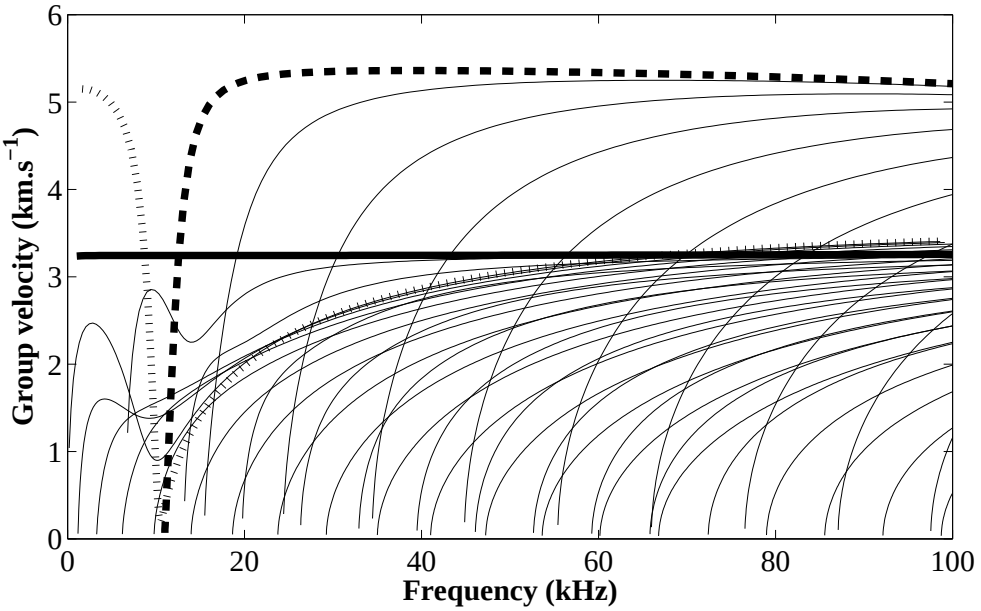

Figure 7: Group velocity dispersion curves computed by WFEM for a steel pipe, outer diameter 168 mm, thickness 11 mm. Solid bold line: torsional mode T(0,1); dot line: longitudinal mode L(0,1); dash line: longitudinal mode L(0,2); solid lines: flexural modes F(n,m).

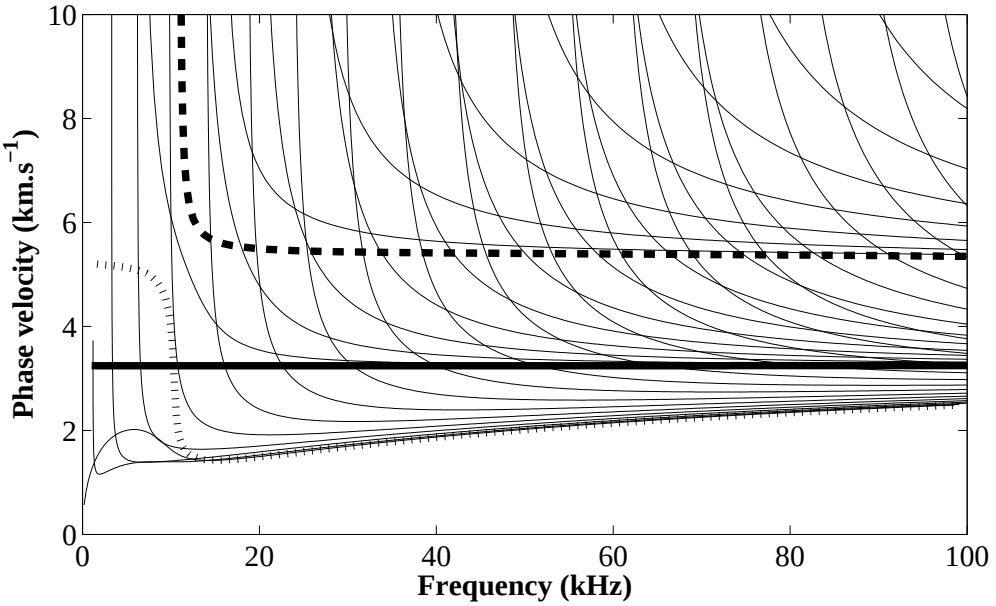

Figure 8: Phase velocity dispersion curves computed by WFEM for a steel pipe, outer diameter 168 mm, thickness 11 mm. Solid bold line: torsional mode T(0,1); dot bold line: longitudinal mode L(0,1); dash bold line: longitudinal mode L(0,2); solid lines: flexural modes F(n,m).

3. Experimental investigation

3.1. Signal treatments

Original signals recorded from the pipeline were hard to interpret. Hence, they need to be treated in order to make curves reading and interpretation easier. Some treatments were performed on these responses involving some signal processing tools. The procedure is illustrated on figure 9 and described below.

Firstly, raw signals were recorded by each sensor in the inspection system. So, we obtained 16 different signals from each channel. Secondly, these responses were processed by the *Wavelet denoise* tool in order to eliminate noise and perturbations that could affect them. Thirdly, denoised signals were averaged and we obtained one denoised response from this measurement. Fourthly, Hilbert Transform was applied in order to get the time signal envelope. Finally, this curve was analyzed and peaks identification was made.

3.1.1. Signal denoising

Raw signals were very noisy due to perturbations coming from background noise or external vibration sources. These signals need to be processed in order to improve the signal-to-noise ratio. The *Wavelet Denoise* is a powerful tool which is based on thresholding the Discrete Wavelet Transform (DWT) of a signal and then reconstructing it. The DWT breaks down approximations successively and acts as low pass filters by removing the details (noise) after a signal decomposition at a certain level. The *Wavelet Packet Analysis* allows splitting both approximations

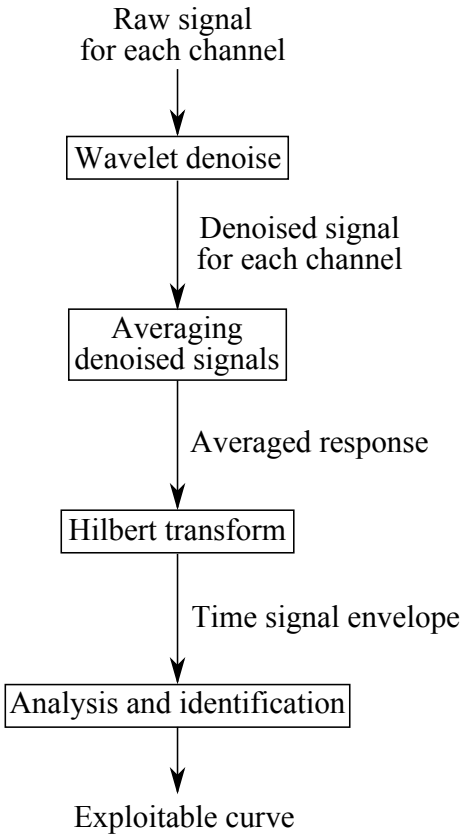

Figure 9: Diagram of experimental-signals treatment.

and details and then removal of noise components, so the rectified signals become smoother. The inverse wavelet transform of the thresholded transform coefficients is the denoised signal. This technique has shown, in many studies [31–35], a good S/N ratio improvement much better than obtained through a bandpass filter. After a threshold value is applied to the levels of detail, the echoes can be better visualized for denoised than original signals. In figure 10, we can see the decomposition of a signal recorded from a single transducer channel. Response was obtained at 10 kHz for the first measurement point in the pipeline. The original signal s was split into details ($d1$ to $d6$) and approximations ($a1$ to $a6$) according to figure 11 using the *Symlet Wavelet (sym8)*. The decomposition until the 6^{th} level seems to be sufficient since it allows the elimination of noise details from $d1$ to $d4$. The $a6$ approximation represents a low-frequency perturbation corresponding to the mains voltage (50 Hz), so it should be avoided. The sum of $d5$ and $d6$ represents the denoised signal. The result of the denoising tool can be observed in figure 12, which contains a comparison between original and processed signals. The added value is evident here. The same process was used for all recorded raw-signals.

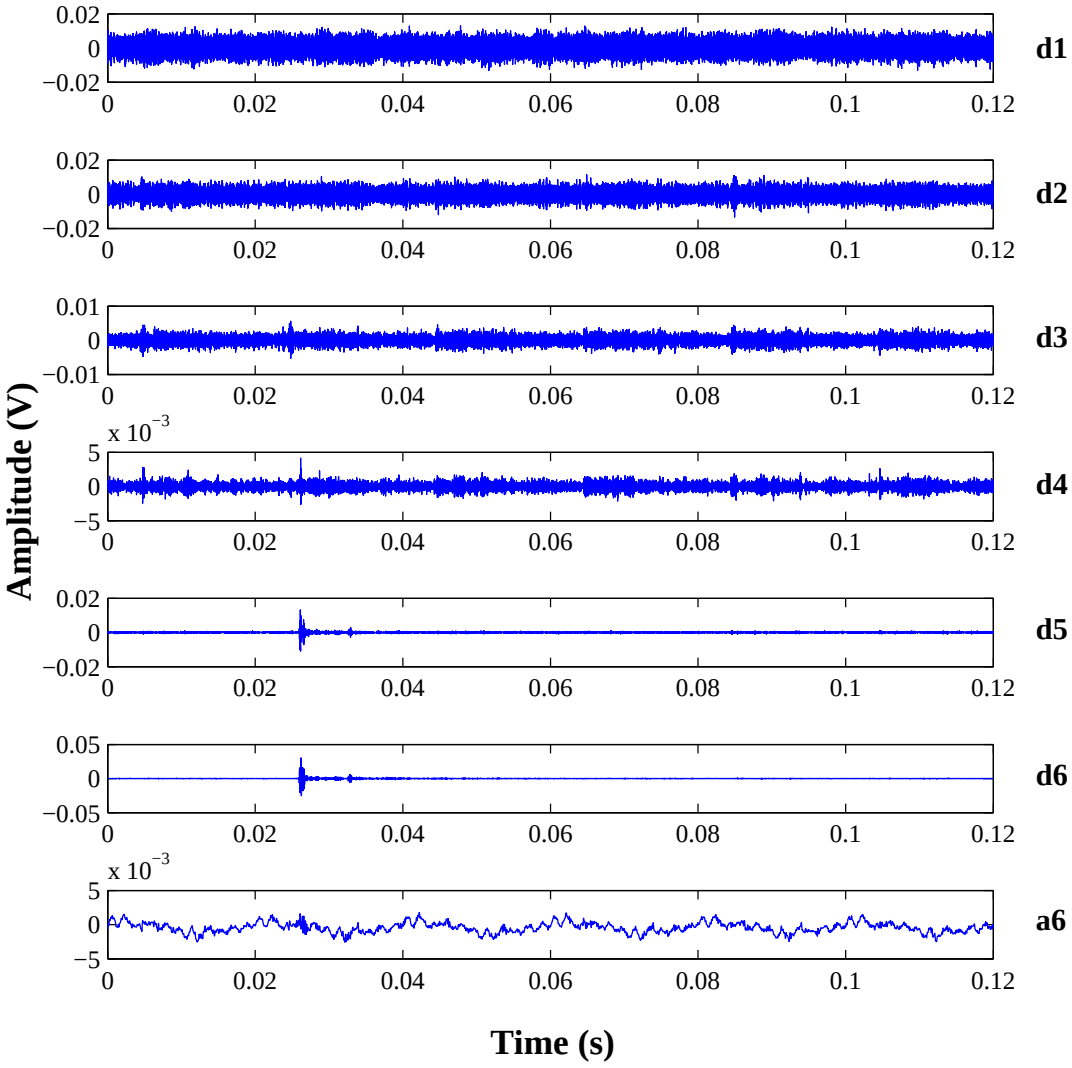

Figure 10: Signal decomposition into details of one channel response at 10 kHz, measurement point 1.

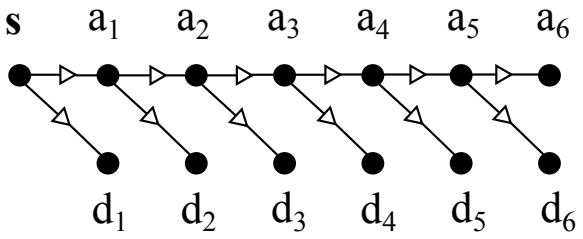

Figure 11: Wavelet decomposition tree.

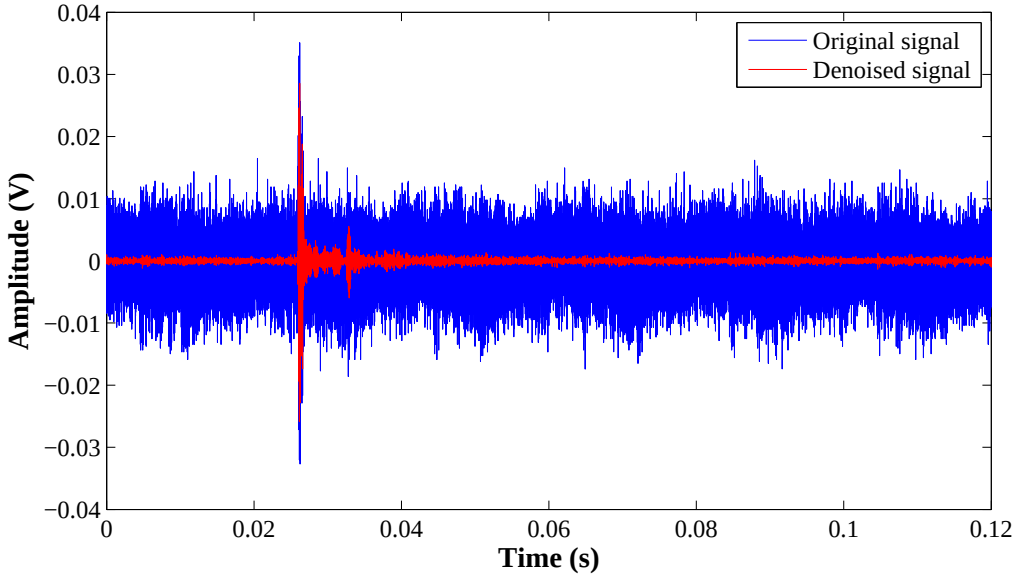

Figure 12: Comparison between original and denoised signals at 10 kHz for the 1st measurement point.

3.1.2. Averaging denoised signals

The aim of averaging signals was to eliminate unwanted modes that could be generated by the wave generator (due to mounting faults or design imperfections). These modes were essentially non-axisymmetric waves, which were dispersive and make obtained curves difficult to interpret. The average should suppress these waves on condition that sensors were equally distributed on the circumference of the pipe.

3.1.3. Hilbert transform

The Hilbert Transform (HT) is one of the integral transforms (like Laplace and Fourier). The HT of a real-valued function $x(t)$ extending from $-\infty$ to $+\infty$ is a real-valued function $\tilde{x}(t)$ defined by Equation 19 [36, 37].

$$H[x(t)] = \tilde{x}(t) = \pi^{-1} \int_{-\infty}^{+\infty} \frac{x(\tau)}{t-\tau} d\tau. \tag{19}$$

The HT application to the initial signal provides some additional information about an amplitude, instantaneous phase and frequency of vibrations. Physically, the HT is an equivalent to a special kind of a linear filter, where all the amplitudes of the spectral components are left unchanged, but their phases are shifted by $-\pi/2$ [36, 38]. The envelope means an integral curve which determines a singular position of the initial function [39]. The envelope may be constant (in which case the wave is a continuous harmonic) or may vary with time. The form or the shape of the instantaneous-amplitude variation is called a wave envelope. By using the HT, the rapid oscillations can be removed from the amplitude modulated signal to produce a direct representation of the slow envelope alone. An amplitude modulated wave

$x(t) = A(t)cos\psi(t)$ should be processed in some way to preserve only the modulating envelope function $A(t)$ and to throw away the oscillations $cos\psi(t)$.
When measured data contains damage events or an information on a damage condition of the structure, it is important to extract as much of this information from the data as possible. The HT is able to not only detect the presence of a defect in the structure, but also quantify the extent of the damage [40]. Thus, the modal-based methods can identify quantitatively structural system properties before and after damages, including the modal mass, stiffness, and damping matrices. Several recently appeared applications of the HT methods to structural dynamics are devoted to damage detection by using experimentally measured mode shapes and natural frequencies [41].
In this work, the HT was applied to denoised and averaged signals in order to get only the amplitudes envelope. Thus, oscillations were omitted and the full concentration, when identifying reflections, was made on these envelope curves.

3.1.4. Analysis and identification

The defect identification was established by analyzing time signals in two measuring points for each inspected area of the pipeline. This allows to verifying and validating defect positions relative to the inspection-system location. Indeed, for each inspected zone, we recorded the time signal associated with a first measuring point (for example point 5), then the receiver ring was moved while keeping the generator ring in place (point 6 in our example) and we re-recorded the response. Therefore, for any reflecting discontinuity in the pipeline, there will be a temporal shift of the peak associated with it by comparing the two responses. Taking into account reflections associated with structured singularities (concrete blocks, clamps ...), which have known locations in the pipeline, we compare every time two signals to confirm the defect positions.

3.2. Defect identification and results discussion

In this subsection, we present experimental curves obtained after numerical treatments and analysis performed on the raw signals. Responses were recorded at different excitation frequencies. In these curves the passage of the incident wave was used to validate the estimation on the propagation velocity of torsional waves. The peak corresponding to the incident wave is distinguished when the receiver is far from the transmitter of a certain distance. Figures from 13 to 21 shows the time signals obtained after numerical treatments for all measurement points at a chosen frequency. In each figure, the defects and features identification was mentioned. The x-axis corresponds to the distance traveled by the wave as it leaves the wave-generator ring E to return to the receiver ring R. The peaks correspond to the identified reflections coming from obstacles and captured by R. Spatial representation facilitates the location of detected obstacles.

Based on the plan of the pipeline and by calculating the propagation duration of the torsional wave, we manage to sort out the singularities of architecture, which are

known, and the singularities of the defects. The identification of successive reflections of known singularities can be made by correcting the signal amplitude using the estimation of the wave attenuation.
Regarding the measurement points 1 and 2, the inspection system was placed in an area where waves can propagate in both directions, so we expected to detect echoes from discontinuities located on both right and left sides. By examining figures 13 and 14, and focusing on the right side, we see that the measured distance between clamp C1 and concrete wall M4 (4.2 m in figure 13 and 4.5 m in figure 14) is close to the real distance of 4.4 m, while the weld G-G, which is shown in figure 13, is hidden in figure 14 by the peak of the incident signal. The measured distance between G-G and C1 of 0.6 m is close to the real one which is about 0.8 m. With regard to the left side, the distance between the echoes of the weld I-I and the clamp C2 are estimated to 0.65 m in figure 13, close to that calculated in figure 14 (0.6 m). The distance between C2 and M5 is evaluated to 4.24 m in figure 13 and 4.2 m in figure 14; these values were close to the real distance in the pipeline. These remarks show that moving the receiver R1 to R2, the physical distance between structured singularities remains constant.
Figures 15 and 16 correspond to measurement points 3 and 4, where we putted the inspection system close to bends 1 and 2. The wave is emitted in both directions. We detect in figure 15 reflections from concrete blocks M2, M3 and finally that of M4. The position of M2, being pretty close to R3 (0.56m), leads to the superposition of the incident wave with that reflected from M2.
We can see in figure 17 that the wave, emitted by the generator E5, travels to the right. We can note two echoes from the weld A-A and the concrete wall M1 respectively at abscissas 11.4 m and 13.2 m which gives a distance of 1.8 m. Comparing with the real distance between A-A and M1, which is 0.8 m, this distance is coherent because the detected peak represents an outward and return of the wave. Therefore, halving the distance measured on the curve gives a value of 0.9 m which is close to the theoretical value of 0.8 m. We must take into account the uncertainty on the position of the echo from the concrete wall M1 given its width (0.4 m). In figure 18, there will be moving of abscissas echoes from A-A and M1 since the receiver is moved to E6 from a distance of 1.3 m (2.1 m - 0.8 m). We pick up the abscissas of A-A and M1 from the curve which are 10.3 m and 12 m respectively. We note here that we keep almost the same distance between A-A and M1. Other echoes observed in figures 17 and 18 are possible structured singularities or defects present in the pipeline, they can also be echoes of non-axisymmetric waves related to the conversion of torsional wave.
Positions of E7/R7 and E8/R8 allow emitting and receiving waves in both directions of propagation. By examining figure 19, we see that the measured distance between E7 and M7 is about 6.6 m (13.6/2-0.2), which is equal to the real distance. The abscissa of the weld O-O is about 11.5 m, which means a calculated distance of 0.85 m between O-O and M7 close to the real one (0.8 m). In Figure 20, the position of M7 from E7 is estimated to 4.9 m (10/2-0.1) close to the real value of 4.8 m.
Concerning the measurement point 9, the response is a little particular, reflection

from the end of the pipe 13 is not easily identifiable. This may be due to the geometry of the tee rather special that can changes transmitted waveform.

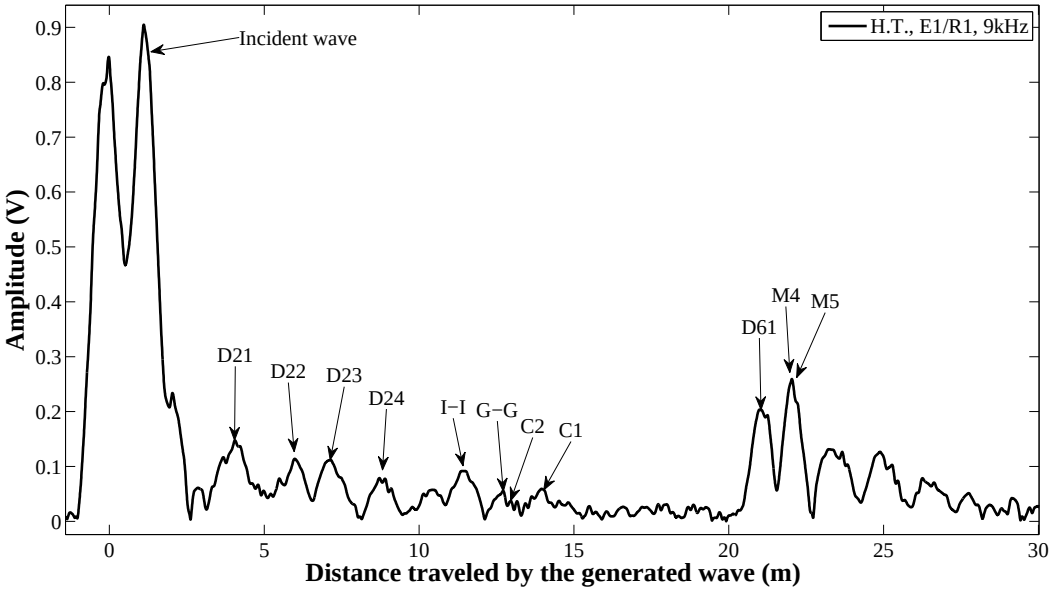

Figure 13: Hilbert Transform of the signal obtained at 9 kHz for the 1st measurement point.

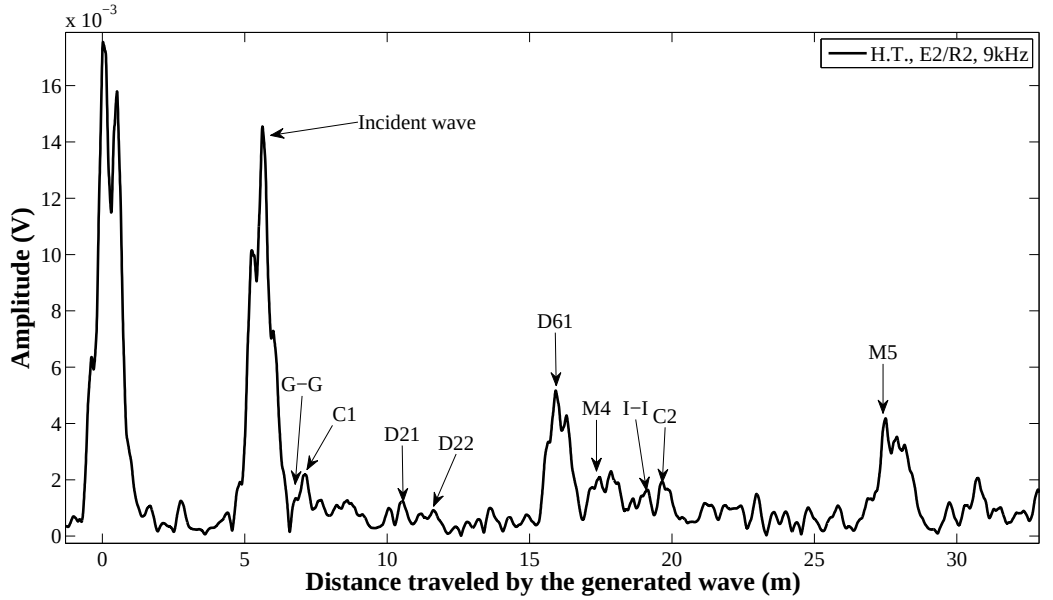

Figure 14: Hilbert Transform of the signal obtained at 9 kHz for the 2nd measurement point.

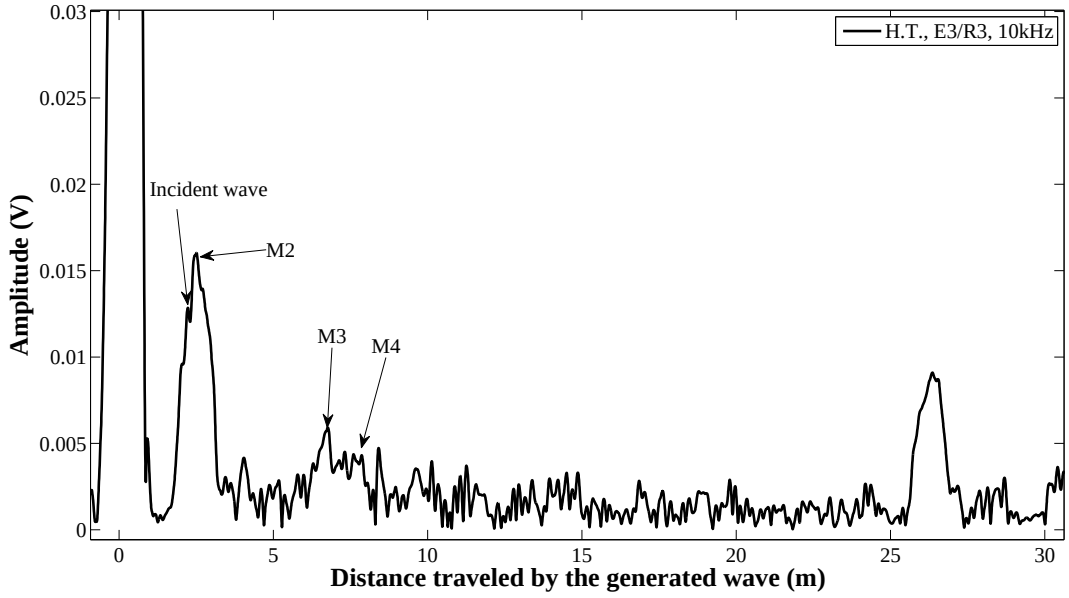

Figure 15: Hilbert Transform of the signal obtained at 10 kHz for the 3$^{\text{rd}}$ measurement point.

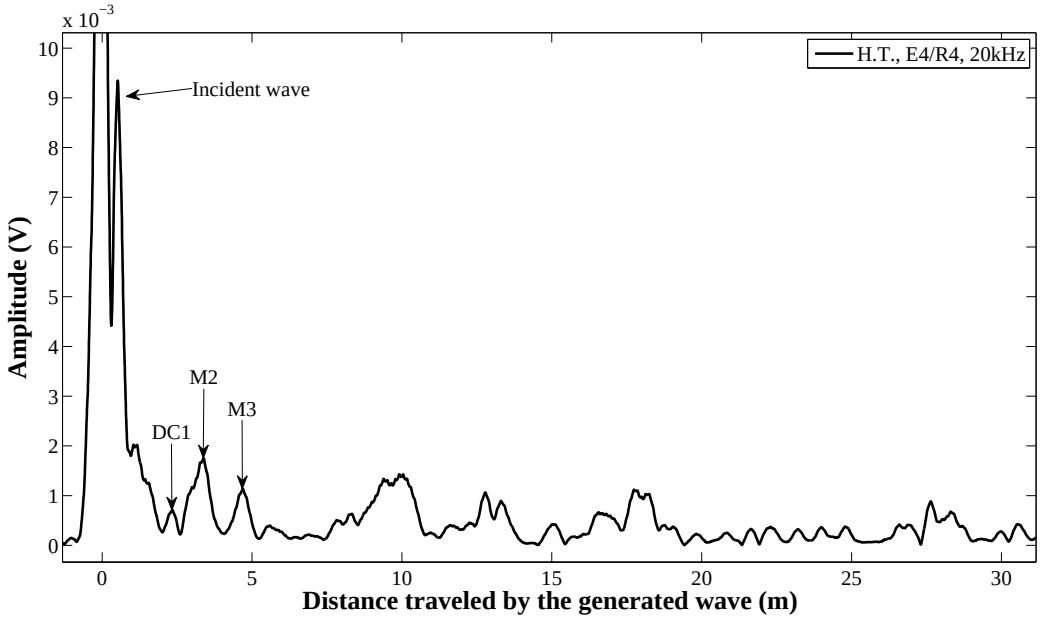

Figure 16: Hilbert Transform of the signal obtained at 20 kHz for the 4$^{\text{th}}$ measurement point.

3.3. Defect positioning in the pipeline

Defect positions can be synthesized in Table 1, in which defects are arranged for each pipe and measurement points leading to detect them. Defects are located relative to the free end of the pipe 3. These defects can be seen on the schema of

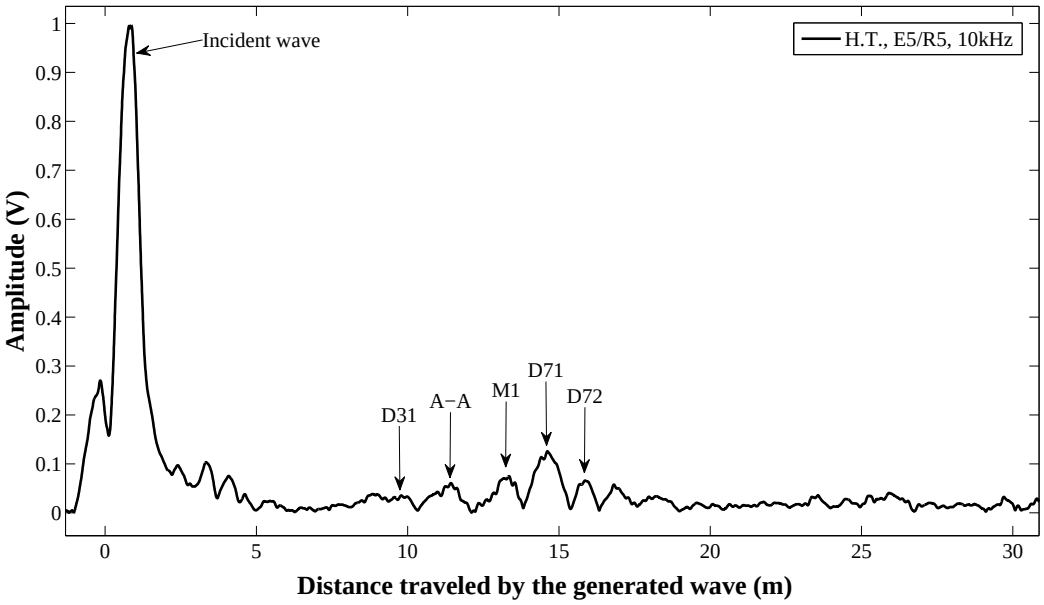

Figure 17: Hilbert Transform of the signal obtained at 10 kHz for the 5^{th} measurement point.

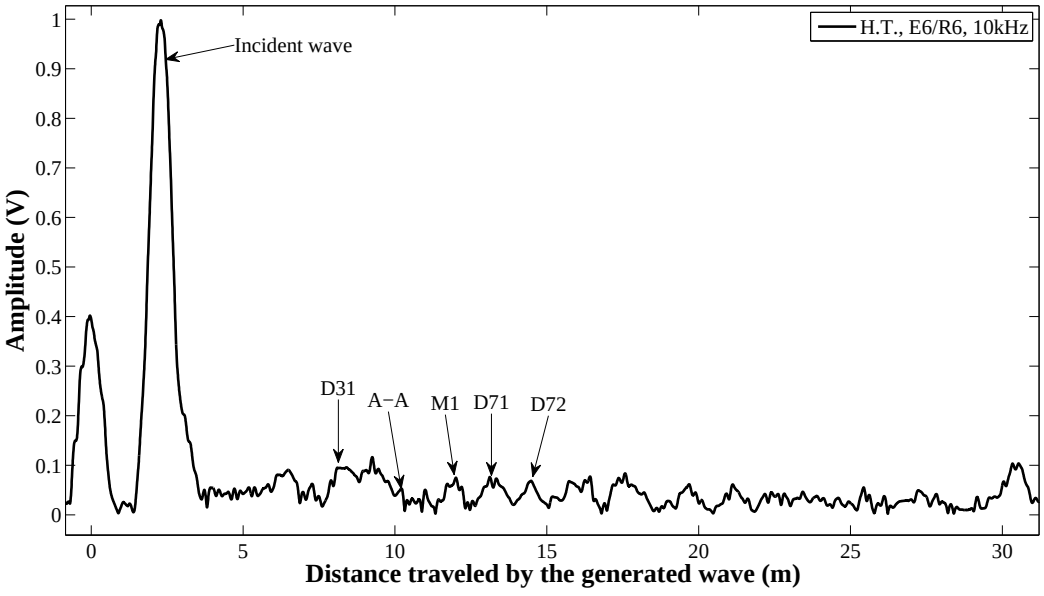

Figure 18: Hilbert Transform of the signal obtained at 10 kHz for the 6^{th} measurement point.

the pipeline in figure 22.

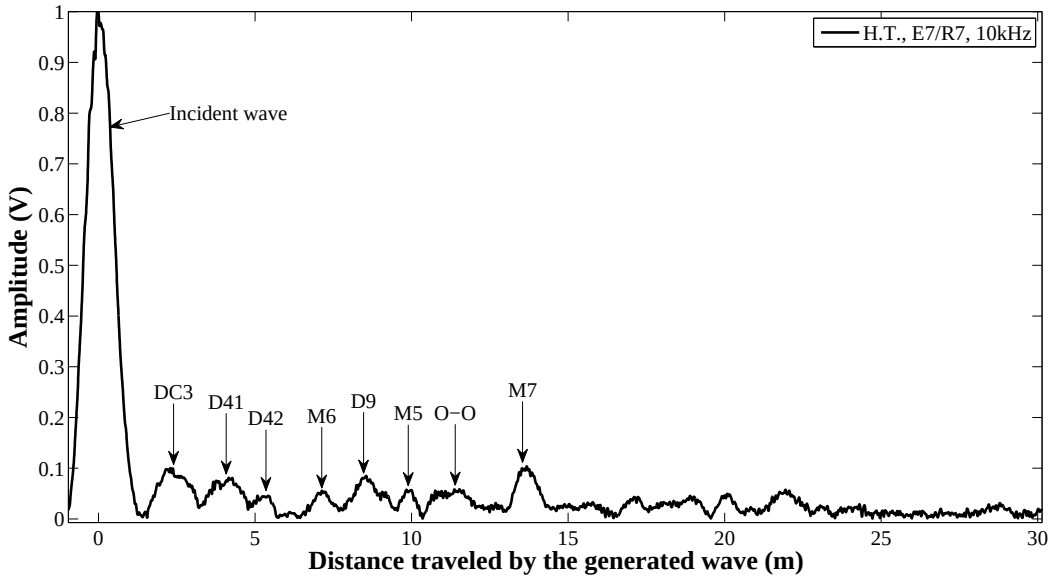

Figure 19: Hilbert Transform of the signal obtained at 10 kHz for the 7^{th} measurement point.

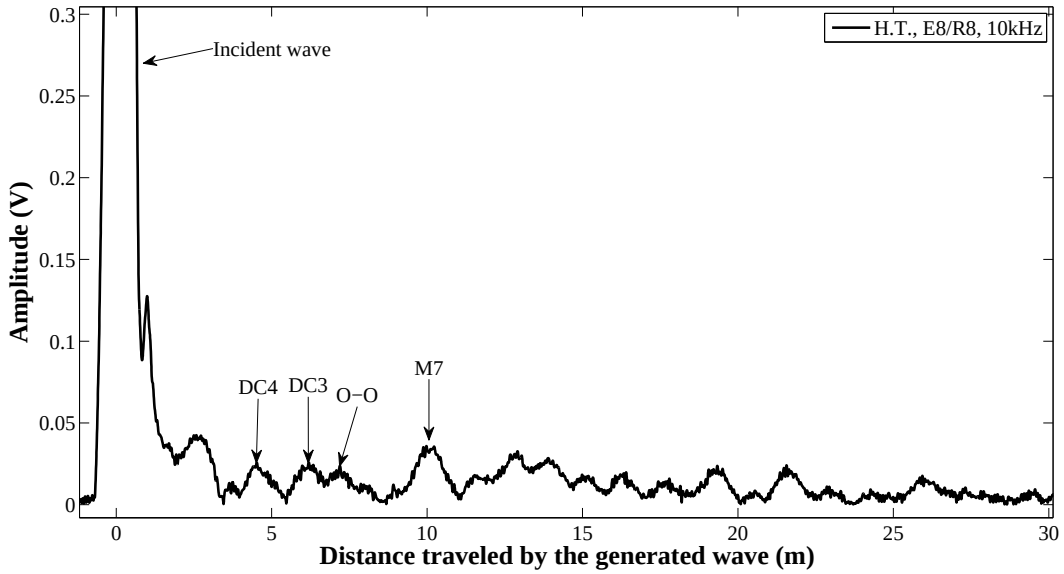

Figure 20: Hilbert Transform of the signal obtained at 10 kHz for the 8^{th} measurement point.

4. Conclusion

A pipeline was tested in this work by an inspection system designed and developed by the authors. The tested pipeline is an industrial mock-up that brings together hollow pipes, features and machined defects. It was placed in conditions close to real industrial environment in order to simulate and involve almost all sources of influence

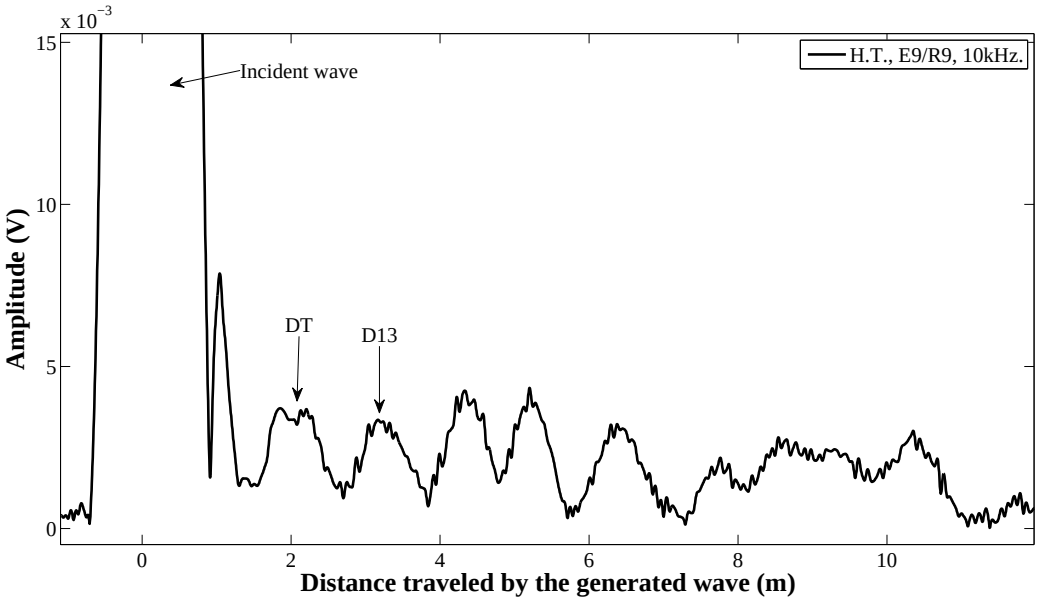

Figure 21: Hilbert Transform of the signal obtained at 10 kHz for the 9$^{\text{th}}$ measurement point.

Table 1: Defect positions in the pipeline.

Measurement points	Pipes	Defects	Positions
1 ; 2	2	D21	30.48 m
		D22	31.45 m
		D23	31.95 m
		D24	32.85 m
	6	D61	18.12 m
3 ; 4	Elbow 1	DC1	12.2 m
5 ; 6	3	D31	5.2 m
	7	D71	7.67 m
		D72	8.31 m
7 ; 8	4	D41	46.3 m
		D42	47.3 m
	5 ; 9	D9	40.4 m
	Elbow 3	DC3	43.5 m
	Elbow 4	DC4	44.26 m
9	Tee	DT	57 m
	13	D13	57.6 m

on the performed measurements. The inspection system is composed of two piezoelectric transducer-rings, one for generating torsional guided-waves, and the other for receiving reflected waves. The system can be clamped around the pipe and allows the fast screening of the structure. The Wave Finite Element Method was used to compute dispersion curves of propagating waves along the tested pipeline. Mea-

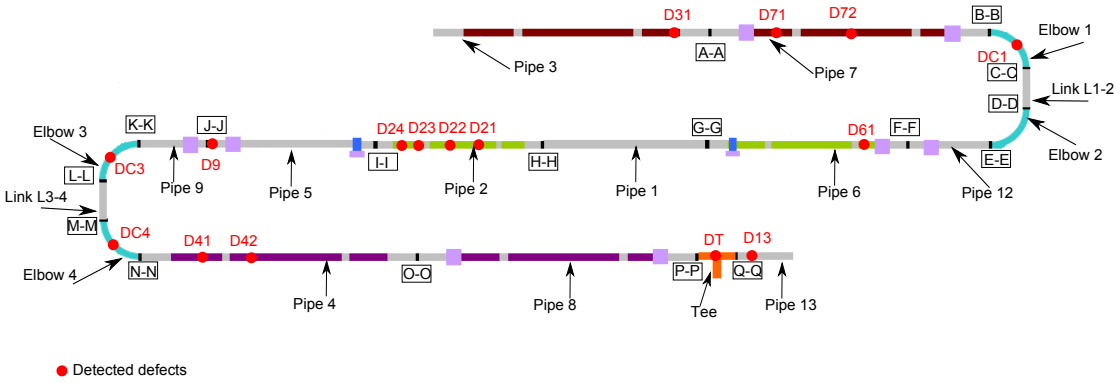

Figure 22: Localization of defects in the pipeline.

surements were performed according to well-defined points sweeping all the pipeline. Recorded signals was subjected to a series of treatments like signal denoising tools and Hilbert transform in the aim of obtaining comprehensible curves. Based on the pipeline architecture, the identification of reflections in obtained curves was performed in order to distinguish between peaks related to defects from those related to structured singularities.

The findings presented in this paper can be ameliorated by automating the reflections identification process, which could leads to more accurate and more fast analysis of inspected pipelines. Once defect detection and localization successfully done, the sizing of these anomalies should be addressed in future works. In fact, the severity of anomalies in structures is a relevant criteria in structural health monitoring and evaluation of pipelines.

References

[1] D. Alleyne, P. Cawley, Long range propagation of lamb waves in chemical plant pipework, Materials Evaluation 55 (4) (1997) 504–508.

[2] H. Kwun, S. Kim, G. Light, Long-range guided wave inspection of structures using the magnetostrictive sensor, J. Korean Soc. NDT 21 (2001) 383–390.

[3] M. Lozev, R. Smith, B. Grimmett, Evaluation of methods for detecting and monitoring of corrosion damage in risers, Journal of Pressure Vessel Technology 127 (3) (2005) 244–254.

[4] A. Carvalho, J. Rebello, L. Sagrilo, C. Camerini, I. Miranda, Mfl signals and artificial neural networks applied to detection and classification of pipe weld defects, NDT & E International 39 (8) (2006) 661–667.

[5] F. Bertoncini, M. Raugi, F. Turcu, Pipeline long-range inspection and monitoring by an innovative magnetic collar for magnetostrictive guided-wave systems, NDT.net - The e-Journal of Nondestructive Testing.

[6] C. Lee, S. Park, Damage classification of pipelines under water flow operation using multi-mode actuated sensing technology, Smart Materials and Structures 20 (11) (2011) 115002.

[7] X. Wang, P. W. Tse, A. Dordjevich, Evaluation of pipeline defect's characteristic axial length via model-based parameter estimation in ultrasonic guided wave-based inspection, Measurement Science and Technology 22 (2) (2011) 025701.

[8] J.-W. Kim, C. Lee, S. Park, Real-time health monitoring of pipeline structures using piezoelectric guided wave propagation, Advanced Science Letters 4 (3) (2011) 696–701.

[9] M. Park, I. Kim, Y. Yoon, Ultrasonic inspection of long steel pipes using lamb waves, NDT & E International 29 (1) (1996) 13–20.

[10] J. Rose, A baseline and vision of ultrasonic guided wave inspection potential, Transactions - American society of mechanical engineers journal of pressure vessel technology 124 (3) (2002) 273–282.

[11] J. Rose, Ultrasonic guided waves in structural health monitoring, Key Engineering Materials 270 (2004) 14–21.

[12] J. Li, On circumferential disposition of pipe defects by long-range ultrasonic guided waves, Journal of pressure vessel technology 127 (2005) 530–537.

[13] J. Rose, J. Mu, Y. Cho, Recent advances on guided waves in pipe inspection, in: 17th World Conference on Nondestructive Testing, Shanghai, China, 2008.

[14] R. Thompson, G. Alers, M. Tennison, Application of direct electromagnetic lamb wave generation to gas pipeline inspection, in: Ultrasonics Symposium, IEEE, 1972, pp. 91–94.

[15] M. Silk, K. Bainton, The propagation in metal tubing of ultrasonic wave modes equivalent to lamb waves, Ultrasonics 17 (1) (1979) 11–19.

[16] D. Alleyne, P. Cawley, The excitation of lamb waves in pipes using dry-coupled piezoelectric transducers, Journal of nondestructive evaluation 15 (1) (1996) 11–20.

[17] X. Wang, P. W. Tse, C. K. Mechefske, M. Hua, Experimental investigation of reflection in guided wave-based inspection for the characterization of pipeline defects, NDT & E International 43 (4) (2010) 365 – 374.

[18] J. Rose, S. Pelts, M. Quarry, A comb transducer model for guided wave nde, Ultrasonics 36 (1-5) (1998) 163–169.

[19] H. Shin, J. Rose, Guided waves by axisymmetric and non-axisymmetric surface loading on hollow cylinders, Ultrasonics 37 (5) (1999) 355–363.

[20] D. N. Alleyne, P. Cawley, The long range detection of corrosion in pipes using lamb waves, Review of Progress in Quantitative NDE 14 (1995) 2073–2080.

[21] D. N. Alleyne, M. Lowe, P. Cawley, The reflection of guided waves from circumferential notches in pipes, Journal of Applied Mechanics 65 (3) (1998) 635–641.

[22] M. Lowe, Characteristics of the reflection of lamb waves from defects in plates and pipes, Plenum Publishing Corp., Review of Progress in Quantitative Nondestructive Evaluation.

[23] M. Lowe, D. Alleyne, P. Cawley, The mode conversion of a guided wave by a part-circumferential notch in a pipe, Journal of Applied mechanics 65 (1998) 649–656.

[24] D. Alleyne, P. Cawley, The effect of discontinuities on the long-range propagation of lamb waves in pipes, ARCHIVE: Proceedings of the Institution of Mechanical Engineers, Part E: Journal of Process Mechanical Engineering 1989-1996 (vols 203-210) 210 (35) (1996) 217–226.

[25] A. Demma, P. Cawley, M. Lowe, A. Roosenbrand, The reflection of the fundamental torsional mode from cracks and notches in pipes, The Journal of the Acoustical Society of America 114 (2003) 611–625.

[26] D. Alleyne, B. Pavlakovic, M. Lowe, P. Cawley, Rapid long range inspection of chemical plant pipework using guided waves, Key Engineering Materials 270 (2004) 434–441.

[27] J. Ma, F. Simonetti, M. J. S. Lowe, Scattering of the fundamental torsional mode by an axisymmetric layer inside a pipe, The Journal of the Acoustical Society of America 120 (4) (2006) 1871–1880.

[28] W. Zhong, F. Williams, On the direct solution of wave propagation for repetitive structures, Journal of Sound and Vibration 181 (1995) 485–501.

[29] D. Mackey, N. Mackey, C. Mehl, V. Mehrmann, Structured polynomial eigenvalue problems: good vibrations from good linearizations, SIAM Journal on Matrix Analysis and Applications 28 (2006) 1029–1058.

[30] R. Lehoucq, D. Sorensen, C. Yang, ARPACK Users' guide: solution of large-scale eigenvalue problems with implicitly restarted arnoldi methods, SIAM Publications, Philadelphia, 1998.

[31] G. Acciani, G. Brunetti, G. Fornarelli, A. Giaquinto, Angular and axial evaluation of superficial defects on non-accessible pipes by wavelet transform and neural network-based classification, Ultrasonics 50 (1) (2010) 13–25.

[32] H. Kim, H. Melhem, Damage detection of structures by wavelet analysis, Engineering Structures 26 (3) (2004) 347–362.

[33] P. Rizzo, I. Bartoli, A. Marzani, F. L. di Scalea, Defect classification in pipes by neural networks using multiple guided ultrasonic wave features extracted after wavelet processing, Journal of Pressure Vessel Technology 127 (3) (2005) 294–303.

[34] M. Siqueira, C. Gatts, R. da Silva, J. Rebello, The use of ultrasonic guided waves and wavelets analysis in pipe inspection, Ultrasonics 41 (10) (2004) 785–797.

[35] S.-p. Song, P.-w. Que, Wavelet based noise suppression technique and its application to ultrasonic flaw detection, Ultrasonics 44 (2) (2006) 188–193.

[36] S. Hahn, Hilbert transforms in signal processing, Vol. 2, Artech House Norwood, MA, 1996.

[37] A. Korpel, Gabor: frequency, time, and memory, Applied Optics 21 (20) (1982) 3624–3632.

[38] F. King, Hilbert Transforms, Cambridge University Press, Cambridge, 2009.

[39] A. Kultyshev, Envelope, frequency, and phase representation in terms of a family of oscillations, Measurement Techniques 33 (8) (1990) 839–842.

[40] M. Feldman, Hilbert transform, envelope, instantaneous phase, and frequency, in: C. Boller, F. Chang, Y. Fujino (Eds.), Encyclopedia of Structural Health Monitoring, John Wiley & Sons, Ltd, Chichester, UK, 2009.

[41] M. Feldman, Hilbert transform in vibration analysis, Mechanical Systems and Signal Processing 25 (3) (2011) 735–802.

Chapter 5

Pipeline inspection using a torsional guided-waves inspection system. Part 2: Defect sizing by the Wave Finite Element Method

Abstract

This paper deals with the torsional-mode reflection from defects and structural singularities in an industrial pipeline in order to perform the defect sizing. The Wave Finite Element Method (WFEM) has been used to construct a numerical database of reflection coefficients from rectangular defects by varying thickness, axial and circumferential extents. Calculation was made depending on frequency. The approximation of defect sizes is carried out by sweeping the numerical database to find the suitable combination of dimensions for a given defect. Axial and circumferential extents is evaluated by limited intervals for each possible thickness. Reflections from structural singularities (elbows, concrete blocks, clamps, and welds) were also treated by comparing reflection coefficients obtained by WFEM to those evaluated experimentally. Results show a good agreement for most of the structured singularities but not for the others. Results may be improved by including damages in the structural singularities.

Keywords: Torsional guided waves, Defect sizing, Reflection coefficient, Wave Finite Element Method.

1. Introduction

Traditional ultrasonic testing is not suitable for detecting localized damage in pipelines. Applying guided waves for defect screening had shown a relevant efficiency since many years. Defect localization can be easily evaluated from the reflection of a well tuned wave packet. Practically, the time frequency analysis or denoise processing of the obtained testing signal is necessary. Furthermore, guided waves can be also employed for the sizing of defects, which is much more difficult and requires detailed knowledge about the interaction of the incident wave with different possible defect types. Indeed, the reflection or transmission signal depends not only the defect size or shape, but also the mode type and frequency, potential mode conversion, and the attenuation due to dissipation, leakage or geometry. However, the wave-defect interaction analysis will help to find out which type of modes are sensitive to a given type of defects. The character of scattering should be quite different if the defect is transverse such as crack or notch, axially distributed such as delamination in layered structures, or due to the loss of mass, presence of inclusions, etc., which probably causes the failure of the inspection if the mode is not properly chosen. In the other hand, the numerical wave-defect interaction analysis will provide a reference of the sizing in the practical test, at least to some extent.

The effect of defect size on the reflection and transmission characteristics in pipes has been investigated by many researchers [1–10]. These studies deal with many types of defects like cracks [4, 5], notches [1, 6–8], and circular holes [9, 10]. J.L. Rose et al. [11] have used the boundary element analysis in seeking out some techniques that might be used for flaw sizing potential with guided waves. It is shown that a very simple algorithm of examining amplitude of the reflection or transmission from

a defect as being proportional to depth of the defect is indeed sometimes true. A long range ultrasonic guided wave test system was used by Jing Mu et al. [12] to measure the circumferential size of volumetric corrosion defects and a transverse saw cuts by sweeping the focal position around the pipe. A quantitative study of the reflection of the T(0,1) mode from defects in pipes was carried out by A. Demma et al. [5], finite element predictions being validated by experiments on selected cases. Another work [2] by A. Demma et al. presents a systematic analysis of the effect of pipe size, defect size, guided wave mode and frequency on the reflection from notches. J. Davies and P. Cawley [13] quantify the performance of a synthetically focused guided-waves technique for detection, location, and sizing of circumferential crack-like defects in pipelines.

Many useful frequency-domain information, such as wave dispersibility, reflection from damage, interface or boundary, sensitivity of specific mode to various types of damages, mode conversions, etc. [14], can be obtained directly from the eigensolutions in spectral methods, or by the global-local techniques such as hybrid methods [15–20]. The Wave Finite Element Method (WFEM), which is a simple spectral method based on the standard finite element (FE) formulation, can be applied to examine the wave interaction with the local defects and the structural features [17–20]. The hybrid WFE/FE method is one of the hybrid methods for global-local analysis, which is very suitable to the case that wavelength is larger than the axial extension of FE model for complex local defect.

Although the application of FE simulations to calculate the reflection coefficient from defects and to quantify their sizes appears in several works, the WFEM has not been used for the defect dimensioning. The purpose of this study is to investigate the reflections of the torsional mode T(0,1) from previously detected defects localized in a pipeline in order to approximate defect sizes. The hybrid WFE/FE method has been employed to construct a database of reflection coefficients from a rectangular defect with variable axial, circumferential and thickness extents. Calculations was made depending on the excitation frequency with the torsional mode T(0,1) as incident wave. The basis of the numerical simulation procedure is presented in section 2 and the formulation of the WFEM is described. The next section is devoted to the description of the defect-sizing process. Some results of reflection coefficients depending on size and frequency are shown. Signals obtained from different measurement points in the pipeline has been used to calculate experimental reflection coefficients from defects and structural singularities such as bends, welds and clamps. The comparison between experimental values and numerical abacuses of reflection coefficients conducts us to the approximation of defect sizes. Finally, in section 4, experimental reflection coefficients from structural singularities at some frequencies are compared to numerical ones obtained by WFEM.

2. Wave response in an infinite structural waveguide with a coupling structure

Consider an infinitely long structure with the local inhomogeneities which are due to the geometry or material variation. A monochromatic incident wave, which comprises a single or multiple wave modes, is assumed to be generated at $x - \infty$ and travel in the positive $x + \infty$ direction. Scattering phenomenon emerges when the incident wave impinges on those inhomogeneities as is shown in figure 1. The resultant wave field consists of the incident and scattered components (both reflection and transmission).

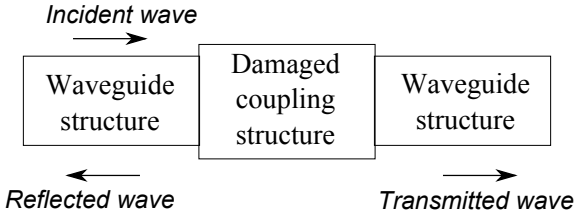

Figure 1: Wave propagation through a damaged coupling structure.

The modelling of damaged cell is similar to that of typical one for modes extraction, except that additional interior dofs might be included. The coupling condition is governed by the dynamics equation of coupling structures,

$$[\mathbf{M}^c]\left\{\begin{array}{ccc}(\ddot{\mathbf{q}}_l^c)^T & (\ddot{\mathbf{q}}_i^c)^T & (\ddot{\mathbf{q}}_r^c)^T\end{array}\right\}^T+[\mathbf{K}^c]\left\{\begin{array}{ccc}(\mathbf{q}_l^c)^T & (\mathbf{q}_i^c)^T & (\mathbf{q}_r^c)^T\end{array}\right\}^T=\left\{\begin{array}{ccc}(\mathbf{F}_l^c)^T & \mathbf{0} & (\mathbf{F}_r^c)^T\end{array}\right\}^T, \tag{1}$$

where $[\mathbf{M}^c]$ and $[\mathbf{K}^c]$ denote the mass and stiffness matrices of coupling structures, respectively. Equation 1 can be condensed as:

$$\left[\begin{array}{cc}\mathbf{S}_{ll}^c & \mathbf{S}_{lr}^c\\ \mathbf{S}_{rl}^c & \mathbf{S}_{rr}^c\end{array}\right]\left\{\begin{array}{c}\mathbf{q}_l^c\\ \mathbf{q}_r^c\end{array}\right\}=\left\{\begin{array}{c}\mathbf{F}_l^c\\ \mathbf{F}_r^c\end{array}\right\}. \tag{2}$$

Considering the coupling conditions

$$\mathbf{q}_l^c=[\mathbf{q}^+]\mathbf{A}^{in}+[\mathbf{q}^-]\mathbf{A}^{re},\ \mathbf{q}_r^c=[\mathbf{q}^+]\mathbf{A}^{tr}, \tag{3}$$

and

$$\mathbf{F}_l^c=[\mathbf{F}^+]\mathbf{A}^{in}+[\mathbf{F}^-]\mathbf{A}^{re},\ \mathbf{F}_r^c=-[\mathbf{F}^+]\mathbf{A}^{tr}, \tag{4}$$

Equation 2 can be re-formed as the governing equations for the scattering problem:

$$\left[\begin{array}{cc}\mathbf{S}_{ll}^c[\mathbf{q}^-]-[\mathbf{F}^-] & \mathbf{S}_{lr}^c[\mathbf{q}^+]\\ \mathbf{S}_{rl}^c[\mathbf{q}^-] & \mathbf{S}_{rr}^c[\mathbf{q}^+]+[\mathbf{F}^+]\end{array}\right]\left\{\begin{array}{c}\mathbf{A}^{re}\\ \mathbf{A}^{tr}\end{array}\right\}=\left[\begin{array}{c}[\mathbf{F}^+]-\mathbf{S}_{ll}^c[\mathbf{q}^+]\\ -\mathbf{S}_{rl}^c[\mathbf{q}^+]\end{array}\right]\left\{\mathbf{A}^{in}\right\}. \tag{5}$$

Given a single or a set of incident modes as the input in Equation 5, scattered modes (reflection and transmission) acting as the output can be obtained. Numerically, the base number N_r is suggested to be frequency dependent, which can be

implemented by a routine to include those slightly evanescent wave modes into the bases.

Since the coupling structure might contain a large number of interior DOFs, the dynamic reduction can be used to accelerate the spectral solution by using the assumed modes of coupling structure. The system matrices of coupling parts at each frequency in Eq.2 have to be taken into calculation. In this case, a convenient way is to model the coupling structure using component mode synthesis (CMS) method, which gives better approximation than Guyan reduction (exact for stiffness matrices but approximate for mass) when dealing with higher frequency problems. For the sake of simplicity, the fixed-boundary CMS method is used here [21]. In the fixed-boundary CMS method, a substructure is considered to be composed of interior and interface dofs. It condenses the system matrices by assuming the displacements of the interior dofs as a linear superposition of the constraint modes and the internal normal modes. By introducing the transformation matrix $[\mathbf{T}]$, the displacement vector of coupling substructure is represented in terms of generalized coordinates:

$$\left\{ \begin{array}{ccc} (\mathbf{q}_l^c)^T & (\mathbf{q}_i^c)^T & (\mathbf{q}_r^c)^T \end{array} \right\}^T = [\mathbf{T}] \left\{ \begin{array}{ccc} (\mathbf{q}_l^c)^T & (\mathbf{q}_\delta^c)^T & (\mathbf{q}_r^c)^T \end{array} \right\}^T, \tag{6}$$

where the $\mathbf{q}_\delta^c$ is the modal displacement. The transformation matrix for the fixed-boundary method has the form

$$[\mathbf{T}] = \left[\begin{array}{ccc} \mathbf{I} & \mathbf{0} & \mathbf{0} \\ -[\mathbf{K}_{ii}^c]^{-1}[\mathbf{K}_{il}^c] & \mathbf{\Phi}_{ii} & -[\mathbf{K}_{ii}^c]^{-1}[\mathbf{K}_{ir}^c] \\ \mathbf{0} & \mathbf{0} & \mathbf{I} \end{array} \right], \tag{7}$$

where $\mathbf{\Phi}_{ii}$ is the fixed interface normalized modal matrix, $\mathbf{K}_{ii}^c$, $\mathbf{K}_{il}^c$ and $\mathbf{K}_{ir}^c$ are the interior DOFs related components in the stiffness matrix. Other modes such as attachment modes can also be used as required. Thus Equation 1 can be simplified as

$$[\mathbf{M}_{CB}^c] \left\{ \begin{array}{ccc} (\ddot{\mathbf{q}}_l^c)^T & (\ddot{\mathbf{q}}_\delta^c)^T & (\ddot{\mathbf{q}}_r^c)^T \end{array} \right\}^T + [\mathbf{K}_{CB}^c] \left\{ \begin{array}{ccc} (\mathbf{q}_l^c)^T & (\mathbf{q}_\delta^c)^T & (\mathbf{q}_r^c)^T \end{array} \right\}^T = \left\{ \begin{array}{ccc} (\mathbf{F}_l^c)^T & \mathbf{0} & (\mathbf{F}_r^c)^T \end{array} \right\}^T \tag{8}$$

where the condensed mass matrix $[\mathbf{M}_{CB}^c] = [\mathbf{T}]^T [\mathbf{M}^c] [\mathbf{T}]$, stiffness matrix $[\mathbf{K}_{CB}^c] = [\mathbf{T}]^T [\mathbf{K}^c] [\mathbf{T}]$, $\mathbf{q}_\delta$ is the truncated set of generalized modal displacement associated to the modal matrix $\mathbf{\Phi}_{ii}$.
Consequently, Equation 5 can be modified as

$$\left[\begin{array}{cc} \widehat{\mathbf{S}}_{ll}^c[\mathbf{q}^-] - [\mathbf{F}^-] & \widehat{\mathbf{S}}_{lr}^c[\mathbf{q}^+] \\ \widehat{\mathbf{S}}_{rl}^c[\mathbf{q}^-] & \widehat{\mathbf{S}}_{rr}^c[\mathbf{q}^+] + [\mathbf{F}^+] \end{array} \right] \left\{ \begin{array}{c} \mathbf{A}^{re} \\ \mathbf{A}^{tr} \end{array} \right\} = \left[\begin{array}{c} [\mathbf{F}^+] - \widehat{\mathbf{S}}_{ll}^c[\mathbf{q}^+] \\ -\widehat{\mathbf{S}}_{rl}^c[\mathbf{q}^+] \end{array} \right] \left\{ \mathbf{A}^{in} \right\}, \tag{9}$$

where $\widehat{\mathbf{S}}_{ll}^c$, $\widehat{\mathbf{S}}_{lr}^c$, $\widehat{\mathbf{S}}_{rl}^c$, $\widehat{\mathbf{S}}_{rr}^c$ are the reduced system matrices obtained by eliminating the modal displacement $\mathbf{q}_\delta$:

$$\begin{array}{ll} \widehat{\mathbf{S}}_{ll}^c = \mathbf{D}_{ll}^c - \mathbf{D}_{l\delta}^c {\mathbf{D}_{\delta\delta}}^{-1} \mathbf{D}_{\delta l}^c \ ; & \widehat{\mathbf{S}}_{lr}^c = \mathbf{D}_{lr}^c - \mathbf{D}_{l\delta}^c {\mathbf{D}_{\delta\delta}}^{-1} \mathbf{D}_{\delta r}^c \ ; \\ \widehat{\mathbf{S}}_{rl}^c = \mathbf{D}_{rl}^c - \mathbf{D}_{r\delta}^c {\mathbf{D}_{\delta\delta}}^{-1} \mathbf{D}_{\delta l}^c \ ; & \widehat{\mathbf{S}}_{rr}^c = \mathbf{D}_{ri}^c - \mathbf{D}_{r\delta}^c {\mathbf{D}_{\delta\delta}}^{-1} \mathbf{D}_{\delta r}^c . \end{array}$$

The spectral solution for wave scattering is therefore calculated by two kind of superelements: the eigensolutions for guided wave modes and the superelements of coupling structures. After solving Equation 9, the whole scattered wave fields can be obtained through Equations 6–8 for near field and the wave representation for far field. It should be noted that the eigensolution of the coupling substructure model can be used for different wave inputs, which is particularly applicable to the systems comprising certain standard local features. Another advantage over the direct condensation is that the number of the normal modes of coupling substructures can also be frequency dependent, not only that of the truncated bases, which further improves the numerical efficiency if the solution in the wide frequency range is desired.

3. Defect sizing

3.1. Database construction of reflection-coefficients from a defect

To approximate the size of the defect, the idea was to build a digital database containing the different probabilities of defect sizes that could exist while assuming that it was modeled with a form similar to that shown in figure 2. The parameters that characterize the defect are 'a, b, c', which are axial extent, depth, and circumferential extent respectively. Calculations was made by varying these three parameters. The axial extent sweeps the interval [4-20] mm in steps of 4 mm. The circumference of the pipe was divided to 44 elements, the circumferential extent was varied by eliminating an element in every step. Knowing that the pipe diameter is of 168 mm, each element measures 12 mm in the circumferential direction. Finally, the depth of the defect varies from 2 mm with a step of 3 mm until the whole pipe thickness which is 11 mm. The material properties of the steel pipes are: $E = 2.1 \times 10^{11}\ Pa$, $\rho = 7800\ Kg.m^{-3}$, $\nu = 0.3$. Reflection coefficients calculation was established depending on frequency in the range [5-15] kHz. This latter corresponds practically to the signal frequency at which the pipe under test was excited. The torsion mode was considered in the calculation process. In fact, the inspection system use this mode to generate guided waves for the defect detection. Several iterations conduct us to obtain a database that contain reflection coefficients as a function of four variables: a, b, c and the frequency.

Calculations were performed based on the connexion between two homogeneous waveguides through inhomogeneous one including the defect as shown in figure 3. The waveguide 1 is a pipe section connected to a damaged coupling structure which is in turn connected to waveguide 2 similar to the first one. To numerically describe the wave mode scattering, the reflection and transmission coefficients are defined by the solution of response from Equation 5:

$$R_i = \frac{A_i^{re}}{A_i^{in}}, \quad T_i = \frac{A_i^{tr}}{A_i^{in}} \tag{10}$$

where $i = 1, 2, ..., N_r$. It should be mentioned that the coefficients depend not only on the defects, but also on the normalization method of eigenmodes and the size

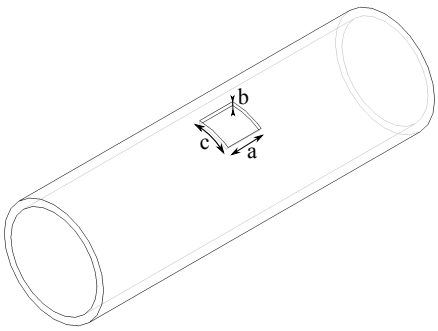

Figure 2: Damaged pipe with defect dimensions.

of intact part of waveguide that included for the reduction of high order near-field modes. The change of the phase of the coefficient with the frequency is partially owing to the size of intact part of waveguide in coupling structure model.

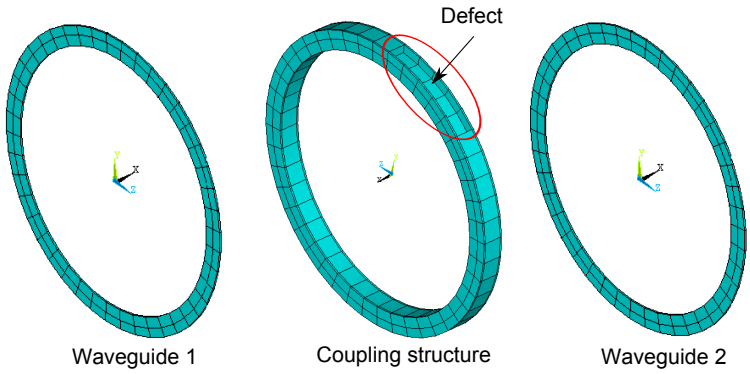

Figure 3: Finite element models of waveguides with a damaged coupling structure.

Figure 4 shows the reflection coefficients variation with frequency for different defect sizes. These curves prove the dependence of reflection coefficients with the excitation frequency. Generally speaking, these coefficients increase with the frequency. Figure 5 shows the reflection coefficients variation with axial, circumferential and depth defect extents at 10kHz for different sizes. These curves demonstrate the increase of the reflection coefficients with the defect sizes.
The database constructed by a large diversity of defect sizes let us to plot the 3-D curves showing the evolution of reflection coefficients with two chosen variables from the defect dimensions (a, b or c) at a given frequency. In figure 6 we can see 3-D graphs of the reflection coefficients variation with defect sizes at 10 kHz. It is clear that the reflection monotonically increases with axial extent at constant depth and vice versa, it also increases with circumferential extent at constant axial extent and vice versa.

Figure 7 shows color maps of the 3-D reflection plot in figure 6. The lines are

isolines of constant reflection coefficient as described by the color bar. From these isolines we can observe that the reflection coefficient obtained for example at a certain depth and axial extent is also obtained at smaller depth and larger axial extent.

3.2. Experimental reflection-coefficients calculation

To determine the approximate dimensions of the detected defects, the calculation of experimental reflection coefficients has been established. For each obtained signal, we trace attenuation curve of the incident wave and calculate at each frequency the reflection coefficient of each defect. The wave motions can be theoretically expressed by the exponential function e^{-ikx}, k being the wavenumber, which is frequency dependent, and x being the wave propagation distance. The reflection coefficient is defined as the ratio between the averaged maximum-amplitude of reflected signal from the singularity and the maximum-amplitude of incident signal at the same moment of detection. Results for each measurement point are presented in table 1.

Table 1: Experimental reflection-coefficients from defects.

Defects	*f = 8 kHz*	*f = 9 kHz*	*f = 10 kHz*
D21		0.186	0.167
D22		0.156	0.125
D23	0.124	0.161	0.202
D24		0.122	0.126
D61	0.531	0.54	0.55
D31	0.127	0.089	0.055
D71	0.286	0.253	0.25
D72	0.194	0.127	0.138
D41		0.112	0.1
D42	0.144	0.104	0.06
D91	0.153	0.171	0.13
D13	0.051	0.024	0.022

3.3. Defect sizes determination

In this subsection, we present the results of investigations established based on the numerical abacus of the reflection coefficients. Defects listed in table 1 do not include those detected in structural singularities. Indeed, the numerical tool does not allow currently to size defects located in coupling structures like elbow, concrete block, clamp or tee. Table 2 shows for most of the defects the presence of more than a possibility sizing. In fact, a value of reflection coefficient can induce several combination of size (a, b, c). The uncertainties can be reduced by increasing the number of excitation frequencies per measurement point, which helps the restriction of intervals sizing.

Table 2: Approximate dimensions of detected defects.

Defects	Axial extent (mm)	Circumferential extent (mm)	Thickness (mm)
D21	[11 - 20]	[360 - 528]	5
	[4 - 20]	[370 - 432]	8
	[4 - 20]	[140 - 155]	11
D22	[9 - 20]	[306 - 528]	5
	[4 - 20]	[165 - 288]	8
	[4 - 20]	[115 - 132]	11
D23	[11 - 20]	[354 - 528]	5
	[4 - 20]	[200 - 390]	8
	[4 - 20]	[132 - 168]	11
D24	[7 - 20]	[246 - 528]	5
	[4 - 20]	[126 - 290]	8
	[4 - 20]	[78 - 132]	11
D61	[17 - 20]	[500 - 528]	8
	[4 - 20]	[354 - 370]	11
D31	[4 - 20]	[180 - 306]	5
	[4 - 20]	[96 - 132]	8
	[4 - 20]	[54 - 66]	11
D71	[17 - 20]	[465 - 528]	5
	[7 - 20]	[260 - 510]	8
	[4 - 20]	[180 - 200]	11
D72	[7 - 20]	[250 - 528]	5
	[4 - 20]	[140 -320]	8
	[4 - 20]	[80 - 140]	11
D41	[6 - 20]	[225 - 528]	5
	[4 - 20]	[120 - 252]	8
	[4 - 20]	[70 - 90]	11
D42	[4 - 20]	[205 - 335]	5
	[4 - 20]	[110 - 150]	8
	[4 - 20]	66	11
D91	[11 - 20]	[330 - 528]	5
	[4 - 20]	[186 - 310]	8
	[4 - 20]	[130 - 138]	11
D13	[4 - 20]	[48 - 130]	5
	[4 - 20]	[30 - 66]	8
	[4 - 20]	[18 - 28]	11

4. Reflection of torsional mode from structural singularities

In order to prove the reflections associated to structural singularities (elbows, concrete blocks, clamps, and welds) in the tested pipeline (figure 8), the WFEM has been used to determine the reflection coefficients from these features without defects.

A finite element model was created for each one of them as seen on figure 9. Elbows have a bending angle of 90° and an upper radius of curvature equal to 1.5×pipe diameter. Concrete blocks have 468 mm long, 400 mm wide and 520 mm high. Their mechanical properties are: $E = 20\ GPa$, $\rho = 2200\ Kg.m^{-3}$, $\nu = 0.2$. Clamps have 10 mm thick and a 150 mm wide along the axial direction. Finally, the weld are axially symmetric and has a width of 10 mm and a thickness of 15 mm. The mechanical properties of the weld beads are assumed higher than those of the pipes.

Thereafter, the WFE results are compared to experimental ones. Calculation has been made through the frequency range [5-15]kHz for each structural singularity. Measurements have been taken at three frequencies: 8, 9 and 10 kHz. Figures from 10 to 13 show the results for some selected structural singularities.

The experimental values are close to the numerical curves for most figures. However, there are some gaps between them, this is may be due to the approximation made on the geometric models of the structural singularities in one hand, and on their physical properties in other hand. The differences between experimental points of some elbows and numerical results may be due to the presence of susceptible defects in these elbows, since our calculation do not take into account damaged structural singularities.

5. Conclusion

A parametric study of the torsional-mode reflection from defects and structural singularities in an industrial pipeline was established. The Wave Finite Element Method was used to construct a numerical database of reflection coefficients from rectangular defects by varying thickness, axial and circumferential extents. Calculation was made depending on frequency. Experiments lead us to estimate reflection coefficients from detected defects. Since the defect identification and localization can be made by analyzing experimental signals, the reflection coefficient can be evaluated based on the attenuation curve of the incident wave, at different frequencies. Then, the approximation of defect sizes was carried out by sweeping the numerical abacuses to find the suitable combination of dimensions for a given defect. Axial and circumferential extents was evaluated by limited intervals for each possible thickness. Subsequently, a comparison between reflection coefficients from structural singularities (elbows, concrete blocks, clamps, and welds) obtained by WFEM and experiments has been carried out. A good agreement was found for most of the structured singularities, but clear gaps was noted for the others. This can be justified by the fact that we did not take into account the presence of defects in these singularities. Future works can focus on this issue in order to deal with the effect of damaged structural singularities on the reflection coefficient.

References

[1] P. Cawley, M. Lowe, F. Simonetti, C. Chevalier, A. Roosenbrand, The variation of the reflection coefficient of extensional guided waves in pipes from defects as

a function of defect depth, axial extent, circumferential extent and frequency, Proceedings of the Institution of Mechanical Engineers, Part C: Journal of Mechanical Engineering Science 216 (11) (2002) 1131–1143.

[2] A. Demma, P. Cawley, M. Lowe, A. Roosenbrand, B. Pavlakovic, The reflection of guided waves from notches in pipes: a guide for interpreting corrosion measurements, NDT & E International 37 (3) (2004) 167–180.

[3] W. Zhu, An fem simulation for guided elastic wave generation and reflection in hollow cylinders with corrosion defects, Journal of pressure vessel technology 124 (1) (2002) 108–117.

[4] M. Ratassepp, S. Fletcher, M. Lowe, Scattering of the fundamental torsional mode at an axial crack in a pipe, The Journal of the Acoustical Society of America 127 (2010) 730–740.

[5] A. Demma, P. Cawley, M. Lowe, A. Roosenbrand, The reflection of the fundamental torsional mode from cracks and notches in pipes, The Journal of the Acoustical Society of America 114 (2003) 611–625.

[6] R. Carandente, J. Ma, P. Cawley, The scattering of the fundamental torsional mode from axi-symmetric defects with varying depth profile in pipes, The Journal of the Acoustical Society of America 127 (2010) 3440–3448.

[7] M. Lowe, D. Alleyne, P. Cawley, The mode conversion of a guided wave by a part-circumferential notch in a pipe, Journal of Applied mechanics 65 (1998) 649–656.

[8] D. N. Alleyne, M. Lowe, P. Cawley, The reflection of guided waves from circumferential notches in pipes, Journal of Applied Mechanics 65 (3) (1998) 635–641.

[9] A. Lovstad, P. Cawley, The reflection of the fundamental torsional guided wave from multiple circular holes in pipes, NDT & E International 44 (7) (2011) 553 – 562.

[10] A. Lovstad, P. Cawley, The reflection of the fundamental torsional mode from pit clusters in pipes, NDT & E International 46 (0) (2012) 83 – 93.

[11] J. Rose, S. Pelts, Y. Cho, Modeling for flaw sizing potential with guided waves, Journal of nondestructive evaluation 19 (2) (2000) 55–66.

[12] J. Mu, L. Zhang, J. L. Rose, J. Spanner, Defect sizing in pipe using an ultrasonic guided wave focusing technique, AIP Conference Proceedings 820 (1) (2006) 760–766.

[13] J. Davies, P. Cawley, The application of synthetic focusing for imaging crack-like defects in pipelines using guided waves, Ultrasonics, Ferroelectrics and Frequency Control, IEEE Transactions on 56 (4) (2009) 759–771.

[14] S. Gopalakrishnan, A. Chakraborty, D. R. Mahapatra, Spectral Finite Element Method: Wave Propagation, Diagnostics and Control in Anisotropic and Inhomogeneous Structures, Springer, 2008.

[15] N. Hu, H. Fukunaga, M. Kameyama, D. R. Mahapatra, S. Gopalakrishnan, Analysis of wave propagation in beams with transverse and lateral cracks using a weakly formulated spectral method, Journal of Applied Mechanics 74 (2007) 119–127.

[16] J. Galán, R. Abascal, Numerical simulation of lamb wave scattering in semi-infinite plates, International Journal for Numerical Methods in Engineering 53 (2002) 1145–1173.

[17] W. Zhou, M. Ichchou, J.-M. Mencik, Analysis of wave propagation in cylindrical pipes with local inhomogeneities, Journal of Sound and Vibration 319 (1-2) (2009) 335–354.

[18] M. Ichchou, J. Mencik, W. Zhou, Wave finite elements for low and mid-frequency description of coupled structures with damage, Computer Methods in Applied Mechanics and Engineering 198 (15-16) (2009) 1311–1326.

[19] W. Zhou, M. Ichchou, Wave propagation in mechanical waveguide with curved members using wave finite element solution, Computer Methods in Applied Mechanics and Engineering 199 (33-36) (2010) 2099–2109.

[20] W. Zhou, M. Ichchou, Wave scattering by local defect in structural waveguide through wave finite element method, Structural Health Monitoring 10 (4) (2011) 335–349.

[21] R. Craig, M. Bampton, Coupling of substructures for dynamic analysis, AIAA Journal 12 (1968) 1313–1319.

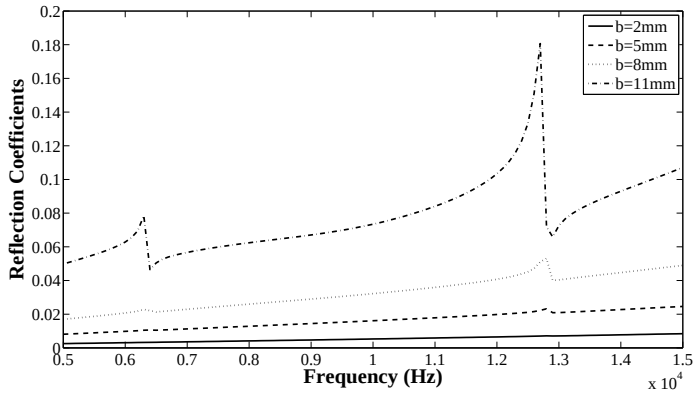

(a)

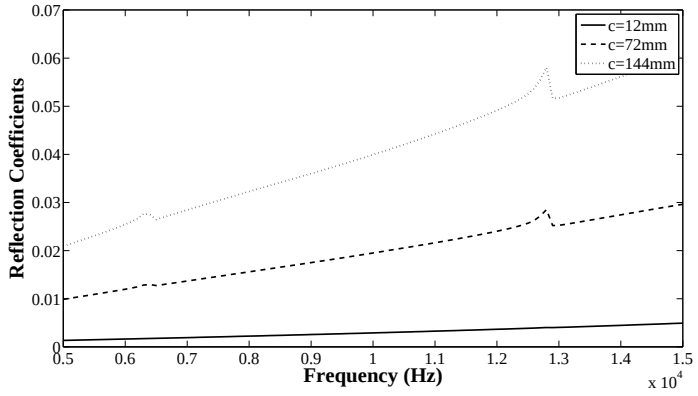

(b)

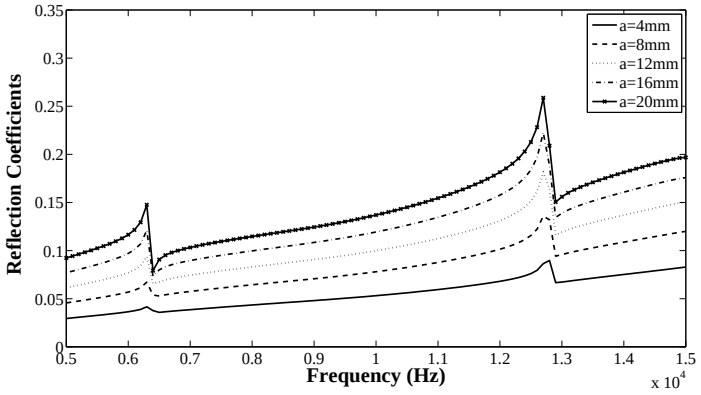

(c)

Figure 4: Reflection coefficients variation with frequency for: (a) different defect depth with $a = 8mm$, $c = 60mm$; (b) different defect circumferential-extents with $a = 8mm$, $b = 5mm$; and (c) different defect axial-extents with $c = 132mm$, $b = 8mm$

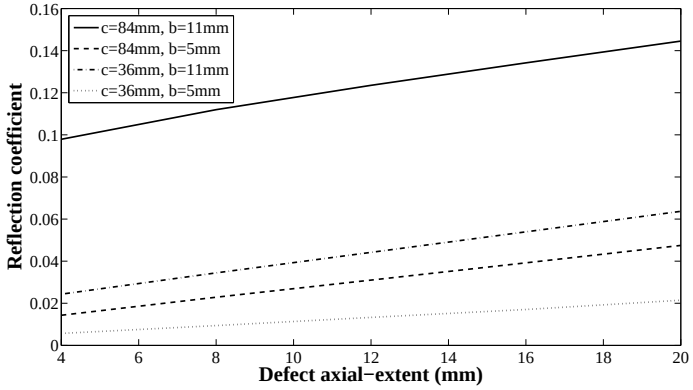

(a)

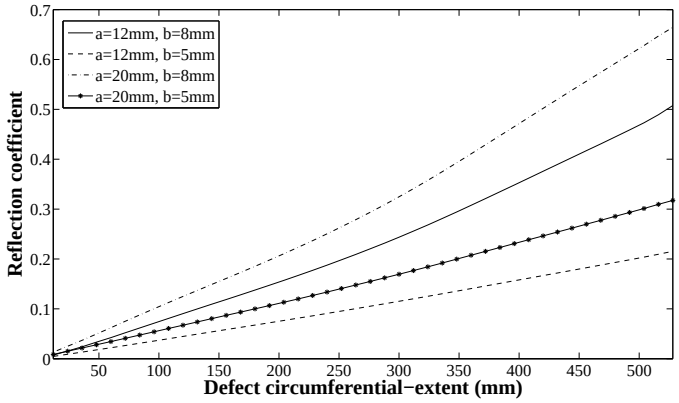

(b)

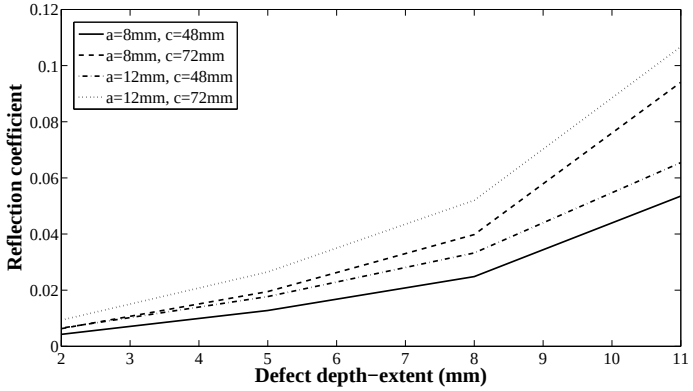

(c)

Figure 5: Reflection coefficients variation with: (a) defect axial-extents for different circumferential and depth sizes; (b) defect circumferential-extents for different axial and depth sizes; and (c) defect depth for different circumferential and axial sizes; at 10 kHz.

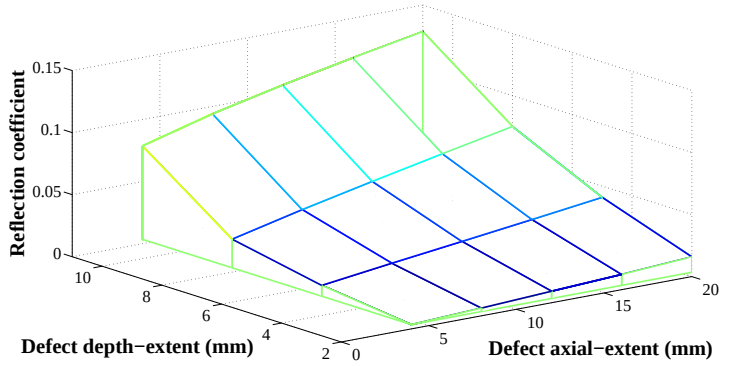

(a)

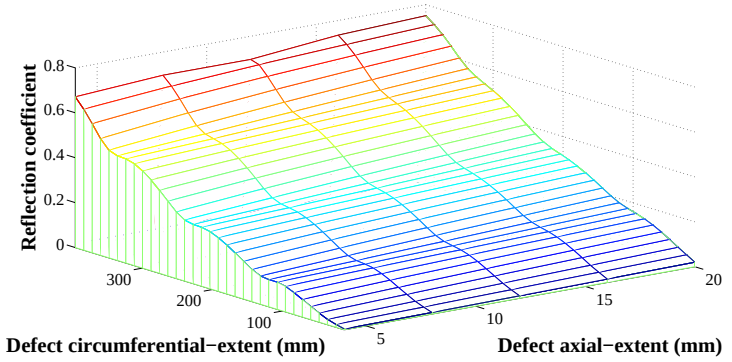

(b)

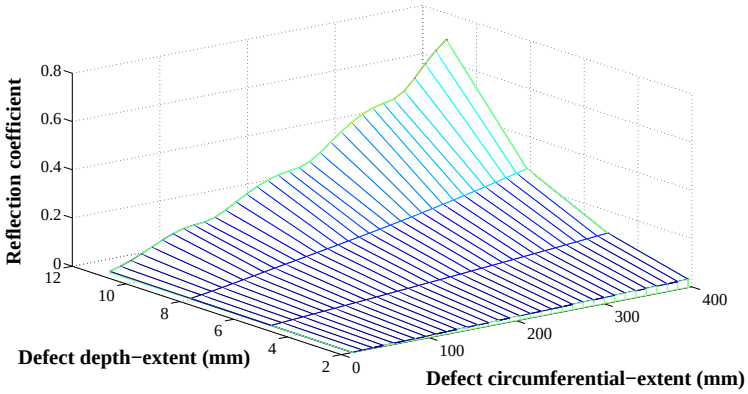

(c)

Figure 6: 3D graph of reflection coefficients at 10 kHz with: (a) varying depth and axial extent ($c = 72mm$), (b) varying circumferential and axial extents (through thickness defect) and, (c) varying depth and circumferential extent ($a = 8mm$).

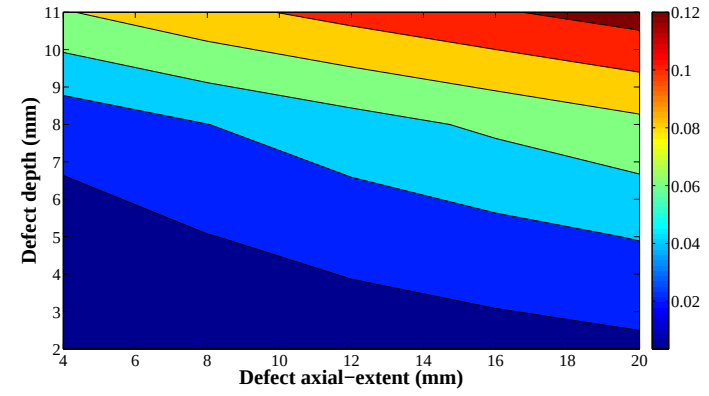

(a)

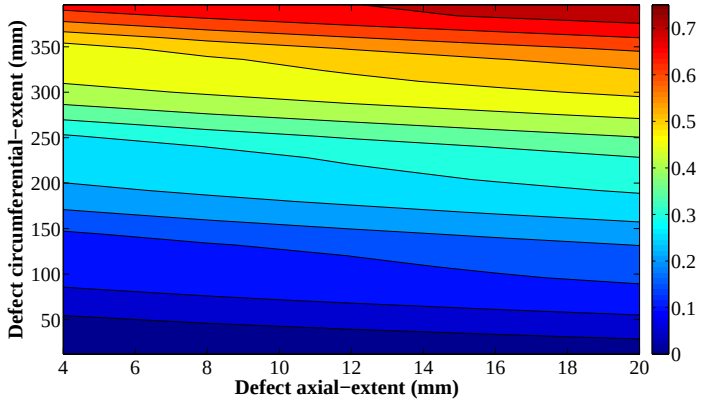

(b)

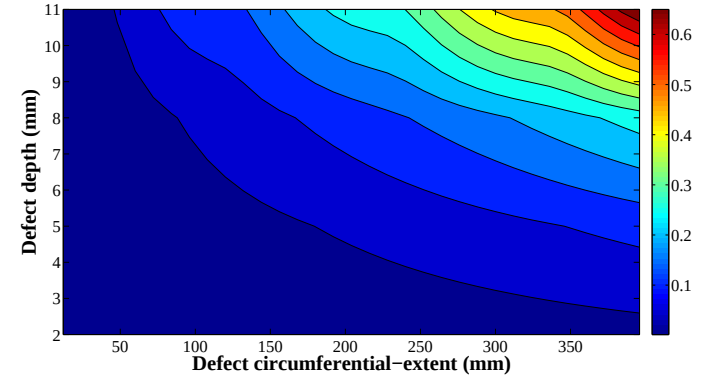

(c)

Figure 7: Color map of reflection coefficients at 10 kHz with: (a) varying depth and axial extent ($c = 72mm$), (b) varying circumferential and axial extents (through thickness defect) and, (c) varying depth and circumferential extent ($a = 8mm$).

(a) Elbow (b) Concrete block (c) Clamp

Figure 8: Structural singularities in the pipeline.

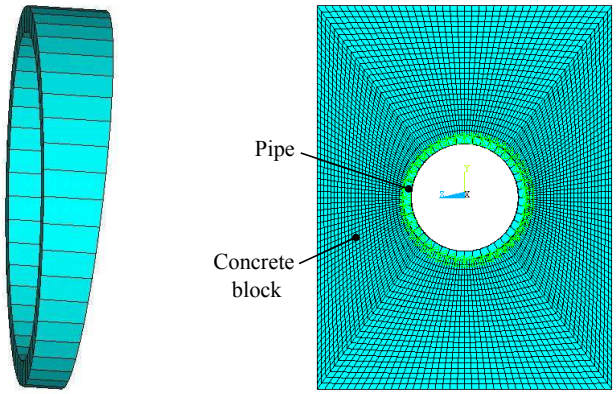

(a) Elbow (b) Concrete block assembly

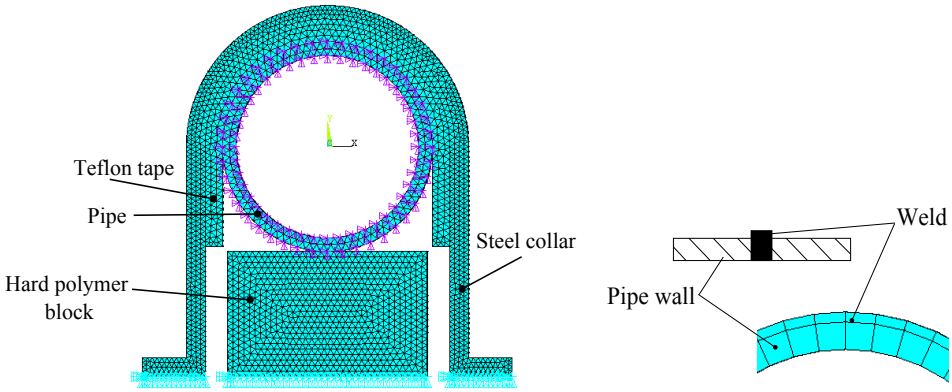

(c) Clamp assembly (d) Weld

Figure 9: Finite elements models of structural singularities.

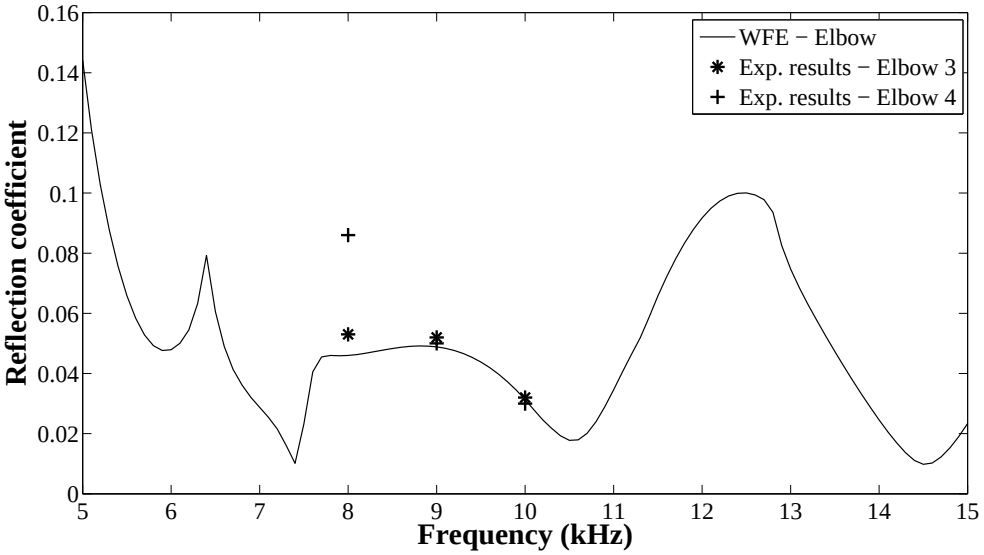

Figure 10: Comparison between WFEM and experimental reflection coefficients from elbow.

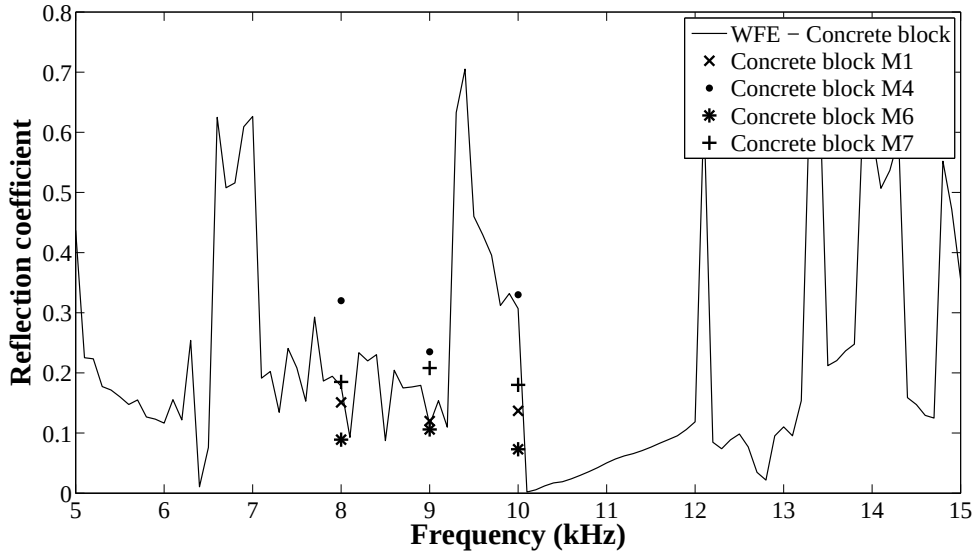

Figure 11: Comparison between WFEM and experimental reflection coefficients from concrete block.

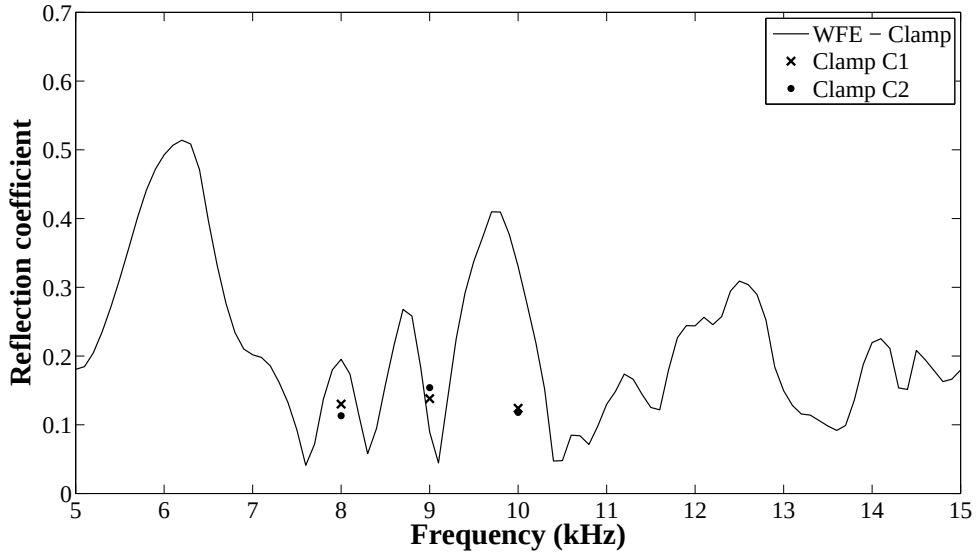

Figure 12: Comparison between WFEM and experimental reflection coefficients from clamp.

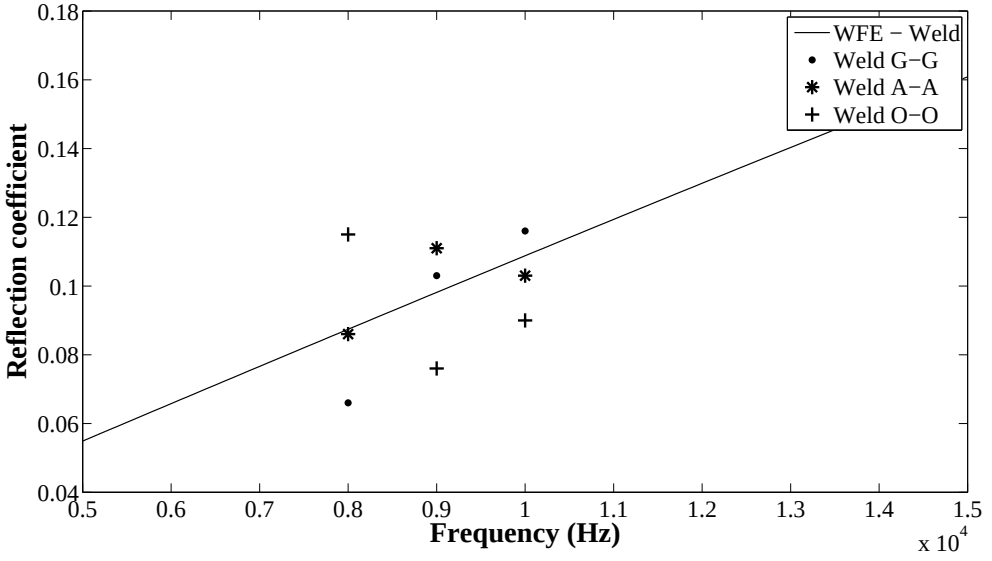

Figure 13: Comparison between WFEM and experimental reflection coefficients from weld.

Chapter 6

Effect of defect angular-position on the wave reflection and transmission coefficients: numerical investigation by the Wave Finite Element Method

Abstract

This paper provides a numerical investigation concerning the effect of defect angular-position on reflection and transmission coefficients while exciting by different types of waves. The spectral method Wave Finite Element has been used to carry out calculation. Twelve angular positions was studied while impinging the modeled defect by torsional mode T(0,1), longitudinal mode L(0,2) and flexural mode F(1,2). Results show that the type of incident wave as well as the examined reflected and transmitted waves play an important role in circumferential localization of the defect.

Keywords: Guided waves, Defect localization, Angular position, Reflection and transmission coefficient, Wave Finite Element Method.

1. Introduction

A considerable progress has been made over the last few years on the subject of long-range guided wave inspection in pipes [1–3]. The generation of different modes depends on source loading conditions. Axisymmetric modes like longitudinal modes have been studied carefully in earlier years because of their uniform circumferential energy distribution. Different kinds of generation methods for axisymmetric modes have been widely used.

The subject of guided wave tuning principles and focusing for defect detection is introduced in many works [4–10]. This hypothesis is being explored in detail today, that of establishing wave resonances from a defect inside a structure by controlling phase velocity and frequency. It becomes possible to focus the ultrasonic energy onto the defect of interest that gives us the best dynamic response and hence the best potential for detection classification and sizing of the particular defect. Guided waves via a four dimensional tuning process of adjusting circumferential loading length, circumferential position, phase and frequency, can create a natural focusing effect almost anywhere inside the pipe. Shin and Rose [11] discussed the use of both axisymmetric and nonaxisymmetric surface loading in hollow cylinders and illustrates the basic principles behind nonaxisymmetric wave propagation. Use of these flexural mode waves are being tried in order to assist in the flaw detection classification and sizing process. Further work on the excitation of nonaxisymmetric guided waves is reported by Li and Rose [12]. It is shown in this paper how it becomes possible to load the upper surface of a pipe and to inspect, for example, the bottom side of a pipe, at a certain distance away. J. Davies and P. Cawley [13] quantify the performance of a synthetically focused guided-waves technique for detection, location, and sizing of circumferential crack-like defects in pipelines.

The wave-defect interaction analysis will help to find out which type of modes are sensitive to a given type of defects. The character of scattering should be quite different if the defect is transverse such as crack or notch, axially distributed such as delamination in layered structures, or due to the loss of mass, presence of inclusions,

etc., which probably causes the failure of the inspection if the mode is not properly chosen. In the other hand, the numerical wave-defect interaction analysis will provide a reference of the sizing in the practical test, at least to some extent.

Many useful frequency-domain information, such as wave dispersibility, reflection from damage, interface or boundary, sensitivity of specific mode to various types of damages, mode conversions, etc. [14], can be obtained directly from the eigensolutions in spectral methods, or by the global-local techniques such as hybrid methods [15–20]. The Wave Finite Element Method (WFEM), which is a simple spectral method based on the standard finite element (FE) formulation, can be applied to examine the wave interaction with the local defects and the structural features [17–20]. The hybrid WFE/FE method is one of the hybrid methods for global-local analysis, which is very suitable to the case that wavelength is larger than the axial extension of FE model for complex local defect.

This paper aims to investigate numerically reflection and transmission coefficients from a defined defect in a pipe while varying its angular position at a fixed axial location. Three different waves are tested: the torsional mode T(0,1), the longitudinal L(0,2) mode, and the flexural F(1,2) mode are incident separately. In the first case, reflection and transmission coefficients of T(0,1) and L(0,2) as well as those of F(1,2), F(2,2) and F(3,2) are examined. In the second case, reflection and transmission coefficients of L(0,2) and T(0,1) as well as those of F(1,3) and F(2,3) are observed. Finally, in the third case when F(1,2) is incident, its reflection and transmission coefficients are also analyzed. The hybrid WFE/FE method has been employed in this study to compute diffusion matrices from the defect, in order to find an approach for the angular localization of the defect.

Firstly, theoretical foundation – containing the WFEM formulation and the wave response of a waveguide with a coupling structure – is presented. The next section is devoted to the numerical implementation including methodology and dispersion curves as well as obtained results and a detailed discussion.

2. Theoretical foundation

2.1. WFE method formulation

By using axisymmetric elements, WFE method for the 1-D wave propagation problem is employed to extract the wavenumbers and mode shapes for all modes susceptible to propagate in the pipe. Those eigenmodes are then superposed to form a scattering equation by connecting with FE formulation of the pipe segment with inhomogeneities.

For the one-dimensional wave propagation in the waveguide, as is shown in figure 1, the finite element formulation of a repetitive segment may be written as

$$\begin{bmatrix} \mathbf{S}_{ll} & \mathbf{S}_{lr} \\ \mathbf{S}_{rl} & \mathbf{S}_{rr} \end{bmatrix} \begin{Bmatrix} \mathbf{q}_l \\ \mathbf{q}_r \end{Bmatrix} = \begin{Bmatrix} \mathbf{F}_l \\ \mathbf{F}_r \end{Bmatrix}, \tag{1}$$

where $\mathbf{S}_{rl}$, $\mathbf{S}_{ll}$ and $\mathbf{S}_{rr} \in \mathbb{C}^{N\times N}$ are block dynamic stiffness matrices, and subscripts l or r denote the left or right components respectively.

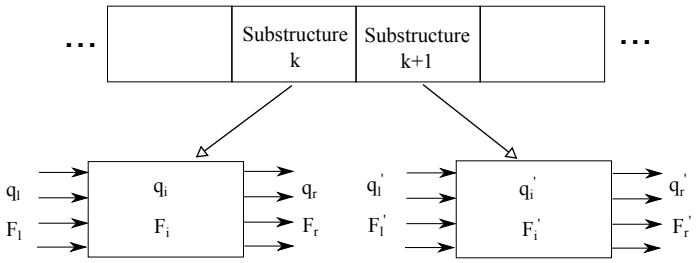

Figure 1: Structure discretized to identical cells (one-dimensional periodic system).

The harmonic wave motions can be theoretically treated using the exponential function e^{-jkx} ($j = \sqrt{-1}$), where x-axis is the propagation direction. Provided the DOFs are in the same order, the displacement and force relationships between two adjacent segments can be written as

$$\mathbf{q}'_l = \lambda \mathbf{q}_l, \quad \mathbf{F}'_l = \lambda \mathbf{F}_l, \tag{2}$$

where $\lambda = e^{-jkd}$ with d denoting the length of the repetitive segment in wave propagation direction. Considering the displacement continuity $\mathbf{q}'_l = \mathbf{q}_r$ and force equilibrium condition $\mathbf{F}'_l = -\mathbf{F}_r$, Equation 1 can be written as

$$\begin{bmatrix} \mathbf{S}_{ll} & \mathbf{S}_{lr} \\ \mathbf{S}_{rl} & \mathbf{S}_{rr} \end{bmatrix} \begin{Bmatrix} \mathbf{q}_l \\ \lambda \mathbf{q}_l \end{Bmatrix} = \begin{Bmatrix} \mathbf{F}_l \\ -\lambda \mathbf{F}_l \end{Bmatrix}, \tag{3}$$

Eliminating the force component of Equation 3 leads to a special case of quadratic eigenvalue problem for (λ, $\mathbf{q}_l$)

$$[\mathbf{S}_1/\lambda + \mathbf{S}_2 + \lambda \mathbf{S}_1^{\mathrm{T}}]\boldsymbol{\varphi} = \mathbf{0}, \tag{4}$$

where $\boldsymbol{\varphi} = \mathbf{q}_l$, $\mathbf{S}_1 = \mathbf{S}_{rl}$, $\mathbf{S}_2 = \mathbf{S}_2^{\mathrm{T}} = \mathbf{S}_{ll} + \mathbf{S}_{rr}$.

If the spectral problem for both propagating and evanescent modes is of interest, the propagation constant must be obtained for a given frequency in order to find the dispersion relationship. The eigenequation may be solved using the classical linearization method to obtain the dispersion relationship and eigenmodes:

$$\begin{bmatrix} \mathbf{0} & \mathbf{S}_1 \\ -\mathbf{S}_1 & -\mathbf{S}_2 \end{bmatrix} \begin{Bmatrix} \boldsymbol{\varphi} \\ \lambda \boldsymbol{\varphi} \end{Bmatrix} = \lambda \begin{bmatrix} \mathbf{S}_1 & \mathbf{0} \\ \mathbf{0} & \mathbf{S}_1^{\mathrm{T}} \end{bmatrix} \begin{Bmatrix} \boldsymbol{\varphi} \\ \lambda \boldsymbol{\varphi} \end{Bmatrix}. \tag{5}$$

The solution of such standard generalized eigenvalue problem yields the displacement vectors $\mathbf{q}_l^i$ ($i = 1, 2, \ldots, 2N$) for propagating and non-propagating waves. The corresponding force vectors can be written as

$$\mathbf{F}_l^i = \left(\mathbf{S}_{ll} + \lambda^i \mathbf{S}_{lr}\right) \mathbf{q}_l^i, \tag{6}$$

which can be obtained from Equation 3.

Another structured linearization method may be used to directly calculate both the displacement and the force vectors for propagating and non-propagating modes:

$$\begin{bmatrix} -\mathbf{S}_{ll} & \kappa \mathbf{I} \\ \mathbf{S}_1 & \mathbf{0} \end{bmatrix} \begin{Bmatrix} \boldsymbol{\varphi} \\ \boldsymbol{\psi} \end{Bmatrix} = \lambda \begin{bmatrix} \mathbf{S}_1^{\mathrm{T}} & \mathbf{0} \\ -\mathbf{S}_{rr} & -\kappa \mathbf{I} \end{bmatrix} \begin{Bmatrix} \boldsymbol{\varphi} \\ \boldsymbol{\psi} \end{Bmatrix} \tag{7}$$

where $\kappa = \|\mathbf{S}_1\|$, $\boldsymbol{\psi} = \mathbf{F}_l/\kappa$.

The symmetry of the eigenvalues of Equation 5 might be lost due to roundoff errors, if no preservation routine is used in the eigenvalue computation. In the case of large matrices produced, it is better to employ the structured linearization method proposed by Zhong and Williams [21], which calculates the reciprocal pairs $(\lambda,\ 1/\lambda)$ by constructing Equation 4 to the eigenvalue problem about two skew symmetric matrices

$$\begin{bmatrix} \mathbf{S}_1 - \mathbf{S}_1^{\mathrm{T}} & -\mathbf{S}_2 \\ \mathbf{S}_2 & \mathbf{S}_1 - \mathbf{S}_1^{\mathrm{T}} \end{bmatrix} \begin{Bmatrix} \boldsymbol{\varphi} \\ \lambda\boldsymbol{\varphi} \end{Bmatrix} = \mu \begin{bmatrix} \mathbf{0} & \mathbf{S}_1 \\ -\mathbf{S}_1^{\mathrm{T}} & \mathbf{0} \end{bmatrix} \begin{Bmatrix} \boldsymbol{\varphi} \\ \lambda\boldsymbol{\varphi} \end{Bmatrix}, \tag{8}$$

where $\mu = (1/\lambda + \lambda)$. The pairing of eigenvalues is automatically guaranteed, as the linearization itself preserves the symmetry. However eigensolution of Equation 8 need specific iteration procedure to be developed [21], so does the linearization method proposed by Mackey *et al.* [22]. As the left system matrix is most likely well-conditioned, Equation 8 can be formulated as the standard eigenvalue problem:

$$[\mathbf{S}_{Std}] \begin{Bmatrix} \boldsymbol{\varphi} \\ \lambda\boldsymbol{\varphi} \end{Bmatrix} = \frac{1}{\mu} \begin{Bmatrix} \boldsymbol{\varphi} \\ \lambda\boldsymbol{\varphi} \end{Bmatrix}, \tag{9}$$

where $[\mathbf{S}_{Std}]$ equals to the left division of the right system matrix by the left one. This transformation may not be realized explicitly which usually leads to a dense matrix. The eigenvalues $1/\mu$ with the larger real parts correspond to the wavenumbers with the smaller amplitudes of imaginary parts, although not very strictly. This allows the ARPACK routine for nonsymmetric complex eigenvalue problems to be used [23], which is faster than the QZ algorithm if only a few eigenpairs are of interest.

It should be mentioned that if the dispersion relationships in undamped systems are of interest, Equation 4 can be re-formed to the generalized eigenvalue problem for ω^2, which provides a rapid dispersion calculation scheme

$$\tilde{\mathbf{K}}\boldsymbol{\varphi} = \omega^2\tilde{\mathbf{M}}\boldsymbol{\varphi} \tag{10}$$

where

$$\begin{cases} \tilde{\mathbf{K}} = \mathbf{K}_{rl}/\lambda + \mathbf{K}_{ll} + \mathbf{K}_{rr} + \lambda\mathbf{K}_{rl}^{\mathrm{T}} \\ \tilde{\mathbf{M}} = \mathbf{M}_{rl}/\lambda + \mathbf{M}_{ll} + \mathbf{M}_{rr} + \lambda\mathbf{M}_{rl}^{\mathrm{T}} \end{cases}$$

Both $\tilde{\mathbf{K}}$ and $\tilde{\mathbf{M}}$ are Hermitian matrices when $k \in \mathbb{R}$. The stable eigenequation facilitates the mode tracing, since the property that eigenvectors of distinct eigenvalues are mutually orthogonal can be used by introducing the criterion $\mid \boldsymbol{\varphi}_{i+1}^{\mathrm{T}}\tilde{\mathbf{M}}\boldsymbol{\varphi}_i \mid$ to classify the waves with different normalized modal shape.

The spectral eigensolutions sometimes need to be classified for the computational purpose. Equation 3 can be used to trace the kindred modes at different frequencies. However it concerns the operation of a large number of vectors. An alternative is to combine the curve tracing of the wave numbers with the mode assurance criterion (MAC). Polynomial fitting can be used to predict the eigenvalue of the subsequent

frequency step. In case of more than one solution being found within the prescribed tolerance δ, a criterion

$$\varepsilon = \left|\varphi_{f+\Delta f}^{H} \cdot \varphi_f\right|, \tag{11}$$

can be introduced to distinguish the kindred modes from the others when $\varepsilon\,(\varepsilon \leq 1)$ is maximum, where φ_f and $\varphi_{f+\Delta f}$ are the unitary displacement vectors at frequency step f and its subsequent frequency step $f + \Delta f$. Thus the eigenmodes can be traced by the consistency rather than the orthogonality. The unitary displacement vectors may not contain all the DOFs if only one or some of the low order modes need to be classified (partial modal assurance criterion, PMAC).

2.2. Wave response in an infinite structural waveguide with a coupling structure

Consider an infinitely long structure with the local inhomogeneities which are due to the geometry or material variation. A monochromatic incident wave, which comprises a single or multiple wave modes, is assumed to be generated at $x - \infty$ and travel in the positive $x + \infty$ direction. Scattering phenomenon emerges when the incident wave impinges on those inhomogeneities as is shown in figure 2. The resultant wave field consists of the incident and scattered components (both reflection and transmission).

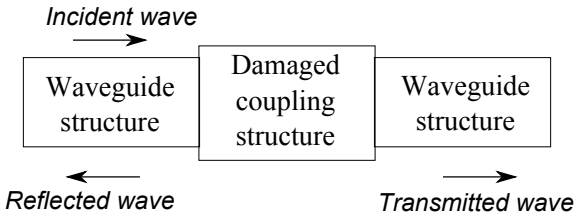

Figure 2: Wave propagation through a damaged coupling structure.

The modeling of damaged cell is similar to that of typical one for modes extraction, except that additional interior dofs might be included. The coupling condition is governed by the dynamics equation of coupling structures,

$$[\mathbf{M}^c]\left\{\begin{array}{ccc}(\ddot{\mathbf{q}}_l^c)^T & (\ddot{\mathbf{q}}_i^c)^T & (\ddot{\mathbf{q}}_r^c)^T\end{array}\right\}^T + [\mathbf{K}^c]\left\{\begin{array}{ccc}(\mathbf{q}_l^c)^T & (\mathbf{q}_i^c)^T & (\mathbf{q}_r^c)^T\end{array}\right\}^T = \left\{\begin{array}{ccc}(\mathbf{F}_l^c)^T & \mathbf{0} & (\mathbf{F}_r^c)^T\end{array}\right\}^T, \tag{12}$$

where $[\mathbf{M}^c]$ and $[\mathbf{K}^c]$ denote the mass and stiffness matrices of coupling structures, respectively. Equation 12 can be condensed as:

$$\left[\begin{array}{cc}\mathbf{S}_{ll}^c & \mathbf{S}_{lr}^c \\ \mathbf{S}_{rl}^c & \mathbf{S}_{rr}^c\end{array}\right]\left\{\begin{array}{c}\mathbf{q}_l^c \\ \mathbf{q}_r^c\end{array}\right\} = \left\{\begin{array}{c}\mathbf{F}_l^c \\ \mathbf{F}_r^c\end{array}\right\}. \tag{13}$$

Considering the coupling conditions

$$\mathbf{q}_l^c = [\mathbf{q}^+]\mathbf{A}^{in} + [\mathbf{q}^-]\mathbf{A}^{re},\ \mathbf{q}_r^c = [\mathbf{q}^+]\mathbf{A}^{tr}, \tag{14}$$

and

$$\mathbf{F}_l^c = [\mathbf{F}^+]\mathbf{A}^{in} + [\mathbf{F}^-]\mathbf{A}^{re},\ \mathbf{F}_r^c = -[\mathbf{F}^+]\mathbf{A}^{tr}, \tag{15}$$

Equation 13 can be re-formed as the governing equations for the scattering problem:

$$\begin{bmatrix} \mathbf{S}^c_{ll}[\mathbf{q}^-] - [\mathbf{F}^-] & \mathbf{S}^c_{lr}[\mathbf{q}^+] \\ \mathbf{S}^c_{rl}[\mathbf{q}^-] & \mathbf{S}^c_{rr}[\mathbf{q}^+] + [\mathbf{F}^+] \end{bmatrix} \begin{Bmatrix} \mathbf{A}^{re} \\ \mathbf{A}^{tr} \end{Bmatrix} = \begin{bmatrix} [\mathbf{F}^+] - \mathbf{S}^c_{ll}[\mathbf{q}^+] \\ -\mathbf{S}^c_{rl}[\mathbf{q}^+] \end{bmatrix} \left\{ \mathbf{A}^{in} \right\}. \quad (16)$$

Given a single or a set of incident modes as the input in Equation 16, scattered modes (reflection and transmission) acting as the output can be obtained. Numerically, the base number N_r is suggested to be frequency dependent, which can be implemented by a routine to include those slightly evanescent wave modes into the bases.

Since the coupling structure might contain a large number of interior DOFs, the dynamic reduction can be used to accelerate the spectral solution by using the assumed modes of coupling structure. The system matrices of coupling parts at each frequency in Equation 13 have to be taken into calculation. In this case, a convenient way is to model the coupling structure using component mode synthesis (CMS) method, which gives better approximation than Guyan reduction (exact for stiffness matrices but approximate for mass) when dealing with higher frequency problems. For the sake of simplicity, the fixed-boundary CMS method is used here [24]. In the fixed-boundary CMS method, a substructure is considered to be composed of interior and interface dofs. It condenses the system matrices by assuming the displacements of the interior dofs as a linear superposition of the constraint modes and the internal normal modes. By introducing the transformation matrix $[\mathbf{T}]$, the displacement vector of coupling substructure is represented in terms of generalized coordinates:

$$\left\{ \begin{array}{ccc} (\mathbf{q}^c_l)^T & (\mathbf{q}^c_i)^T & (\mathbf{q}^c_r)^T \end{array} \right\}^T = [\mathbf{T}] \left\{ \begin{array}{ccc} (\mathbf{q}^c_l)^T & (\mathbf{q}^c_\delta)^T & (\mathbf{q}^c_r)^T \end{array} \right\}^T, \quad (17)$$

where the $\mathbf{q}^c_\delta$ is the modal displacement. The transformation matrix for the fixed-boundary method has the form

$$[\mathbf{T}] = \begin{bmatrix} \mathbf{I} & \mathbf{0} & \mathbf{0} \\ -[\mathbf{K}^c_{ii}]^{-1}[\mathbf{K}^c_{il}] & \mathbf{\Phi}_{ii} & -[\mathbf{K}^c_{ii}]^{-1}[\mathbf{K}^c_{ir}] \\ \mathbf{0} & \mathbf{0} & \mathbf{I} \end{bmatrix}, \quad (18)$$

where $\mathbf{\Phi}_{ii}$ is the fixed interface normalized modal matrix, $\mathbf{K}^c_{ii}$, $\mathbf{K}^c_{il}$ and $\mathbf{K}^c_{ir}$ are the interior DOFs related components in the stiffness matrix. Other modes such as attachment modes can also be used as required. Thus Equation 12 can be simplified as

$$[\mathbf{M}^c_{CB}] \left\{ \begin{array}{ccc} (\ddot{\mathbf{q}}^c_l)^T & (\ddot{\mathbf{q}}^c_\delta)^T & (\ddot{\mathbf{q}}^c_r)^T \end{array} \right\}^T + [\mathbf{K}^c_{CB}] \left\{ \begin{array}{ccc} (\mathbf{q}^c_l)^T & (\mathbf{q}^c_\delta)^T & (\mathbf{q}^c_r)^T \end{array} \right\}^T = \left\{ \begin{array}{ccc} (\mathbf{F}^c_l)^T & \mathbf{0} & (\mathbf{F}^c_r)^T \end{array} \right\}^T \quad (19)$$

where the condensed mass matrix $[\mathbf{M}^c_{CB}] = [\mathbf{T}]^T [\mathbf{M}^c] [\mathbf{T}]$, stiffness matrix $[\mathbf{K}^c_{CB}] = [\mathbf{T}]^T [\mathbf{K}^c] [\mathbf{T}]$, $\mathbf{q}_\delta$ is the truncated set of generalized modal displacement associated to the modal matrix $\mathbf{\Phi}_{ii}$.

Consequently, Equation 16 can be modified as

$$\begin{bmatrix} \widehat{\mathbf{S}}^c_{ll}[\mathbf{q}^-] - [\mathbf{F}^-] & \widehat{\mathbf{S}}^c_{lr}[\mathbf{q}^+] \\ \widehat{\mathbf{S}}^c_{rl}[\mathbf{q}^-] & \widehat{\mathbf{S}}^c_{rr}[\mathbf{q}^+] + [\mathbf{F}^+] \end{bmatrix} \begin{Bmatrix} \mathbf{A}^{re} \\ \mathbf{A}^{tr} \end{Bmatrix} = \begin{bmatrix} [\mathbf{F}^+] - \widehat{\mathbf{S}}^c_{ll}[\mathbf{q}^+] \\ -\widehat{\mathbf{S}}^c_{rl}[\mathbf{q}^+] \end{bmatrix} \left\{ \mathbf{A}^{in} \right\}, \quad (20)$$

where $\widehat{\mathbf{S}}^c_{ll}$, $\widehat{\mathbf{S}}^c_{lr}$, $\widehat{\mathbf{S}}^c_{rl}$, $\widehat{\mathbf{S}}^c_{rr}$ are the reduced system matrices obtained by eliminating the modal displacement $\mathbf{q}_\delta$.

The spectral solution for wave scattering is therefore calculated by two kind of superelements: the eigensolutions for guided wave modes and the superelements of coupling structures. After solving Equation 20, the whole scattered wave fields can be obtained through Equations 17–19 for near field and the wave representation for far field. It should be noted that the eigensolution of the coupling substructure model can be used for different wave inputs, which is particularly applicable to the systems comprising certain standard local features. Another advantage over the direct condensation is that the number of the normal modes of coupling substructures can also be frequency dependent, not only that of the truncated bases, which further improves the numerical efficiency if the solution in the wide frequency range is desired.

3. Numerical implementation and results

3.1. Methodology

The principle of the study is to vary the circumferential position of the defect while keeping the axial position constant, and observe the influence of this variation on the reflection and transmission coefficients. The modeled defect is a through-thickness cut having 12 mm for the circumferential extent and 20 mm for the axial extent (see figure 3). The modeled pipe is made of steel and has 168 mm outer diameter and 11 mm of thickness. Material properties of the pipe are: $E = 2.1 \times 10^{11}\ Pa$, $\rho = 7800\ Kg.m^{-3}$, $\nu = 0.3$.

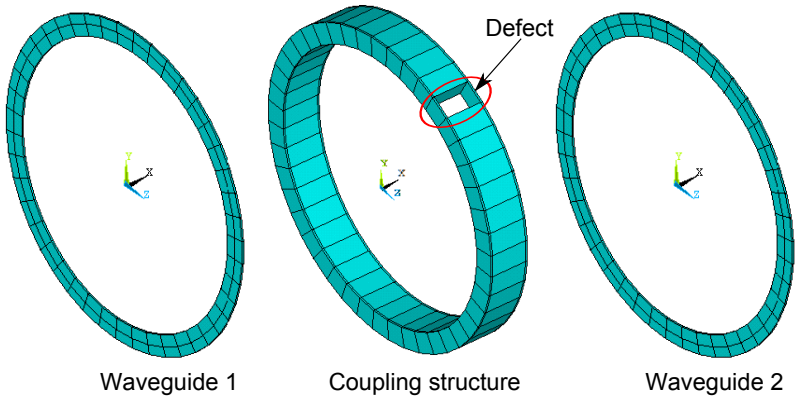

Figure 3: Defect positions around the circumference of the pipe.

Calculation was made based on the connexion between two homogeneous waveguides through inhomogeneous one including the defect as shown in figure 3. The waveguide 1 is a pipe section connected to a damaged coupling structure which is in turn connected to waveguide 2 similar to the first one. To numerically describe the wave mode scattering, the reflection and transmission coefficients are defined by the

solution of response from Equation 16:

$$R_i = \frac{A_i^{re}}{A_i^{in}}, \quad T_i = \frac{A_i^{tr}}{A_i^{in}} \tag{21}$$

where $i = 1, 2, ..., N_r$.

The circumference of the pipe is divided into 44 elements. Positions of the defect around the pipe are varied by an increment of 4 elements, that is an angle of about $\Delta\alpha = 32.73°$. Thus, 11 positions were treated in this study as illustrated in figure 4.

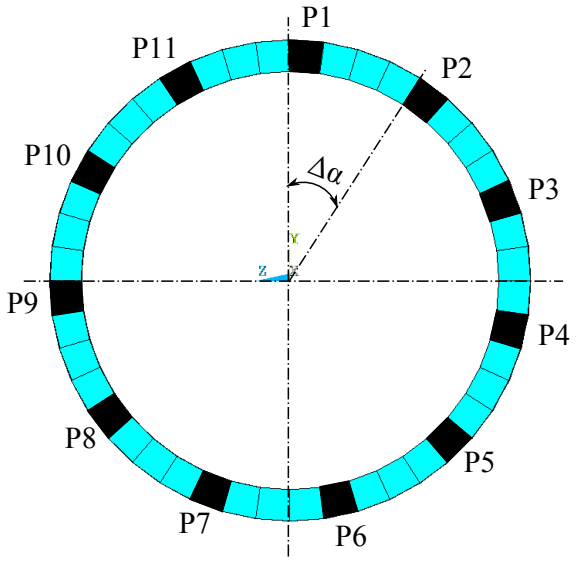

Figure 4: Defect positions around the circumference of the pipe.

Three types of incident waves are used: fundamental torsional mode T(0,1), longitudinal mode L(0,2), and flexural mode F(1,2). In the case of torsional T(0,1) as incident mode, reflection and transmission coefficients of T(0,1) and L(0,2) are checked, as well as those of three flexural modes: F(1,2), F(2,2) and F(3,2). When the longitudinal L(0,2) mode is incident, reflection and transmission coefficients of L(0,2), T(0,1) and two flexural modes: F(1,3) and F(2,3) are observed. The choice of these flexural modes to be verified is not arbitrary. In fact, when the axisymmetric torsional wave T(0,1) encounters a nonaxisymmetric feature (like a metal loss or localized weld), mode conversion could occurs. The T(0,1) mode can be converted to nonaxisymmetric flexural waves F(1,2), F(2,2) and F(3,2). When the L(0,2) mode impinges on a nonaxisymmetric feature, mode conversion manifests by the appearance of nonaxisymmetric flexural waves F(1,3) and F(2,3). The last tested incident mode is the flexural F(1,2). Its reflection and transmission coefficients were turned out. Calculations were carried out in the frequency range [5-30] kHz, in which the above-mentioned incident and reflected waves are present.

3.2. Dispersion curves in the pipe

The wavenumber k is frequency dependent and can be expressed as:

$$k(\omega) = j\frac{ln(\lambda)}{d} \tag{22}$$

The unknown propagation constants are obtained for a given frequency by the WFE method in order to find the dispersion relationship. Wavenumbers of the common modes can be thereafter evaluated and plotted as a frequency function for the modeled pipe as shown in figure 5.

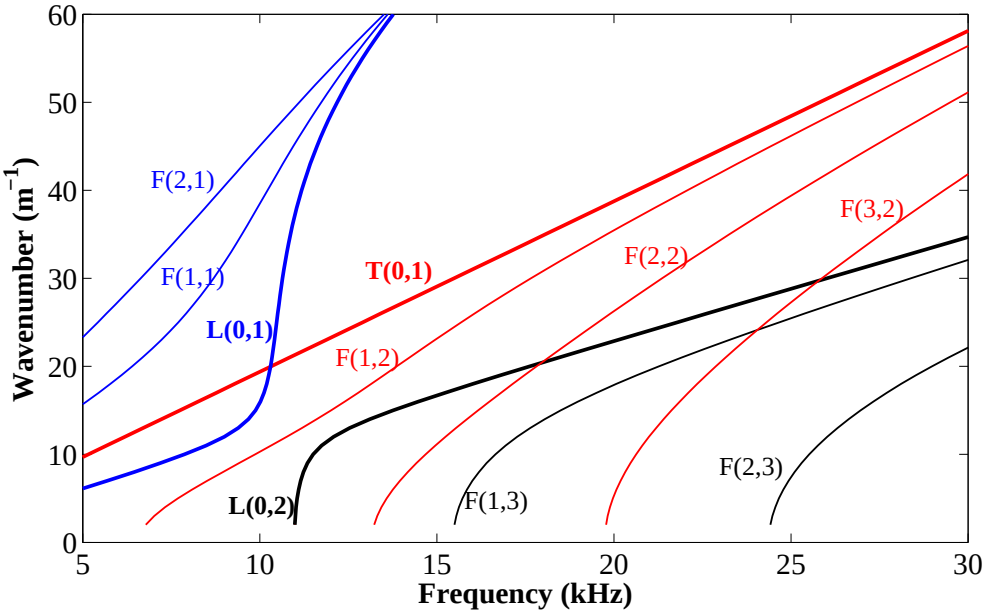

Figure 5: Wavenumber computed by WFEM for modes propagating in a steel pipe with 168 mm outer diameter, 11 mm-thick. Red bold line: torsional mode T(0,1); red normal lines: flexural torsional modes F(1,2), F(2,2) and F(3,2); black bold line: longitudinal mode L(0,2); black normal lines: flexural longitudinal modes F(1,3) and F(2,3); blue bold line: longitudinal mode L(0,1); blue normal lines: flexural longitudinal modes F(1,1) and F(2,1).

From the calculated wavenumbers, the group an phase velocities can be readily determined and plotted in the frequency range considered (figures 6 and 7).

Dispersion curves show all of the constructive interference zones that could occur as the waves reflect inside a structure, demonstrating the kinds of waves and modes that could actually propagate. These curves show that the L(0,2) mode in the frequency range 20-100 kHz is practically nondispersive, that is to say its group velocity is essentially constant with frequency so that there is minimal distortion of the wave packet over long propagation distances. L(0,2) is also the fastest mode, which means that it will be the first signal to arrive at the receiver. The L(0,1) mode is another axisymmetric longitudinal wave, which will be generated and received along with L(0,2). However, the velocity of this latter is approximately twice that

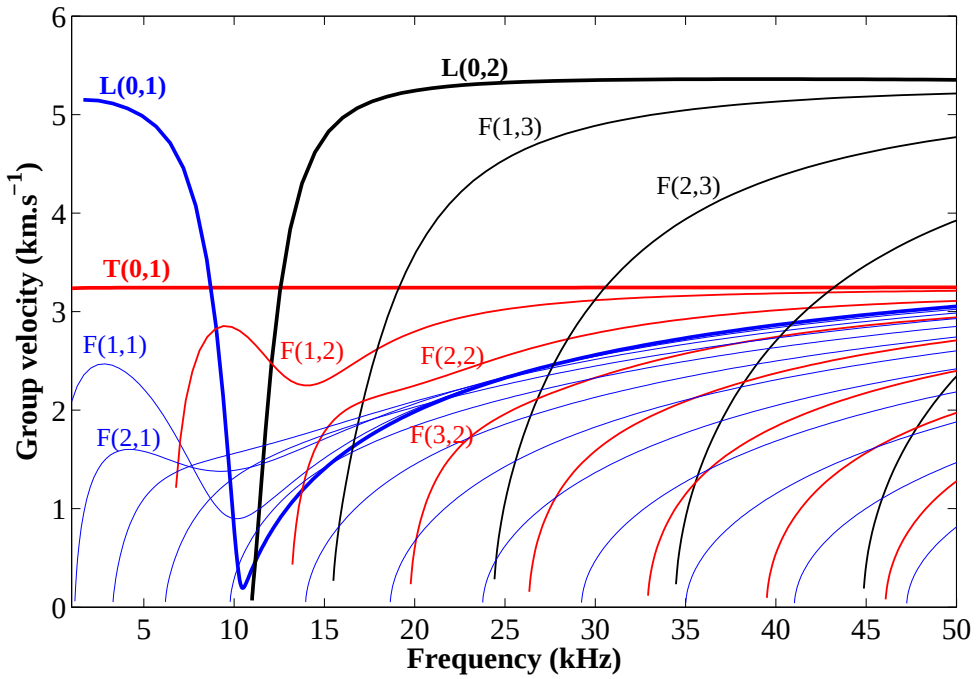

Figure 6: Group velocity dispersion curves computed by WFEM for a steel pipe, outer diameter 168 mm, thickness 11 mm. Red bold line: torsional mode T(0,1); red normal lines: flexural torsional modes F(n,2); black bold line: longitudinal mode L(0,2); black normal lines: flexural longitudinal modes F(n,3); blue bold line: longitudinal mode L(0,1); blue normal lines: flexural longitudinal modes F(n,1).

of the former. The T(0,1) mode is the only wave that keeps its velocity constant in the whole frequency range. Thus, it is an ideal nondispersive mode. Flexural modes converge to either a longitudinal or torsional mode at high frequencies where the wavelength to radius ratio is small. For example, F(n,1) modes converge to L(0,1), F(n,2) modes converge to T(0,1) and F(n,3) converge to L(0,2).

3.3. Numerical results and discussion

3.3.1. T(0,1) as incident wave

The torsional mode T(0,1) has shown a relevant capability for defect detection in pipes and possesses a lot of advantages in the long range guided waves inspection domain [25–28]. The first test in our investigation consists of impinging the considered defect by the T(0,1) mode. When this latter is incident in a such nonaxisymmetric discontinuity, three flexural modes F(1,2), F(2,2) and F(3,2) are mostly produced due to the mode conversion.

When T(0,1) is incident, reflection and transmission coefficients of T(0,1), L(0,2) and the three above-mentioned flexural modes are calculated. Several important observations could be taken from the obtained curves. Figure 8 shows the reflection and transmission coefficients of the T(0,1) mode from the considered defect for the 11 positions around the circumference of the pipe. We can note that there is no

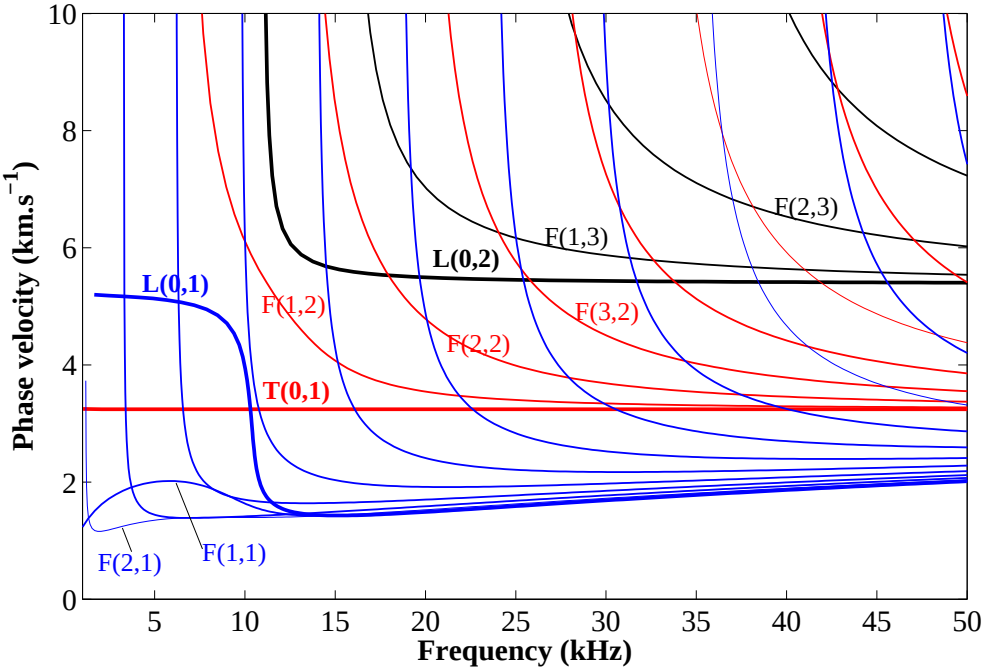

Figure 7: Phase velocity dispersion curves for a steel pipe, outer diameter 168 mm, thickness 11 mm. Red bold line: torsional mode T(0,1); red normal lines: flexural torsional modes F(n,2); black bold line: longitudinal mode L(0,2); black normal lines: flexural longitudinal modes F(n,3); blue bold line: longitudinal mode L(0,1); blue normal lines: flexural longitudinal modes F(n,1).

variation in the obtained curves depending on the circumferential position of the defect. This is obvious regarding the axisymmetry of the T(0,1) mode that makes it insensitive to an angular rotation of the defect.

Figure 9 shows the reflection and transmission coefficients of the L(0,2) mode. The result indicates that these coefficients are very negligible (around 10^{-7}). Thus, we can say that there is no reflection and transmission of the L(0,2) mode when the T(0,1) is incident.

Figures from 10 to 15 show the reflection and transmission coefficients of F(1,2), F(2,2) and F(3,2) respectively when T(0,1) is incident. From these figures we can note that for modes F(1,2) and F(3,2) each two positions have the same reflection/transmission coefficient curve except position P9; for example curves of P1 and P6 are confused. That is to say a given reflection/transmission coefficient at a given frequency refers to two possible circumferential positions, which is practically not convenient to localize the circumferential position of the defect.

However, the result found in the F(2,2) case shows that each position produces its own reflection/transmission coefficient curve. The F(2,2) mode seems to be more suitable for circumferential localization of the defect when T(0,1) mode is incident.

It should be mentioned that these flexural waves, as they are nonaxisymmetric, are sensible to the circumferential position of the defect. Nevertheless, each mode

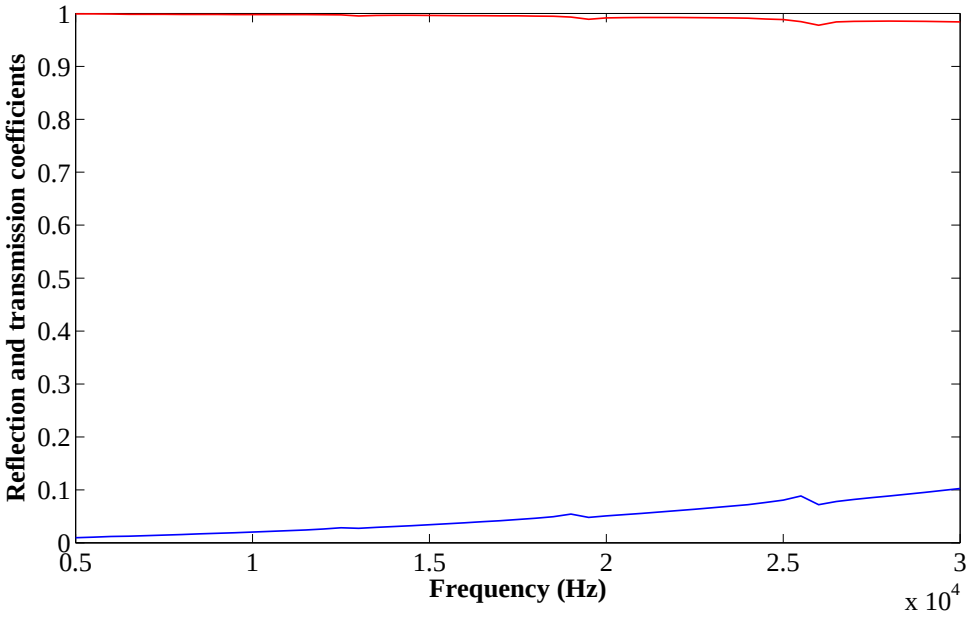

Figure 8: Reflection coefficients (blue line) and transmission coefficients (red line) of T(0,1) from a 12 $mm \times 20$ mm through-thickness defect with a T(0,1) incident mode. WEFM results for a defect having constant axial position and variable circumferential position from P1 to P11.

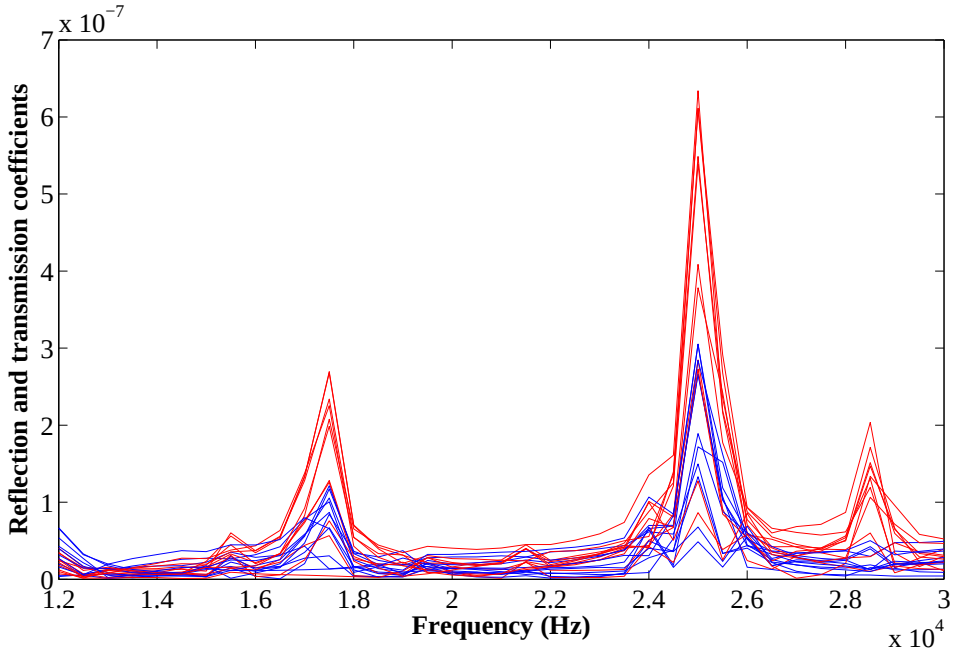

Figure 9: Reflection coefficients (blue lines) and transmission coefficients (red lines) of L(0,2) from a 12 $mm \times 20$ mm through-thickness defect with a T(0,1) incident mode. WEFM results for a defect having constant axial position and variable circumferential position from P1 to P11.

has his own mode shape which impacts on the result.

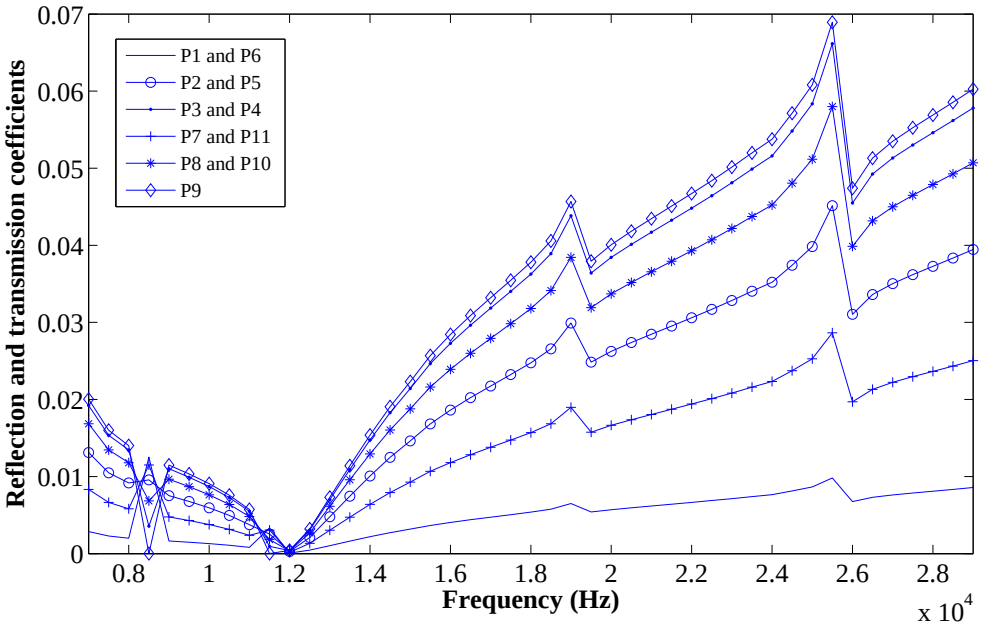

Figure 10: Reflection coefficients of F(1,2) from a 12 $mm \times 20$ mm through-thickness defect with a T(0,1) incident mode. WEFM results for a defect having constant axial position and variable circumferential position from P1 to P11.

3.3.2. L(0,2) as incident wave

The L(0,2) mode has drew attention of many researchers [1, 29–31]. It has been widely used in guided waves testing and employed in many inspection systems. It has the advantage to achieve the entire pipe wall coverage since it is axisymmetric and has a near constant mode shape through the wall thickness. Defects located at any circumferential position and anywhere the pipe wall thickness can be detected. The L(0,2) mode is dispersive but has been employed in relatively non-dispersive frequency regimes around 30-100 kHz.

The second test in our investigation consists of impinging the considered defect by the L(0,2) mode. When this latter is incident in a such nonaxisymmetric discontinuity, two flexural modes F(1,3) and F(2,3) are mostly produced due to the mode conversion.

Reflection and transmission coefficients of L(0,2), T(0,1) and the two abovementioned flexural modes are calculated. Several important observations could be taken from the obtained curves. Figure 16 shows the reflection and transmission coefficients of the L(0,2) mode from the considered defect for the 11 positions around the circumference of the pipe. We can note that there is no variation in the obtained curves depending on the circumferential position of the defect. This is obvious regarding the axisymmetry of the L(0,2) mode that makes it insensitive to an angular rotation of the defect.

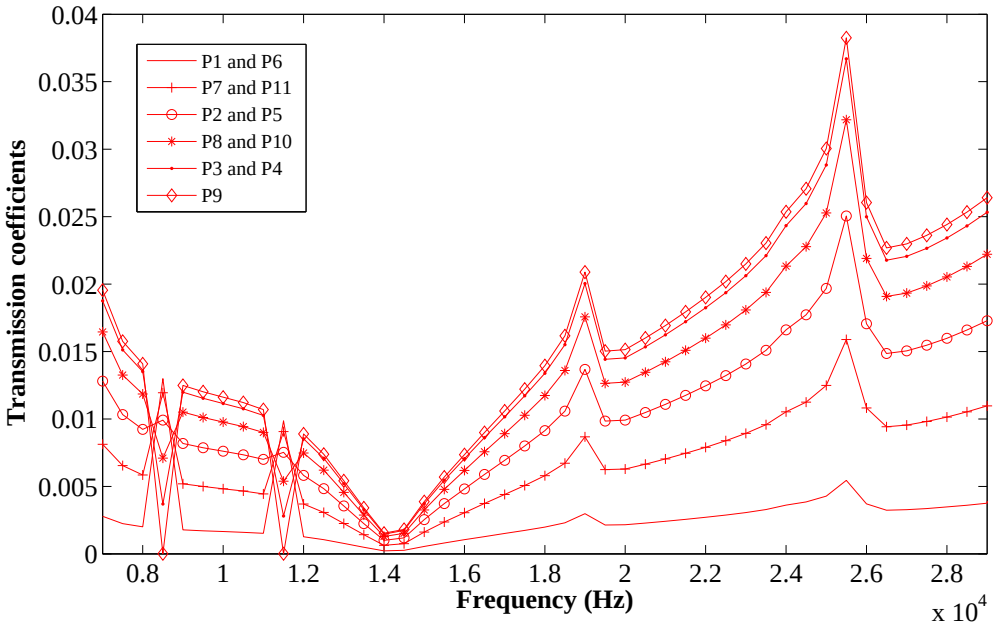

Figure 11: Transmission coefficients of F(1,2) from a 12 $mm \times 20$ mm through-thickness defect with a T(0,1) incident mode. WEFM results for a defect having constant axial position and variable circumferential position from P1 to P11.

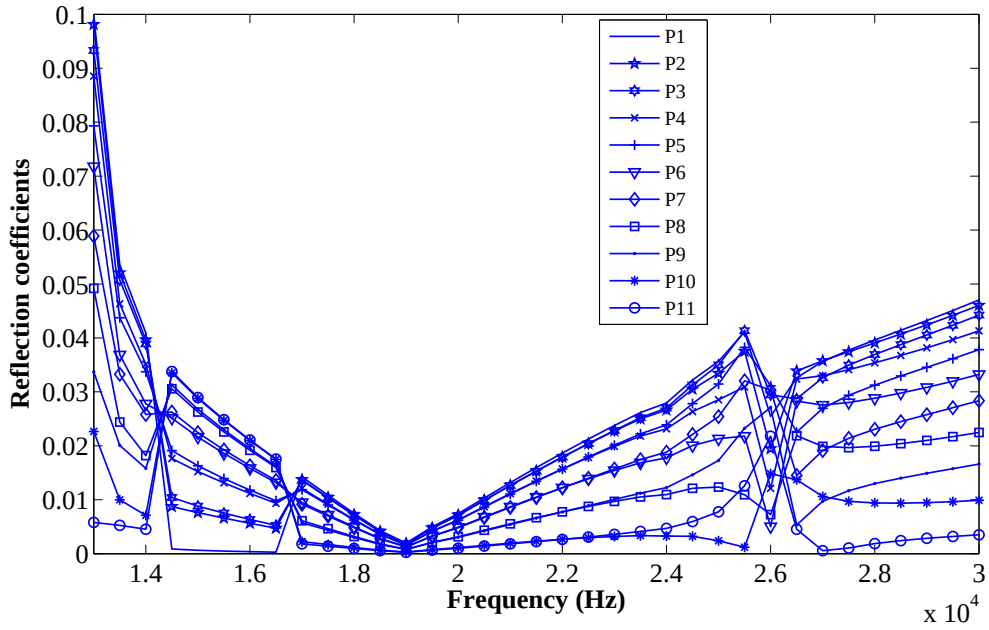

Figure 12: Reflection coefficients of F(2,2) from a 12 $mm \times 20$ mm through-thickness defect with a T(0,1) incident mode. WEFM results for a defect having constant axial position and variable circumferential position from P1 to P11.

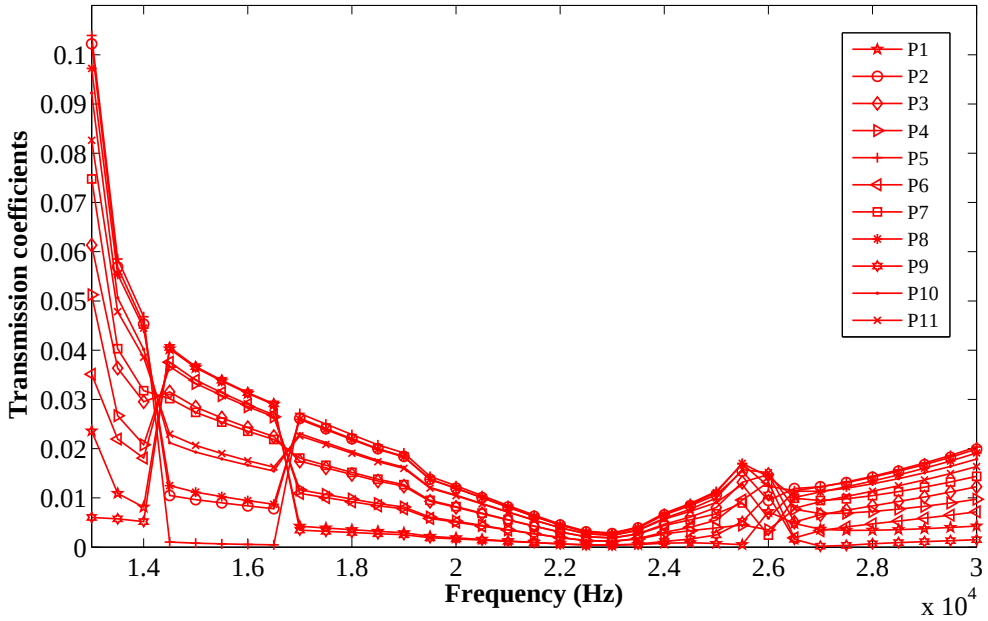

Figure 13: Transmission coefficients of F(2,2) from a 12 $mm \times 20$ mm through-thickness defect with a T(0,1) incident mode. WEFM results for a defect having constant axial position and variable circumferential position from P1 to P11.

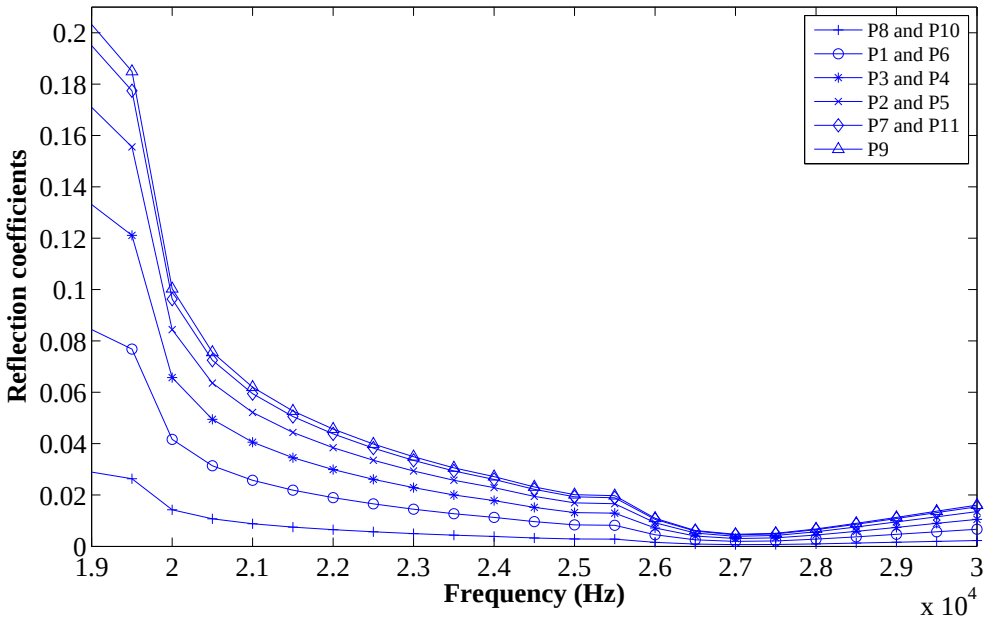

Figure 14: Reflection coefficients of F(3,2) from a 12 $mm \times 20$ mm through-thickness defect with a T(0,1) incident mode. WEFM results for a defect having constant axial position and variable circumferential position from P1 to P11.

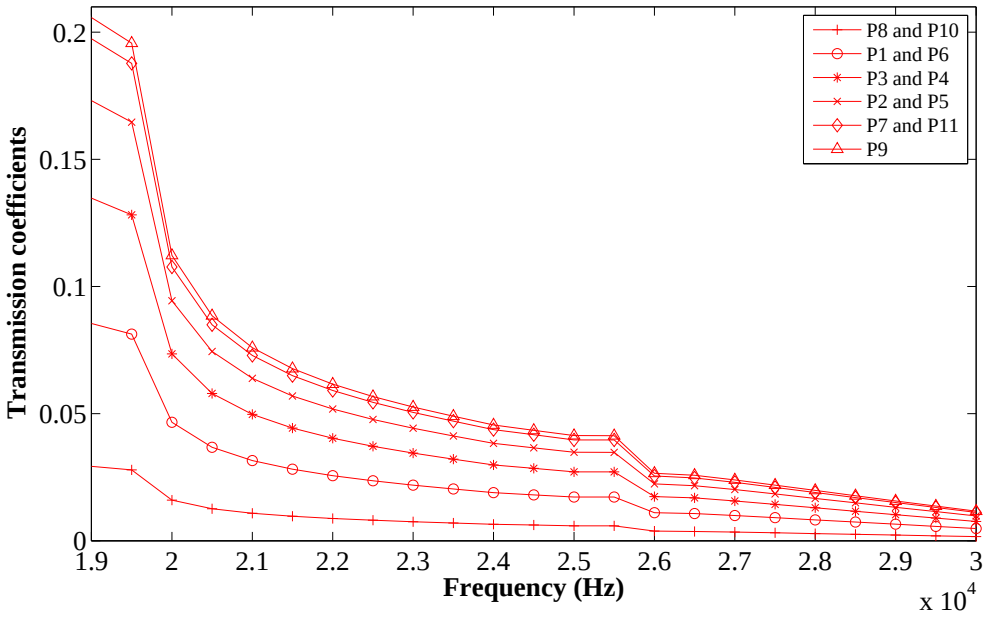

Figure 15: Transmission coefficients of F(3,2) from a 12 $mm \times 20$ mm through-thickness defect with a T(0,1) incident mode. WEFM results for a defect having constant axial position and variable circumferential position from P1 to P11.

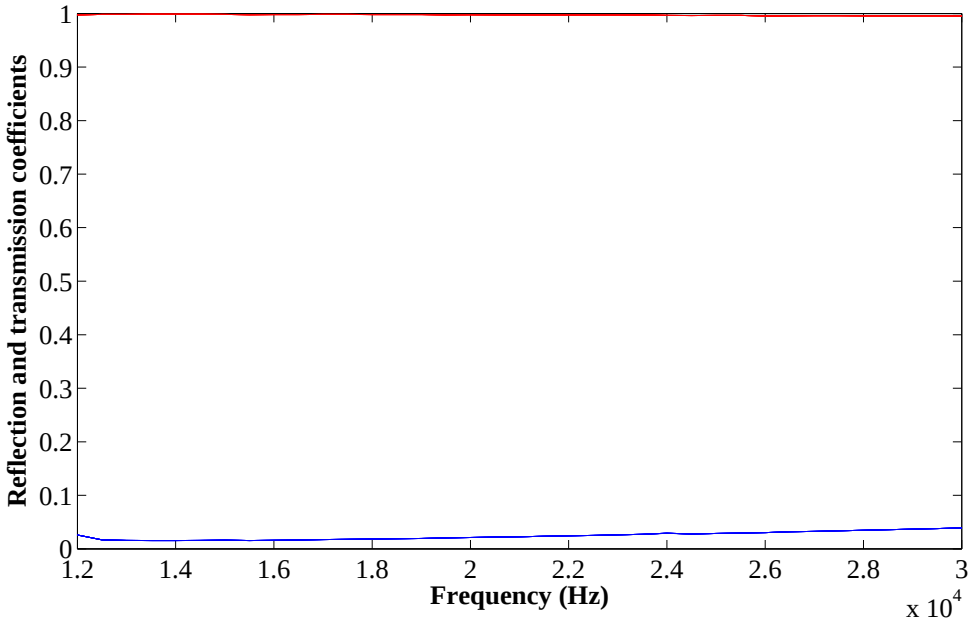

Figure 16: Reflection coefficients (blue line) and transmission coefficients (red line) of L(0,2) from a 12 $mm \times 20$ mm through-thickness defect with a L(0,2) incident mode. WEFM results for a defect having constant axial position and variable circumferential position from P1 to P11.

Figure 17 shows the reflection and transmission coefficients of the T(0,1) mode. The result indicates that these coefficients are very negligible (around 10^{-6}). Thus, we can say that there is no reflection and transmission of the T(0,1) mode when the L(0,2) is incident.

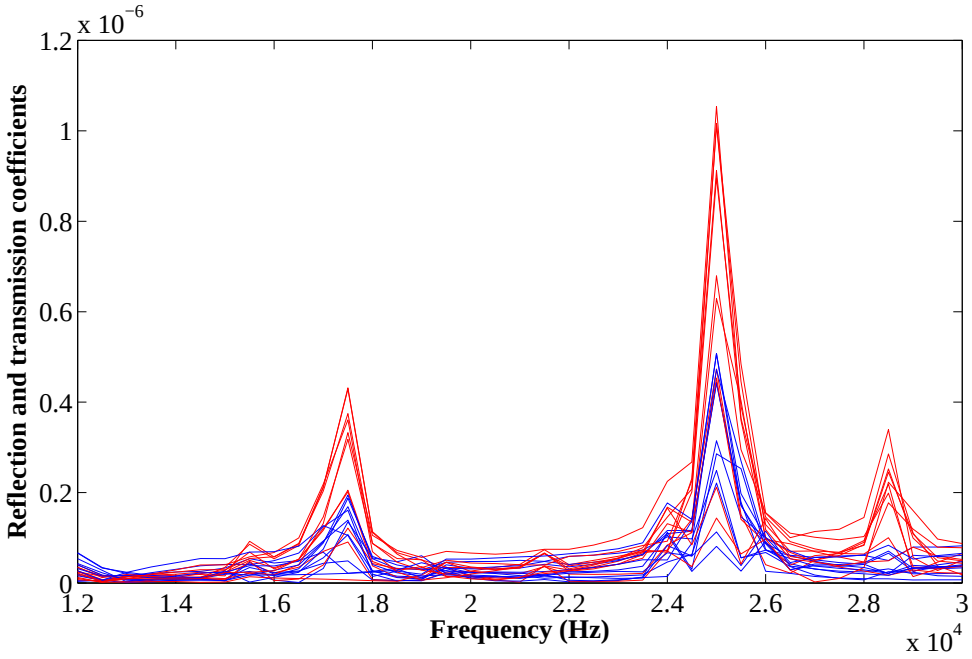

Figure 17: Reflection coefficients (blue line) and transmission coefficients (red line) of T(0,1) from a 12 $mm \times 20$ mm through-thickness defect with a L(0,2) incident mode. WEFM results for a defect having constant axial position and variable circumferential position from P1 to P11.

Figures from 18 to 21 show the reflection and transmission coefficients of F(1,3) and F(2,3) respectively when L(0,2) is incident. From these figures we can note that for the F(1,3) mode each two positions have the same reflection/transmission coefficient curve except position P9; for example curves of P1 and P6 are confused. That is to say a given reflection/transmission coefficient at a given frequency refers to two possible circumferential positions, which is practically not efficient to localize the circumferential position of the defect.

However, the result found in the F(2,3) case shows that each position produces its own reflection/transmission coefficient curve. The F(2,3) mode seems to be more suitable for circumferential localization of the defect when L(0,2) mode is incident.

3.3.3. F(1,2) as incident wave

Flexural modes could be excited via partial loading around the circumference of the pipe. If we have a transducer ring clamped around a pipe, only a part of these transducers have to be excited in order to create a nonaxisymmetric wave. Some parameters like number, type and position of the transducers as well as the frequency, play an important role in the type of the generated mode. When non-axisymmetric guided waves are generated, the acoustic field is more complicated and the energy

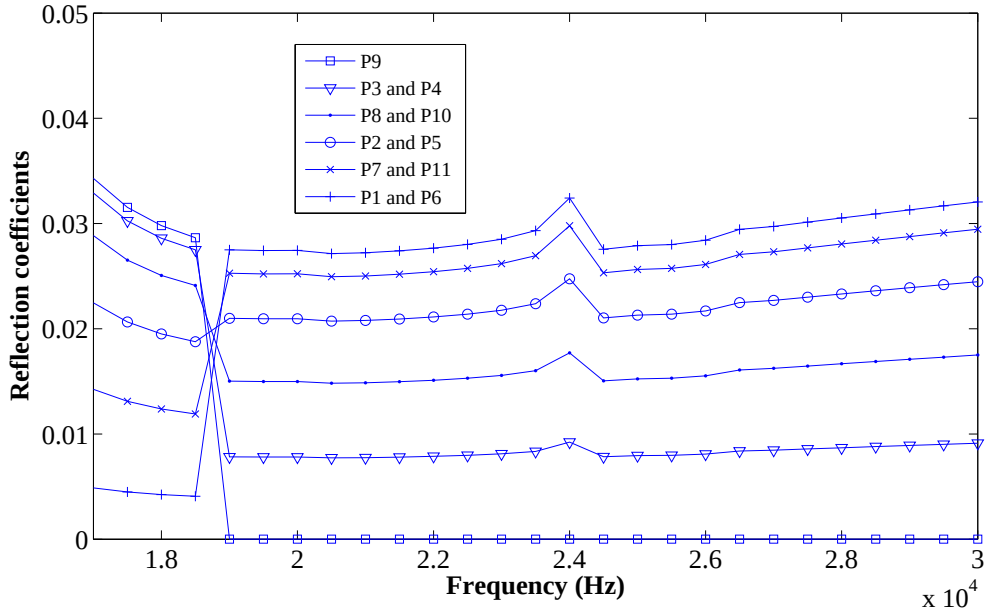

Figure 18: Reflection coefficients of F(1,3) from a 12 $mm \times 20$ mm through-thickness defect with a L(0,2) incident mode. WEFM results for a defect having constant axial position and variable circumferential position from P1 to P11.

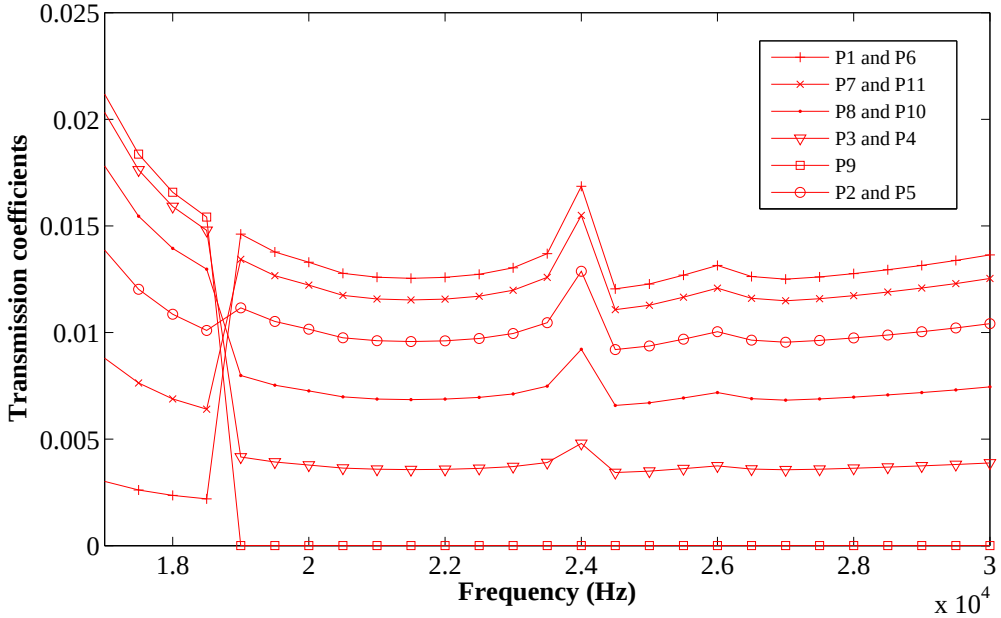

Figure 19: Transmission coefficients of F(1,3) from a 12 $mm \times 20$ mm through-thickness defect with a L(0,2) incident mode. WEFM results for a defect having constant axial position and variable circumferential position from P1 to P11.

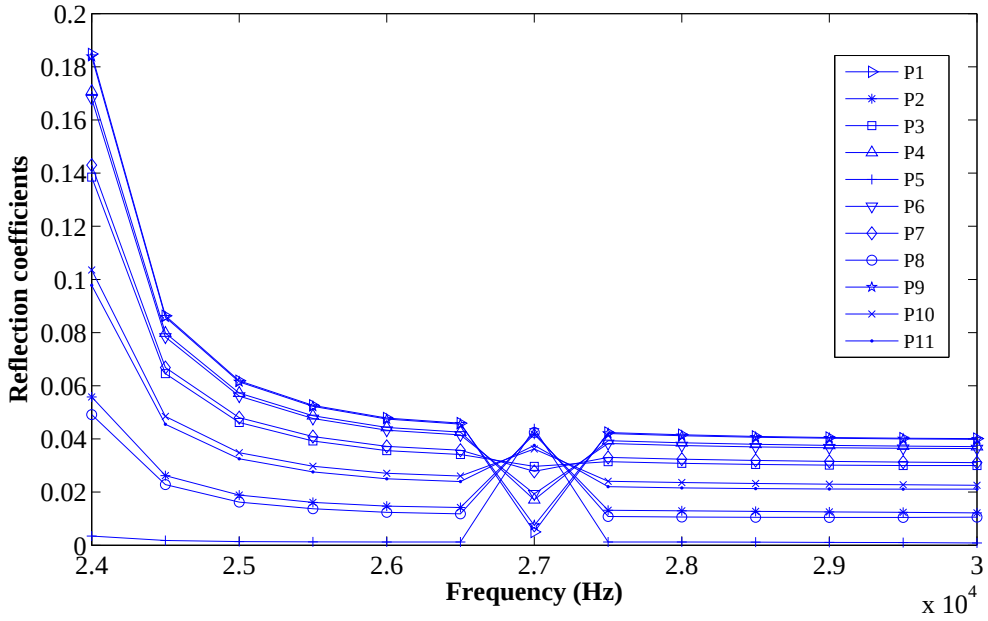

Figure 20: Reflection coefficients of F(2,3) from a 12 $mm \times 20$ mm through-thickness defect with a L(0,2) incident mode. WEFM results for a defect having constant axial position and variable circumferential position from P1 to P11.

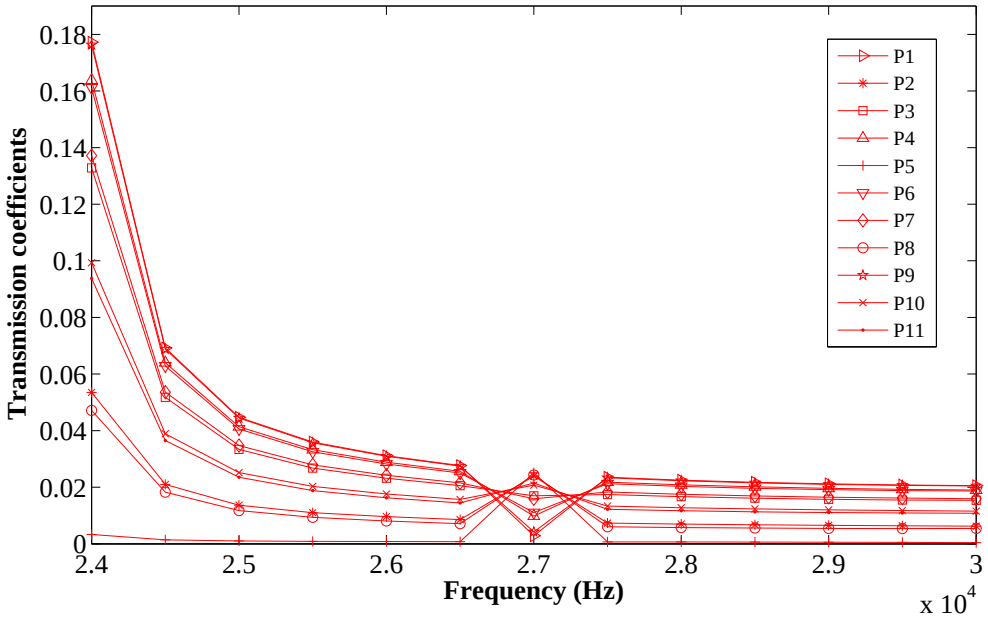

Figure 21: Transmission coefficients of F(2,3) from a 12 $mm \times 20$ mm through-thickness defect with a L(0,2) incident mode. WEFM results for a defect having constant axial position and variable circumferential position from P1 to P11.

distribution of the wave propagation needs to be known in order to evaluate the guided wave inspection ability and to perform frequency and angle tuning.

The F(1,2) mode was chosen to be incident to the considered defect for the purpose of testing its sensitivity to angular position. Reflection and transmission coefficients of the F(1,2) mode were computed for positions from P1 to P11 as shown in figures 22 and 23. We may remark the same phenomena of coincidence between each two positions (P1 with P6, P2 with P5 and so on). For a given reflection/transmission coefficient at a given frequency we have two possible circumferential positions, which is practically not efficient to localize the circumferential position of the defect.

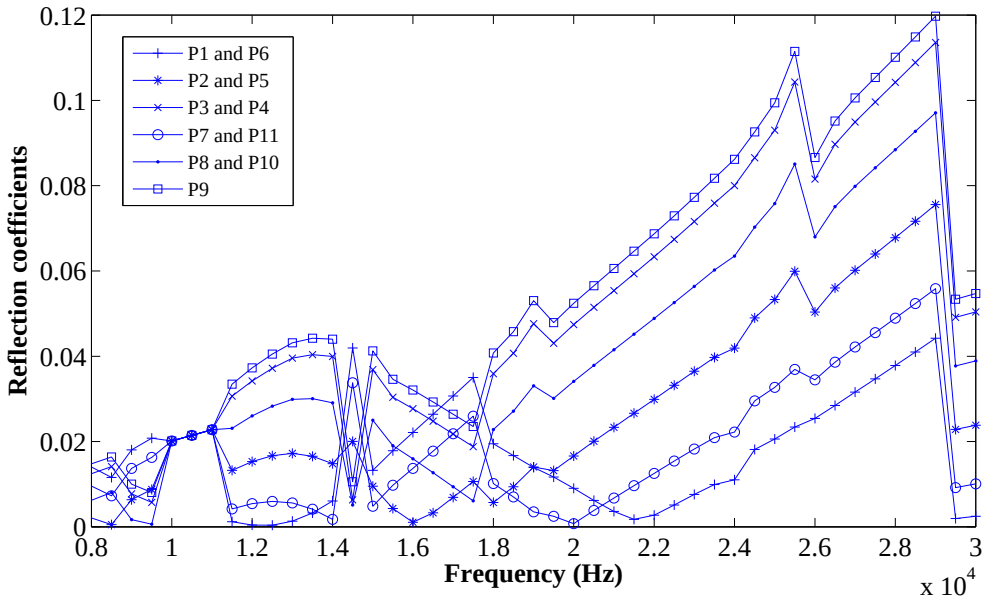

Figure 22: Reflection coefficients of F(1,2) from a 12 $mm \times 20$ mm through-thickness defect with a F(1,2) incident mode. WEFM results for a defect having constant axial position and variable circumferential position from P1 to P11.

4. Conclusion

In this work, a numerical investigation into the effect of defect angular-position on the reflection and transmission coefficients has been performed. The Wave Finite Element Method has been used to carry out calculations depending on frequency. The principle was to vary the circumferential position of the defect while keeping the axial position constant, and observe the influence of this variation on the reflection and transmission coefficients. Results have shown many important remarks. While exciting the pipe by the torsional T(0,1) mode, there is no effect on the reflection and transmission coefficients of T(0,1) regarding its axisymmetry. Almost neither reflection nor transmission of the L(0,2) mode have been found. However, results obtained for flexural waves show that the F(2,2) mode has a good potential to reveal

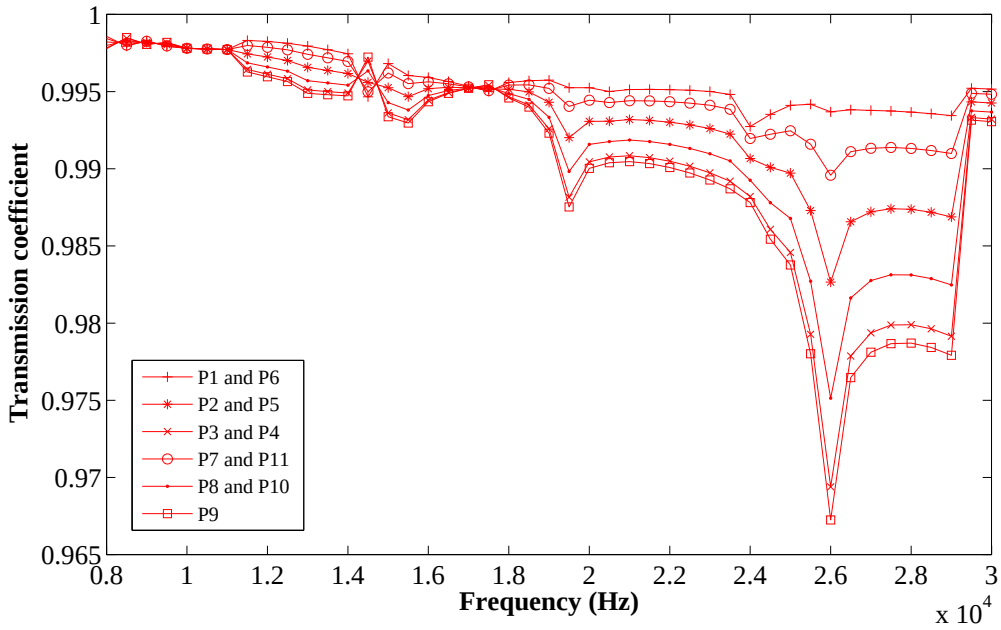

Figure 23: Transmission coefficients of F(1,2) from a 12 $mm \times 20$ mm through-thickness defect with a F(1,2) incident mode. WEFM results for a defect having constant axial position and variable circumferential position from P1 to P11.

the angular position of the defect. When L(0,2) mode is incident, there is no effect on the reflection and transmission coefficients of L(0,2) due to its axisymmetry. Almost neither reflection nor transmission of the T(0,1) mode have been detected. However, results obtained for flexural waves show that the F(2,3) mode has a good potential to reveal the angular position of the defect. When F(1,2) mode is incident, the result is not so accurate since we obtain two possible angular positions for the defect.

This investigation gives guidance to circumferential localization of defects in pipes by a numerical way. This approach could be improved by refining the mesh of the pipe which leads to a more accurate scanning of the circumference.

References

[1] D. Alleyne, P. Cawley, The long range detection of corrosion in pipes using lamb waves, Review of Progress in Quantitative NDE 14 (1995) 2073–2080.

[2] J. Barshinger, J. Rose, M. Avioli Jr, Guided wave resonance tuning for pipe inspection, Journal of Pressure Vessel Technology 124 (2002) 303–310.

[3] J. Rose, J. Mu, Y. Cho, Recent advances on guided waves in pipe inspection, in: Proceedings of the 17th World Conference on Nondestructive Testing, Shanghai, China, 2008.

[4] H. Shin, J. Rose, Guided wave tuning principles for defect detection in tubing, Journal of nondestructive evaluation 17 (1) (1998) 27–36.

[5] J. Rose, X. Zhao, Flexural mode tuning for pipe elbow inspection, Materials Evaluation 59 (5) (May 2001) 621–624.

[6] J. Li, J. Rose, Implementing guided wave mode control by use of a phased transducer array, Ultrasonics, Ferroelectrics and Frequency Control, IEEE Transactions on 48 (3) (2001) 761–768.

[7] J. Rose, Z. Sun, P. Mudge, M. Avioli, Guided wave flexural mode tuning and focusing for pipe testing, Materials evaluation 61 (2) (2003) 162–167.

[8] Z. Sun, L. Zhang, J. L. Rose, Flexural torsional guided wave mechanics and focusing in pipe, Journal of Pressure Vessel Technology 127 (2005) 471–478.

[9] T. Hayashi, K. Kawashima, Z. Sun, J. Rose, Guided wave focusing mechanics in pipe, Journal of pressure vessel technology 127 (2005) 317–321.

[10] L. Zhang, W. Luo, J. Rose, Ultrasonic guided wave focusing beyond welds in a pipeline, in: AIP Conference Proceedings, Vol. 820 A, Institute of physics publishing LTD, 2005, pp. 877–884.

[11] H. Shin, J. Rose, Guided waves by axisymmetric and non-axisymmetric surface loading on hollow cylinders, Ultrasonics 37 (5) (1999) 355–363.

[12] J. Li, J. Rose, Excitation and propagation of non-axisymmetric guided waves in a hollow cylinder, The Journal of the Acoustical Society of America 109 (2001) 457–464.

[13] J. Davies, P. Cawley, The application of synthetic focusing for imaging crack-like defects in pipelines using guided waves, Ultrasonics, Ferroelectrics and Frequency Control, IEEE Transactions on 56 (4) (2009) 759–771.

[14] S. Gopalakrishnan, A. Chakraborty, D. R. Mahapatra, Spectral Finite Element Method: Wave Propagation, Diagnostics and Control in Anisotropic and Inhomogeneous Structures, Springer, 2008.

[15] N. Hu, H. Fukunaga, M. Kameyama, D. R. Mahapatra, S. Gopalakrishnan, Analysis of wave propagation in beams with transverse and lateral cracks using a weakly formulated spectral method, Journal of Applied Mechanics 74 (2007) 119–127.

[16] J. Galán, R. Abascal, Numerical simulation of lamb wave scattering in semi-infinite plates, International Journal for Numerical Methods in Engineering 53 (2002) 1145–1173.

[17] W. Zhou, M. Ichchou, J.-M. Mencik, Analysis of wave propagation in cylindrical pipes with local inhomogeneities, Journal of Sound and Vibration 319 (1-2) (2009) 335–354.

[18] M. Ichchou, J. Mencik, W. Zhou, Wave finite elements for low and mid-frequency description of coupled structures with damage, Computer Methods in Applied Mechanics and Engineering 198 (15-16) (2009) 1311–1326.

[19] W. Zhou, M. Ichchou, Wave propagation in mechanical waveguide with curved members using wave finite element solution, Computer Methods in Applied Mechanics and Engineering 199 (33-36) (2010) 2099–2109.

[20] W. Zhou, M. Ichchou, Wave scattering by local defect in structural waveguide through wave finite element method, Structural Health Monitoring 10 (4) (2011) 335–349.

[21] W. Zhong, F. Williams, On the direct solution of wave propagation for repetitive structures, Journal of Sound and Vibration 181 (1995) 485–501.

[22] D. Mackey, N. Mackey, C. Mehl, V. Mehrmann, Structured polynomial eigenvalue problems: good vibrations from good linearizations, SIAM Journal on Matrix Analysis and Applications 28 (2006) 1029–1058.

[23] R. Lehoucq, D. Sorensen, C. Yang, ARPACK Users' guide: solution of large-scale eigenvalue problems with implicitly restarted arnoldi methods, SIAM Publications, Philadelphia, 1998.

[24] R. Craig, M. Bampton, Coupling of substructures for dynamic analysis, AIAA Journal 12 (1968) 1313–1319.

[25] A. Demma, P. Cawley, M. Lowe, A. Roosenbrand, The reflection of the fundamental torsional mode from cracks and notches in pipes, The Journal of the Acoustical Society of America 114 (2003) 611–625.

[26] D. Alleyne, B. Pavlakovic, M. Lowe, P. Cawley, Rapid long range inspection of chemical plant pipework using guided waves, Key Engineering Materials 270 (2004) 434–441.

[27] A. Demma, P. Cawley, M. Lowe, A. Roosenbrand, B. Pavlakovic, The reflection of guided waves from notches in pipes: a guide for interpreting corrosion measurements, NDT & E International 37 (3) (2004) 167–180.

[28] J. Ma, F. Simonetti, M. J. S. Lowe, Scattering of the fundamental torsional mode by an axisymmetric layer inside a pipe, The Journal of the Acoustical Society of America 120 (4) (2006) 1871–1880.

[29] D. Alleyne, P. Cawley, The excitation of lamb waves in pipes using dry-coupled piezoelectric transducers, Journal of nondestructive evaluation 15 (1) (1996) 11–20.

[30] J. Barshinger, J. Rose, Guided wave propagation in an elastic hollow cylinder coated with a viscoelastic material, Ultrasonics, Ferroelectrics and Frequency Control, IEEE Transactions on 51 (11) (2004) 1547–1556.

[31] T. Hayashi, K. Kawashima, Z. Sun, J. Rose, Guided wave propagation mechanics across a pipe elbow, Journal of pressure vessel technology 127 (2005) 322–327.

Conclusion

The work presented in this manuscript form part of the research aimed at provide a novel solution to defect detection in piped using guided waves. This domain of research belongs to the Nondestructive Testing field, which is under continuous progress. The current market of long range pipe monitoring exhibits a strong competition. Actually, some commercial inspection systems exist, each one has its own characteristics.

An inspection system prototype for defect detection in pipes was designed in this work. It consists of two rings of 16 piezoelectric transducers for each one. The generator ring aims at creating torsional guided waves that can travel along the pipeline. When they encountered discontinuity in the structure, a part of these waves were reflected back to the receiver ring. The received time signals were then analyzed in order to determine the position and the nature of defects.

The use and the need of such a device for structural health monitoring was illustrated by preliminary numerical simulations. These simulations had shown the promising potential of torsional wave motion among all the propagative waves in pipe. In the design process, many finite element simulations were carried out on intact and damaged pipes in order to visualize the torsional wave propagation and to verify the sensitivity to defects. Time responses obtained from standard FE and WFE methods have shown the generation of the torsional mode by clamping the piezoelectric transducers in the proper orientation. These simulated signals have proven also the defect detection.

Many experimental tests have been performed by the prototype on intact and damaged pipes for two different materials: PVC and steel. Results validate the ability of the inspection system to generate the desired waves. Damping, as a property of structure, was identified and was evaluated experimentally for the two material types. The generated waves could propagate along the pipe and detect discontinuities like defects. The interaction between waves and a machined notch was determined by the estimation of reflection coefficients at different excitation frequencies. These values were compared with WFE results and have shown a good agreement. The wave interaction with curved structure was also evaluated by comparing intact and damaged bends. The obtained time signals have indicated a good detection potential.

The long distance application involving the treatment of reflected traveling waves is then the next step. For this purpose, a pipeline was tested by our inspection system. The tested pipeline is an industrial mock-up that brings together hollow pipes, features and machined defects. It was placed in conditions close to real industrial environment in order to simulate and involve almost all sources of influence on the

performed measurements. The Wave Finite Element Method was used to compute dispersion curves of propagating waves along the tested pipeline. Measurements were performed according to well-defined points sweeping all the pipeline. Yet, regarding the complexity of the time signal for field applications, some post-treatment of such signals was necessary. Recorded signals was subjected to a series of treatments like signal denoising tools and Hilbert transform in the aim of obtaining comprehensible curves. Based on the pipeline architecture, the identification of reflections in obtained curves was performed in order to distinguish between peaks related to defects from those related to structured singularities.

Guided wave techniques have two main objectives: defect localization and defect sizing. The former being realized, the latter needs some interest. For this goal, a parametric study of the torsional-mode reflection from defects and structural singularities in an industrial pipeline was established. The Wave Finite Element Method was used to construct a numerical database of reflection coefficients from rectangular defects by varying thickness, axial and circumferential extents. Calculation was made depending on frequency. Experiments lead us to estimate reflection coefficients from detected defects. Since the defect identification and localization can be made by analyzing experimental signals, the reflection coefficient can be evaluated based on the attenuation curve of the incident wave, at different frequencies. Then, the approximation of defect sizes was carried out by sweeping the numerical abacuses to find the suitable combination of dimensions for a given defect. Axial and circumferential extents was evaluated by limited intervals for each possible thickness. Subsequently, a comparison between reflection coefficients from structural singularities (elbows, concrete blocks, clamps, and welds) obtained by WFEM and experiments has been carried out. A good agreement was found for most of the structured singularities, but clear gaps was noted for the others. This can be justified by the fact that we did not take into account the presence of defects in these singularities. Future works can focus on this issue in order to deal with the effect of damaged structural singularities on the reflection coefficient.

The last task in this thesis was to find out a solution to angular localization of a knowing defect. That is why a numerical investigation into the effect of defect angular-position on the reflection and transmission coefficients has been performed. The Wave Finite Element Method has been used to carry out calculations depending on frequency. The principle was to vary the circumferential position of the defect while keeping the axial position constant, and observe the influence of this variation on the reflection and transmission coefficients. Results have shown many important remarks. While exciting the pipe by the torsional T(0,1) mode, there is no effect on the reflection and transmission coefficients of T(0,1) regarding its axisymmetry. Almost neither reflection nor transmission of the L(0,2) mode have been found. However, results obtained for flexural waves show that the F(2,2) mode has a good potential to reveal the angular position of the defect. When L(0,2) mode is incident, there is no effect on the reflection and transmission coefficients of L(0,2) due to its axisymmetry. Almost neither reflection nor transmission of the T(0,1) mode have been detected. However, results obtained for flexural waves show that the F(2,3) mode has a good potential to reveal the angular position of the defect. When F(1,2) mode is incident, the result is not so accurate since we obtain two possible angular

positions for the defect. This investigation gives a guidance to circumferential localization of defects in pipes by a numerical way. This approach could be improved by refining the mesh of the pipe which leads to a more accurate scanning of the circumference.

The developed inspection system is just at its prototype phase. Thus, a lot of improvement could be brought for its design in order to provide a more robust system able to inspect structures at more severe conditions. The excitation frequency have also to be increased in order to be able to detect small defects. Numerical side, the process of defect sizing needs to be automated based on the numerical database constructed by WFEM in one hand, and experimental evaluations in the other hand.

Appendix A

Piezoelectric transducers properties

Piezoelectric transducers contained in the inspection system prototype are shear plates made of 'PIC 255', which is a modified lead zirconate titanate (PZT) with a high curie temperature, coupling factor and charge constant. Transducers have the dimensions: 20 mm x 10 mm x 5 mm. Shear direction is parallel to the 20 mm edge. The material is optimized for actuator application under dynamic or high-temperature working conditions. Due to its high coupling efficiency, low mechanical quality factor and low temperature coefficient, it is also well suited low-power ultrasonic transducers, non-resonant boardband devices, sensors for load and sound transducers and is preferred for vacuum applications (Table A.1).

Parameter		Unit	Value
Density	p	g/cm^3	7.8
Curie Temperature	T_c	$^\circ C$	350
Relative Dielectric Permittivity	$\epsilon_{33}^T/\epsilon_0$		1750
	$\epsilon_{11}^T/\epsilon_0$		1650
Dielectric Dissipation Factor	$tan\delta$		0.02
Electromechanical Coupling Factor	k_p		0.62
	k_t		
	k_{31}		0.35
	k_{33}		0.69
Mechanical Quality Factor	Q_m		80
Frequency Constant	N_p	H_{zm}	2000
	N_1	H_{zm}	1420
	N_3	H_{zm}	
	N_t	H_{zm}	2000
Piezoelectric Deformation (Charge) Coefficient	d_{31}	pm/V	-180
	d_{33}	pm/V	400
	d_{15}	pm/V	500
Piezoelectric Voltage Coefficient	g_{31}	$10^{-3}\ Vm/N$	-11.3
	g_{33}	$10^{-3}\ Vm/N$	25
Elastic Compliance Coefficient	s_{11}^E	$10^{-12}\ m^2/N$	16.1
	s_{33}^E	$10^{-12}\ m^2/N$	20.7
Elastic Stiffness Coefficient	c_3^D	$10^{10}\ N/m^2$	13.4
Temperature Coefficient	$TC\epsilon_{33}$	$10^{-3}/K$	4

Table A.1: Material properties of PIC 255 (PI Ceramic) [83]

Appendix B

CAD model of the inspection system prototype

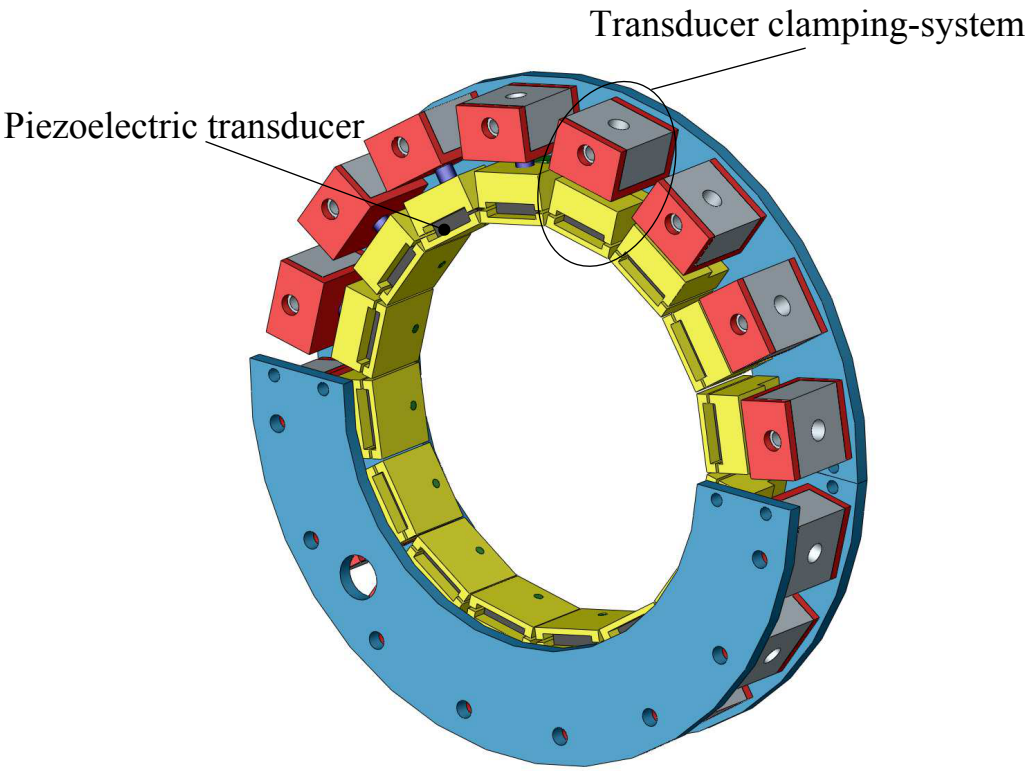

Figure B.1: 3D representation of the prototype.

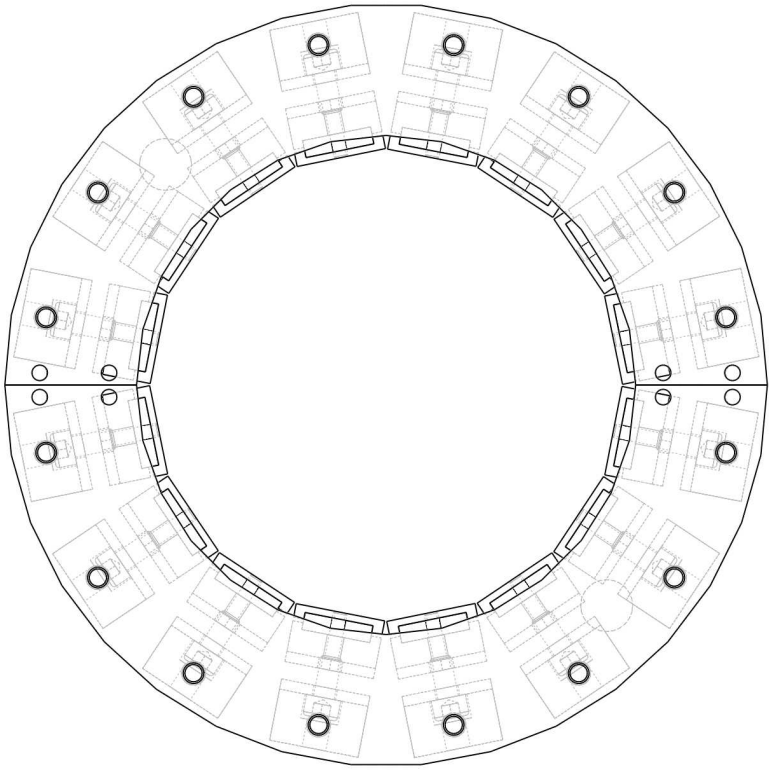

Figure B.2: Planar representation of the prototype.

Bibliography

[1] M. G. Lozev, R. W. Smith, and B. B. Grimmett. Evaluation of methods for detecting and monitoring of corrosion damage in risers. *Journal of Pressure Vessel Technology*, 127(3):244–254, 2005.

[2] D.L. Atherton. Magnetic inspection is key to ensuring safe pipelines. *NDT & E International*, 30(1):40, 1997.

[3] A. Plotnicov and L. Clapham. Stress effects and magnetic NDE methods for pipeline inspection: A study of interacting defects. *Insight (Northampton)*, 44(2):74–78, 2002.

[4] Y.S. Sun, M.X. Qu, J.T. Si, C.T. Lu, X.Y. Zhou, and D.L. Atherton. Improvement in remote-field eddy current probe structure. *NDT & E International*, Vol. 50(No. 5):pp. 600–604, May 1992.

[5] T.R. Schmidt. The remote field eddy current inspection technique. *Materials evaluation*, 42(2):225–230, 1984.

[6] W.N. Reynolds. Radiographic, ultrasonic and infra-red NDT techniques for ceramics. *British ceramic. Transactions and journal*, 88(4):124–126, 1989.

[7] R.B. Thompson, G.A. Alers, and M.A. Tennison. Application of direct electromagnetic lamb wave generation to gas pipeline inspection. In *1972 Ultrasonics Symposium*, pages 91–94. IEEE, 1972.

[8] MG Silk and KF Bainton. The propagation in metal tubing of ultrasonic wave modes equivalent to lamb waves. *Ultrasonics*, 17(1):11–19, 1979.

[9] D.N. Alleyne and P. Cawley. The excitation of lamb waves in pipes using dry-coupled piezoelectric transducers. *Journal of nondestructive evaluation*, 15(1):11–20, 1996.

[10] J.L. Rose. A baseline and vision of ultrasonic guided wave inspection potential. *Transactions-American society of mechanical engineers journal of pressure vessel technology*, 124(3):273–282, 2002.

[11] W. Mohr and P. Höller. On inspection of thin-walled tubes for transverse and longitudinal flaws by guided ultrasonic waves. *IEEE Transactions on Sonics and Ultrasonics*, 23:369–374, 1976.

[12] R.B. Thompson, R.K. Elsley, W.E. Peterson, and C.F. Vasile. An emat system for detecting flaws in steam generator tubes. *DARPA/AFML Review of Progress in Quantitative Nondestructive Evaluation*, pages 562–567, 1979.

[13] W. Böttger, H. Schneider, and W. Weingarten. Prototype emat system for tube inspection with guided ultrasonic waves. *Nuclear engineering and design*, 102(3):369–376, 1987.

[14] D.N. Alleyne and P. Cawley. The long range detection of corrosion in pipes using lamb waves. *Review of Progress in Quantitative NDE*, 14:2073–2080, 1995.

[15] D. N. Alleyne, M.J.S. Lowe, and P. Cawley. The reflection of guided waves from circumferential notches in pipes. *Journal of Applied Mechanics*, 65(3):635–641, 1998.

[16] M. Lowe. Characteristics of the reflection of lamb waves from defects in plates and pipes. *Plenum Publishing Corp., Review of Progress in Quantitative Nondestructive Evaluation*, 1998.

[17] M.J.S. Lowe, D.N. Alleyne, and P. Cawley. The mode conversion of a guided wave by a part-circumferential notch in a pipe. *Journal of Applied mechanics*, 65:649, 1998.

[18] D.N. Alleyne and P. Cawley. The effect of discontinuities on the long-range propagation of lamb waves in pipes. *ARCHIVE: Proceedings of the Institution of Mechanical Engineers, Part E: Journal of Process Mechanical Engineering 1989-1996 (vols 203-210)*, 210(35):217–226, 1996.

[19] A. Demma, P. Cawley, M. Lowe, and A.G. Roosenbrand. The reflection of the fundamental torsional mode from cracks and notches in pipes. *The Journal of the Acoustical Society of America*, 114:611, 2003.

[20] D.N. Alleyne, B. Pavlakovic, M.J.S. Lowe, and P. Cawley. Rapid, long range inspection of chemical plant pipework using guided waves. *Key Engineering Materials*, 270:434–441, 2004.

[21] J. Ma, F. Simonetti, and M. J. S. Lowe. Scattering of the fundamental torsional mode by an axisymmetric layer inside a pipe. *The Journal of the Acoustical Society of America*, 120(4):1871–1880, October 2006.

[22] J.L. Rose, S.P. Pelts, and M.J. Quarry. A comb transducer model for guided wave nde. *Ultrasonics*, 36(1-5):163–169, 1998.

[23] H.J. Shin and J.L. Rose. Guided wave tuning principles for defect detection in tubing. *Journal of nondestructive evaluation*, 17(1):27–36, 1998.

[24] J. Barshinger and M.J. Avioli Jr. Guided wave resonance tuning for pipe inspection. *Journal of Pressure Vessel Technology*, 124:303, 2002.

[25] J.L. Rose, Z. Sun, P.J. Mudge, and M.J. Avioli. Guided wave flexural mode tuning and focusing for pipe testing. *Materials evaluation*, 61(2):162–167, 2003.

[26] Z. Sun, L. Zhang, and J.L. Rose. Flexural torsional guided wave mechanics and focusing in pipe. *Journal of Pressure Vessel Technology*, 127:471, 2005.

[27] T. Hayashi, K. Kawashima, Z. Sun, and J.L. Rose. Guided wave focusing mechanics in pipe. *Journal of pressure vessel technology*, 127:317, 2005.

[28] J.L. Rose, J. Mu, and Y. Cho. Recent advances on guided waves in pipe inspection. In *Proceedings of the 17th World Conference on Nondestructive Testing, Shanghai, China*, 2008.

[29] H.J. Shin and J.L. Rose. Guided waves by axisymmetric and non-axisymmetric surface loading on hollow cylinders. *Ultrasonics*, 37(5):355–363, 1999.

[30] J. Li and J.L. Rose. Excitation and propagation of non-axisymmetric guided waves in a hollow cylinder. *The Journal of the Acoustical Society of America*, 109:457, 2001.

[31] W. Luo, J. L. Rose, J. K. van Velsor, M. Avioli, and J. Spanner. Circumferential Guided Waves for Defect Detection in Coated Pipe. In D. O. Thompson & D. E. Chimenti, editor, *Review of Progress in Quantitative Nondestructive Evaluation Volume 25*, volume 820 of *American Institute of Physics Conference Series*, pages 165–172, March 2006.

[32] W. Luo and J.L. Rose. Phased array focusing with guided waves in a viscoelastic coated hollow cylinder. *The Journal of the Acoustical Society of America*, 121:1945, 2007.

[33] J.N. Barshinger and J.L. Rose. Guided wave propagation in an elastic hollow cylinder coated with a viscoelastic material. *Ultrasonics, Ferroelectrics and Frequency Control, IEEE Transactions on*, 51(11):1547–1556, 2004.

[34] J.L. Rose and X. Zhao. Flexural mode tuning for pipe elbow inspection. *Materials Evaluation*, 59(5):621–624, May 2001.

[35] T. Hayashi and J.L. Rose. Guided wave simulation and visualization by a semianalytical finite element method. *Materials evaluation*, 61(1):75–79, 2003.

[36] T. Hayashi, K. Kawashima, Z. Sun, and J.L. Rose. Guided wave propagation mechanics across a pipe elbow. *Journal of pressure vessel technology*, 127:322, 2005.

[37] A. Demma, P. Cawley, M. Lowe, and B. Pavlakovic. The effect of bends on the propagation of guided waves in pipes. *Journal of pressure vessel technology*, 127:328, 2005.

[38] P. Cawley, M.J.S. Lowe, F. Simonetti, C. Chevalier, and AG Roosenbrand. The variation of the reflection coefficient of extensional guided waves in pipes from defects as a function of defect depth, axial extent, circumferential extent

and frequency. *Proceedings of the Institution of Mechanical Engineers, Part C: Journal of Mechanical Engineering Science*, 216(11):1131–1143, 2002.

[39] A. Demma, P. Cawley, M. Lowe, A.G. Roosenbrand, and B. Pavlakovic. The reflection of guided waves from notches in pipes : a guide for interpreting corrosion measurements. *NDT & E International*, 37(3):167–180, 2004.

[40] W. Zhu. An fem simulation for guided elastic wave generation and reflection in hollow cylinders with corrosion defects. *Journal of pressure vessel technology*, 124(1):108–117, 2002.

[41] M. Ratassepp, S. Fletcher, and M.J.S. Lowe. Scattering of the fundamental torsional mode at an axial crack in a pipe. *The Journal of the Acoustical Society of America*, 127:730, 2010.

[42] R. Carandente, J. Ma, and P. Cawley. The scattering of the fundamental torsional mode from axi-symmetric defects with varying depth profile in pipes. *The Journal of the Acoustical Society of America*, 127:3440, 2010.

[43] A. Lovstad and P. Cawley. The reflection of the fundamental torsional guided wave from multiple circular holes in pipes. *NDT & E International*, 44(7):553 – 562, 2011.

[44] A. Lovstad and P. Cawley. The reflection of the fundamental torsional mode from pit clusters in pipes. *NDT & E International*, 46(0):83 – 93, 2012.

[45] J. Rose, S. Pelts, and Y. Cho. Modeling for flaw sizing potential with guided waves. *Journal of nondestructive evaluation*, 19(2):55–66, 2000.

[46] J. Mu, L. Zhang, J.L. Rose, and J. Spanner. Defect sizing in pipe using an ultrasonic guided wave focusing technique. *AIP Conference Proceedings*, 820(1):760–766, 2006.

[47] J. Davies and P. Cawley. The application of synthetic focusing for imaging crack-like defects in pipelines using guided waves. *Ultrasonics, Ferroelectrics and Frequency Control, IEEE Transactions on*, 56(4):759–771, 2009.

[48] S. Gopalakrishnan, A. Chakraborty, and D. Roy Mahapatra. *Spectral Finite Element Method: Wave Propagation, Diagnostics and Control in Anisotropic and Inhomogeneous Structures*. Springer, 2008.

[49] N. Hu, H. Fukunaga, M. Kameyama, D. Roy Mahapatra, and S. Gopalakrishnan. Analysis of wave propagation in beams with transverse and lateral cracks using a weakly formulated spectral method. *Journal of Applied Mechanics*, 74:119–127, 2007.

[50] J.M. Galán and R. Abascal. Numerical simulation of lamb wave scattering in semi-infinite plates. *International Journal for Numerical Methods in Engineering*, 53:1145–1173, 2002.

[51] W. Zhou, M.N. Ichchou, and J.-M. Mencik. Analysis of wave propagation in cylindrical pipes with local inhomogeneities. *Journal of Sound and Vibration*, 319(1-2):335–354, 2009.

[52] M.N. Ichchou, J.-M. Mencik, and W. Zhou. Wave finite elements for low and mid-frequency description of coupled structures with damage. *Computer Methods in Applied Mechanics and Engineering*, 198(15-16):1311–1326, 2009.

[53] W.J. Zhou and M.N. Ichchou. Wave propagation in mechanical waveguide with curved members using wave finite element solution. *Computer Methods in Applied Mechanics and Engineering*, 199(33-36):2099–2109, 2010.

[54] W. Zhou and M.N. Ichchou. Wave scattering by local defect in structural waveguide through wave finite element method. *Structural Health Monitoring*, 10(4):335, 2011.

[55] L. Cartz. *Nondestructive testing: radiography, ultrasonics, liquid penetrant, magnetic particle, eddy current*. ASM International, 1995.

[56] B. Raj, T. Jayakumar, and M. Thavasimuthu. *Practical non-destructive testing*. Woodhead, 2002.

[57] C.E. Betz. *Principles of Magnetic Particle Testing*. Amer Society for Nondestructive, 1985.

[58] D.J. Hagemaier. *Fundamentals of Eddy Current Testing*. ASNT, 1990.

[59] P.M. Morse and H. Feshbach. *Methods of Theoretical Physics*. McGraw-Hill Book Company, 1953.

[60] B.A. Auld. *Acoustic fields and waves in solids vol. 1*. R.E. Krieger, 1990.

[61] B.A. Auld. *Acoustic fields and waves in solids vol. 2*. R.E. Krieger, 1990.

[62] L.E. Malvern. *Introduction to the mechanics of a continuous medium*. Prentice-Hall, 1969.

[63] D.C. Gazis. Three-dimensional investigation of the propagation of waves in hollow circular cylinders. I. analytical foundation. *The Journal of the Acoustical Society of America*, 31:568–578, 1959.

[64] D.C. Gazis. Three-dimensional investigation of the propagation of waves in hollow circular cylinders. II. numerical results. *The Journal of the Acoustical Society of America*, 31(5):573–578, 1959.

[65] J. Zemanek. An experimental and theoretical investigation of elastic wave propagation in a cylinder. *The Journal of the Acoustical Society of America*, 51(1B):265–283, 1972.

[66] I. Mirsky. Wave propagation in transversely isotropic circular cylinders, part 1: Theory. *The Journal of the Acoustical Society of America*, 37(6):1016–1021, 1965.

[67] J.L. Rose. *Ultrasonic Waves in Solid Media*. Cambridge University Press, August 1999.

[68] A.H. Fitch. Observation of elastic-pulse propagation in axially symmetric and nonaxially symmetric longitudinal modes of hollow cylinders. *The Journal of the Acoustical Society of America*, 35:706–708, 1963.

[69] J.W.S. Rayleigh. *The theory of sound*. Dover, 1945.

[70] J.M. Mencik and MN Ichchou. Multi-mode propagation and diffusion in structures through finite elements. *European Journal of Mechanics-A/Solids*, 24(5):877–898, 2005.

[71] M.N. Ichchou, S. Akrout, and J.M. Mencik. Guided waves group and energy velocities via finite elements. *Journal of sound and vibration*, 305(4):931–944, 2007.

[72] J.M. Mencik and MN Ichchou. A substructuring technique for finite element wave propagation in multi-layered systems. *Computer Methods in Applied Mechanics and Engineering*, 197(6-8):505–523, 2008.

[73] A. Demma and D. Alleyne. Inspection of pipes using guided waves : state of the art. In *Proceedings of the 5th Pan American Conference for NDT*. NDT.net, 2011.

[74] J.O. Davies. *Inspection of pipes using low frequency focused guided waves*. PhD thesis, University of London, 2008.

[75] http://www.guided-ultrasonics.com/.

[76] J.J. Ditri, J.L. Rose, and A. Pilarski. Generation of guided waves in hollow cylinders by wedge and comb type transducers. *Review of progress in quantitative nondestructive evaluation*, 12:211–211, 1993.

[77] T.R. Hay and J.L. Rose. Flexible pvdf comb transducers for excitation of axisymmetric guided waves in pipe. *Sensors and Actuators A: Physical*, 100(1):18–23, 2002.

[78] J. Li and J.L. Rose. Implementing guided wave mode control by use of a phased transducer array. *Ultrasonics, Ferroelectrics and Frequency Control, IEEE Transactions on*, 48(3):761–768, 2001.

[79] D.N. Alleyne and P. Cawley. Long range propagation of lamb waves in chemical plant pipework. *Materials Evaluation*, 55(4):504–508, 1997.

[80] P. Wilcox, M. Lowe, and P. Cawley. Omnidirectional guided wave inspection of large metallic plate structures using an emat array. *Ultrasonics, Ferroelectrics and Frequency Control, IEEE Transactions on*, 52(4):653–665, 2005.

[81] Y.Y. Kim, C.I. Park, S.H. Cho, and S.W. Han. Torsional wave experiments with a new magnetostrictive transducer configuration. *The Journal of the Acoustical Society of America*, 117(6):3459–3468, 2005.

[82] H. Kwun, S.Y. Kim, and G.M. Light. The magnetostrictive sensor technology for long range guided wave testing and monitoring of structures. *Materials evaluation*, 61(1):80–84, 2003.

[83] *PIC Catalog: Piezo Ceramic Actuators and Custom Subassemblies*. Physik Instrumente (PI) GmbH & Co. KG, 2006.

dernière page de la thèse

AUTORISATION DE SOUTENANCE

Vu les dispositions de l'arrêté du 7 août 2006,

Vu la demande du Directeur de Thèse

Monsieur M. ICHCHOU

et les rapports de

Monsieur J. HOLNICKI-SZULC
Professeur - Institute of Fundemental Technological Research - Pawinskiego 5b - 02-106 Varsovie Pologne

Et de

Monsieur M. HADDAR
Professeur - Ecole Nationale d'Ingénieurs de Sfax - Route de Soukra - 3038 Sfax - Tunisie

Monsieur KHARRAT Mohamed

est autorisé à soutenir une thèse pour l'obtention du grade de **DOCTEUR**

Ecole doctorale MECANIQUE, ENERGETIQUE, GENIE CIVIL ET ACOUSTIQUE

Fait à Ecully, le 5 juillet 2012

P/Le directeur de l'E.C.L.
La directrice des Etudes

ECOLE CENTRALE DE LYON
SCOLARITE
3ème Cycle

M-A. GALLAND